

4. SITES 677 AND 678¹

Shipboard Scientific Party²

HOLE 677A

Date occupied: 0800 hr, 30 September 1986
Date departed: 1545 hr, 3 October 1986
Time on hole: 3 days, 7 hr, 45 min.
Position: 1°12.138'N, 83°44.220'W
Water depth (sea level; corrected m, echo-sounding): 3461.2
Water depth (rig floor; corrected m, echo-sounding): 3472.3
Bottom felt (m, drill pipe): 3472.3
Total depth (m): 3781.7
Penetration (m): 309.4
Number of cores: 34
Total length of cored section (m): 309.4
Total core recovered (m): 279.44
Core recovery (%): 89.7
Oldest sediment cored:
Depth sub-bottom (m): 309
Nature: nannofossil chalk
Age: 5.6–5.9 m.y. (late Miocene)
Measured velocity (km/s): 1.66
Basement rocks:
Depth sub-bottom (m): 309.4
Nature: basalt

Age: late Miocene
Measured velocity (km/s): not measured

HOLE 677B

Date occupied: 1645 hr, 3 October 1986
Date departed: 0830 hr, 4 October 1986
Time on hole: 15 hr, 45 min.
Position: 1°12.142'N, 83°44.220'W
Water depth (sea level; corrected m, echo-sounding): 3461.2
Water depth (rig floor; corrected m, echo-sounding): 3472.3
Bottom felt (m, drill pipe): 3473.4
Total depth (m): 3566.5
Penetration (m): 93.10
Number of cores: 10
Total length of cored section (m): 93.10
Total core recovered (m): 93.03
Core recovery (%): 99.9
Oldest sediment cored:
Depth sub-bottom (m): 93.1
Nature: nannofossil ooze
Age: late Pliocene
Measured velocity (km/s): not measured

HOLE 678A

Date occupied: 1100 hr, 4 October 1986
Date departed: 1545 hr, 4 October 1986
Time on hole: 4 hr, 45 min.
Position: 1°13.006'N, 83°43.392'W
Water depth (sea level; corrected m, echo-sounding): 3435.7
Water depth (rig floor; corrected m, echo-sounding): 3446.8
Bottom felt (m, drill pipe): 3463.9
Total depth (m): 3464.4
Penetration (m): 0.54
Number of cores: 1
Total length of cored section (m): 0.54
Total core recovered (m): 0.54
Core recovery (%): 100
Oldest sediment cored:
Depth sub-bottom (m): 0.54
Nature: clayey radiolarian-nannofossil-foraminifer ooze
Age: late Pleistocene
Measured velocity (km/s): not measured

HOLE 678B

Date occupied: 1545 hr, 4 October 1986
Date departed: 0500 hr, 5 October 1986

¹ Becker, K., Sakai, H., et al., 1988. *Proc. ODP, Init. Repts. (Pt. A)*, 111: College Station, TX (Ocean Drilling Program).

² Keir Becker (Co-Chief Scientist), Rosenstiel School of Marine and Atmospheric Sciences, University of Miami, Miami, FL 33149; Hitoshi Sakai (Co-Chief Scientist), Ocean Research Institute, University of Tokyo, Tokyo 164, Japan; Russell B. Merrill, Staff Scientist, Ocean Drilling Program, Texas A&M University, College Station, TX 77843; Andrew C. Adamson, Ocean Drilling Program, Texas A&M University, College Station, TX 77843; Joanne Alexandrovich, Lamont-Doherty Geological Observatory, Palisades, NY 10964; Jeffrey C. Alt, Department of Earth and Planetary Sciences, Washington University, St. Louis, MO 63130; Roger N. Anderson, Lamont-Doherty Geological Observatory, Palisades, NY 10964; Daniel Bideau, IFREMER/Centre de Brest, BP 337, 29273 Brest Cedex, France; Robert Gable, Bureau Recherche de Géologie et Minières, BP 6009, 45060 Orleans Cedex-2, France; Peter M. Herzig, Institute of Mining and Economic Geology, Aachen University of Technology, D-5100 Aachen 1, Federal Republic of Germany; Simon Houghton, Department of Earth Sciences, Open University, Milton Keynes, Buckinghamshire MK7 6AA, United Kingdom; Hideo Ishizuka, Department of Geology, Kochi University, 2-5-1 Akebonocho, Kochi 780, Japan; Hodaka Kawahata, Department of Geology, University of Toronto, Toronto, Ontario M5S 1A1, Canada; Hajimu Kinoshita, Department of Earth Sciences, Chiba University, 1-33 Yayoi-cho, Chiba 260, Japan; Michael A. Lovell, Department of Geology, University of Nottingham, University Park, Nottingham NG7 2RD, United Kingdom; John Malpas, Earth Sciences Department, Memorial University, St. John's, Newfoundland A1B 3X5, Canada; Harue Masuda, Ocean Research Institute, University of Tokyo, Tokyo 164, Japan; Roger H. Morin, U.S. Geological Survey, Denver Federal Center, Denver, CO 80225; Michael J. Mottl, Hawaii Institute of Geophysics, University of Hawaii, Honolulu, HI 96822; Janet E. Pariso, School of Oceanography, University of Washington, Seattle, WA 98195; Philippe Pezard, Lamont-Doherty Geological Observatory, Palisades, NY 10964; Joseph Phillips, Institute for Geophysics, University of Texas at Austin, Austin, TX 78751; Joel Sparks, Department of Geology and Geography, University of Massachusetts, Amherst, MA 01003; Stefan Uhlig, Institut für Geowissenschaften und Lithosphärenforschung, Universität Giessen, D-6300 Giessen, Federal Republic of Germany.

Time on hole: 13 hr, 15 min

Position: 1°13.006'N, 83°43.392'W

Water depth (sea level; corrected m, echo-sounding): 3435.7

Water depth (rig floor; corrected m, echo-sounding): 3446.8

Bottom felt (m, drill pipe): 3464.5

Total depth (m): 3636.3

Penetration (m): 171.8

Number of cores: 4

Total length of cored section (m): 28.8

Total core recovered (m): 27.72

Core recovery (%): 96

Oldest sediment cored:

Depth sub-bottom (m): 169

Nature: nannofossil chalk

Age: 5.7–5.9 m.y. (late Miocene)

Measured velocity (km/s): not measured

Basement rocks:

Depth sub-bottom (m): 171.8

Nature: basalt

Age: late Miocene

Measured velocity (km/s): not measured

Principal results: Site 677 is located in a band of slightly low heat flow about 3 km south of Site 504. Coring first with the APC (hydraulic piston corer) and then with the XCB (extended core barrel), Leg 111 penetrated 309.4 m of siliceous nannofossil ooze and chalk and a thin stringer of chert before reaching basement. Recovery with the APC was excellent, averaging over 100% of the cored interval. The thickness of the sediment was surprising, as site survey data indicated that the traveltime to basement was less than at Site 504, where the sediment cover is 275 m. Analyses of pore waters suggested that ocean bottom water is slowly recharging through the sediment cover, at rates on the order of a few millimeters per year. After basement was reached in Hole 677A, Hole 677B was spudded with the APC 10 m north, to ensure complete recovery of the Pleistocene section for biostratigraphic and paleoceanographic studies. As time was limited, coring in Hole 677B was terminated at a total depth of 93.1 mbsf, when Pliocene sediments were first recovered.

Site 678 is located 2 km northeast of Site 677, in a local maximum of heat flow. Time allowed only a brief program of washing and coring to basement at Site 678, primarily for geothermal and geochemical studies of advection of pore waters and diagenesis of the sediments. Recovery of the mud-line section was important for these objectives, so Hole 678A was abandoned when the mud-line core recovered only 54 cm. Hole 678B was immediately spudded, and 7.5 m was recovered in the mud-line core. Time allowed a total of only five cores (three with APC, two with XCB) to be recovered and the hole was mostly washed until chert and basalt were recovered at 171.8 mbsf. Chemical analyses of pore waters confirmed that altered seawater is flowing upward through the sediments at Site 678 at rates of a few millimeters per year.

The compositions of formation waters from the basal sediments are similar at Sites 677 and 678; at both sites, concentrations of dissolved calcium in pore waters were about 6 times greater and those of dissolved magnesium were about 5 times less than in seawater. This suggests that the chemical fluxes through the sediments are negligible compared with advective fluxes within basement.

BACKGROUND AND OBJECTIVES

During Leg 111 of the Ocean Drilling Program (ODP), the *JOIDES Resolution* spent 5 days coring sedimentary sections at Sites 677 (Holes 677A and 677B) and 678. Site 677 is located on a heat-flow low 2750 m south-southwest of Hole 504B, and Site 678 is on a heat-flow high 1360 m southeast of Hole 504B (Fig. 1).

The objectives of drilling at Sites 677 and 678 were:

1. To obtain detailed biostratigraphic and paleoceanographic records, including stable isotopic and palynomorphic data, and

to document environmental changes in the tropical eastern Pacific Ocean and adjacent terrestrial biosphere for the past few million years. Site 677 was the major target for this purpose because the low heat flow at the site should have resulted in better preservation of microfossils.

2. To test the widely adopted hypothesis that warm, altered seawater forms and flows laterally in the upper section of the basement of this area and wells up through the sediment column at localized heat-flow highs, whereas heat-flow lows represent recharge zones of cold seawater into the basement. Depth profiles of pore water chemistry including helium and its isotopes and of temperature were critical measurements to be made at both sites.

3. To study the effect of high heat flow and upwelling warm water on the early diagenesis of pelagic sediments. Comparison of diagenetic alteration of organic as well as inorganic substances in sediments from both sites will document chemical and mineralogical changes that occur in the sediment cover on the ridge flank geothermal areas.

Sites 677/678, southern extensions of Sites 501/504, are covered with 170–310 m of sediment, which is mainly a siliceous calcareous (nannofossil) ooze of pelagic origin containing a continuous biostratigraphic and paleoceanographic record from the late Miocene to the Holocene (Cann et al., 1983). The sedimentary section at Sites 501/504 is classified into three lithologic units, mainly depending on the degree of diagenetic alteration of carbonate- and silica-fossil remains: (1) Unit I (0–143.5 mbsf) consisting of late Pleistocene to late Pliocene siliceous-nannofossil and nannofossil-radiolarian oozes, (2) Unit II (143.5–227.2 mbsf) of late Pliocene to late Miocene siliceous nannofossil chalk, and (3) Unit III (227.2 mbsf to basement) of late late Miocene nannofossil chalk, limestone, and chert (Cann et al., 1983). The diatom biostratigraphy at this site marks the Pliocene-Pleistocene boundary at 70 mbsf and the Miocene-Pliocene boundary at 215 mbsf (Sancetta, 1983), with an average sedimentation rate of 50 m/m.y. The sedimentation rate is not only high but also very uniform over almost the entire sedimentary section (Shackleton and Hall, 1983). Therefore, in spite of the accelerated diagenetic alteration in the lower portion of Unit II from Hole 504B, Shackleton and Hall (1983) were able to obtain a high-resolution (2500 yr) oxygen isotopic record of climatic variation for the eastern equatorial Pacific Ocean during the Pleistocene. They further demonstrated that the Pliocene section of Hole 504B may also preserve the isotopic record with higher resolution than any other places so far studied. The sediments of Sites 501/504 are the best materials obtainable for the biostratigraphic and geochemical studies of climatic variation during the lower Pleistocene and late Pliocene.

In calcareous Pliocene/Miocene sediments under normal deep-sea heat-flow conditions, silicification takes place only below a burial depth of 400 m (Riech and von Rad, 1979). Therefore, the shallower depth of silicification at Sites 501/504 may imply accelerated diagenesis under high-heat-flow conditions. Eighty kilometers north of Sites 501/504, no chert was recovered at Site 505, where the heat flow is low. A comparative study of diagenetic alteration at heat-flow highs and lows, which are closely spaced to each other and thus have similar sedimentary records, would be important to understanding early diagenesis of sediments on young oceanic crust.

The first extensive study of the hydrothermal circulation of this area was made by DSDP Legs 68 and 69, during which five holes were drilled at Sites 501/504, approximately along an east-west line extending over a total distance of 500 m. A surprising discovery was a large monotonic lateral gradient from east to west in the composition of pore waters from the five closely spaced sediment columns; at a given depth, Ca and Si increased westward, whereas Mg, SO₄, and ¹⁸O decreased. The pore wa-

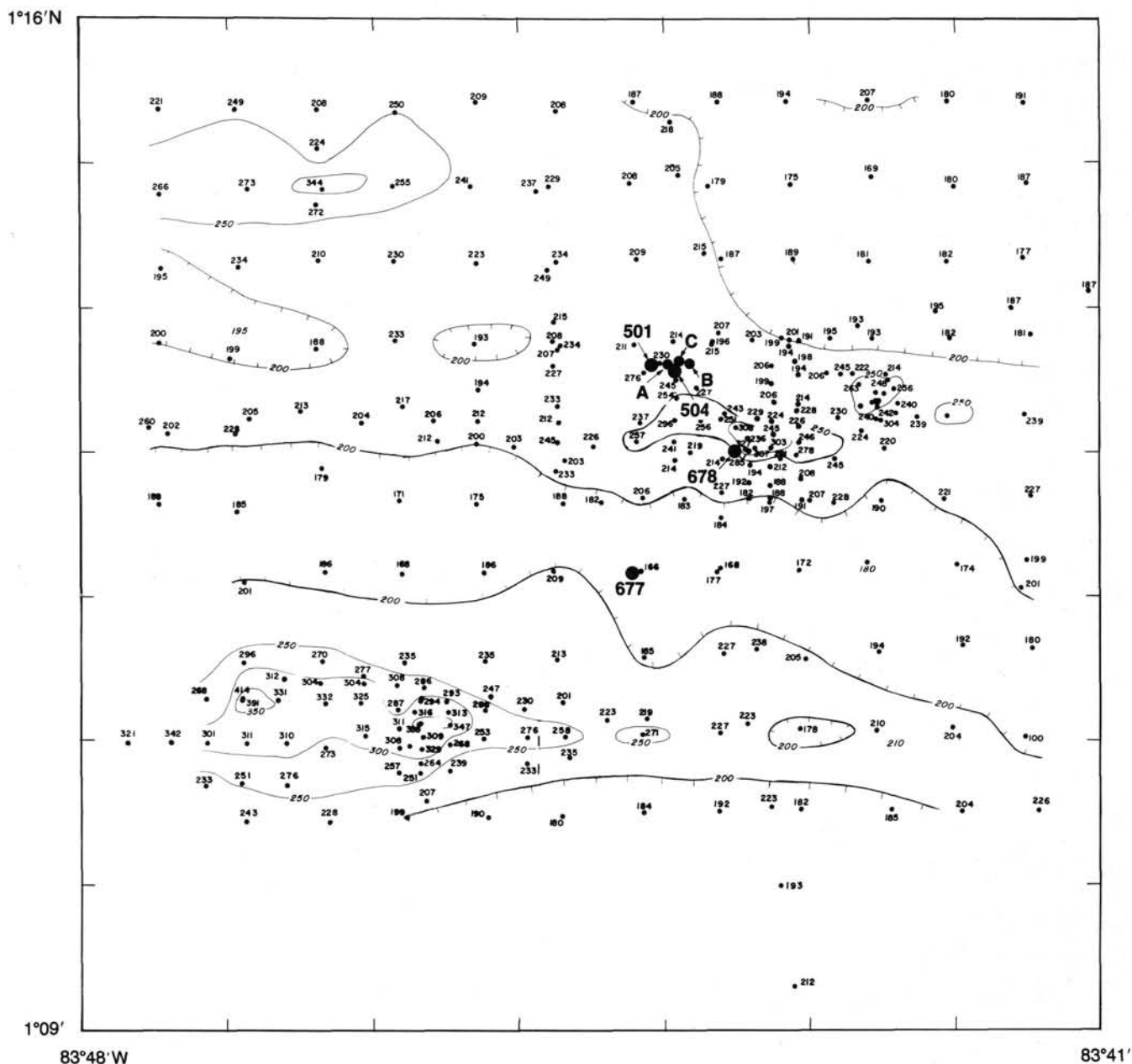


Figure 1. Locations of Sites 501/504 and 677/678 in relation to heat flow. Heat-flow data and contours (in mW/m^2) Langseth et al. (this volume).

ters indicated typical vertical gradients in these species. Such vertical gradients in the sediment column on moderately young oceanic crust have been attributed to basalt alteration in the upper basement beneath the sediment. However, such a large lateral gradient had never been observed before. This trend is nearly parallel with an increasing trend of heat flow from east to west and was interpreted as resulting from the difference in the temperature and extent of reaction within basaltic rocks of seawater flowing through the upper basement (Mottl et al., 1983).

Another important discovery was the presence of an underpressured region in the upper 100 m of the basement in Hole 504B. Downhole temperature measurements performed in Hole 504B on Legs 69, 70, 83, 92, and 111 indicated that ocean bottom water has been flowing into this underpressured region, although the downhole flow has slowed considerably over a period of 7 yr.

After Leg 83, extensive heat-flow surveys and piston coring for pore-water chemistry at Sites 501/504 were made during two research cruises, RC 23-5 (*Robert Conrad*) in 1982 and TT-198 (*Thomas G. Thomson*) in 1986, with M. Langseth and M. Mottl being the co-chief scientists in both cruises. The vertical gradients of pore-water chemistry were positively correlated with heat flow at the site, a strong indication of upward advection of pore water in areas of high heat flow (Langseth et al., this volume).

The sediment cover in this area is sufficiently thick to prevent regional-scale exchange of seawater with underlying basaltic basement (Anderson and Hobart, 1976). The cooling of the basement is governed predominantly by conductive heat loss across the overlying sediment column. However, the previous studies on the porewater chemistry combined with heat-flow data and the downhole flow of seawater in Hole 504B suggest that in

spite of the thick sediment cover, convective heat flow due to circulation of warm seawater through the sediment column may still persist in the area where there are isolated heat-flow highs.

The optimum positions for Sites 677 and 678 were chosen on the basis of the heat-flow and basement temperature maps provided by M. Hobart and M. Langseth using the geophysical data obtained by TT-198, designed to be a site survey cruise for Sites 677 and 678, combined with precisely navigated data from RC-2305 and RC-2606. The heat-flow map with location of Sites 501/504 and Sites 677/678 is reproduced in Figure 1.

In order to achieve the first objective, the coring program originally planned at Site 677 consisted of double APC to refusal and one XCB to the basement. However, because the time was short, APC cores were taken only to the Pliocene/Pleistocene boundary at the second APC hole, Hole 677B. For the same reason, four to five sediment cores were planned to be taken by APC and XCB, with about 70-m wash intervals, at Site 678. However, time was lost by two consecutive failures in obtaining a good mud-line core in the first hole 678A, which was subsequently abandoned as the shortest hole ever drilled by DSDP/ODP. Hole 678B hit basalt at 171.8 mbsf, and the drilling was terminated there, with four good sediment cores.

OPERATIONS

Between 30 September and 5 October, Leg 111 spent slightly more than 5 days in coring the sediments near Site 504, with an emphasis on measuring temperatures and sampling pore waters. Site 677 was located in a local minimum of heat flow 3 km south of Hole 504B; Site 678 was located in a sharp maximum of heat flow about 1.5 km northeast of Site 677. The coring results and temperature/pore-water operations are summarized in Tables 1 and 11, respectively.

Site 677

JOIDES Resolution departed Hole 504B at 0645, 30 September, and steamed 3 km south at less than 1 knot to Site 677. The scientific requirements for Site 677 included two holes cored with the APC to refusal, with one of these holes continued to basement with the XCB. The water depth at Site 677 was verified to be 3472.3 mbrf when Hole 677A was spudded with the APC at 1640, 30 September. APC coring, with orientation and temperature measurements on selected cores, proceeded uneventfully to 3555 mbrf. At that point, the sand line broke at the rope socket while pulling an inner core barrel loose from the outer barrel, and a second wireline trip was required to retrieve the core barrel. APC coring continued to 3612 m where, after a heat-flow test, the overpull reached 85,000 lb. The APC was swapped for an XCB assembly and coring continued to 3781.7 m (309.4 mbsf), where the rate of penetration decreased drastically and basalt was recovered in the core catcher.

The bottom-hole assembly was then pulled clear of the mud line, and the ship was moved 10 m north. Hole 677B was spudded at 1650, 3 October. Hole 677B was cored with the APC at intervals staggered from those at Hole 677A, to 3566.5 mbrf or 93.1 mbsf. To preserve enough time for even a minimal program at Site 678, coring in Hole 677B was stopped when Pliocene sediments were first recovered, in Core 677B-10H. Recovery with the APC in both Holes 677A and 677B was excellent, averaging 99.9%, thus fulfilling the primary Site 677 objective of recovering a complete Pleistocene section for biostratigraphic and paleoceanographic studies.

Site 678

The bottom-hole assembly was pulled clear of the mud line, and the ship was moved to Site 678 beginning at 0830, 4 October. The drill string was left in the water, and the ship steamed at less than 1 knot slightly more than 2 km northeast to Site

Table 1. Coring summary Sites 677 and 678.

Core no.	Date (1986)	Time	Depths (mbsf)	Cored (m)	Recovered (m)	Recovery (%)
Hole 677A						
1H	Sep 30	1730	0.0-6.2	6.2	6.24	100.0
2H	30	1915	6.2-15.7	9.5	9.80	103.0
3H	30	2120	15.7-25.2	9.5	9.78	103.0
4H	30	2300	25.2-34.7	9.5	9.51	100.0
5H	Oct 1	0030	34.7-44.2	9.5	9.51	100.0
6H	1	0215	44.2-53.7	9.5	9.92	104.0
7H	1	0345	53.7-63.2	9.5	9.73	102.0
8H	1	0530	63.2-72.7	9.5	9.81	103.0
9H	1	1000	72.7-82.2	9.5	9.17	96.5
10H	1	1130	82.2-91.7	9.5	9.79	103.0
11H	1	1345	91.7-101.2	9.5	10.00	105.2
12H	1	1515	101.2-110.7	9.5	9.89	104.0
13H	1	1715	110.7-120.2	9.5	9.98	105.0
14H	1	1845	120.2-129.7	9.5	9.84	103.0
15H	1	2015	129.7-139.2	9.5	10.02	105.5
16X	1	2245	139.2-144.2	5.0	9.50	190.0
17X	2	0030	144.2-153.8	9.6	7.67	79.9
18X	2	0230	153.8-163.5	9.7	6.01	61.9
19X	2	0700	163.5-173.2	9.7	8.97	92.5
20X	2	0845	173.2-182.8	9.6	7.79	81.1
21X	2	1030	182.8-192.4	9.6	2.95	30.7
22X	2	1230	192.4-202.1	9.7	7.34	75.7
23X	2	1430	202.1-211.7	9.6	7.09	73.8
24X	2	1830	211.7-221.4	9.7	9.60	98.9
25X	2	2030	221.4-231.1	9.7	7.69	79.3
26X	2	2230	231.1-240.8	9.7	8.73	90.0
27X	3	0045	240.8-250.4	9.6	8.45	88.0
28X	3	0245	250.4-260.0	9.6	6.41	66.8
29X	3	0415	260.0-269.7	9.7	5.55	57.2
30X	3	0615	269.7-279.3	9.6	6.10	63.5
31X	3	0800	279.3-288.9	9.6	9.70	101.0
32X	3	0945	288.9-298.6	9.7	8.22	84.7
33X	3	1145	298.6-308.4	9.8	7.97	81.3
34X	3	1345	308.4-309.4	1.0	0.71	71.0
				309.4	279.44	
Hole 678A						
1H	4	1445	0.0-0.6	0.6	0.54	90.0
				0.6	0.54	
Hole 677B						
1H	3	1715	0.0-7.6	7.6	7.56	99.5
2H	3	1845	7.6-17.1	9.5	9.37	98.6
3H	3	2045	17.1-26.6	9.5	9.78	103.0
4H	3	2200	26.6-36.1	9.5	9.61	101.0
5H	3	2345	36.1-45.6	9.5	9.72	102.0
6H	4	0100	45.6-55.1	9.5	9.71	102.0
7H	4	0215	55.1-64.6	9.5	9.93	104.0
8H	4	0330	64.6-74.1	9.5	8.70	91.6
9H	4	0445	74.1-83.6	9.5	9.27	97.6
10H	4	0700	83.6-93.1	9.5	9.38	98.7
				93.1	93.03	
Hole 678B						
1H	4	1615	0.0-7.5	7.5	7.41	98.8
2H	4	1815	18.2-27.7	9.5	9.84	103.0
3H	4	2145	95.5-105.0	9.5	9.92	104.0
4W	5	0215	105.0-169.5	64.5	7.38	11.4
5X	5	0430	169.5-171.8	2.3	0.55	23.9
				93.3	35.10	

678. The primary scientific objectives for Site 678 were to study hydrologic processes at a local maximum of heat flow, involving sampling pore waters and temperatures. There were less than 24 hours available for this work. Unfortunately, Site 678 was located near a small ridge or fault scarp, which resulted in a misleading estimate of mud-line depth from the PDR (precision depth recorder). The first attempt at a mud-line core came up

empty, and only 0.54 m was recovered when Hole 678A was spudded. As recovering a complete mud-line section was critical to the study of the pore-water chemistry, a second mud-line core was required, and a new hole was spudded, Hole 678B.

At this stage, time was very short, and it was necessary that Hole 678B be only spot-cored with a minimum number of temperature measurements. Only five cores (three APC and two XCB) and two temperature measurements were taken, as the hole was mostly washed to basement. Difficult drilling was encountered at an unexpectedly shallow depth, and pieces of basalt were recovered from 169.5 and 171.8 mbsf. When this evidence of basement was recovered, the ship returned to Hole 504B, departing Site 678 at 0500, 5 October.

SEDIMENTOLOGY AND LITHOSTRATIGRAPHY

SITE 677

Introduction

Two holes were cored at Site 677 (1°12.14'N, 83°44.22'W) in a water depth of 3461 m. Hole 677A was cored to 309.4 mbsf with 279.44 m of sediments recovered. Cores 111-677A-1H through 111-677A-15H were cored with the APC technique reaching 139.2 mbsf and averaging over 100% recovery. Using the XCB technique, Cores 111-677A-16X through 111-677A-34X were recovered with 136.45 m of sediment and basal basalt fragments, and reached 309.4 mbsf averaging 80% recovery. Hole 677B was offset from Hole 677A by 10–30 m. Ten cores were recovered at Hole 677B using the APC, reaching 93.1 mbsf with an average recovery of 99.9%.

Three major sedimentary units and a basal basalt unit are recognized at Site 677. Unit I consists of alternating clayey biogenic calcareous siliceous oozes and clayey biogenic siliceous calcareous oozes ranging in age from early Pliocene to late Pleistocene. Unit II is composed of siliceous nannofossil ooze and chalk, and ranges in age from late Miocene to early Pliocene. Unit III consists of cherty limestone and nannofossil chalk and is late Miocene in age. Unit I has been divided into four subunits, Unit II has been divided into two subunits, and Unit III has been divided into two subunits. All units are described in detail below. Unit IV consists of iron oxide- and smectite-rich sediments intermixed with glassy basement basalts of late Miocene age. Only Unit I, Subunits IA, IB, and IC sediments were recovered at Hole 677B.

Lithologic Units

Unit I: Cores 111-677A-1H to 111-677A-17X; Depth: 0–153.8 mbsf; Age: early Pliocene to late Pleistocene. Cores 111-677B-1H to 111-677B-10H; Depth: 0–93.1 mbsf; Age: late Pliocene to late Pleistocene.

Unit II: Core 111-677A-18X to Section 111-677A-33X-4, 20 cm; Depth: 153.8–303.3 mbsf; Age: late Miocene to early Pliocene.

Unit III: Section 111-677A-33X-4, 20 cm, to Section 111-677A-34X-1, 10 cm; Depth: 303.3–308.5; Age: late Miocene.

Unit IV: Section 111-677A-34X-1, 10 cm, to Section 111-677A-34X, CC; Depth: 308.5–309.4 mbsf; Age: late Miocene.

Unit I

Unit I is composed of alternating clayey calcareous siliceous ooze and clayey siliceous calcareous ooze. Unit I is subdivided into four subunits. The boundaries of the subunits are determined mainly by the fluctuating carbonate content at this site. Subunits were determined with the information obtained from smear slide analyses; however, they agree well with the carbonate record of this site (Fig. 2). The average carbonate content of Unit I of Hole 677A is 37.2%. Subunits IA and IC have average

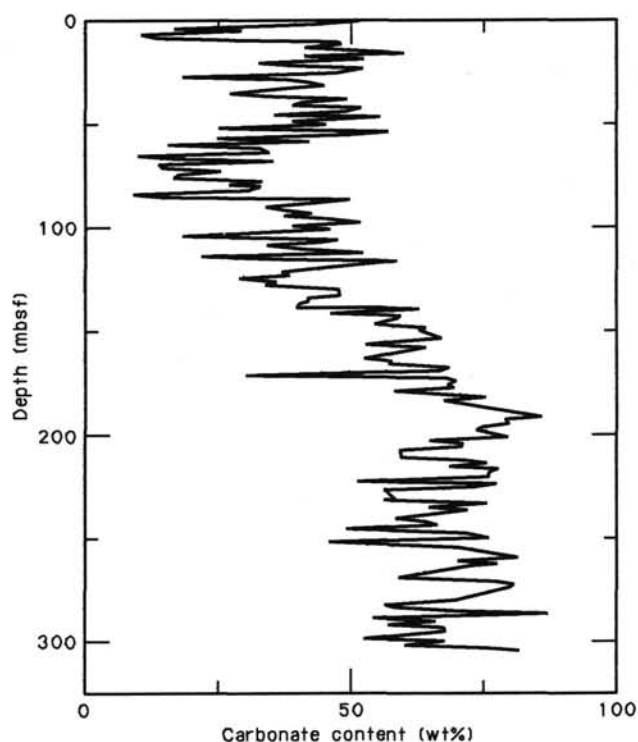


Figure 2. Weight percent carbonate plotted against depth, Hole 677A.

carbonate contents below 37.2% (30.1% and 25.5%, respectively) whereas Subunits IB and ID have average carbonate contents higher than 37.2% (40.9% and 44.3%, respectively). When carbonates are present in lower percentages, the biogenic oozes are classified as siliceous, and when carbonate percentages are higher than the total percent of siliceous material, the sediments are classified as biogenic calcareous. Clay is present in these sediments varying between 5% and 25% (as estimated from smear slides). Pyrite is common and contributes to the mottled appearance of the cores.

Subunit IA

Core 111-677A-1H to Section 111-677A-2H-4, 50 cm; Depth: 0–11.2 mbsf; Age: late Pleistocene.

Core 111-677B-1H; Depth 0–7.6 mbsf; Age: late Pleistocene.

Subunit IA consists of olive gray, olive green, and light gray green clayey foraminiferal-nannofossil radiolarian-diatom ooze, mottled with darker shades of gray green and dusky yellow green. Burrowing is usually haloed and streaked with pyrite particles. Open burrows as well as fat and simple Zoophycos occur in this unit. As the name specifies, clay, foraminifers, radiolarians, and diatoms are all present in excess of 10%. Sponge spicules and silicoflagellates are minor components. The top of Core 111-677A-1H (Sections 1 and 2) is composed of clayey radiolarian foraminiferal ooze, but was not distinguished in Hole 677B, so it was not identified as a separate subunit.

In Hole 677A a volcanic ash layer was identified in this unit at 8.4 mbsf. An ash layer that correlates to this same layer was found in Hole 677B at 9.2 mbsf but is contained in Subunit IB. It is likely that the sediments containing this ash layer in Hole 677B are part of Subunit IA, but this could not be discerned due to the lack of smear slides in this interval.

Subunit IB

Section 111-677A-2H-4, 50 cm, to Core 111-677A-7H; Depth 11.2–63.2 mbsf; Age: early Pleistocene to late Pleistocene.

Cores 111-677B-2H to 111-677B-8H; Depth 7.6–74.1 mbsf; Age: early Pleistocene to late Pleistocene.

Subunit IB consists of clayey diatom foraminiferal-nannofossil ooze varying in color from light gray green to olive gray green alternating with dusky yellow green, mottled with darker olive green and pyrite streaks. Bioturbation is moderate to intense with numerous *Cylindrichnus* and *Zoophycos* trace fossils. Radiolarians are present with less than 10% abundance. Sponge spicules are common and silicoflagellates are present but rare except for a slight increase to 5% midway through the section.

Subunit IC

Cores 111-677A-8H to 111-677A-10H; Depth: 63.2–91.7 mbsf; Age: late Pliocene to early Pleistocene.

Cores 111-677B-9H to 111-677B-10H; Depth: 74.1–93.1 mbsf; Age: late Pliocene to early Pleistocene.

Subunit IC consists of alternating gray green, olive green, and yellow green mottled clayey nannofossil radiolarian-diatom ooze. Bioturbation ranges from minor to strong. Gray pyritic streaking is common. Several pyritized burrows are noted, as well as shell fragments and a shark tooth in Hole 677B. Foraminifers become less abundant (less than 10%) and remain in low abundances downsection. In Core 111-677A-10H an inclusion of light gray green sediment is found which probably was derived from higher in the section, and included by the coring process.

Subunit ID

Cores 111-677A-11H to 111-677A-17X; Depth 91.7–153.8 mbsf; Age: early Pliocene.

Subunit ID is composed of clayey diatom nannofossil ooze. It is moderately to intensely bioturbated and mottling ranges in color from yellow green, gray green, olive green to olive. Pyritic streaking is common, as well as *Zoophycos*, *Cylindrichnus*, and *Planolites*. At the base of Core 111-677A-11H, Section 7 and CC, a flow-in diapiric structure is noted.

Unit II

Unit II consists of siliceous nannofossil ooze and siliceous nannofossil chalk. Unit II was divided into two subunits based on the relative amount of induration. The sediments of Unit II have an average carbonate content of 64.7%. Subunit IIA has a slightly lower carbonate content (60.7%) than Subunit IIB (68.7%). Pyrite and clay are less abundant (1% for pyrite and 5% for clay) than in Unit I.

Subunit IIA

Cores 111-677A-18X to 111-677A-20X; Depth: 153.8–182.8 mbsf; Age: early Pliocene.

Subunit IIA is composed of alternating layers of siliceous nannofossil ooze and siliceous nannofossil chalk. Bioturbation is moderate. The chalks and oozes are light gray to grayish yellow green with yellow and gray mottling. Diatoms are the most abundant siliceous component (radiolarians, sponge spicules, and silicoflagellates are also present) but remains with an abundance of less than 10%. The alternating layers of chalk and ooze range in thickness from 6 to 30 cm. The distinction between oozes and chalks is strictly by the subjective judgment of hardness (see "Introduction and Explanatory Notes" chapter, this volume). Using these criteria it appears that the transition from chalk to ooze occurs gradually over an interval of 29 m.

Subunit IIB

Core 111-677A-21X to Section 111-677A-33X-4, 20 cm; Depth: 182.8–303.3 mbsf; Age: late Miocene to early Pliocene.

Subunit IIB is composed entirely of light gray, olive gray, pale green, gray green, and white siliceous nannofossil chalk.

Bioturbation is minor to moderate with olive mottling. Pyrite mottling is slight. Diatom tests are the most dominant of the siliceous components within these chalks, but rarely do they occur in excess of 10% as estimated in smear slides. In Core 111-677A-23X at 203.8 mbsf a volcanic ash layer was noted. The ash consists mainly of sand- and silt-sized volcanic glass and pyrite.

Unit III

Unit III sediments are composed of cherty limestone and nannofossil chalk. This unit was divided into two subunits based on the degree of induration and the presence of siliceous material.

Subunit IIIA

Section 111-677A-33X-4, 20–50 cm; Depth: 303.3–303.6 mbsf; Age: late Miocene.

Subunit IIIA is composed of cherty limestone intermixed with siliceous nannofossil chalk. This section is disturbed by drilling in that the cherty limestones have been fragmented. The cherty limestones are tan to brown in color and show a large amount of bioturbation mottling, and in some portions appear thinly laminated (less than 1 mm). The silicified areas of the limestones cut across primary sedimentary structures (bioturbation).

Subunit IIIB

Sections 111-677A-33X-4, 50 cm, to 111-677A-34X-1, 10 cm; Depth 303.6–308.5 mbsf; Age: late Miocene.

Subunit IIIB is nannofossil chalk. No biogenic siliceous remains are found in the smear slides of this unit. Foraminifers are present in abundances of less than 5%. Clay, pyrite, and other accessory minerals occur in minor abundance. The lack of any siliceous component in this unit is almost certainly a diagenetic effect. The original silicic components of this chalk were probably dissolved and mobilized, later forming the cherts found in Subunit IIIA.

Unit IV

Sections 111-677A-34X-1, 10 cm, to 111-677A-34X, CC; Depth 308.5–309.4 mbsf; Age: late Miocene.

Unit IV consists of iron oxide- and smectite-rich basal sediments mixed with glassy basalt fragments. There are dark green sediments mixed with the basalt fragments at the top of this unit. Below this mixture the sediments are brown and are probably highly weathered basalts. Below these brown sediments are brecciated basalts.

SITE 678

Introduction

Two holes were cored at Site 678 (1°13.01'N, 83°43.39'W) in a water depth of 3435 m. At Hole 678A the APC recovered 0.54 m of clayey radiolarian nannofossil-foraminiferal ooze, and the hole was abandoned. Hole 678B was cored to 171.8 mbsf recovering 35.1 m of sediment. Cores 111-678B-1H through 111-678B-3H were cored with the APC with wash intervals in between each core. Recovery from the APC averaged over 100%. The XCB Core 111-678B-5X recovered 0.55 m of limestone and brecciated basalt.

Three sedimentary units and one basaltic unit are recognized at Site 678. Unit I is composed of clayey calcareous siliceous ooze. Unit II consists of clayey diatom nannofossil chalk. Unit III is composed of limestone, and Unit IV consists of basalt fragments and conglomerates.

Lithologic Units

Unit I: Cores 111-678B-1H to 111-678B-2H; Depth: 0.0–27.7 mbsf; Thickness: 17.3 m; Age: late Pliocene to late Pleistocene.

Unit II: Core 111-678B-3H to Section 111-678B-4W, CC (15 cm); Depth: 95.5–111.8 mbsf; Thickness: 16.3 m; Age: late Miocene.

Unit III: Sections 111-678B-4W, CC (15 cm) to 111-678B-5X, CC (10 cm); Depth: 111.8–169.8 mbsf; Thickness: 0.7 m; Age: late Miocene.

Unit IV: Sections 111-678B-5X, CC (10 cm) to 111-678B-5X, CC (41 cm); Depth: 169.8–170.1 mbsf; Thickness: 0.3 m; Age: late Miocene.

Unit I

Unit I consists of gray green to olive clayey calcareous radiolarian-diatom ooze. Foraminifers, sponge spicules, and silicoflagellates are rare (present in abundance of less than 5%). Nannofossils make up 10% of the calcareous fraction, the rest consisting of unidentifiable calcite. Bioturbation is moderate to intense. Simple Zoophycos, Planolites, Cylindrichnus, and pyritic streaking and mottling are common.

Unit II

Unit II is composed of clayey diatom nannofossil chalk. The chalk is mottled, predominantly olive gray green in color, with gray pyritic streaks and halos around burrow features. Bioturbation is moderate to intense. Some simple Zoophycos were noted as well as numerous Cylindrichnus. Foraminifers and radiolarians are present in abundance of less than 5% while silicoflagellates and sponge spicules occur in trace amounts. In Section 111-678B-3H-3, 8 cm (98.5 mbsf), a 5-in. volcanic ash layer was noted. The ash is composed of volcanic glass and pyrite of sand and silt size.

Unit III

Unit III consists of limestone. The limestone ranges from pink to green in color and is found in fragments as large as 3 cm in diameter. Drilling has broken the limestone into very small pieces. The limestones are predominantly composed of micrite, but foraminifers are seen in thin section.

Unit IV

Unit IV consists of dark green and gray (metal-rich) muds, intercalated with basalt pebbles and conglomerates, and white calcitic material. Basalt conglomerates occur near the base of 111-678B-4W, CC (not officially included in Unit IV due to disturbed nature of the recovered cores). Within these poorly indurated conglomerates a pyrite and marcasite concretion was noted. The basalts appear to be samples of pillow lava margins and are sparsely vesicular with varying proportions of glass. They are plagioclase-phyric with the plagioclase occurring as glomerocrysts of approximately 10–12 crystals. The individual plagioclase crystals average 0.8 mm in size, are essentially euhedral, fresh, and have compositions of approximately An₇₀. They form as much as 4% of the rock. In some places the glomerocrysts appear to serve as nucleation sites for varivols of plagioclase and clinopyroxene. Between the varivols and in extremely fine-grained patches, axiolitic texture is seen, but most groundmass is devitrified, hyalopilitic with equal amounts of plagioclase and clinopyroxene, the former occurring as skeletal acicular crystals which show fluxion alignment, and the latter often plumose. Oxides are ubiquitous and small groundmass crystals of chromite are observed. Alteration of the basalts represents early diagenetic processes, very shallow burial, and possibly low-pressure/low-temperature hydrothermal processes. Generally, alteration occurs in areas adjacent to and paralleling cracks and fractures and surrounding vesicles. Alteration produces Fe-oxides, K-rich and K-poor smectites, and possibly pyrite.

BIOSTRATIGRAPHY

SITE 677

Two holes were drilled at Site 677 in a water depth of 3461 m: Hole 677A to a depth of 309.4 mbsf and Hole 677B to a depth of 93.1 mbsf. The sediments range in age from late Miocene to Pleistocene and consist mainly of calcareous siliceous ooze, muddy nannofossil siliceous ooze, and siliceous nannofossil ooze. Figure 3 shows the age and zonal assignments of the cores recovered from Site 677.

Calcareous Nannofossils

Calcareous nannofossils occur in all samples examined; their abundance generally varies from few to common. Preservation of the nannofossils ranges from moderate to poor. Placoliths frequently show signs of dissolution. The Miocene/Pliocene dis-coaster assemblages are consistently overgrown, particularly in Miocene sediments. Species identification of discoaster taxa recovered from the basement sediments is often difficult because of poor preservation. The discoasters commonly occur as isolated fragments. Ceratoliths are the other nannofossil group that consistently occur with overgrowth. The Pliocene/Pleistocene boundary lies within Cores 111-677A-9H and 111-677B-9H. The early/late Pliocene boundary is placed in the middle of Core 111-677A-17X. The Miocene/Pliocene boundary is assigned to the upper part of Core 111-677A-24X.

Based on nannofossil biochronological evidence the oldest sediment recovered at Site 677 (Hole 677A) has an age between 5.6 and 7.4 Ma. Reworking at Site 677 is a fairly consistent, but minor, component of the nannofossil assemblages, limited to discoasters and a few robust placolith species (e.g., *Reticulofenestra pseudoumbilica*). Nannofossil species events observed in Hole 677A are listed in Table 2.

Pleistocene

The Pleistocene assemblages are dominated by *Gephyrocapsa* spp. and *Pseudoemiliania lacunosa*. *Calcidiscus leptoporus* is the only other species which consistently forms over 1% of the assemblages. Minor species (0.1%–1%) include *Helicosphaera sellii*, *H. carteri*, *Pontosphaera japonica*, *P. multipora*, *Syracosphaera* spp., and *Rhabdosphaera clavigera*. Rare species include *Umbilicosphaera sibogae*, *Ceratolithus cristatus*, *C. telesmus*, *C. simplex*, *Thoracosphaera* sp., and scyphosphaerids. Most of these species have a sporadic occurrence within the Pleistocene sediments. Early Pleistocene assemblages contain additional species such as *Calcidiscus macintyreii*, *Helicosphaera neogranulata*, *Coccolithus pelagicus*, and *Ceratolithus rugosus*.

Shipboard scanning electronic microscope (SEM) studies on Samples 111-677A-1H, CC, and 111-677B-1H, CC, recorded the rare occurrence of *Emiliania huxleyi*. The presence of this species allows these cores to be placed within the NN21 *Emiliania huxleyi* Zone. Further analysis of younger samples failed to show any dominance of *E. huxleyi* in the nannofossil assemblages; *Gephyrocapsa* species still dominate these samples. The *Emiliania huxleyi* Acme Zone of Gartner (1977) (base 0.085 Ma) may therefore not be delineated in these cores. The low dominance of *E. huxleyi* may be the result of poor preservation; the rare specimens of *E. huxleyi* found in Cores 111-677A-1H and 111-677B-1H are very badly corroded, and no intact coccoliths could be found. Preservation of other coccolith species is also poor in these latest Pleistocene sediments. Isolated shields of *Calcidiscus leptoporus* frequently show signs of etching and breakage. *Gephyrocapsa* spp. appear to be the most robust, solution-resistant taxa in the Pleistocene sediments. Most specimens have their bridges intact, although etching of suture boundaries is apparent.

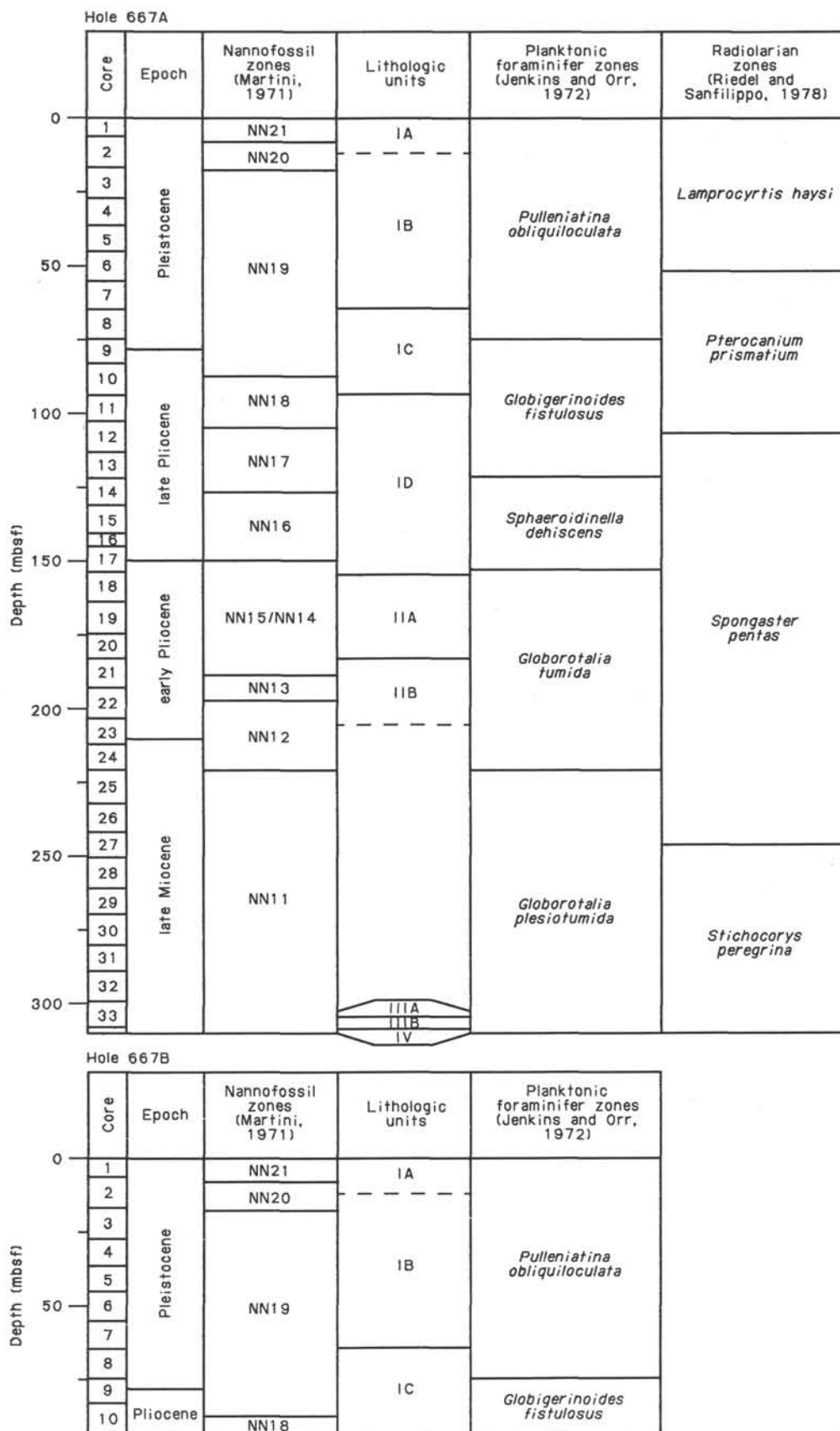


Figure 3. Zonal assignments, epoch boundaries, lithostratigraphy within cores, and depth in Holes 677A and 677B.

Table 2. Nannofossil and planktonic foraminiferal species events, their stratigraphic placement (depth in Hole 677A), and their assigned age estimates.

Datum	Depth (mbsf)	Age (Ma)
f.o. <i>Emiliania huxleyi</i>	6.2–15.7	0.275
l.o. <i>Pseudoemiliania lacunosa</i>	15.7–16.45	0.475
l.o. <i>Helicosphaera sellii</i>	48.8–54.00	1.37
l.o. <i>Calcidiscus macintyreii</i>	57.1–62.00	1.45
l.o. <i>Discoaster brouweri</i>	85.8–87.5	1.89
l.o. <i>D. pentaradiatus</i>	105.2–111.7	2.35
l.o. <i>D. surculus</i>	120.2–129.7	2.41
l.o. <i>Sphenolithus</i> spp.	144.2–147.9	3.45
l.o. <i>Reticulofenestra pseudumbilica</i>	147.9–153.8	3.56
f.o. <i>D. pentaradiatus</i>	182.8–192.4	4.1
f.o. <i>Ceratolithus rugosus</i>	192.4–202.1	4.6
l.o. <i>C. acutus</i>	211.7–221.4	5.0
f.o. <i>Pulleniatina primalis</i>	260.0–269.7	5.8

Note: f.o. = first occurrence; l.o. = last occurrence.

E. huxleyi is not recorded in Samples 111-677A-2H, CC, and 111-677B-2H, CC, probably indicating that the NN21 *Gephyrocapsa oceanica* Zone is present. *Pseudoemiliania lacunosa* occurs in Sample 111-677A-3H-1, 75 cm, indicating the base of Zone NN20 and an age of 0.475 Ma.

Helicosphaera sellii has its highest occurrence in Cores 111-677A-6H-6, 78 cm. In Hole 677B this event occurs in Core 111-677B-7H. The extinction of *Calcidiscus macintyreii* (1.45 Ma) occurs between Samples 111-677A-7H-6, 84 cm, and 111-677A-7H-3, 45 cm. In Hole 677B *C. macintyreii* was recorded in Sample 111-677B-7H, CC.

Below the extinction level of *C. macintyreii* the nannofossil assemblages become enriched by few to common *C. pelagicus*. Bukry (1980) noted that the decrease in abundance and extinction datum of *C. pelagicus* were not uniform in the eastern Pacific. *C. pelagicus* disappeared at the northern Siqueiros sites (about 10°N lat.) earlier than at the equatorial Galapagos sites (DSDP Leg 54). *C. pelagicus* was recorded from the *Ceratolithus cristatus* Zone (= *Gephyrocapsa oceanica* Zone in the NN zonal scheme) at Hole 424. Although an isolated specimen of *C. pelagicus* was recorded in the core catcher of Sample 111-677H-3H, the species was not recorded again until Sample 111-677A-7H-3, 45 cm, just below the *C. leptoporus* extinction datum (1.45 Ma). The species also has a similar l.o. (last occurrence) datum in Site 677B where it was recorded in the core catcher of Sample 111-677B-7H. At the northern Siqueiros sites *C. pelagicus* was recorded by Bukry (1980) below the extinction datum of *G. caribbeanica* (about 1.65 Ma). Therefore the extinction datum of *C. pelagicus* in the cores from Site 677 is younger than that reported from the more northern sites in the tropical Pacific.

The position of the Pliocene/Pleistocene boundary can be calculated by assuming a constant sediment accumulation rate in the interval spanning the extinctions of *C. macintyreii* and *Discoaster brouweri*. This boundary lies within the middle of Cores 111-677A-9H and 111-677B-9H, although its exact location is complicated by the possible absence of latest Pliocene sediments (see below).

Pliocene

The final discoaster extinction (*D. brouweri*, dated at 1.89 Ma) occurs between Samples 111-677A-10H-4, 75 cm, and 111-677-10H-3, 61 cm. Backman and Shackleton (1983) have shown that the final 0.1–0.2 m.y. of the range of *D. brouweri* is characterized by a high proportion (in excess of 20%) of the tri-radiate form. The only core in which this pattern was not observed was in Site 504 where a minor hiatus was inferred to

cover most of this critical time interval. A similar scarcity of the tri-radiate form was also observed at Site 677 which suggests that a minor hiatus occurred during the period 1.9–2.1 Ma.

The dominance of *Gephyrocapsa* species decreases rapidly near the extinction level of *D. brouweri* (1.88 Ma), and below the appearance of *D. brouweri*, small reticulofenestrids dominate the placolith assemblages. The extinction of *D. pentaradiatus* (2.35 Ma) occurs between Samples 111-677A-12H-3, 95 cm, and 111-677A-12H, CC. *D. surculus* occurs in the core catcher of Core 111-677A-14H. Preservation of discoasters is poor in the late Pliocene cores, with specimens frequently broken. *D. tamilis* shows increased abundance in Core 111-677A-16X.

The next reliable nannofossil event of the Pliocene is the extinction of *R. pseudumbilica* (base of Zone NN16) at 3.56 Ma. This species has its highest occurrence in Sample 111-677A-17X, CC. In the CN zonal scheme of Bukry (1980) the extinctions of *R. pseudumbilica* and *Sphenolithus* species are considered coeval, and both designate the base of CN12a. Backman and Shackleton (1983) have shown that in tropical environments these events are separated by about 0.1 m.y. These events are separated at Site 677; sphenoliths occur without *R. pseudumbilica* in Sample 111-677A-17X-3, 70 cm. *Sphenolithus abies* and *S. neoabies* also occur consistently throughout the rest of the Pliocene.

Zones NN14 and NN15 could not be separated in Hole 677A because of the scarcity of the species *Amaurolithus tricorniculatus* which is used to define the top of the *D. asymmetricus* Zone. A similar scarcity of this form was noted in Pliocene sediments from DSDP Site 503, Leg 68 (Prell et al., 1982). The base of Zone NN14 can be placed within Core 111-677A-21X, as *D. asymmetricus* has its first appearance within the core catcher of Sample 111-677A-20X. The base of Zone NN13 is marked by the first appearance of *Ceratolithus rugosus*. This species together with *Ceratolithus acutus* was observed in Sample 111-677A-22X, CC, so an age of about 4.6 Ma may be assigned to the sample.

The first occurrence of *Ceratolithus acutus* occurs just above the Miocene/Pliocene boundary. This species has its initial occurrence in Sample 111-677A-23X, CC; the Miocene/Pliocene boundary is therefore placed within the upper part of Core 111-677A-24X.

Miocene

The top of the NN11 (*Discoaster quinqueramus* Zone) is defined as the last occurrence of the marker species, *D. quinqueramus* was recorded in Sample 111-677A-25X, CC. The NN11 Zone may be assigned to the bottom 80 m of sediment recovered from Site 677. The late Miocene discoaster assemblages contain the species *D. quinqueramus*, *D. berggrenii*, *D. stellus*, *D. intercalaris*, *D. variabilis*, *D. pentaradiatus*, and *D. brouweri*. Common placoliths include *Reticulofenestra pseudumbilica*, small reticulofenestrids, *Dictyococcocites antarcticus*, and *C. macintyreii*. *C. leptoporus* and *C. pelagicus* form a consistent but rare component. Sphenoliths are common and include *S. abies*, *S. neoabies*, and *S. metula*. *Amaurolithus primus* and *A. amplificus* also occur in the late Miocene assemblages. *Amaurolithus* species have a f.o. (first occurrence) at 7.4 Ma in the eastern equatorial Atlantic sediments cored during Leg 108 (J. Backman, 1987, pers. commun.) The presence of *A. amplificus* in Sample 111-677A-34X, CC, indicates the maximum age of the basement sediments (i.e., 7.4 Ma).

The preservation of discoasters in the late Miocene is generally poor. *D. quinqueramus* and *D. berggrenii* appear to be robust taxa; they generally occur as intact specimens. Both these taxa have sturdy well-developed central areas, which probably impart rigidity to the discoaster structure. Other species which have a larger arm/central area ratio occur mainly as fragments,

e.g., *D. pentaradiatus*, *D. brouweri*, and *D. variabilis*. Most of these discoasters are also overgrown with diagenetic calcite, making species assignment difficult.

Planktonic Foraminifers

Introduction

This report is based on an examination of core-catcher material from Samples 111-677A-1H through 111-677A-32X and 111-677B-1H through to 111-677B-10H. The planktonic foraminifer zonation is that of Jenkins and Orr (1972) developed for the eastern Pacific and subsequently used by Keigwin (1982) for sediments cored on DSDP Leg 68. Preservation of the planktonic foraminiferal tests generally varies from very good in the late Pleistocene to poor in the lower Pliocene and late Miocene. Some specimens have been filled with pyrite as in Sample 111-677A-6H, CC.

Pleistocene

Pleistocene sediments are assigned to the *Pulleniatina obliquiloculata* Zone according to the zonal scheme of Jenkins and Orr (1972) and yield well-preserved and abundant species of planktonic foraminifers including the zone fossil. Other abundant species include *Neoglobobulimina dutertrei*, *Globigerinoides ruber*, and *Globorotalia tumida*. *Globorotalia unguolata* occurs in the core catchers of Samples 111-677A-1H, 111-677A-2H, 111-677B-1H, and 111-677B-2H and is normally recorded from the Holocene. Rare specimens of dextrally coiled *N. pachyderma* were recorded in both Samples 111-677A-2H, CC, and 111-677A-3H, CC, and possible specimens in 111-677A-6H, CC. There is a significant coiling change from sinistral to dextral in the *P. obliquiloculata* populations between Samples 111-677A-3H, CC, and 111-677A-4H, CC. The Pliocene/Pleistocene boundary at Site 677 as defined by the last occurrence of *Globigerinoides fistulosus* (1.6 Ma) is found between Samples 111-677A-7H, CC, and 111-677A-8H, CC, and between Samples 111-677B-8H, CC, and 111-677B-9H, CC.

Pliocene

Late Pliocene sediments are assigned to the *Globigerinoides fistulosus* Zone. The zonal fossil ranges throughout the zone and is found in Samples 111-677A-8H, 111-677A-9H, 111-677A-12H, and 111-677A-13H, but is rare in contrast to the abundant specimens of *N. dutertrei* and *Orbulina universa*. *G. ruber* is common in some of the samples. There is a significant coiling change of *P. obliquiloculata* from dextral in 111-677A-10H, CC, to sinistral in 111-677A-9H, CC. *G. obliquis* became extinct in 111-677A-13H, CC.

Sphaeroidinella dehiscens has its first occurrence within Sample 111-677A-17X, CC, and delineates the lower boundary of the *S. dehiscens* Zone. This species has a reported first occurrence datum at 5.1 Ma (Saito et al., 1975). In Hole 677A *S. dehiscens* is first recorded from the top of the NN15 Zone near the extinction level of *R. pseudumbilica* (3.56 Ma). Therefore the first appearance of the species at Site 677 occurs very much later than previously reported. Interestingly, Keigwin (1982) recorded the first appearance of *S. dehiscens* within various levels at Sites 502 and 503 in the basal Gilbert magnetic chron. The late appearance of *S. dehiscens* at Site 677 is unlikely to be the result of dissolution effects, the species having a most solution-resistant test, a feature which first promoted its use as zonal fossil in the zonal scheme of Jenkins and Orr (1972). The zonal fossil is rare to common throughout the zone, which contains relatively high diversity faunas. Abundant species are *Neoglobobulimina humerosa* and *O. universa*. *Pulleniatina primalis* is dextrally coiled throughout the zone and *G. altispira* became extinct in Sample 111-677A-14H, CC.

The base of the *Globorotalia tumida* Zone is based on the first occurrence of the marker species. This datum is also used to locate the position of the Miocene/Pliocene boundary. The initial occurrence of *G. tumida* (5.2 Ma) is reported to be a reliable datum in the equatorial Pacific (Saito et al., 1975). This species was first recorded from Sample 111-677A-23X, CC, and is a common component of the assemblages. Abundant species include *P. primalis*, *N. humerosa*, *N. acostaensis*, and *G. menardii*. Although the preservation was reasonably good throughout, there were fewer specimens per sample in the lower part of the zone. An important change in the coiling of *G. tumida* occurs from dextral in Sample 111-677A-22X, CC, to sinistral in 111-677A-21X, CC.

Miocene

Samples 111-677A-24X, CC, to 111-677A-32X, CC, are assigned to the *Globorotalia plesiotumida* Zone. The marker species is common throughout the Zone except for Sample 111-677A-24X, CC, which only yielded three species: *G. trilobus*, *G. cf. variabilis*, and *S. semminulina*. The faunas in the zone are relatively low in species diversity and in actual numbers of specimens, and this is probably due to dissolution of the tests. Important stratigraphical markers include the first appearance of *P. primalis* in Sample 111-677A-29X, CC, and the change from sinistral to dextral in *N. acostaensis* populations in Samples 111-677A-29X, CC (sinistral), and 111-677A-28X, CC (dextral).

The age of the older samples in the *G. plesiotumida* Zone is not known but they are older than 5.8 Ma, the age of Sample 111-677A-29X marked by the first evolutionary appearance of *P. primalis*.

Benthic Foraminifers

At Site 677, benthic foraminifers occur throughout the samples, and genera recorded include *Dentalina*, *Gyroldina*, *Cibicides*, *Cassidulina*, *Uvigerina*, and various miliolids.

Radiolarians

Samples from Hole 677A core catchers 111-677A-1H to 111-677A-33X were examined for 65 radiolarian species (see "Introduction and Explanatory Notes" chapter, this volume). The samples yielded extremely well preserved, high diversity radiolarian assemblages with one exception. Sample 111-677A-33X, CC (308.4 mbsf), found below the cherty limestone lithologic Subunit IIIA (303.3–303.6 mbsf) was devoid of radiolarians except for a few robust eucitonid and spongodiscid spumellarians.

The zones of Riedel and Sanfilippo (1978) are noted on Hole 677A barrel sheets. Use of this zonation however, does not present an accurate age model for the sediments of Hole 677A. The late Miocene to Recent radiolarian zonal boundaries of Riedel and Sanfilippo (1978) are based mainly on evolutionary limits. Since evolutionary limits must be based on quantitative species counts and morphologic measurements, they were not determined in this preliminary study. All events are based on recognized morphotypic limits (however evolutionary intermediate forms were noted).

Radiolarian event stratigraphy (both morphotypic and evolutionary) should prove to be an excellent method for dating the sediments of Hole 677A. With 65 species searched for in the samples, at least 16 reliable and previously dated events have been located (Table 3). Ten additional datums have been determined at this site, but have no ages assigned to them. The radiolarian species events occurring in Hole 677A are discussed below.

Zonal Assignments

The first appearance of *Lamprocyrtis nigrinae*, (*L. haysi*), occurred in 111-677A-5H, CC. In this sample and above it *L. nigrinae* is consistently present. The *L. haysi* zone as defined is

Table 3. Radiolarian species events, their stratigraphic placement (depth in Hole 677A), and their assigned age estimates.

Datum	Depth (mbsf)	Age (m.y.b.p.)	Ref.
l.o. <i>Stylatractus universus</i>	6.2–15.7	0.41–±0.005	1
l.o. <i>Theocorythium vetulum</i>	44.2–53.7	1.1–1.2	3
f.o. <i>T. trachelium</i>	63.2–72.7	1.5–1.6	3
l.o. <i>Pterocanium prismatium</i>	63.2–72.7	1.5–1.6	3
f.o. <i>T. davisiana</i>	101.2–110.7	2.63	2
l.o. <i>Stichocorys peregrina</i>	110.7–120.2	2.77	2
f.o. <i>Lamprocyrtis neoheteroporus</i>	129.7–139.2	3.19	2
f.o. <i>Botryostrobus</i> sp.	139.2–144.2	3.28	2
l.o. <i>Phormostichoartus doliolus</i>	153.8–163.5	3.57	2
f.o. <i>Spongaster tetras</i>	163.5–173.2	3.67	2
f.o. <i>Amphirhopalum ypsilon</i>	163.5–173.2	3.6–3.7	3
f.o. <i>P. prismatium</i>	173.2–182.8	4.2–4.3	3
l.o. <i>Didymocyrtis penultima</i>	182.8–192.4	3.71	2
l.o. <i>Solenosphaera omnitubus</i>	202.1–211.7	4.7–4.8	3
l.o. <i>Siphostichoartus corona</i>	240.8–250.4	4.9–5.0	3
l.o. <i>Eucyrtidium</i> sp. cf. <i>E. diaphanes</i>	279.3–288.9	5.9–6.0	3

Note: f.o. = first occurrence; l.o. = last occurrence. Ref. = Ages are from the following references: 1, Hays and Shackleton (1976); 2, J.M. Alexandrovich (unpubl. data); 3, Johnson and Nigrini (1985).

well constrained in Hole 677A. The base of the *Pterocanium prismatium* zone is defined by the morphotypic last appearance of *S. peregrina*. This event is clearly delineated (in 111-677A-13H, CC) since when present *S. peregrina* is common in the radiolarian assemblages. Since the top of the *P. prismatium* zone is defined by the base of the *L. haysi* zone, the *P. prismatium* zone is also well constrained. The *Spongaster pentas* zone is defined by the base of the *P. prismatium* zone and the evolutionary bottom of *S. pentas*. The top of this zone is easily recognized in Hole 677A, but the bottom is very uncertain. *S. pentas* is extremely rare in these sediments (*S. tetras* however, is not). The last zone recognized in the sediments of Hole 677A is the *Stichocorys peregrina* zone. The bottom, based on the evolutionary bottom of *S. peregrina* could not be located, although several morphologically defined *S. delmontensis* have been found in Samples 111-677A-32X, CC, through 111-677A-28X, CC. The top of the *S. peregrina* zone defined by the evolutionary bottom of *S. pentas* is poorly constrained.

Quaternary

Four dated radiolarian events occur in the Quaternary (*S. universus* through *P. prismatium*, Table 3). Six additional undated events have been defined with certainty. These are the f.o. and l.o. of *A. anthropiscus* (Samples 111-677A-9H, CC, and 111-677A-4H, CC, respectively), the f.o. of *P. minithorax* (111-677A-5H, CC), the l.o. of *L. neoheteroporus* (111-677A-4H, CC), the f.o. of *L. nigrinae* (111-677A-5H, CC), and the l.o. (probably a local l.o.) of *L. bacca* (111-677A-7H, CC). The ranges of *C. invaginata* and *C. tuberosa* could not be defined with confidence due to the resolution of the sampling interval. Only one specimen of *A. angulare* was observed (111-677A-1H, CC). Other Quaternary indicators (see Goll, 1980) could not be used as datums in Hole 677A due to either low abundances, inconsistent ranges, or identification problems. *T. hertwiggi* was not found.

Pliocene

Ten dated radiolarian events occur consistently in the Pliocene interval of Hole 677A (f.o. *T. davisiana* through l.o. *S. omnitubus*, Table 3). Another consistent datum found in this interval is the l.o. of *D. avita* (111-677A-10H, CC) but it has not been dated. The l.o. of *B. bramlettei*, the f.o. of *S. tetras*, and the l.o. of *S. ambus* could not be confidently located. The l.o.

of *L. audax* (111-677A-29X, CC) does not appear in this interval as would be predicted by the data of Johnson and Nigrini (1985). *L. heteroporus* was not found in any sample.

Miocene

Two reliable and dated radiolarian datums were found in the Miocene interval of Hole 677A (*S. corona* and *E. sp. cf. E. diaphanes*, Table 3). The morphotypic l.o. of *D. antepenultima* was found in Sample 111-677A-28X, CC. One specimen of *A. tritubus* was observed in Sample 111-677A-31X, CC. *C. thermophila* was not encountered, but a similar form, tentatively identified as *Botryopyle dictyocephalus* has a consistent occurrence in 111-677A-30X, 111-677A-31X, and 111-677A-32X, CC, and one specimen encountered in the Pliocene interval in 111-677A-18X, CC. One specimen of *D. ontongensis* was found in 111-677A-29X, CC. *S. omnitubus* is consistently present in the lowest sample with good radiolarian preservation (111-677A-32X, CC) which indicates that this sample must be younger than 6.4 Ma (Johnson and Nigrini, 1985), and older than 6.0 Ma (the l.o. of *E. sp. cf. diaphanes*, Johnson and Nigrini, 1985).

Other Microfossils

Fish teeth are present in Samples 111-677A-22X, CC, 111-677A-23X, CC, 111-677A-31X, CC, 111-677B-7H, CC, and 111-677B-8H, CC. Possible echinoid spines occur in Samples 111-677A-25X, CC, and 111-677A-26X, CC.

Sediment-Accumulation Rate

The sediment-accumulation rates at Site 677 were established using 29 chronostratigraphic events (Tables 2 and 3). Unfortunately no magnetic datums are included here because of problems with the cryogenic magnetometer during Leg 111. The resultant curve (Fig. 4) suggests a high fairly continuous rate of deposition from the late Miocene to the Pleistocene with no major hiatus discernible, although nannofossil evidence suggests a minor hiatus around 1.9–2.1 Ma. The established sedimentation (mean 48 m/m.y.) appears to show little variation down to the last datum at 5.95 Ma (l.o. *E. cf. diaphanes*). There are no reliable datums within the last 40 m of sediment, although the presence of *S. omnitubus* (f.o. 6.45 Ma, Johnson and Nigrini, 1985) indicates that the core-catcher material of Sample 111-677A-32X is younger than 6.45 Ma. No radiolarians occur below the core catcher of Sample 111-677A-32X, but the presence of *Amaurolithus* spp. in the basement sediments gives a maximum age of 7.4 Ma (J. Backman, 1987, pers. commun.). Tropical sediments from the eastern Atlantic cored during Leg 108, have a similarly high sedimentation rate down to this datum (7.4 Ma); therefore it is not unreasonable to assume that the high sedimentation rates continue down to the basement sediment at Site 677.

SITE 678

Introduction

Two holes were drilled at Site 678 in a water depth of 3425 m; Hole 678A to a depth of 0.6 m; Hole 678B to a sub-bottom depth of 171.8 m. Hole 678B was only cored at specific stratigraphic intervals (0–7.5, 18.2–27.7, 95.5–105.0, and 169.5–171.8 mbsf). Core 111-678B-4W represents a washed interval between 105 and 169.5 mbsf. The sediments recovered from Site 678 consist of calcareous siliceous ooze, siliceous nannofossil chalk, and limestone.

The sediments cored at Site 678 range in age from late Miocene to late Pleistocene. Figure 5 shows the age and zonal assignments of the cores recovered. Calcareous nannofossils occur in all cores although they are rare in Core 111-678B-5X.

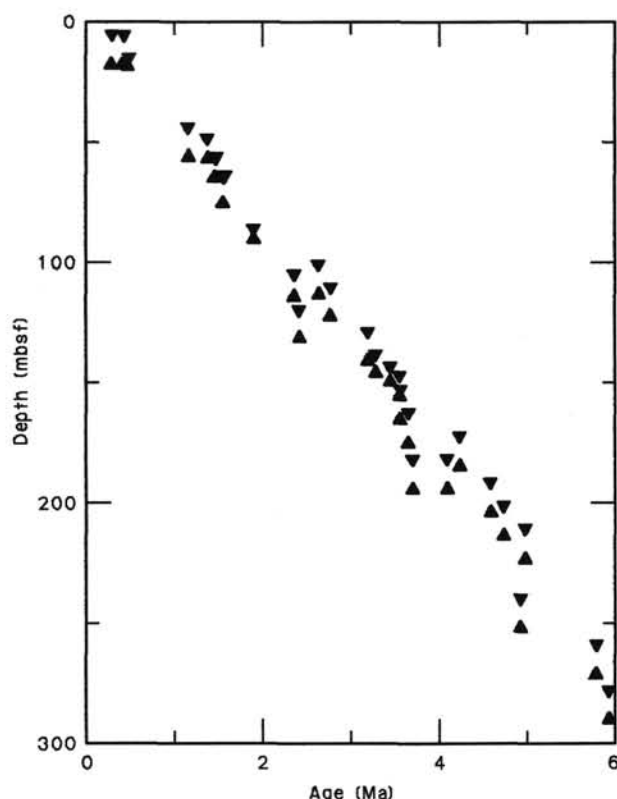


Figure 4. Graphic representation of sediment age in Hole 677A. Downward-pointing triangles mark top and upward-pointing triangles mark bottom of chronostratigraphic events used to establish rate of deposition.

Pleistocene

Sample 111-678A-1H, CC, may be placed within the latest Pleistocene Zone NN21: rare specimens of the marker species *Emiliania huxleyi* were recorded by SEM from this sample. *Gephyrocapsa* spp. dominate the assemblage, and *Calcidiscus leptoporus* is the only other species to form > 1%. Other species include *Pontosphaera japonica*, *H. carteri*, *H. inversa*, *C. telesmus*, and *C. simplex*. Reworked specimens of *H. sellii* also occur. Calcareous nannofossils are common in the sample; preservation is moderate to poor. The low abundance of *E. huxleyi* and the dominance of *Gephyrocapsa* spp. in the near-surface sediments is similar to that recorded from Site 677. Once again preservation of the nannofossils is poor in the late Pleistocene, with evidence of moderate to strong dissolution of placolith crystal sutures.

Sample 111-678B-2H contains *Pseudoemiliania lacunosa*: therefore, the core may be placed within Zone NN19. *Gephyrocapsa* spp. dominate the assemblage. Other species recorded include *P. multipora*, *H. inversa*, *H. neogranulata*, and a diverse ceratolith assemblage (*C. cristatus*, *C. simplex*, *C. rugosus*, and *C. telesmus*). The presence of *H. inversa* indicates that the sample is above the extinction datum of *Helicosphaera sellii* (Gartner, 1977). The sample, therefore, has a maximum age of 1.37 Ma. The top of the NN19 Zone is placed at 0.475 Ma.

Pliocene

The occurrence of *D. brouweri* in the core catcher of Core 111-678B-3H places the core within the late Pliocene Zone NN18 (top 1.89 Ma, base 2.35 Ma). *D. triradiatus* and *D. intercalaris* are the only other discoasters present. Small reticulofenestrids and *P. lacunosa* dominate the assemblage. Other species include

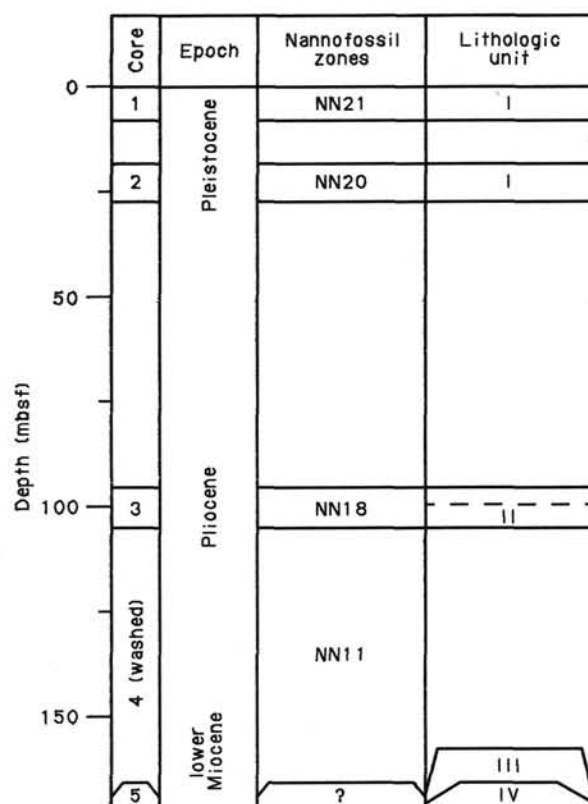


Figure 5. Zonal assignments, epoch boundaries, and lithostratigraphy within cores and sub-bottom depth in Hole 678B.

C. leptoporus, *C. macintyreii*, *H. sellii*, *H. carteri*, and *Ceratolithus rugosus*. Nannofossil preservation is moderate in the sample. Specimens of reworked discoasters include *D. quinquaramus*, *D. surculus*, and *D. challengerii*.

Miocene

The occurrence of *D. quinquaramus* in the core catcher of Core 111-678B-4W places the core within the latest Miocene Zone NN11 (top 5.0–5.6 Ma). *Amaurolithus amplificus* and *A. primus* are also present. The f.o. datum of *A. amplificus* species in the equatorial Atlantic is about 7.4 Ma (J. Backman 1987, pers. commun.). The nannofossil assemblages are dominated by *R. pseudumbilica*. Other common placoliths include small reticulofenestrids and *Dictyococcites antarcticus*. Rare placoliths of *C. macintyreii*, *C. leptoporus*, and *C. pelagicus* are also present.

The discoaster assemblages are dominated by *D. quinquaramus* and *D. berggrenii*. Intermediate forms between these two species were also reported. Other forms include *D. brouweri*, *D. stellus*, *D. variabilis*, and *D. pentaradiatus*.

Nannofossil preservation in the core-catcher sample is very poor. Both placoliths, particularly *R. pseudumbilica* and discoaster, are extensively overgrown. Most of the discoasters are irregularly thickened by extensive overgrowth making species identification difficult. The late Miocene age of Core 111-678B-4W suggests that the sediment was cored from the bottom of the washed interval (105–169.5 m).

A sparse low-diversity nannofossil flora comprising large placoliths was recorded from Core 111-678B-5X. Occasional specimens of *C. macintyreii*, *R. pseudumbilica*, *C. leptoporus*, and *D. antarcticus* occur in the sediments. Most of the coccoliths show extensive overgrowth. Very rare broken arms of discoasters also occur.

SEDIMENT PORE-WATER CHEMISTRY

Introduction

One of the major objectives of drilling at Sites 677 and 678 was to characterize further the hydrothermal processes occurring within the sediments and basement in the vicinity of DSDP Site 504. The presence of such processes in this area had originally been indicated by heat-flow data collected on the 504 Site Survey (Langseth et al., 1983). Five holes drilled at Sites 501/504 on DSDP Leg 69 revealed large lateral as well as vertical gradients in sediment pore-water chemistry. These were attributed by Mottl et al. (1983) to hydrothermal circulation and basalt-seawater interaction in basement, accompanied by vertical and lateral propagation of the basement alteration signal through the sediment column by diffusion and possibly also advection. The relationship between heat flow and sediment pore-water chemistry in this area was further investigated by M. Langseth, M. Hobart, and M. Mottl on cruises 23-5 of the *Robert Conrad* in 1982 and 198 of the *Thomas G. Thompson* in 1986. A strong correlation was found between lateral variations in heat flow and sediment pore-water chemistry within the upper 17 m of the sediments, that part which was accessible using piston coring and "pogo" heat-flow measurements on the two cruises. These correlations have been used to locate Sites 677 and 678, in zones of low and high heat flow, respectively.

Including the site survey, nearly 300 heat-flow measurements and 25 piston cores have now been collected from a 100 km² area surrounding Site 504, most of them on cruise 198 using precision bottom-mounted transponder navigation. The resulting map shows broad and regular undulations in heat flow that strike east-west parallel to seafloor topography and the Costa Rica Rift spreading axis to the north (Langseth et al., this volume). The wavelength of the variation is about 8 km and the amplitude is 15% on either side of the mean heat flow for the area of 216 mW/m². These broad heat-flow variations are believed to result from hydrothermal circulation in basement.

Within the east-west bands of high heat flow are several more restricted areas where the heat flow exceeds 250 to 350 mW/m², to a measured maximum of 391. Within these restricted areas, extremely large lateral and vertical gradients in pore water chemistry were measureable in the piston cores. In one area 2.4 km east of Hole 504B, for example, Mg²⁺ was found to decrease from 52 to 4 mmol/kg within the upper 7 m of sediment in three cores, while one core taken only 200 m south of these showed no decrease in Mg²⁺ over its length of 7 m. The steepness of the vertical chemical gradients correlates well with the measured heat flow. This correlation and the size of the lateral gradients strongly suggest that the localized thermal and chemical anomalies are maintained by slow upward seepage of warm, altered seawater through the sediment column beneath these restricted areas. The convex-upward curvature of the pore-water chemical profiles suggests flow velocities of a few millimeters/year. This rate is sufficiently slow to be consistent with the linear temperature gradients measured in the shallow sediments.

Prior to drilling at Sites 677 and 678, the localized areas of high heat flow were believed to be of two types. Two examples of the first type lie 600 m south-southeast and 2.5 km east of Hole 504B, respectively, and were investigated in detail on cruise 198. They are narrow, only 500 m from north to south, and vary in length from 500 m to 3 km. They lie in an area of generally thick sediment, greater than 250 m from seismic reflection data. The second type occurs 6 km southwest of Hole 504B. It is larger, as wide as 2 km from north to south and at least 5 km from east to west, and occurs in an area of generally thinner sediment, less than 200–250 m.

Site 678 was located in one of the areas of the first type, 1360 m southeast of Hole 504B and 50 m southwest of a 198 heat-flow station of 307 mW/m². The two holes were located

near the crest of a small hill which rises 20–30 m above the surrounding seafloor, near the center of a 4-km wide trough which runs east-west through the area. Two 198 piston cores were collected nearby, one 200 m to the east and the other 100 m to the west. Both showed very large, convex-upward vertical gradients in sediment pore-water composition.

Site 677, in contrast, was located near the center of the band of low heat flow which lies to the south of Hole 504B. The holes were drilled 100 m southwest of the lowest heat-flow measurement made anywhere in the 100-km² area, 166 mW/m². The site is located on the southern edge of the topographic trough mentioned above, 2.8 km south-southwest of Hole 504B and 2.3 km southwest of Site 678. Based on seismic reflection data, it lies in an area of sediment thickness in excess of 250 m.

A major surprise of the drilling was that the depth to basement differed from that predicted from seismic reflection records for both sites. Basement was not encountered until 309 m depth at Site 677, while it was hit much shallower than expected at Site 678, at only 170 m. That this is basement was confirmed by recovery of basalt, coupled with a biostratigraphic age for the basal sediments of 5.8–6.4 m.y. (see discussion at "Biostratigraphy" section, this chapter). It appears that Site 678 is located in an area with sediment generally in excess of 250 m, but that the localized area of high heat flow which was targeted overlies a narrow basement peak or ridge.

The major objectives at Sites 677 and 678 with regard to pore-water chemistry were (1) to test further the hypothesis that warm, altered seawater is seeping upward from basement through the sediments at rates of a few millimeters/year in a localized area at Site 678, (2) to determine whether the low heat-flow areas such as that surrounding Site 677 represent the complementary downflow zones, and (3) to determine whether the composition of formation water in the shallow basement, as reflected in the composition of the basal sediment pore water, varies laterally across the larger area, from the low- to the high-heat-flow regions.

Procedures

Sediment pore-water samples were obtained both by squeezing and, in Hole 677A only, with the Barnes *in-situ* sampler. Details of these procedures are provided in the "Introduction and Explanatory Notes" chapter of this volume. Sediments were squeezed at as close to *in-situ* temperatures as possible (see Table 5), using the temperature gradients measured on cruise 198 as a guide. No attempt was made to squeeze at higher than room temperature, however.

All samples were filtered through 0.22- μ m Millipore cellulose acetate filters and analyzed in the shipboard laboratory for pH, alkalinity, chlorinity, Ca²⁺, Mg²⁺, SO₄²⁻, Si, NH₄⁺, PO₄³⁻, and NO₃⁻ following the methods detailed in the shipboard manual written by Gieskes and Peretsman (1986). These methods are summarized in Table 4.

Table 4. Analytical methods used for pore-water analysis.

Species	Method
pH	pH electrode.
Alkalinity	Potentiometric titration with 0.1N HCl.
Chlorinity	Mohr titration with silver nitrate.
Ca ²⁺	Compleximetric titration with EDTA.
Mg ²⁺	Calculated after titration with EDTA for total alkaline earths (Ca + Mg + Sr).
Si	Colorimetry with molybdate blue (812 nm).
Ammonium	Colorimetry by phenol-hypochlorite method (640 nm).
Phosphate	Colorimetry with molybdate (885 nm).
Nitrate	Catalytic reduction to nitrite followed by colorimetry using sulfanilamide (543 nm).

Results and Discussion

Results are presented in Table 5.

Ca^{2+} and Mg^{2+}

The concentrations of Ca^{2+} and Mg^{2+} are plotted vs. depth in Figure 6. These two elements are known to change dramatically during reaction of seawater with basalt at elevated temperatures, as Mg^{2+} is taken up in secondary alteration minerals in exchange for Ca^{2+} leached from the rock. The correlation between Ca^{2+} enrichment and $\delta^{18}\text{O}$ depletion in sediment pore waters from Site 504 led Mottl et al. (1983) to conclude that Ca^{2+} enrichment in these waters results largely from basalt-seawater reaction in basement.

The depth profiles in Figure 6 show a marked contrast between the low- and high-heat-flow sites. Holes 677A and 677B, drilled with a nominal zero-offset from each other, both show concentrations of Ca^{2+} and Mg^{2+} nearly identical to that in bottom seawater to a depth of 110 m. Below that Ca^{2+} increases and Mg^{2+} decreases by about 10 mmol/kg over a 70-m interval, after which the slope decreases greatly until 14 m above basement, when it again increases drastically. Most of the change to the measured extremes of 69 mmol/kg Ca^{2+} and 10 mmol/kg Mg^{2+} occurs over the last 7 m above basement.

In contrast, Hole 678B, in the high-heat-flow area, shows a rapid increase in Ca^{2+} with depth to 36 mmol/kg at 7 m and 45 mmol/kg at 19 m, accompanied by a complementary decrease in Mg^{2+} . These gradients are very similar to those in the two 198 piston cores taken within 200 m of Hole 678B, indicating that we hit our target exactly. The concentrations near the surprisingly shallow basement are difficult to determine due to the large scatter of the lowermost six samples. These all came from the core catcher and were taken after the core had been split. Note that four of the six came from a wash core; they have been assigned to the lower extreme of the washed interval because penetration of the XCB was stopped there by a much harder layer, which these samples are believed to represent. The samples include chalk, limestone, and clay containing basalt fragments. Because of their hardness and small size, five of the six yielded only 1–7 mL of pore water each (Table 5). From their scattered chlorinities, these samples suffered both evaporation and contamination with fresh water during handling of the core catcher on deck. The marine technicians have confirmed that this is highly likely. In any case, the data for these few samples have been corrected in the various figures to a chlorinity of 550 mmol/kg, so that the scatter cannot be due to these factors alone. Some seawater contamination may have occurred during recovery, but the low alkalinity of sample IW16 limits this to a small amount, at least for this one larger sample.

The depth profiles for Ca^{2+} and Mg^{2+} at Sites 677 and 678 bracket those in Holes 501, 504, 504A, and 504C shown by Mottl et al. (1983). The profiles from the low-heat-flow Site 677 show the same S-shaped curve as the Site 504 holes, but to a lesser degree, while the convex-upward profile at Site 678 is similar to that in Hole 501, but to a greater degree. The other major difference is that no samples were available from the lower 12 m of the sediments at Sites 501/504, and only three from three different holes from the lower 27 m above basement. Large gradients in the basal sediments thus would not have been detectable in the data set from Sites 501/504.

The contrast in the depth profiles from Sites 677 and 678, and their correlation with heat flow, would seem to offer substantial proof of the hypothesis that water is seeping through the sediments, downward at Site 677 and upward at Site 678. Except for a slight gradient from 110 to 180 m depth and an altered composition from that of seawater from 180 to 290 m, the profile from Site 677 is a classic concave-upward convective pro-

file indicating downward flow. The deviations from an ideal flow profile may be due to reactions in the sediments which are rapid relative to a very slow rate of seepage. The major diagenetic boundary in this hole, that between ooze and chalk, is gradational and occurs between 157 and 192 m. Thin beds of cherty limestone occur sporadically only in the lower 6 m above basement. Whether the steep gradient near basement can be attributed in whole or in part to a lower diffusion coefficient in the altered basal sediments can only be determined after formation factor data become available.

The profile from Site 678 is likewise a typical convective profile, this time convex-upward indicating upward flow, except for the possible complications very near basement. Whether these are real or an artifact is indeterminate at present. The diagenetic boundaries at Site 678 were not sampled, as the site was spot-cored, but chalk was first sampled at 96 m and limestone free of chert at 169 m, only 1 m above basement. If these are convective profiles, then the similar distances over which most of the gradient occurs near the upper and lower boundaries of the sediment column indicate that the upward and downward flow rates are of comparable magnitude, on the order of a few millimeters/year (Langseth et al., this volume).

As to whether the shallow basement formation water varies laterally from the low- to the high-heat-flow localities, this seems unlikely in light of the present data. We cannot demonstrate that the basal sediment pore waters are identical in the two areas, but they certainly are not very different. If they are in fact the same, it would mean that the hydrothermal circulation in basement postulated to explain the broader heat-flow variations would occur largely as a closed system chemically. The inputs and outputs of unaltered and altered seawater, respectively, flowing through the sediment column would be negligible compared with the rate of convective overturn in basement.

Alkalinity and Ammonium

Figure 7 shows the depth profiles for alkalinity and ammonium. These two species show similar profiles at the low-heat-flow Site 677, increasing to a constant value at mid-depth in the sediments and then decreasing again toward basement. As with Ca^{2+} and Mg^{2+} , the gradients steepen greatly within the lower 7 m. Increases in alkalinity and ammonium in sediment pore waters are commonly attributed to reduction of seawater sulfate by bacteria utilizing organic matter.

The depth profile for the high-heat-flow Site 678 again contrasts greatly with that for 677. Alkalinity drops by 80% within the upper 7 m and then remains low to basement. Ammonium increases to high values within the upper 25 m, then decreases after an unsampled interval, and finally becomes highly scattered near basement. As with Ca^{2+} and Mg^{2+} , the values near basement are comparable at the two sites.

Si and Chlorinity

Figure 8 shows the depth profiles for Si and chlorinity. For Si, the profiles are similar for the two sites, showing an increase with depth which is sharply reversed a short distance above basement. A similar reversal occurs at Sites 501/504 over a larger distance (about 30 m) within the basal sediments, where they are recrystallized to chert and cherty limestone. Neither chert nor cherty limestone was found at Site 678, and cherty limestone was sampled only within the lower 6 m above basement at Site 678. As noted by Mottl et al. (1983), the pore waters are greatly supersaturated with quartz over most of the sediment section, but become just saturated with quartz where the chert appears and below.

Chlorinity increases with depth over the upper 40 m at Site 677, from the bottom seawater concentration to a constant value of about 550 mmol/kg. The profile for Site 678 is less clear be-

cause of the intermittent sampling. The scatter near basement in the core catcher samples has already been discussed in the section on Ca^{2+} and Mg^{2+} . The profile at Site 677 differs from that at Sites 501/504, where a maximum is reached at about 100 m depth followed by a decrease to greater depths. What these profiles imply for the convective hypothesis is not clear at present. They seem to be consistent with upward convection at Site 678, but they may not be with downward convection at Site 677, unless the chlorinity increase is due to uptake of water by the shallow sediments, or to penetration of bottom seawater of gradually lowered salinity following the last glaciation.

Phosphate and Nitrate

Phosphate increases from the bottom seawater concentration in the shallow sediments, reaching a maximum in the upper 10 m (Fig. 9). It then decreases with depth to low values. This decrease occurs much more rapidly with depth at Site 678 than it does at Site 677. The nitrate data apparently are seriously affected by contamination, in spite of the use of Whatman 1 filter papers in the squeezer which had been pre-rinsed with distilled water and dried.

Summary and Conclusions

The profiles of sediment pore-water composition vs. depth differ greatly between Sites 677 and 678, which have low and high heat flow, respectively. Profiles for Ca^{2+} and Mg^{2+} are concave upward at Site 677 and convex-upward at Site 678. Alkalinity also is convex upward at Site 678. These differences are consistent with the hypothesis that water is flowing through the sediments at velocities of a few millimeters/year, downward at Site 677 and upward at Site 678. Profiles for ammonium, Si, and phosphate are dominated by reactions in the sediments. All of these species except phosphate show large gradients near basement at Site 677 and near the seafloor at Site 678, again consistent with the convection hypothesis. Chlorinity is constant with depth except for an increase in the upper 40 m of the sediments. More detailed modeling will be required to confirm the convection hypothesis, especially for downward flow at Site 677. The data suggest that the composition of formation water in the shallow basement does not vary much laterally between sites of high and low heat flow in this area.

PALEOMAGNETICS

Introduction

ODP Site 677 is located in an area of low heat flow approximately 3 km south of Site 504B. During Leg 111 two adjacent holes, Holes 677A and 677B, were cored in order to (1) characterize the geochemical and hydrogeological signals associated with regions of low heat flow and (2) provide a biostratigraphic and paleoceanographic record for this region. Paleomagnetic studies were conducted in order to determine the reversal stratigraphy through the cored section.

Experimental Methods

Remanent magnetization measurements were made on minicube samples taken at intervals of 1.5 m from the recovered drill core. As these are equatorial sediments and should have little or no vertical component of magnetization, accurate declination values are required in order to determine magnetic polarity. Using the Eastman Whipstock Multishot system, azimuthal orientation was attempted on the upper 15 cores of Hole 677A, and measurements of remanent magnetization were thus restricted to these cores. All samples were measured for natural remanent magnetization (NRM) intensity and direction using a MOLSPIN Portable Rock Magnetometer. Demagnetization was performed with a Schonstedt single-axis demagnetization unit (GSD-1) in

steps of 50, 100, 200, and 300 Oe on samples from successfully oriented cores (Cores 677A-2H, 677A-3H, 677A-6H, 677A-9H, 677A-10H, 677A-14H, and 677A-15H). The results of these measurements are displayed in Table 6.

Magnetic susceptibility was measured on cores from Hole 677A using a Bartington Susceptibility Meter (Model MS1). This device uses a loop-type sensor that allows whole cores to be passed through in chosen intervals (10 cm in this case). Prior to measurements, cores were cleaned thoroughly to reduce contamination.

Results

Intensity of Remanent Magnetization (J_0)

The intensity of natural remanent magnetization (J_0) is plotted vs. depth in Figure 10. Nearly all of the samples fall in the range of 10^{-7} emu/cm³ and thus agree with values observed from nearby Site 503 (Kent and Spariosu, 1983). Although J_0 values in the range of 10^{-7} would normally be measured with a more sensitive magnetometer, problems with the shipboard cryogenic magnetometer required that we attempt to use the spinner magnetometer for this study. The noise values of the MOLSPIN magnetometer are displayed in Table 7 and show that the majority of samples have intensities which are roughly an order of magnitude stronger than typical noise levels of intensity. Although the weaker samples obviously will have very large errors, the bulk of the J_0 values should be valid.

On the basis of J_0 values, the upper 150 m of 677A can be divided into the following four zones: Zone Ia which has low J_0 and extends from 0 to 11 m, Zone Ib which has a steadily decreasing J_0 and extends from 11 to 63 m, Zone Ic which has a high mean value of J_0 and extends from 63 to 90 m, and Zone Id which has a low mean value of J_0 and extends from 90 to 140 m. These zones agree well with the stratigraphic subunits of Unit I defined in "Sedimentology and Lithostratigraphy" section, this chapter. The low J_0 values from 0 to 11 m are most likely due to the high water content of this zone (see "Physical Properties" section, this chapter) which effectively decreases the abundance of minerals contributing to the magnetic signal (e.g., magnetite or maghemite).

The variation in J_0 below this can be correlated with fluctuations in carbonate content (see "Physical Properties" section, this chapter). High carbonate contents are associated with low J_0 values and suggest that increasing carbonate effectively dilutes the concentration of magnetic minerals.

Magnetic Susceptibility (X_0)

Values of X_0 are plotted vs. depth in Figures 11 and 12; breaks in the record represent cores that were (1) split before X_0 could be measured, or (2) only partially recovered during use of the extended core barrel (XCB). The large gap between 185 and 250 mbsf was only spot-measured due to a very low, and unchanging value of mean X_0 . Near the bottom of the section, 280 mbsf, detailed measurements resumed as there was a distinct increase in the range and average value of X_0 .

X_0 has a mean value of 5 $\mu\text{G}/\text{Oe}$ to a depth of about 90 mbsf. Below this, there is a slight, but distinct drop to a mean value of 2.5 $\mu\text{G}/\text{Oe}$. This decrease in X_0 is coincident with the decrease in J_0 and most likely represents a change in the abundance of magnetite or maghemite. Between the top of the section and 180 mbsf, values greater than 10 $\mu\text{G}/\text{Oe}$ are nearly always restricted to the top 15 cm of each core and are probably due to a small amount of rust contamination by the core barrel during initial penetration into the section. As these contaminated zones are extremely localized and easily identified, they do not appear to be a serious problem to the magnetic record. Near the bottom of the section, 270–290 mbsf, there is a sharp rise in the amount of scatter in X_0 values. This change is due to

Sample no. Method ^a	Depth (mbsf)	Core ^b		Interval (cm)	Vol. water (ml)	Squeeze temperature (°C)	pH	Chlorinity ^c mmol/kg titration	Alkalinity meq/kg titration	Ca ²⁺ mmol/kg titration (correction) ^d	Mg ²⁺ mmol/kg titration (correction) ^d	NH ₄ ⁺ μmol/kg colorimetry	Si μmol/kg colorimetry	PO ₄ μmol/kg colorimetry	NO ₃ + NO ₂ μmol/kg colorimetry		
Surface seawater (9 Oct. 86)								519.2		9.67	49.88						
Hole 677A:																	
IW1	4.5	1H	3	145-150	102	3.8	7.34	542.6	2.93	10.12	51.88	116	646	1.04	12.0		
IW2	7.0	2H	1	80-89	48	3.8	7.91	541.6	3.49	9.71	53.31	198	781	2.63	3.7		
IW3	21.4	3H	4	120-125	95	3.6	7.45	545.4	3.89	9.47	53.36	285	693	0.64	2.6		
IW4	25.8	4H	1	55-74	34	5.4	7.76	547.3	4.28	9.42	52.93	274	868	3.53	3.2		
IW5	35.3	5H	1	51-69	35	10.1	7.64	548.7	4.35	9.54	53.05	291	1014	3.23	6.1		
IW6	48.4	6H	3	120-125	88	9.4	7.45	553.8	4.21	9.62	53.60	324	847	2.24	1.2		
IW7	76.9	9H	3	120-125	93	15.0	7.69	557.6	5.79	10.34	53.43	413	1095	2.34	<0.1		
IW8	106.9	12H	4	120-125	101	19.0	7.17	556.2	3.98	10.08	53.54	424	1236	0.44	3.2		
IW9	116.7	13H	4	145-150	99	21.2	7.60	555.7	4.99	10.51	52.79	436	1379	0.84	2.8		
IW10	126.2	14H	4	145-150	102	22.7	7.87	548.2	4.93	11.77	51.14	504	1412	0.44	1.6		
IW11	135.4	15H	4	120-125	93	22.6	7.69	550.1	4.92	13.78	50.09	463	1466	0.74	2.1		
IW12	145.2	16X	4	145-150	45	25.0	7.18	550.1	4.51	14.63	48.42	452	1296	1.94	9.5		
IW13	148.7	17X	3	145-150	47	21.2	7.26	546.3	4.60	16.01	47.32	476	1471				
IW14	158.0	18X	3	120-125	89	21.4	7.30	542.6	4.84	16.65	46.55	437	1388	0.34	2.0		
BW15	163.6	B			20		7.35	544.4	6.14	18.83	44.82	419	1815	1.84	1.5		
15ov, ^c					1168			499.3		18.71	45.15		1739				
IW16	169.5	19X	4	145-150	84	20.9	7.21	545.4	3.99	17.74	45.12	395	1417	0.84	1.9		
IW17	179.2	20X	4	145-150	81	21.9	17.18	549.1	5.15	19.23	43.70	417	1649	0.44	2.2		
IW18	196.6	22X	3	120-125	67	22.6	7.37	545.4	4.88	19.36	43.22	432	1658	0.34	5.5		
IW19	208.1	23X	4	145-150	57	22.6	7.60	546.3	4.46	19.92	42.15	440	1761	0.54	2.0		
BW20	211.8	B			18		8.10	541.6	4.69	19.04	44.69	436	2015				
20ov, ^c					760			478.6		19.58	43.88		2163				
IW21	217.7	24X	4	145-150	91	22.4	7.45	547.4	4.88	19.72	42.62	437	1699	4.63	2.1		
IW22	227.1	25X	4	120-125	68	21.4	7.37	552.1	2.74	19.62	42.72	405	1629	1.04	5.0		
IW23	237.1	26X	4	145-150	67	23.3	7.25	553.1	4.46	20.95	41.55</						

Hole 677B:

IW1	1.0	1H	1	95-100	98	1.8	7.89	540.7	2.88	9.92	51.11	17	544	5.62	1.5
IW2	3.0	1H	2	145-150	88	1.7	8.18	538.8	3.08	9.86	51.09	80	640	5.12	2.9
IW3	9.1	2H	1	145-150	95	3.9	7.82	538.8	3.58	9.85	51.34	174	702	7.91	0.6
IW4	12.1	2H	3	145-150	88	3.7	7.70	539.7	3.45	9.41	51.85	222	698	7.51	1.0
IW5	18.6	3H	1	145-150	77	8.9	7.47	545.2	3.74	9.28	52.08	276	723	3.43	0.9
IW6	23.1	3H	4	145-150	77	8.9	7.75	545.2	4.45	9.38	51.97	275	750	5.82	1.9
IW7	28.1	4H	1	145-150	84	8.0	7.66	545.2	4.18	9.51	52.14	264	793	4.13	1.9
IW8	31.1	4H	3	145-150	90	7.3	7.58	548.9	4.16	9.53	52.13	297	798	4.33	0.3
IW9	37.6	5H	1	145-150	48	8.5	7.73	546.5	3.85	9.49	52.32	347	823	1.84	0.9
IW10	40.6	5H	3	145-150	74	8.3	7.55	557.4	4.35	9.85	53.77	314	783	3.73	2.7
IW11	51.3	6H	4	120-125	74	12.3	7.77	554.6	4.00	9.62	53.16	289	857	2.24	1.6
IW12	61.1	7H	4	145-150	91	12.4	7.81	553.6	4.61	10.15	52.92	396	920	2.44	1.9
IW13	70.6	8H	4	145-150	94	15.5	7.92	553.6	5.03	10.32	52.75	479	958	2.14	1.9
IW14	80.1	9H	4	145-150	105	15.3	7.91	549.9	5.43	10.30	53.08	393	1016	2.34	8.0
IW15	89.6	10H	4	145-150	91	18.8	7.59	545.2	5.38	10.22	52.57	443	1034		

Hole 678B:

IW1	0.5	1H	1	45-50	86	3.9	8.16	544.1	2.52	11.86	48.78	33	530	3.83	5.9
IW2	1.5	1H	1	145-150	99	3.9	7.80	541.3	2.66	13.57	46.44	127	592	5.53	2.4
IW3	3.0	1H	2	145-150	107	1.3	7.85	540.4	2.41	17.05	42.25	181	648	4.53	5.3
IW4	6.0	1H	4	145-150	89	1.3	7.55	539.4	1.66	33.00	22.76	326	735	0.74	1.5
IW22	7.2	1H	5	114-125	40	4.7	8.06	540.4	0.69	35.99	16.62	435	725	0.34	16.9
IW5	18.7	2H	1	45-50	57	12.0	7.53	547.9	0.83	45.18	10.26	513	986	0.34	0.6
IW6	19.7	2H	1	145-150	100	12.3	7.76	543.2	0.96	44.90	10.63	535	966	1.24	15.5
IW7	21.2	2H	2	145-150	74	4.9	8.04	549.8	0.84	46.40	10.31	533	835	0.15	1.9
IW8	24.2	2H	4	145-150	90	8.1	6.83	548.4	0.55	47.15	8.77	516	862	0.05	<0.1
IW9	25.7	2H	5	145-150	70	9.2	7.64	545.1	0.89	46.86	8.90	498	993	0.44	
IW10	97.0	3H	1	145-150	84	25.4	7.15	545.1	0.62	48.66	9.22	355	1475	1.04	2.1
IW11	99.7	3H	3	120-125	74	24.4	7.50	547.3	1.12	50.43	7.45	328	1516	0.15	<0.1
IW12	104.5	3H	6	145-150	66	26.0	7.27	549.6	0.60	50.72	8.04	349	1498	0.04	12.0
IW13	138.0	4W	2	55-67	36	24.0	7.49	546.1	0.75	43.49	15.99	398	1199	0.25	62.9
IW14	138.9	4W	3	95-107	36	24.0	6.93	547.3	0.49	50.13	9.74	228	1504	0.05	2.6
IW15	139.9	4W	4	145-150	75	25.0	7.64	546.3	0.68	50.77	8.71	308	1392	0.44	6.9
IW16	168.9	4W	CC	3-15	26	25.0	7.51	546.3	0.58	44.85	16.68	202	447		
IW17 ^c	169.0	4W	CC	18-25	6	25.6		539.0		55.22	14.57	436	145		
IW18 ^c	169.2	4W	CC	30-42	7	25.6		525.8		63.85	12.73	485	152		
IW19	169.4	4W	CC	50-60	2	26.0		554.9		68.50	6.91		158		
IW20 ^c	169.7	5X	CC	5-11	3	26.0		531.0		60.77	12.86		172		
IW21 ^c	169.9	5X	CC	22-32	1.5	26.2		495.9		69.32	7.84		157		
Basement	171.0														

^a Method: IW = squeezed; BW = Barnes *in-situ* sample; ov. = from overflow chamber of Barnes sampler, diluted with distilled water.

^b Type: H = hydraulic piston core; X = extended barrel core; B = Barnes sample; W = wash core; CC = core catcher.

^c Chlorinity listed is as measured; concentrations of all other species as measured in designated (°) samples have been corrected to a chlorinity of 550 mmol/kg in the above table, or, for the Barnes overflow samples, to the chlorinity of the sample from the main coil.

^d Corrected using the equations of Gieskes and Peretsman (1986).

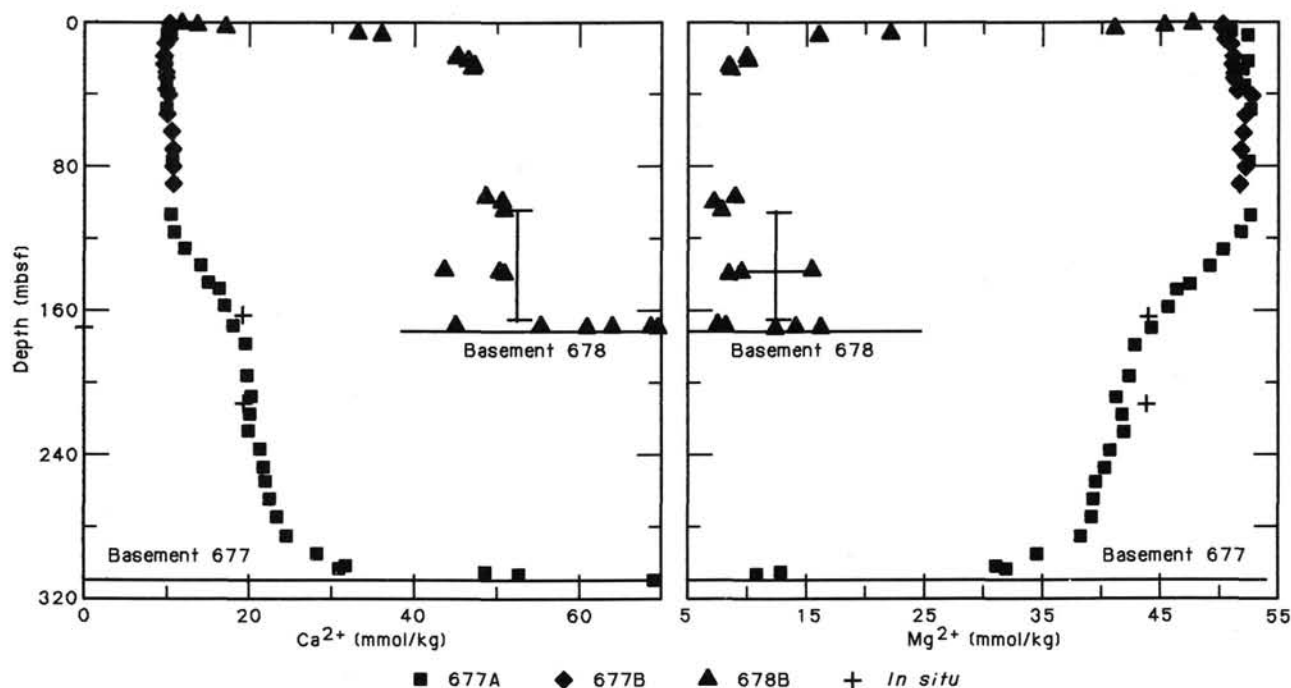


Figure 6. Concentrations of Mg^{2+} and Ca^{2+} vs. depth in sediment pore waters from Sites 677 and 678. Note that Core 678B-4W is a wash core and therefore has an uncertain depth range, as indicated by the vertical bar.

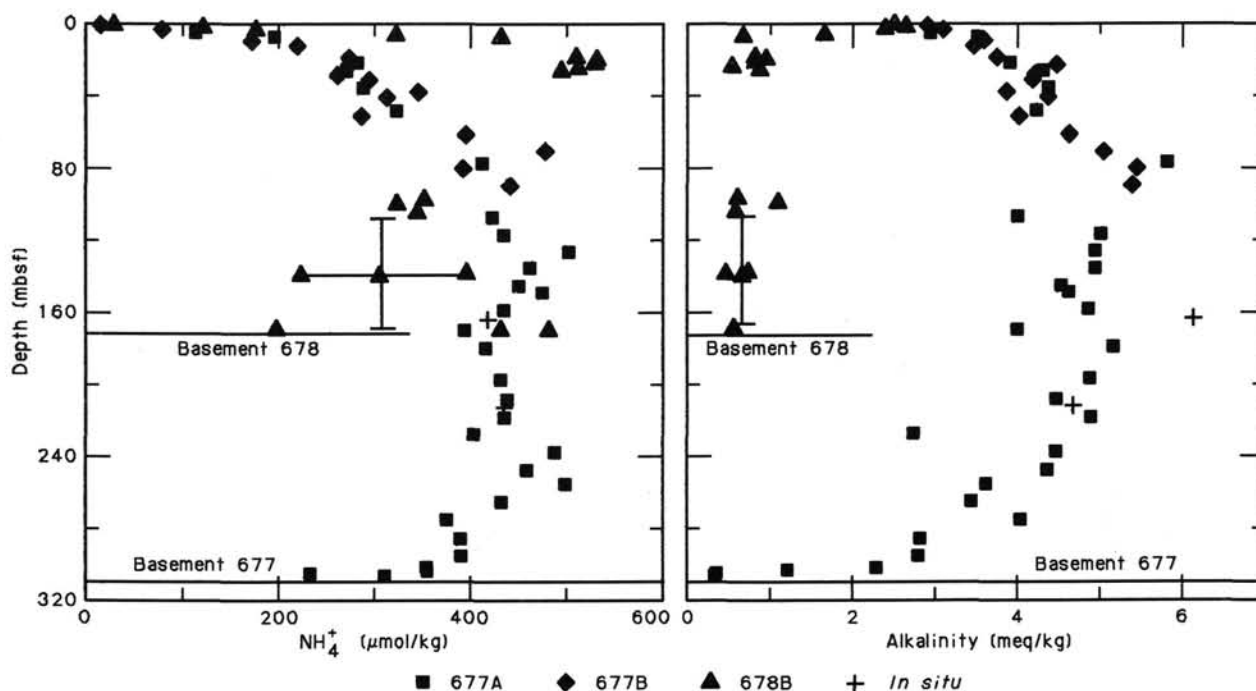


Figure 7. Alkalinity and ammonium concentration vs. depth in sediment pore waters from Sites 677 and 678.

the presence of short (5 cm), intermittent zones of high susceptibility which occur throughout the section and result in an increase in the mean value of X_0 .

Stable Directions

AFD was done on samples from oriented cores in order to determine stable directions of inclination and declination. Be-

cause of the low initial intensity, attempts at demagnetization most frequently resulted in intensity values which were within noise levels, thus making it difficult to find a stable component of magnetization using a Zijderveld plot. As a rough guide to magnetic polarity, then, we have chosen "cleaned" declination and inclination values which represent magnetic directions which were present after weak field demagnetization (typically 100 Oe)

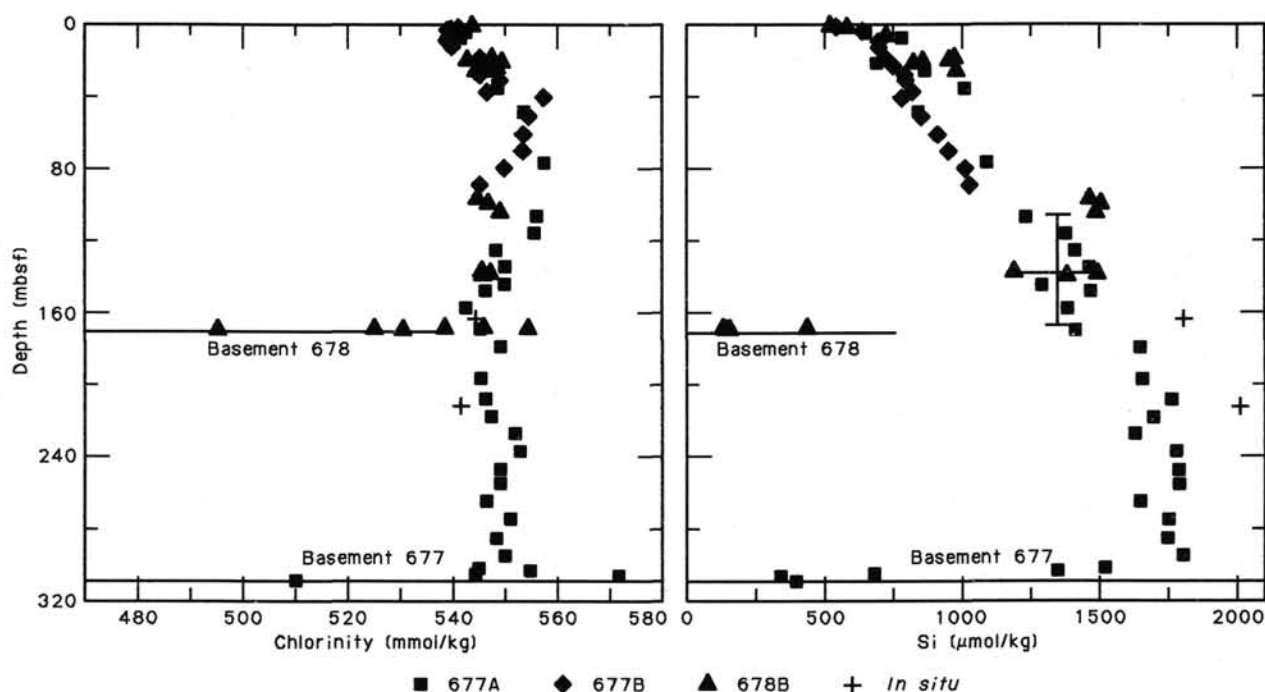


Figure 8. Concentration of Si and chlorinity vs. depth in sediment pore waters from Sites 677 and 678.

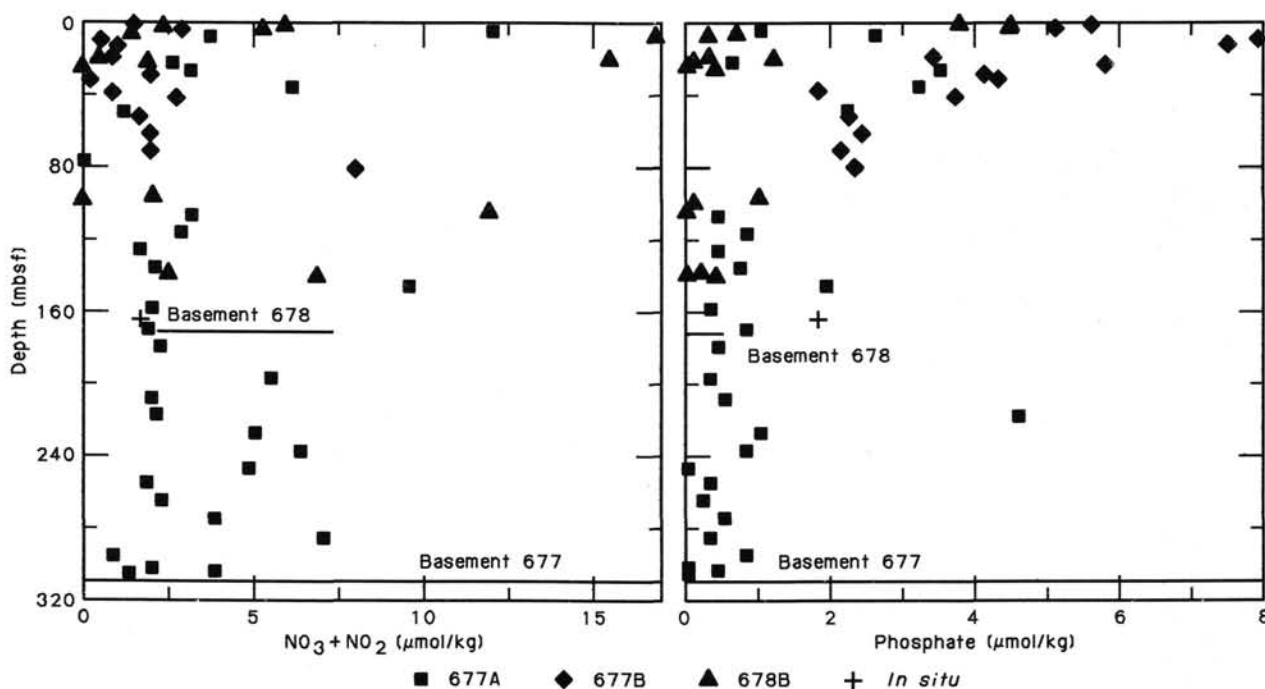


Figure 9. Concentrations of phosphate and nitrate vs. depth in sediment pore waters from Sites 677 and 678.

but which we cannot, with confidence, call "stable" directions. These declination and inclination values are plotted vs. depth in Figure 13. Declination values near 0° represent positive magnetic polarity and those near 180° represent reversed polarity. Although there appear to be only two reversely magnetized samples (at 50 and 89 mbsf) within the section, the extremely low sample density restricts any attempt to construct an accurate reversal chronology for this section.

Conclusions

Both J_0 and X_0 show a distinct decrease below 90 m, suggesting that there may be a decrease in the concentration of magnetic minerals below this depth. Accurate determination of reversal stratigraphy for Site 677A was hampered by extremely low intensities of magnetization and a low number of azimuthally oriented cores. Further paleomagnetic studies would require

Table 6. Remanent magnetic measurements for each sample from Hole 677A are displayed at successive alternating field demagnetization (AFD) steps.

Sample, section, depth (cm)	Depth (mbsf)	AFD (Oe)	Circular standard deviation	Declination	Inclination	Intensity J_0 (10^{-6} emu/cm ³)
1-1, 135	1.35	0	12.7	214.0	-4.4	0.332
135	1.35	50	13.5	212.3	-3.7	0.212
135	1.35	50	23.0	220.3	-7.2	0.140
135	1.35	100	14.1	217.7	-11.7	0.126
135	1.35	200	39.5	191.3	-0.2	0.098
135	1.35	250	29.1	195.8	-36.7	0.062
1-2, 46	1.96	0	22.7	242.9	-14.1	0.171
46	1.96	50	20.7	231.9	-4.8	0.133
46	1.96	100	9.3	191.9	-49.5	0.192
46	1.96	100	15.6	176.0	-34.9	0.222
46	1.96	150	11.2	160.0	-54.1	0.248
46	1.96	200	9.8	288.1	-52.5	0.484
46	1.96	300	14.5	123.2	-54.8	0.173
2-1, 50	6.70	0	4.5	163.2	51.7	0.300
50	6.70	0	12.9	155.5	23.1	0.149
50	6.70	100	11.4	168.3	18.8	0.179
50	6.70	200	22.4	139.6	10.4	0.137
50	6.70	300	25.1	161.2	29.0	0.082
2-2, 7	7.77	0	12.1	173.9	20.6	0.317
7	7.77	50	10.0	172.6	-0.8	0.278
7	7.77	100	10.4	168.5	-0.2	0.186
7	7.77	300	9.8	180.1	4.2	0.315
7	7.77	300	10.0	175.0	-4.7	0.388
7	7.77	400	27.3	165.8	2.1	0.153
2-3, 123	10.43	0	7.9	197.2	39.4	0.499
123	10.43	50	10.4	206.7	9.2	0.414
123	10.43	100	55.1	206.1	12.8	0.249
123	10.43	200	17.2	196.7	4.6	0.283
123	10.43	250	25.2	194.1	2.9	0.148
2-4, 9	10.79	0	11.6	234.4	49.0	0.526
9	10.79	50	15.0	234.3	18.6	0.146
9	10.79	100	18.2	243.5	17.8	0.177
9	10.79	200	28.0	262.1	22.6	0.180
9	10.79	300	23.1	265.2	23.3	0.226
9	10.79	400	30.3	257.0	22.8	0.158
9	10.79	500	43.9	225.5	6.7	0.084
2-5, 126	13.46	0	14.5	221.2	28.2	0.343
129	13.49	50	10.8	224.9	-1.6	0.207
129	13.49	100	14.4	233.2	-1.8	0.235
129	13.49	250	10.9	232.1	-6.3	0.296
129	13.49	350	35.7	229.5	-12.1	0.063
2-6, 125	14.95	0	6.3	23.5	31.0	0.496
125	14.95	100	11.3	236.2	-1.8	0.382
125	14.95	200	16.7	237.7	-0.9	0.285
125	14.95	300	28.1	233.9	9.3	0.199
125	14.95	400	21.2	252.0	17.5	0.191
125	14.95	500	28.1	218.3	8.7	0.168
3-1, 83	16.53	0	13.6	46.2	11.4	0.254
83	16.53	50	16.7	71.4	12.4	0.323
83	16.53	100	13.2	75.7	8.6	0.278
83	16.53	300	20.5	69.9	1.2	0.180
3-2, 83	18.03	50	5.0	77.0	3.4	0.353
83	18.03	100	17.0	87.5	2.1	0.419
83	18.03	200	7.9	71.8	3.6	0.333
83	18.03	200	20.9	78.7	14.2	0.203
83	18.03	300	13.7	79.3	0.4	0.254
3-3, 83	19.53	0	5.0	78.0	2.1	0.881
83	19.53	50	4.6	73.3	1.1	0.850
83	19.53	100	6.8	79.1	2.3	0.985
83	19.53	200	6.7	75.1	-0.1	0.893
83	19.53	300	5.5	74.5	1.8	0.920
3-4, 83	21.03	0	3.3	66.8	-18.1	1.142
83	21.03	50	6.5	73.3	-16.3	0.841
83	21.03	50	6.7	72.0	-14.9	0.869
83	21.03	100	11.0	72.5	-13.2	0.901
83	21.03	200	20.3	84.0	-17.4	0.866
83	21.03	300	11.0	68.0	-17.9	0.233
3-5, 83	22.53	0	11.7	86.2	-1.2	0.326
83	22.53	50	10.6	88.9	0.8	0.340
83	22.53	100	12.8	85.7	4.3	0.281
83	22.53	200	9.2	78.2	1.6	0.383
83	22.53	300	9.7	80.2	2.6	0.350
3-6, 83	24.03	0	8.2	75.4	-16.7	0.220
83	24.03	50	9.8	74.8	-11.1	0.193
83	24.03	100	70.8	259.9	-7.8	0.082
83	24.03	200	8.7	70.9	-11.1	0.208
83	24.03	300	3.1	77.2	-10.7	0.214
4-1, 92	26.12	0	2.5	86.8	20.1	0.891
92	26.12	50	3.5	87.8	6.7	0.634
92	26.12	100	4.1	83.2	5.3	0.593
92	26.12	200	10.3	87.4	5.5	0.293
92	26.12	300	10.6	91.2	-2.8	0.282

Table 6 (continued).

Sample, section, depth (cm)	Depth (mbsf)	AFD (Oe)	Circular standard deviation	Declination	Inclination	Intensity J_0 (10^{-6} emu/cm ³)
4-2, 89	27.59	0	24.9	78.0	-22.4	0.152
89	27.59	100	18.4	81.3	-48.6	0.162
89	27.59	200	23.8	87.2	-29.9	0.126
89	27.59	300	33.7	121.5	-28.0	0.079
89	27.59	400	52.6	98.5	-51.7	0.075
4-3, 92	29.12	0	9.7	100.9	59.2	0.463
92	29.12	50	0.0	96.2	33.4	0.22
92	29.12	100	15.8	101.5	39.2	0.178
92	29.12	200	19.6	84.9	22.1	0.110
4-4, 92	30.62	0	13.2	202.3	84.3	0.079
92	30.62	50	34.1	196.6	-3.5	0.034
92	30.62	200	70.2	284.3	58.1	0.017
4-5, 92	32.12	0	18.3	127.8	83.5	0.117
92	32.12	50	42.6	121.6	50.0	0.038
92	32.12	100	44.1	65.9	-41.7	0.023
4-6, 92	33.62	0	8.6	143.5	71.3	0.320
92	33.62	50	20.9	131.4	39.8	0.140
92	33.62	100	9.7	132.5	48.6	0.145
92	33.62	200	45.5	91.9	44.2	0.066
92	33.62	300	51.1	152.9	12.8	0.033
5-1, 110	35.80	0	42.8	323.5	32.3	0.047
5-2, 110	37.30	0	57.1	279.0	-50.8	0.035
5-3, 110	38.80	0	13.6	300.5	-11.8	0.158
5-4, 110	40.30	0	1.8	296.7	-8.2	0.361
5-5, 110	41.80	0	22.5	302.5	-19.4	0.054
5-6, 110	43.30	0	4.8	325.1	-42.1	0.201
6-1, 107	45.27	0	13.8	101.7	76.2	0.059
6-2, 24	45.94	0	10.6	336.9	72.8	0.144
24	45.94	50	21.9	326.5	47.3	0.100
24	45.94	50	28.0	340.5	42.6	0.081
24	45.94	50	32.0	353.9	46.8	0.099
24	45.94	100	20.9	355.4	44.9	0.091
24	45.94	200	43.0	16.9	64.2	0.055
24	45.94	300	58.1	35.2	49.5	0.017
6-3, 12	47.32	0	24.3	339.3	62.5	0.051
6-4, 124	49.94	0	64.4	332.0	84.9	0.106
124	49.94	50	53.8	335.9	35.6	0.029
124	49.94	100	28.4	308.8	54.9	0.053
6-5, 133	51.53	0	10.2	182.1	64.9	0.136
6-6, 7	51.77	0	15.4	31.8	75.6	0.149
6-7, 7	53.27	0	7.9	65.0	80.8	0.167
7-1, 64	54.34	0	33.0	180.5	41.7	0.081
7-2, 64	55.84	0	67.1	170.3	2.4	0.026
7-3, 64	57.34	0	65.3	254.1	-46.6	0.028
7-4, 64	58.84	0	62.6	53.4	19.6	0.036
7-5, 64	60.34	0	3.0	77.5	-40.4	0.291
7-6, 64	61.84	0	10.7	49.6	-42.8	0.223
8-1, 84	64.04	0	5.9	135.5	46.1	0.492
8-2, 84	65.54	0	5.1	141.2	26.8	0.637
8-3, 84	67.04	0	5.6	146.4	40.7	0.398
8-4, 84	68.54	0	8.1	180.3	69.0	0.420
8-6, 84	71.54	0	19.3	164.5	20.7	0.175
9-1, 61	73.31	0	13.4	204.1	66.3	0.145
9-2, 61	74.81	0	4.7	193.1	-8.1	0.364
9-3, 60	76.30	0	15.7	218.3	-14.2	0.145
9-4, 60	77.80	0	30.8	243.9	-72.9	0.111
10-1, 62	82.82	0	1.7	61.7	7.0	1.224
62	82.82	50	1.5	62.3	1.2	1.180
62	82.82	100	2.8	95.5	-67.5	0.896
62	82.82	200	2.7	245.0	24.1	5.706
62	82.82	300	3.3	14.2	-21.2	10.529
62	82.82	400	1.5	107.8	73.2	13.400
62	82.82	500	1.4	89.6	-7.2	14.967
62	82.82	600	8.5	130.2	77.3	0.286
10-2, 61	84.31	0	73.1	1.9	-24.5	0.786
61	84.31	650	37.3	77.9	35.3	0.167
10-3, 62	85.82	0	22.7	198.8	62.0	0.332
62	85.82	50	13.8	147.9	55.9	0.380
62	85.82	100	51.0	150.5	46.9	0.106
62	85.82	200	74.8	133.5	7.4	0.049
62	85.82	300	54.8	157.7	29.7	0.144
10-4, 61	87.31	0	7.3	91.3	19.9	0.461
61	87.31	50	7.7	100.6	18.1	0.458
61	87.31	100	11.8	94.6	6.8	0.373
61	87.31	200	11.5	98.0	4.7	0.415
61	87.31	300	7.5	91.9	-1.7	0.335
10-5, 62	88.82	0	15.7	191.7	40.0	0.279
62	88.82	50	14.2	195.1	35.4	0.234
62	88.82	100	18.7	206.4	24.2	0.180
62	88.82	200	35.2	198.4	-7.0	0.150
62	88.82	300	22.1	192.9	-18.3	0.128

Table 6 (continued).

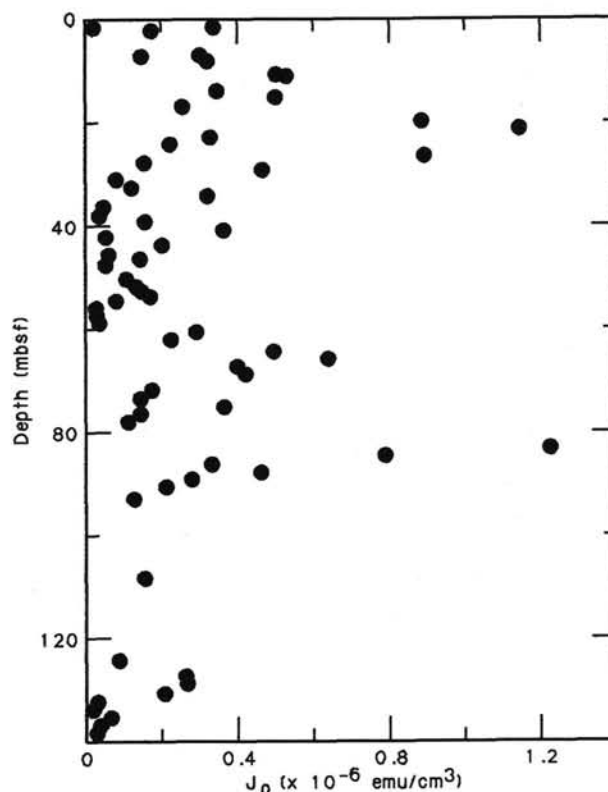
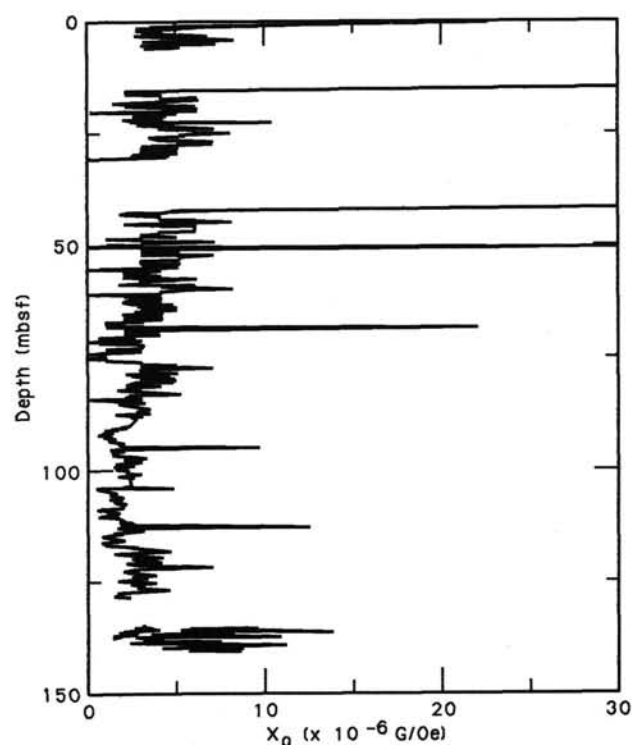
Sample, section, depth (cm)	Depth (mbsf)	AFD (Oe)	Circular standard deviation	Declination	Inclination	Intensity J_0 (10^{-6} emu/cm ³)
10-6, 62	90.32	0	24.7	114.4	23.0	0.212
62	90.32	50	14.7	124.5	5.0	0.274
62	90.32	100	17.9	114.9	4.3	0.259
62	90.32	200	13.9	114.4	-12.9	0.220
62	90.32	300	28.8	122.6	-8.0	0.217
11-1, 84	92.54	0	51.8	81.5	10.9	0.129
11-2, 84	94.04	50	48.7	52.7	39.8	0.111
11-3, 84	95.54	50	51.6	165.1	64.0	0.075
11-4, 84	97.04	50	40.2	210.0	-26.4	0.116
11-5, 84	98.54	50	26.1	340.0	48.2	0.225
11-6, 84	100.04	50	51.1	286.3	-38.8	0.072
12-1, 84	102.04	50	12.4	103.8	63.3	0.316
12-2, 84	103.54	50	24.3	161.2	56.9	0.171
12-3, 84	105.04	50	35.8	77.9	55.5	0.225
12-4, 84	106.54	50	9.3	63.0	42.5	0.485
12-5, 84	108.04	0	7.8	350.2	65.6	0.155
12-6, 84	109.54	50	14.3	78.4	43.7	0.356
13-1, 84	111.54	50	39.2	236.3	25.4	0.122
13-2, 84	113.04	50	16.2	237.6	17.3	0.295
13-3, 84	114.54	50	49.1	195.8	38.9	0.126
13-4, 84	116.04	50	22.0	257.5	20.6	0.118
13-5, 84	117.54	50	28.8	250.9	26.6	0.125
13-6, 84	119.04	50	29.8	239.8	37.2	0.146
14-3, 84	124.04	0	22.6	158.5	47.3	0.088
84	124.04	50	34.9	165.1	44.0	0.069
84	124.04	100	53.4	161.1	67.6	0.065
84	124.04	200	77.3	127.6	4.5	0.027
14-5, 84	127.04	0	7.1	178.8	40.2	0.261
84	127.04	50	16.3	177.0	17.9	0.165
84	127.04	100	22.3	186.4	8.2	0.109
84	127.04	200	0.2	205.0	21.6	0.065
84	127.04	300	47.2	147.8	16.3	0.044
14-6, 84	128.54	0	15.0	218.3	64.3	0.265
84	128.54	50	50.2	192.5	12.9	0.076
84	128.54	100	14.9	83.3	-65.6	0.141
84	128.54	200	4.2	67.3	-54.3	0.659
84	128.54	300	6.7	61.2	-64.3	1.364
84	128.54	400	1.3	66.9	-61.0	2.333
84	128.54	500	3.5	238.0	-60.8	3.431
84	128.54	600	65.5	231.7	-74.6	0.046
15-1, 84	130.54	0	15.4	101.7	8.3	0.207
84	130.54	50	14.5	92.7	0.8	0.144
84	130.54	100	11.2	100.2	-9.3	0.132
84	130.54	200	12.0	114.7	9.5	0.112
84	130.54	300	22.0	99.7	1.8	0.074
15-2, 84	132.04	0	0.0	95.4	18.9	0.030
84	132.04	50	63.5	64.9	17.0	0.042
84	132.04	100	52.1	96.3	47.2	0.022
15-3, 84	133.54	0	53.2	66.9	32.5	0.017
84	133.54	50	66.7	134.5	49.5	0.023
84	133.54	150	22.5	34.6	37.8	0.037
84	133.54	200	34.7	104.7	63.4	0.027
84	133.54	300	4.0	59.9	-56.5	0.504
84	133.54	500	2.7	101.6	-21.4	1.499
84	133.54	600	53.1	116.1	9.2	0.020
15-4, 84	135.04	0	15.6	86.2	35.3	0.066
84	135.04	50	13.5	78.6	44.7	0.063
84	135.04	100	17.8	94.0	17.6	0.075
84	135.04	200	21.1	88.6	-7.3	0.078
84	135.04	300	34.3	70.3	41.2	0.059
84	135.04	400	60.3	254.7	85.1	0.048
15-5, 84	136.54	0	33.2	97.0	33.1	0.038
84	136.54	50	52.1	58.6	63.6	0.017
84	136.54	100	50.2	103.2	46.0	0.020
15-6, 84	138.04	0	23.9	65.1	11.9	0.028
84	138.04	50	56.6	67.9	23.3	0.014

Note: Samples from unoriented cores were measured for NRM properties only.

Table 7. Noise values as measured on the MOLSPIN portable rock magnetometer.

Measurement	X	Y	Z	J_0
1	-0.01	-0.01	-0.06	0.062
2	0.00	-0.01	0.04	0.045
3	-0.02	-0.08	-0.08	0.113
4	0.01	0.00	-0.04	0.042

Note: Four different readings were made (six spins each) using a 24-s spin cycle. Units are in mamps/cm³.

Figure 10. J_0 plotted vs. depth for Cores 111-677A-1H to 111-677A-15H.Figure 11. X_0 plotted vs. depth from 0 to 150 mbsf in Hole 677A.

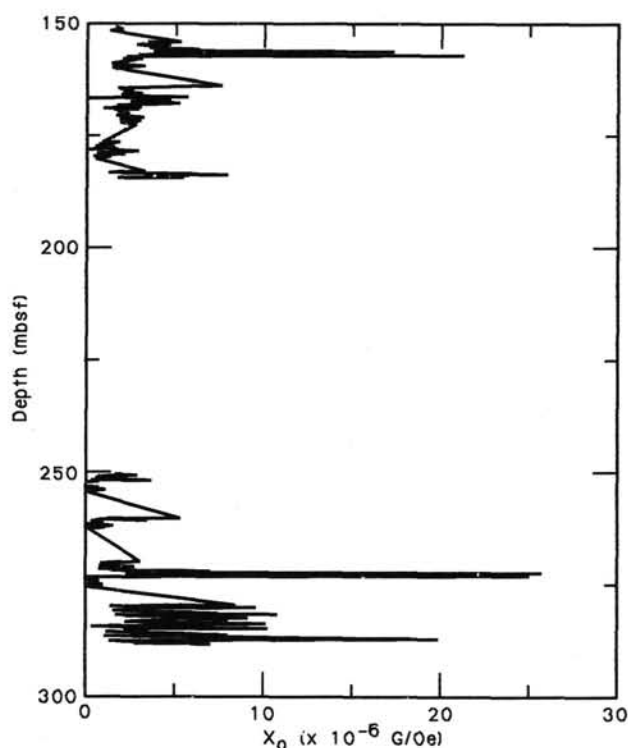


Figure 12. X_0 plotted vs. depth from 150 to 300 mbsf in Hole 677A.

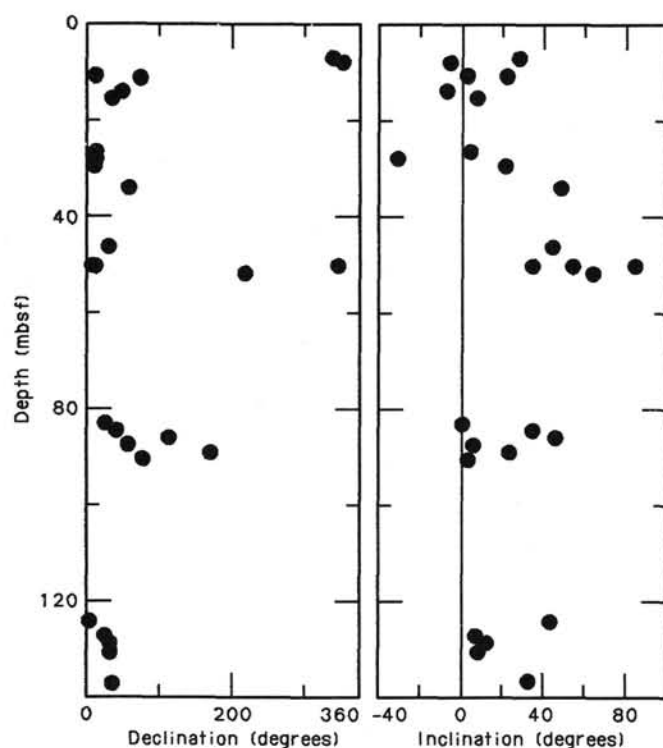


Figure 13. Cleaned inclination and declination values have been corrected according to Multishot orientation data, and plotted against depth. All cores are from Hole 677A and only those cores with successful Multishot runs are included (Cores 111-677A-2H, 111-677A-4H, 111-677A-6H, 111-677A-9H, 111-677A-10H, 111-677A-14H, and 111-677A-15H).

both a higher sampling rate and a more sensitive magnetometer and would provide reversal stratigraphy for those cores which were successfully oriented.

PHYSICAL PROPERTIES

Introduction

Sites 677 and 678 were chosen as part of a regional drilling program located near Site 504 and designed to study ridge-flank geothermal processes. Investigators have identified a recurring pattern of heat-flow highs and lows in this region (Langseth and Mottl, 1982) which is thought to be the surface manifestation of active hydrothermal circulation within the shallow basement. Sites 677 and 678 are located in a low-heat-flow trough and an adjoining high-heat-flow crest, respectively. Extensive APC and XCB coring was planned, intended to yield a continuous string of 9.5-m cores with minimum disturbance to the recovered sediments. A laboratory measurement program was initiated to characterize the sediment physical properties at these two contrasting heat-flow sites and investigate the relationship between the distributions of these parameters within the sedimentary column and geologic processes associated with distinct variations in heat flow, such as pore-water migration and diagenesis.

Double coring at Site 677 produced a continuous sedimentary record from the seafloor to the onset of basement, 309 m below. Laboratory results which are presented in this section and its appendix illustrate the completeness of the recovery. Time constraints limited coring activity at Site 678. Piston cores were retrieved only intermittently, followed by washing to lower depths, again until basement was reached. As a result, data obtained from recovered sediments at this site span relatively narrow depth intervals.

Physical Properties Program

Once sediment cores were split into 1.5-m sections, a systematic physical properties measurement program was begun. This program is depicted in terms of a flow diagram in Figure 14 and includes GRAPE, P -wave logger (PWL), thermal conductivity, Hamilton-Frame compressional wave velocity, vane shear strength, and index properties. Experimental methods regarding these measurements have been discussed in the "Introduction and Explanatory Notes" chapter (this volume).

Thermal conductivity needles were initially calibrated against a rubber standard. Once the sediment-core temperature had stabilized in the laboratory, the conductivity measurements were performed; a linear temperature vs. log time relationship enables this property to be computed directly. Examples of these recorded data are presented in Figures 15 and 16 for a shallow and a deep core, respectively. The Hamilton-Frame apparatus underwent three separate calibration exercises before measurements on split cores were begun: (1) zero-time calibration (see "Introduction and Explanatory Notes" chapter, this volume); (2) dial gauge calibration (Fig. 17); and (3) liner thickness and traveltime corrections (Boyce, 1973). Final corrections to velocity calculations were applied according to these calibration results.

Index properties were routinely measured once per section. These consist of porosity, water content, bulk density, and grain density; they are computed from the sample wet and dry weights and volumes. Sample volumes were determined using the Penta pycnometer. The accuracy of this apparatus was first questioned earlier on Leg 111 during the testing of basalt samples because the volumes of the dry minicores were consistently found to be greater than the volumes of their wet counterparts. In order to investigate this discrepancy, a simple experiment was designed to determine the effect of seawater upon the measurement accuracy of the pycnometer. Four plexiglas samples of known vol-

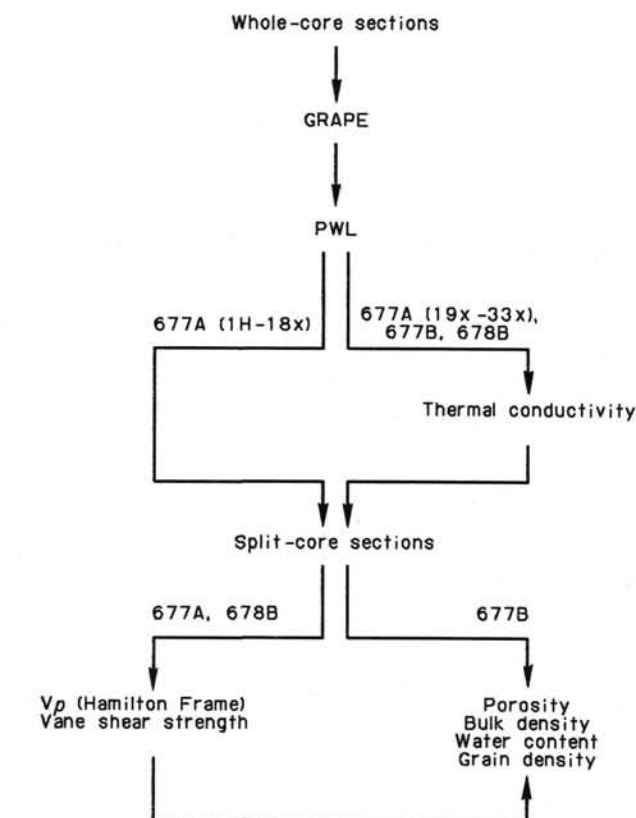


Figure 14. Flow diagram for the physical properties program at Sites 677 and 678.

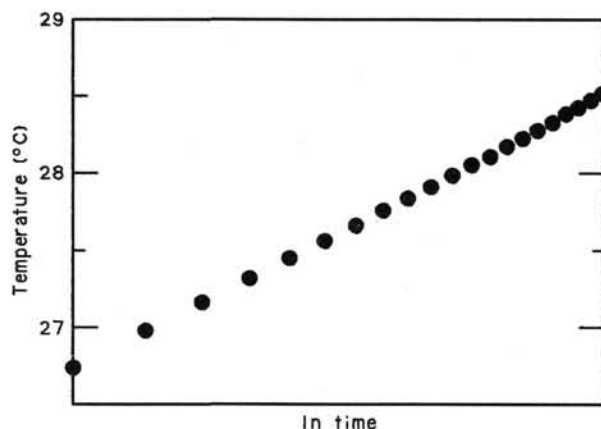


Figure 15. Temperature/log time plot for sediment sample from shallow depth (111-677B-1H-1, 75 cm); thermal conductivity determination. Run 700; 48-348 s.

umes were placed in four pycnometer cells and the corresponding volumes were measured. The measured and true volumes closely agreed, as shown in Figure 18. The test was then repeated, this time adding two drops of seawater to each cell along with the plexiglas standard. Results showed a significant departure between the true and measured volumes, as all of the latter values decreased. It is postulated that liquid within the pycnometer cells absorbs the helium gas, thereby producing systematically lower values for wet volumes. It appears that volumes are reasonably accurate when determined on dry samples, but preferentially low when determined on wet ones. This obser-

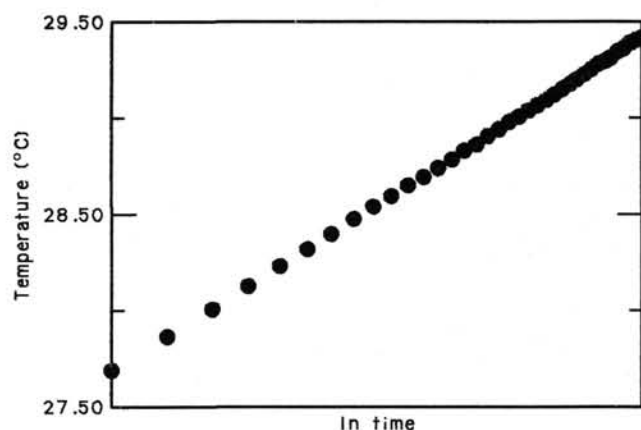


Figure 16. Temperature/log time plot for sediment sample from near the basement (111-677A-33X-2, 80 cm; 301 mbsf); thermal conductivity determination. Run 123; 30-354 s.

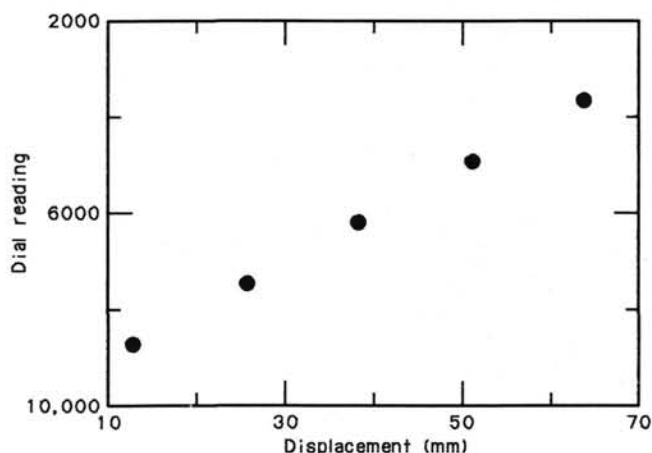


Figure 17. Dial calibration plot for the Hamilton Frame velocimeter.

vation was considered when calculating the index properties presented below; values of porosity, water content, bulk density, and grain density were derived from dry volume measurements.

Results

The physical properties results for the three sediment holes drilled during Leg 111 are presented separately below, although the results for the double hole at Site 677 are also considered together since measurements were not completely duplicated. The precise program adopted at each hole is highlighted in Figure 14. Due to a change in schedule, part way through Hole 677A, there is a gap in the thermal conductivity data at this site. This interval was originally planned to be covered during analysis of sediments from Hole 677B, which was never drilled to sufficient depth because of time constraints.

Hole 677A

Hole 677A was cored from seafloor level to a depth of 309 m. Measurements were made on all recovered cores, generally at a frequency of not less than one per section. Results of the measurements for Hole 677A are documented in Table 8. The data obtained with the GRAPE and the PWL are not presented in full at this stage, although examples of the data are included in this report.

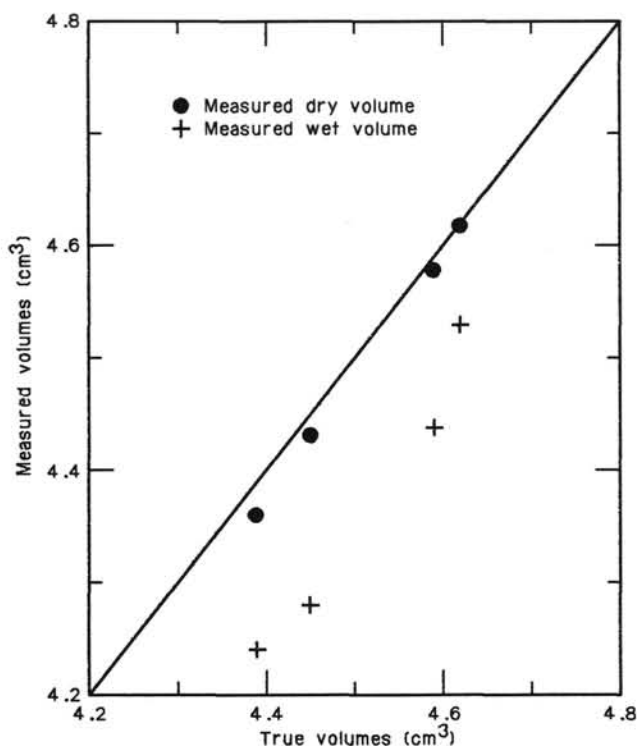


Figure 18. Plot of measured dry and wet volumes against true volumes for the pycnometer. See text for details.

Index Properties

Figures 19 through 22 present the index property data obtained from volumetric and mass determinations on the wet and dry subsamples. There is correlation between the various index properties as would be expected, although the high water content (high porosity and low bulk density) throughout the section is worthy of particular note. This feature will be seen to run throughout the sediment physical property results as it dictates the values of many of the other nonindex parameters measured. The porosity values range from 91.09% at the seafloor surface to 53.13% at the base of the hole. Only in the bottom 2 m of the hole do the porosity values fall below 60%. Corresponding bulk density values range from 1.20 to 1.84 g/cm³; the precise value depending on the grain density value at any particular horizon. Unfortunately, the grain density measurements exhibit noticeable scatter and consequently bulk density values must be viewed in association with the related grain density determinations.

Vane Shear Strength

Values for the shear strength of samples recovered from Hole 677A range from 1.41 to 168.00 kPa. The general range, however, is limited to values below 100 kPa and, similar to the feature shown by the index properties, there is a substantial increase in shear strength at the very bottom of the hole. The results for the entire depth drilled are plotted in Figure 23.

Thermal Conductivity

Thermal conductivity measurements in Hole 677A were made in Cores 111-677A-19X to 111-677A-33X (164–306 mbsf) at a frequency approaching one per section. The results show an increase in thermal conductivity with depth corresponding to a general decrease in porosity, although, again, the trend is small with a distinct increment occurring at the bottom of the hole in

the lower 3 m. Figure 24 shows the variation of thermal conductivity with depth for the lower half of Hole 677A.

Compressional Wave Velocity (Hamilton Frame)

P-wave velocity measurements were made on sediment samples while still in the core liners, a correction being made for propagation through the liner wall, as described by Boyce (1973). The results show considerable scatter (Fig. 25). This is probably due to a combination of the high porosities, and hence low velocities, and the difficulty in setting up the experiment to enable adequate contact between the transducers and sample, while attempting to preserve the fabric of the sample in its undisturbed state. Consequently it is possible that the measured *P*-wave velocities do not relate directly to the measured porosities, although they should provide a relative indication of the variation of the sediment structure between samples. Determinations of velocity by this method yield results varying between 1509 and 1672 m/s. These values are generally much higher than those measured by the *P*-wave logger as discussed below.

Carbonate Content

The carbonate content of the samples varies considerably throughout the hole from less than 10% to more than 87%. The variation has a slight trend of increasing carbonate with depth, but generally appears to be related more to specific horizons than any depth feature. It is possible that these data may help in analyzing the trends in the other physical properties data. Figure 26 is a plot of carbonate content variation with depth for Hole 677A.

P-Wave Logger (PWL)

All cores recovered from Hole 677A were logged with the PWL. The results are of good quality and show the laboratory *P*-wave velocities to be low; this is consistent with the high porosity determinations reviewed above. XCB coring often yields poor recovery with numerous air gaps and incompletely filled sections. The high quality of the data in Figure 27 is, however, typical of the data obtained during Leg 111 for the majority of XCB cores. In Figure 27, the velocity measurements are consistent and fluctuate around a mean of about 1515 m/s. The increase in velocity at a depth of 1.8 m within this core (overall depth in the hole of 204.6 m) correlates with an ash horizon subsequently identified upon opening the core. Full PWL results for the hole will be presented at a later date after further processing of the data.

GRAPE

Simultaneously with the PWL measurements, GRAPE determinations were made on each recovered core. Figure 28 gives an example of the GRAPE data, for part of the same core as the PWL in Figure 27. Note the increase in bulk density at the top of section 2, corresponding, again, to the anomaly in the PWL record subsequently identified as an ash horizon.

Hole 677B

Hole 677B was cored to a depth of 92 m. Consequently, a total of 10 HPC cores were recovered. Measurements of thermal conductivity and index properties were made at a frequency of one per section, in addition to GRAPE and PWL logs being run. The results for Hole 677B are tabulated in Table 9.

Index Properties

Figures 29 through 32 are plots of the index properties (porosity, water content, bulk density, and grain density) for samples taken from each section of the cores from Hole 677B. The results are generally similar to those for Hole 677A with a remarkable agreement between the two. Porosity values are in the

Table 8. Summary of physical properties results for Hole 677A.

Core-section	Interval (cm)	Depth (mbsf)	Water content (%)	Grain density (g/cm ³)	Bulk density (g/cm ³)	Porosity (%)	Shear strength (kPa)	Thermal conductivity (W/m-k)	P-wave velocity (m/s)	CaCO ₃ content (%)
1H-1	70-71	0.70	240.26	4.27	1.31	91.09	1.41		1589.3	51.35
1H-2	75-76	2.25	219.41	2.77	1.27	85.84	3.40		1586.1	42.79
1H-3	75-77	3.76	264.15	2.25	1.20	85.65	4.89		1584.0	16.62
1H-4	75-77	5.26	239.31	2.81	1.26	87.05	9.99		1612.2	29.12
2H-1	70-72	6.91	265.74	2.08	1.19	84.81	8.08		1601.9	10.31
2H-2	70-72	8.41	130.01	2.57	1.38	76.82	8.08		1591.6	13.46
2H-3	70-72	9.91	216.52	3.04	1.29	86.78	8.29		1591.4	29.79
2H-4	70-72	10.62	138.38	4.07	1.49	84.80	13.82			47.32
2H-5	69-71	12.12	144.06	3.09	1.41	81.54	18.07		1656.1	48.25
2H-6	69-71	13.62	146.57	2.42	1.33	77.92	16.03		1550.5	41.14
3H-1	69-71	16.40	133.50	2.48	1.36	76.69	11.78		1602.0	59.75
3H-2	69-71	17.90	165.47	2.99	1.36	83.11	11.78		1598.0	41.20
3H-3	69-71	19.40	159.30	2.97	1.37	82.46	10.84		1615.8	52.14
3H-4	69-71	20.90	187.40	2.84	1.31	84.13	18.85		1571.0	32.63
3H-5	69-71	22.40	178.97	2.06	1.24	78.64	19.80			40.22
3H-6	69-71	23.90	142.89	2.47	1.34	77.79	17.91		1590.8	52.00
4H-1	79-81	26.00	174.94	3.07	1.35	84.24	16.03		1597.1	47.06
4H-2	69-71	27.40	191.53	3.72	1.36	87.63	22.15		1591.1	18.31
4H-3	69-71	28.90	181.19	2.27	1.27	80.43	22.15		1578.1	37.54
4H-4	65-67	30.36	168.61	2.33	1.29	79.66	25.45		1604.0	41.90
4H-5	69-71	31.90	144.76	3.07	1.40	81.51	24.04		1594.8	44.86
4H-6	74-76	33.45	160.29	2.61	1.33	80.63	24.51		1609.5	38.33
5H-1	74-76	35.45	189.31	2.77	1.31	83.94	11.78		1597.3	27.44
5H-2	69-71	36.90	158.32	2.31	1.30	78.49	29.23		1601.4	34.24
5H-3	69-71	38.40	147.66	2.22	1.31	76.58	24.04		1596.9	49.13
5H-4	69-71	39.90	167.41	2.38	1.30	79.91	26.87		1574.1	40.65
5H-5	69-71	41.40	158.60	2.58	1.33	80.29	24.98		1600.6	39.04
5H-6	69-71	42.90	154.03	2.67	1.35	80.37	20.74		1599.2	51.84
6H-1	74-76	44.95	121.13	2.74	1.42	76.71	25.45		1600.0	48.93
6H-2	74-76	46.45	159.37	3.13	1.38	83.19	24.04		1550.1	35.75
6H-3	53-55	47.74	121.11	3.96	1.54	82.59	20.27		1581.9	55.42
6H-4	72-74	49.43	144.04	2.38	1.33	77.31	28.28		1576.7	39.27
6H-5	75-77	50.95	149.16	3.10	1.40	82.12	29.70		1566.5	45.18
6H-6	68-70	52.38	197.15	1.71	1.18	77.25	30.17		1588.8	25.36
6H-7	31-33	53.50	161.07	2.32	1.30	78.82	32.05		1602.0	40.78
7H-1	75-77	54.46	145.82	2.46	1.34	78.10	29.75		1610.4	57.04
7H-2	75-77	55.96	149.82	2.43	1.33	78.36	26.70		1613.3	49.44
7H-3	71-73	57.42	171.17	2.58	1.31	81.45	39.66		1601.7	24.95
7H-4	76-78	58.97	152.26	2.36	1.32	78.13	46.53		1637.8	42.07
7H-5	74-76	60.45	199.31	2.19	1.24	81.37	48.82		1576.0	15.67
7H-6	74-76	61.95	176.71	3.65	1.38	86.50	52.63		1607.3	32.88
7H-7	23-25	62.94	174.70	2.61	1.32	82.33	49.58		1580.9	
8H-1	75-77	63.96	166.75	3.11	1.36	83.75	38.14		1658.2	34.32
8H-2	68-70	65.40	243.94	2.41	1.22	85.50	51.11		1599.2	10.06
8H-3	76-78	66.98	216.42	2.25	1.23	83.00	45.00		1615.6	17.17
8H-4	75-77	68.47	181.48	2.63	1.30	82.61	48.82		1610.3	35.48
8H-5	76-78	69.98	188.46	2.90	1.32	84.47	61.02		1602.5	13.91
8H-6	76-78	71.48	195.63	2.47	1.27	82.86	59.50		1592.2	14.47
9H-1	75-77	73.46	211.18	2.95	1.29	86.13	27.40		1610.7	25.40
9H-2	76-78	74.97	206.22	2.38	1.25	83.09	41.70		1669.7	17.67
9H-3	74-76	76.45	243.19	2.14	1.20	83.94	52.42		1672.0	16.70
9H-4	75-77	77.96	172.21	2.41	1.30	80.57	61.96		1606.8	33.36
9H-5	76-78	79.47	235.07	2.63	1.25	86.09	63.15		1632.7	27.19
9H-6	76-78	80.97	192.05	2.60	1.29	83.27	40.51		1634.8	32.97
10H-1	77-79	82.98	215.05	2.04	1.21	81.47	50.04		1570.1	30.86
10H-2	76-78	84.47	247.87	1.80	1.17	81.90	46.47		1588.3	9.31
10H-3	75-77	85.96	224.37	2.37	1.24	84.21	44.08		1605.5	14.30
10H-4	75-77	87.46	208.82	2.28	1.24	82.63	60.76		1599.9	49.71
10H-5	77-79	88.98	151.49	2.30	1.31	77.65	66.72			41.80
10H-6	77-79	90.48	166.41	2.71	1.33	81.78	78.64		1605.7	34.17
11H-1	71-73	92.42	176.24	2.23	1.27	79.73	28.59		1599.5	37.59
11H-2	60-71	93.90	151.94	2.24	1.30	77.27	33.36		1568.2	42.30
11H-3	69-71	95.40	148.21	2.67	1.36	79.74	30.98		1601.1	37.54
11H-4	69-71	96.90	139.81	3.22	1.43	81.70	56.00		1605.2	45.50
11H-5	69-71	98.40	142.35	2.72	1.38	79.39	48.85		1613.3	51.75
11H-6	69-71	99.90	169.35	2.98	1.35	83.38	51.23		1606.1	38.95
12H-1	69-71	101.90	132.14	2.58	1.38	77.17	59.57		1612.8	45.85
12H-2	69-71	103.40	150.51	2.65	1.35	79.87	50.04		1585.2	32.17
12H-3	69-71	104.90	204.66	2.84	1.29	85.29	57.19		1593.8	18.30
12H-4	69-71	106.4	128.64	3.44	1.47	81.44	54.81		1596.8	47.75
12H-5	69-71	107.9	129.28	2.59	1.39	76.90	71.49		1614.9	44.14
12H-6	69-71	109.4	160.96	2.30	1.30	78.66	81.02		1610.7	34.46
13H-1	69-71	111.4	158.04	2.73	1.35	81.11	63.15		1602.8	40.86
13H-2	69-71	112.9	143.45	2.74	1.37	79.62	57.19		1598.8	52.15
13H-3	69-71	114.4	143.70	2.53	1.35	78.31	57.19		1578.2	21.86
13H-4	69-71	115.9	136.74	2.25	1.33	75.38	65.53		1605.6	38.10
13H-5	69-71	117.4	118.68	2.59	1.41	75.33	72.68			58.68

Table 8 (continued).

Core-section	Interval (cm)	Depth (mbsf)	Water content (%)	Grain density (g/cm ³)	Bulk density (g/cm ³)	Porosity (%)	Shear strength (kPa)	Thermal conductivity (W/m-k)	P-wave velocity (m/s)	CaCO ₃ content (%)
13H-6	69-71	118.9	117.77	2.70	1.43	75.93	71.49		1610.9	52.94
14H-1	69-71	120.9	143.57	3.05	1.40	81.30	76.25		1589.2	43.11
14H-2	69-71	122.4	156.65	2.70	1.35	80.77	79.83		1595.7	37.05
14H-3	69-71	123.9	144.94	2.59	1.36	78.86	64.34		1591.7	38.42
14H-4	69-71	125.4	161.05	2.31	1.30	78.79	97.70		1607.1	29.23
14H-5	69-71	126.9	161.87	2.22	1.29	78.18	101.30		1586.9	35.87
14H-6	69-71	128.4	163.95	2.76	1.34	81.85	96.51		1570.0	33.98
15H-1	69-71	130.4	134.71	3.04	1.42	80.22	44.08			47.75
15H-2	69-71	131.9	136.81	2.81	1.40	79.21	38.13		1583.0	
15H-3	69-71	133.4	152.73	2.42	1.32	78.64	44.08		1567.8	47.96
15H-4	69-71	134.9	144.79	2.41	1.34	77.66	82.21		1590.2	42.07
15H-5	69-71	136.4	139.49	3.10	1.41	81.12	107.20		1600.3	42.08
15H-6	69-71	137.9	132.31	2.57	1.38	77.19	88.17		1610.6	40.40
16X-1	40-42	139.6	131.44	2.59	1.38	77.19	13.11		1580.5	39.88
16X-2	10-12	139.9	152.58	3.01	1.38	82.00	27.40			54.56
16X-3	45-47	140.9								62.91
16X-4	77-79	142.3	141.88	2.25	1.32	76.04	36.94		1580.2	46.40
16X-5	76-78	144.0	120.77	2.43	1.38	74.49	26.21		1558.5	59.50
17X-1	77-79	145.0	110.63	2.37	1.40	72.25	22.64		1559.5	58.99
17X-3	77-79	148.0	92.35	2.52	1.48	69.78	36.94		1616.1	54.65
17X-4	77-79	149.5	110.40	2.39	1.40	72.36	40.51		1571.1	64.00
17X-5	74-76	151.0	88.00	2.69	1.52	70.10	89.36			63.11
18X-1	77-79	154.6	98.84	2.33	1.42	69.55	30.98		1588.7	67.28
18X-2	77-79	156.1	112.11	2.40	1.40	72.75	28.59		1566.7	58.94
18X-3	77-79	157.6	127.84	3.29	1.46	80.65	34.55		1557.8	52.96
18X-4	77-79	159.1	99.18	3.03	1.53	74.81	67.91		1573.3	64.12
19X-1	73-75	164.2	119.76	3.53	1.51	80.71	21.45	0.980		52.36
19X-2	74-76	165.8	132.25	2.48	1.37	76.54	20.25	0.988	1580.8	57.77
19X-3	75-77	167.3	110.33	2.99	1.49	76.56	32.17	1.055		57.12
19X-4	75-77	168.8	106.23	2.92	1.49	75.42	26.21	1.131	1553.0	68.76
19X-5	75-77	170.3	100.89	2.91	1.51	74.37	35.74	1.043	1537.1	66.77
19X-6	76-78	171.8	85.65	2.94	1.57	71.34	65.53	1.082	1584.4	30.43
20X-1	74-76	174.0	89.14	2.84	1.54	71.43	15.49	1.098	1552.0	67.98
20X-2	74-76	175.5	96.00	2.50	1.46	70.37	25.02	1.146	1588.9	69.92
20X-3	74-76	177.0	94.46	2.77	1.51	72.10	14.30	1.130	1578.1	68.46
20X-4	74-76	178.5	83.66	3.07	1.60	71.76	40.51	1.045	1572.6	69.39
20X-5	74-76	180.0	97.13	2.45	1.45	70.24	28.60	1.085		58.39
21X-1	74-76	183.6	94.75	3.02	1.55	73.88	16.68	1.023	1633.3	75.19
21X-2	69-71	185.0	112.71	2.46	1.41	73.35	16.68	1.050	1575.9	67.98
22X-1	69-71	193.1	66.08	3.00	1.69	66.16	29.79	1.243	1609.9	86.03
22X-2	69-71	194.6	76.19	2.86	1.61	68.29	23.83	1.191	1583.5	79.23
22X-3	69-71	196.1	74.94	3.02	1.64	69.12	26.21	1.113	1573.0	79.51
22X-4	69-71	197.6	83.49	2.84	1.57	70.10	64.34	1.012	1592.0	74.83
22X-5	69-71	199.1	83.90	2.94	1.58	70.92	53.62	1.217		73.82
23X-1	69-71	202.8	74.85	2.93	1.63	68.44	23.83	1.201	1577.4	79.66
23X-2	69-71	204.3	96.47	3.32	1.57	75.98	28.59	1.176	1581.9	65.03
23X-3	69-71	205.8	93.71	2.52	1.47	70.06	28.59	1.101	1586.3	71.22
23X-4	69-71	207.3	90.25	2.17	1.41	65.97	47.66	1.204	1585.2	70.92
23X-5	69-71	208.8	101.75	2.38	1.42	70.62	120.30	1.062		59.66
24X-1	69-71	212.4	118.26	3.17	1.48	78.77	23.83	1.046		59.76
24X-2	69-71	213.9	84.36	3.07	1.60	71.92	33.36	1.131		71.80
24X-3	69-71	215.4	83.37	3.00	1.59	71.23	26.21	1.117	1590.2	75.44
24X-4	69-71	216.9	104.00	2.78	1.48	74.12	28.59	1.038	1587.7	69.04
24X-5	69-71	218.4	75.09	2.54	1.55	65.35	22.64	1.174	1592.6	77.80
24X-6	69-71	219.9	80.84	2.46	1.51	66.35	69.10	1.145	1600.5	75.98
25X-1	59-61	222.0	74.72	2.67	1.58	66.37	20.25	1.263	1576.4	75.99
25X-2	69-71	223.6	157.82	2.79	1.35	81.41	17.87	0.906	1588.7	51.39
25X-3	69-71	225.1	83.02	2.48	1.50	67.07	22.64	1.156	1604.9	77.38
25X-4	69-71	226.6	76.04	2.51	1.54	65.34	30.98	1.178		73.29
25X-5	69-71	228.1	111.35	2.87	1.47	76.00	71.49	0.947		56.40
26X-1	69-71	231.8	117.76	2.26	1.36	72.53	20.25	0.988	1575.4	58.69
26X-2	69-71	233.3	115.94	2.56	1.41	74.66	35.74	0.992	1565.2	56.40
26X-3	69-71	234.8	73.90	2.76	1.60	66.86	33.36	1.205	1595.0	75.74
26X-4	69-71	236.3	96.97	2.83	1.51	73.12	57.19	0.994	1565.3	65.27
26X-5	70-72	237.8	70.07	2.80	1.63	65.98	53.62	1.239	1613.1	72.19
26X-6	70-72	239.3	107.23	2.35	1.40	71.47	35.74	1.001	1584.3	66.77
27X-1	75-77	241.6	101.04	2.57	1.46	71.98	16.68	0.993	1577.9	58.85
27X-2	74-76	243.1	94.59	2.38	1.44	69.02	34.55	0.992	1589.6	63.96
27X-3	76-78	244.6	100.14	2.32	1.42	69.75	30.98	1.009	1603.0	67.11
27X-4	75-77	246.1	150.29	2.91	1.38	81.28	32.17	0.855	1588.2	49.08
27X-5	75-77	247.6	80.50	2.92	1.59	69.88	71.49	0.996	1589.3	
27X-6	30-32	248.6	91.18	2.83	1.53	71.88	64.34	1.097	1595.7	71.90
28X-1	74-76	251.2	83.91	2.65	1.53	68.73	34.55	1.200	1595.3	76.15
28X-2	75-77	252.7	155.82	2.17	1.29	77.16	14.30	0.967	1593.4	46.11
28X-3	76-78	254.2	88.64	2.78	1.53	70.88	44.08	1.025	1577.5	
28X-4	77-79	255.7	78.33	2.74	1.58	68.00	73.87	1.066	1595.0	70.64
29X-1	75-77	260.8	65.52	2.70	1.63	63.57	39.32	1.178	1655.2	81.29

Table 8 (continued).

Core-section	Interval (cm)	Depth (mbsf)	Water content (%)	Grain density (g/cm ³)	Bulk density (g/cm ³)	Porosity (%)	Shear strength (kPa)	Thermal conductivity (W/m-k)	P-wave velocity (m/s)	CaCO ₃ content (%)
29X-2	75-77	262.3	80.60	2.63	1.54	67.75	30.98	1.052	1550.6	70.34
29X-3	74-76	263.8	66.29	2.88	1.67	65.34	59.57	1.074		77.72
29X-4	35-37	264.9	73.20	2.43	1.53	63.76	64.34	1.057	1605.9	72.81
30X-1	73-75	270.4	100.59	2.62	1.47	72.30	26.21	0.996	1593.8	59.39
30X-2	74-77	272.0	72.01	2.46	1.54	63.62	22.64	1.252	1610.4	77.11
30X-3	74-76	273.5	59.36	3.23	1.79	65.43	52.42	1.181	1625.9	80.73
30X-4	64-66	274.9	58.82	2.59	1.65	60.04	97.70	1.248	1632.1	79.99
31X-1	75-77	280.1	80.18	2.45	1.51	66.04	33.36	1.179		
31X-2	77-79	281.6	80.95	2.38	1.49	65.61	27.40	1.115	1591.8	70.17
31X-3	75-77	283.1	105.62	2.64	1.45	73.46	22.64	0.973	1588.7	56.61
31X-4	77-79	284.6	92.10	3.07	1.56	73.67	21.45	1.007	1508.8	58.67
31X-5	84-86	286.2	81.55	2.76	1.56	69.00	27.40	0.901	1580.1	70.41
31X-6	73-75	287.6	81.05	2.42	1.50	65.98	46.47	1.151	1594.2	87.21
32X-1	74-76	289.7	112.61	2.78	1.45	75.65	25.02	1.005	1609.0	54.21
32X-2	74-76	291.2	91.92	2.17	1.41	66.46	29.79	1.035	1578.8	65.99
32X-3	74-76	292.7	107.7	2.67	1.45	74.00	35.74	1.065	1605.7	57.37
32X-4	75-77	294.2	84.52	2.39	1.48	66.63	75.06	1.095	1575.3	67.83
32X-5	76-78	295.7	82.30	2.50	1.51	67.10	60.76	1.127	1597.2	67.94
33X-1	67-69	299.3	117.99	2.95	1.46	77.54	30.98	0.935	1568.8	52.63
33X-2	67-69	300.7								67.74
33X-3	78-80	302.4	98.60	2.52	1.46	71.08	60.76	1.084		60.45
33X-4	84-86	304.0	48.37	2.78	1.78	57.05	64.34	1.429	1608.1	75.68
33X-5	76-78	305.4	41.75	2.75	1.84	53.13	168.00	1.447	1662.7	81.67

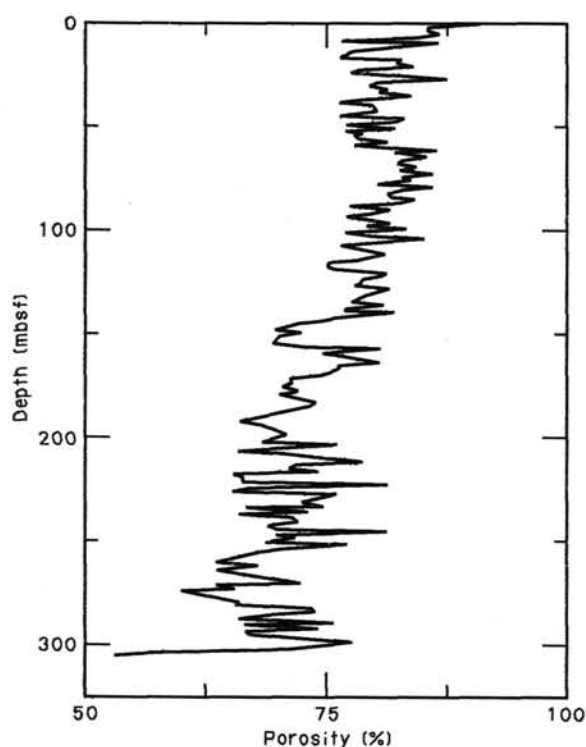


Figure 19. Porosity variation with depth in Hole 677A.

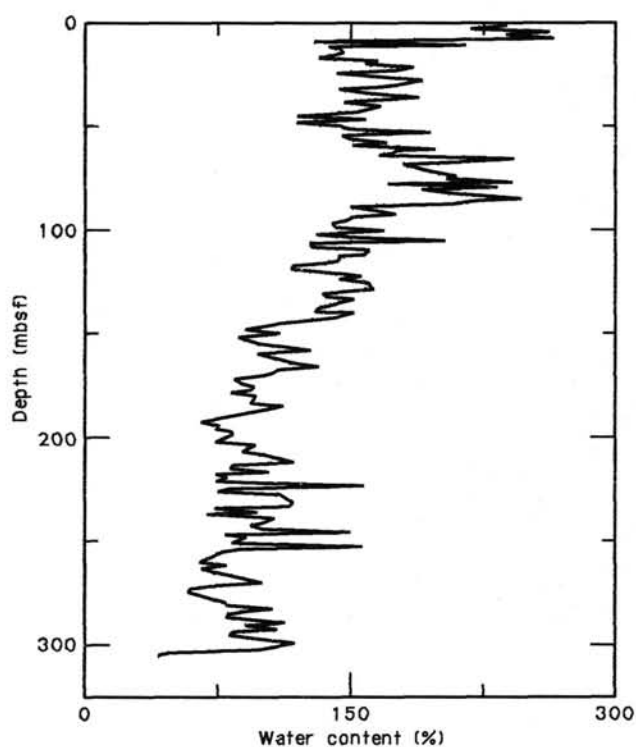


Figure 20. Water content variation with depth in Hole 677A.

high 70%-80% region, with corresponding bulk density values of 1.20-1.60 g/cm³.

Thermal Conductivity

Thermal conductivity determinations were made to supplement those made in Hole 677A. The values reflect the high porosities of the samples with a lowermost value of 0.708 W/m-K (compared with the value for seawater of 0.610 W/m-K) and a highest value of 1.073 W/m-K. The results are plotted in Figure 33, and then again in Figure 34 where they are presented with

the data from Hole 677A; here the overall trend of increasing thermal conductivity with increasing depth (decreasing porosity) is visible.

Hole 678B

Hole 678B, the high-heat-flow site, was drilled in a limited time schedule and consequently only a small number of cores were taken. Although the drilled interval for Hole 678B is some 167 m, suitable samples for physical property determinations were obtained only in the upper 104 m, at three distinct hori-

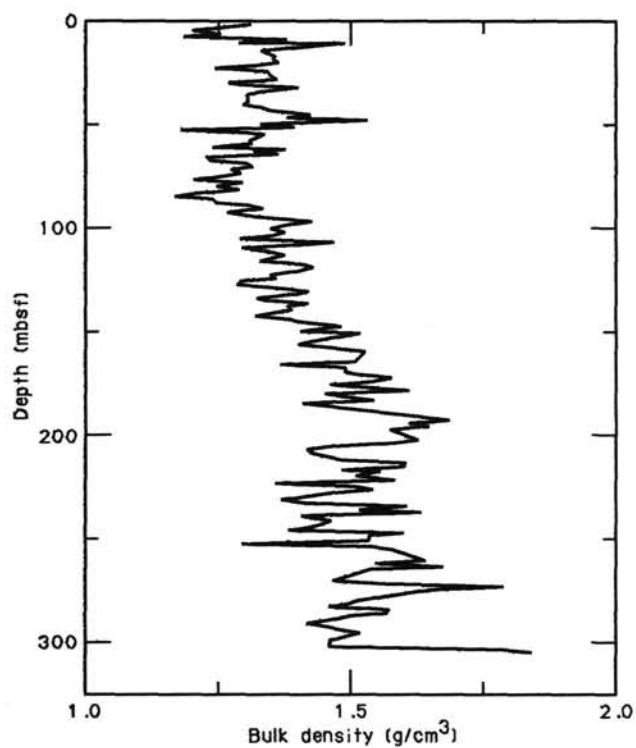


Figure 21. Bulk density variation with depth in Hole 677A.

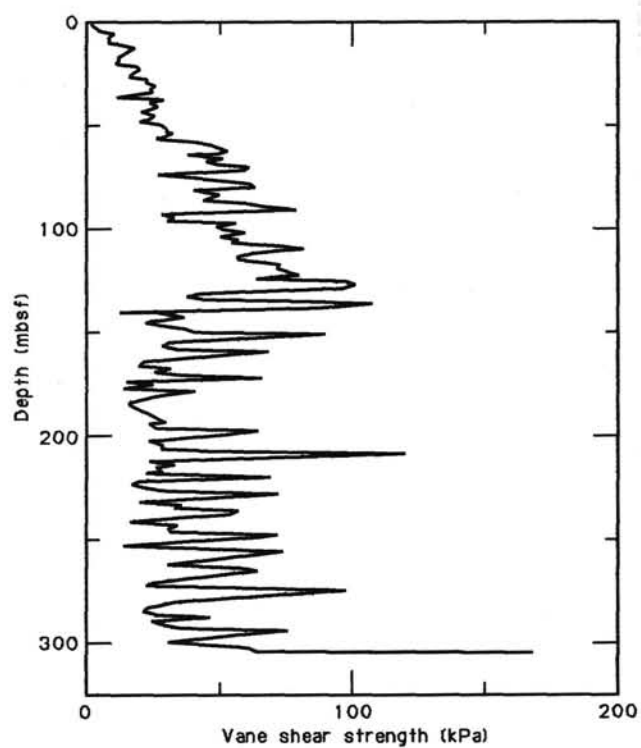


Figure 23. Vane shear strength variation with depth in Hole 677A.

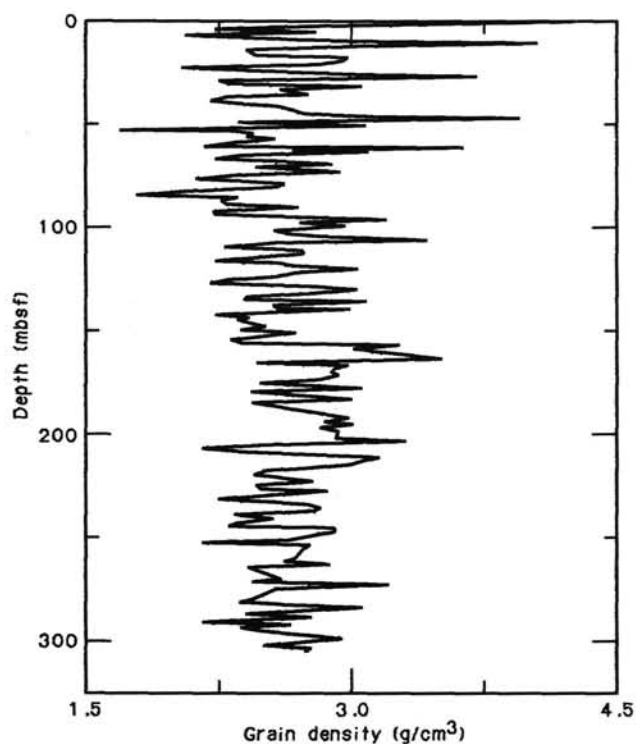


Figure 22. Grain density variation with depth in Hole 677A.

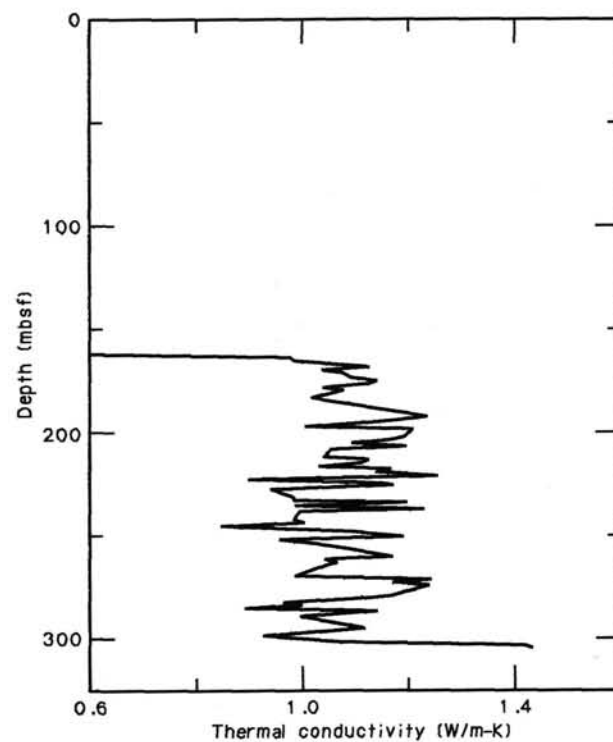


Figure 24. Thermal conductivity variation with depth in Hole 677A.

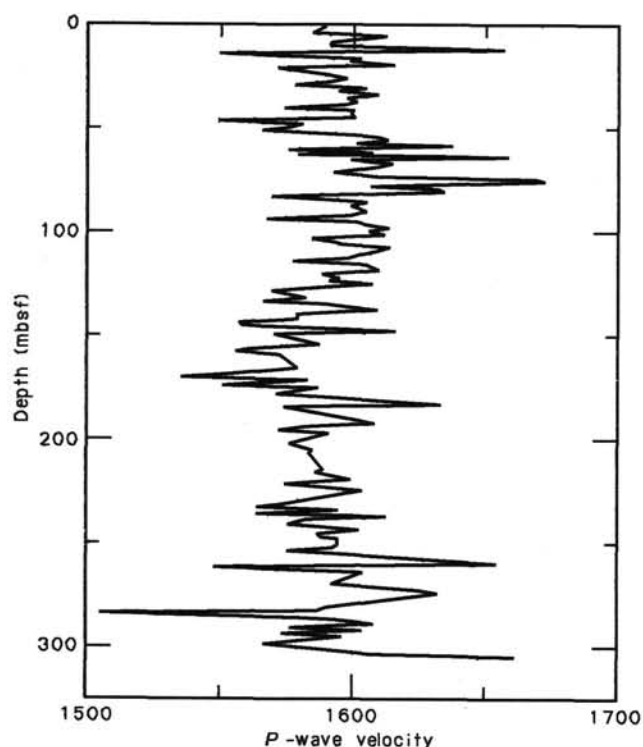


Figure 25. P-wave velocity variation with depth in Hole 677A.

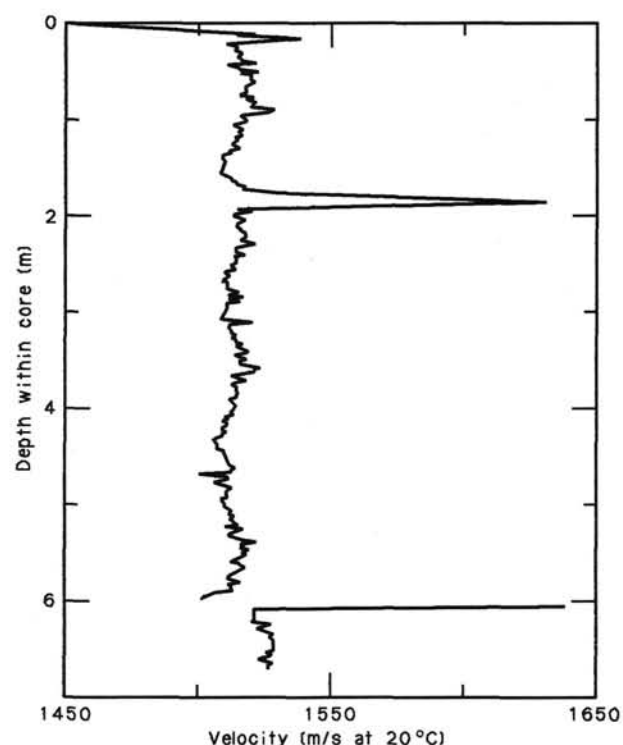


Figure 27. Data record for the P-wave logger; example from Core 111-677A-23X.

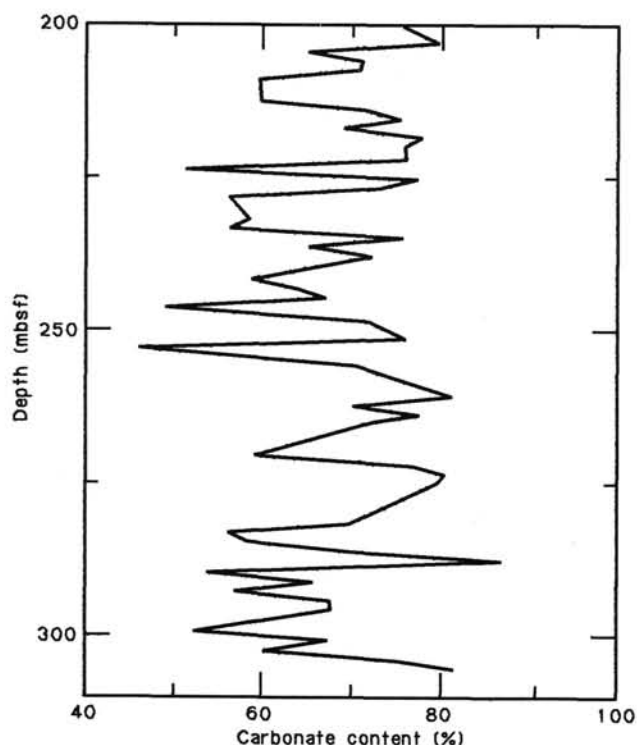


Figure 26. Carbonate content variation with depth in Hole 677A.

zons (see Figs. 35 through 42). The small number of measurements made over the 167 m drilled is reflected in each diagram by the use of a dotted line in showing trends between adjacent samples. The results for Hole 678B are tabulated in Table 10.

Index Properties

Figures 35 through 38 present results of the index property determinations for Hole 678B. The results correlate very well with those for the low-heat-flow site (Holes 677A and 677B), with porosity values ranging between 88% and 71% (bulk densities between 1.17 and 1.562 g/cm³). There is no obvious difference in the absolute values of the physical property measurements made in the topmost 104 m of Sites 677 and 678.

Vane Shear Strength

Measurements of shear strength yield similar values to Site 677 with an increasing trend through the top 98 m of 2.4–83.4 kPa. Below this depth there is a marked increase in shear strength at Hole 678B, occurring midway through Core 111-678B-3H (Fig. 39). The reasons for this are not as yet clear, though as discussed below, there are reasons for changes in shear strength which may be a product of the sampling procedure rather than the state of the *in-situ* material.

Thermal Conductivity

Thermal conductivity values determined for Hole 678B samples range between 0.813 and 1.111 W/m-K (Fig. 40). These are similar to the values determined for samples from Hole 677A over the same depth interval.

Compressional Wave Velocity (Hamilton Frame)

P-wave values measured on cores recovered from Hole 678B range between 1532 and 1632 m/s. There is no discernible trend although the values are similar to those for Hole 677A. Again

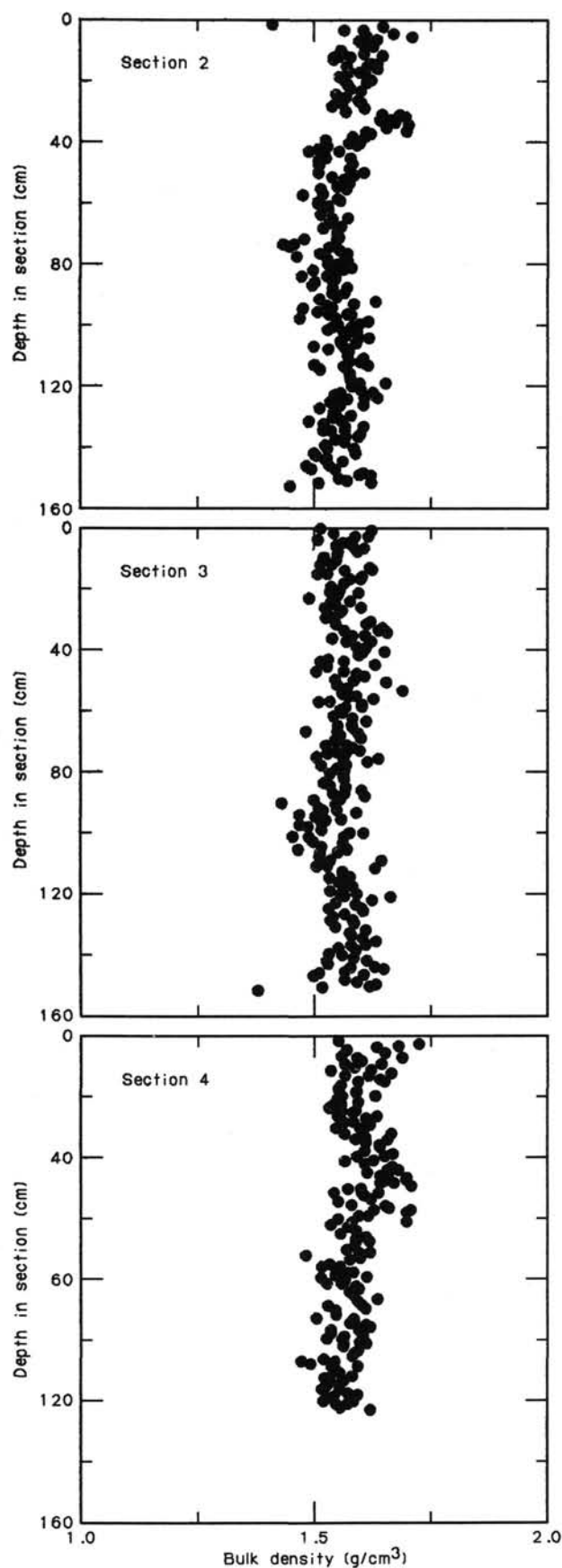


Figure 28. GRAPE data for three sections of Core 111-677A-23X.

Table 9. Summary of physical properties results for Hole 677B.

Core-section	Interval (cm)	Depth (mbsf)	Water content (%)	Grain density (g/cm ³)	Bulk density (g/cm ³)	Porosity (%)	Thermal conductivity (W/m-k)
1H-1	74-76	0.75	250.01	2.08	1.19	83.99	0.818
1H-2	74-76	2.25	229.68	2.28	1.23	83.98	0.929
1H-3	74-76	3.75	204.63	2.80	1.29	85.12	0.832
1H-4	74-76	5.25	240.32	2.83	1.26	87.18	0.826
1H-5	74-76	6.75	190.83	2.74	1.30	83.89	0.899
2H-1	74-76	8.35	215.35	2.15	1.22	82.27	0.903
2H-2	74-76	9.85	155.90	3.00	1.38	82.30	0.906
2H-3	74-76	11.35	184.88	2.34	1.27	81.20	0.928
2H-4	74-76	12.85	200.24	2.90	1.30	85.26	0.875
2H-5	74-76	14.35	174.81	3.02	1.34	84.00	0.880
2H-6	74-76	15.85	173.97	2.70	1.32	82.41	0.884
3H-1	74-76	17.85	174.46	3.05	1.35	84.10	0.842
3H-2	74-76	19.35	154.94	2.36	1.31	78.43	1.073
3H-3	74-76	20.85	191.47	3.23	1.33	86.02	0.852
3H-4	74-76	22.35	163.32	2.31	1.29	78.99	0.941
3H-5	74-76	23.85	184.19	2.24	1.26	80.50	0.818
3H-6	74-76	25.35	163.67	2.61	1.33	80.94	0.872
4H-1	74-76	27.35	146.06	2.32	1.32	77.14	0.907
4H-2	74-76	28.85	173.26	2.23	1.27	79.41	1.021
4H-3	74-76	30.35	158.92	2.64	1.34	80.67	0.914
4H-4	74-76	31.85	124.50	3.27	1.47	80.15	0.954
4H-5	74-76	33.35	182.51	2.87	1.32	83.90	0.851
4H-6	74-76	34.85	135.77	3.14	1.43	80.85	0.901
5H-1	74-76	36.85	166.46	2.81	1.45	76.42	1.026
5H-2	74-76	38.35	134.21	3.10	1.43	80.50	0.882
5H-3	74-76	39.85	186.94	2.62	1.30	83.01	0.890
5H-4	74-76	41.35	178.69	2.21	1.26	79.75	0.877
5H-5	74-76	42.85	141.88	3.29	1.43	82.24	0.846
5H-6	74-76	44.35	116.16	2.70	1.43	75.68	0.950
6H-1	74-76	46.35	153.34	2.34	1.31	78.12	0.898
6H-2	74-76	47.85	151.00	3.04	1.39	82.00	0.855
6H-3	74-76	49.35	137.46	2.35	1.34	76.24	0.952
6H-4	74-76	50.85	144.75	2.64	1.36	79.13	0.900
6H-5	74-76	52.35	131.82	2.53	1.37	76.79	0.938
6H-6	74-76	53.85	161.57	2.33	1.30	78.95	0.945
7H-1	74-76	55.85	135.44	2.68	1.38	78.29	0.839
7H-2	74-76	57.35	166.98	2.33	1.29	79.50	0.928
7H-3	74-76	58.85	131.31	3.01	1.43	79.65	0.981
7H-4	74-76	60.35	150.17	2.69	1.36	80.09	0.964
7H-5	74-76	61.85	150.88	2.58	1.34	79.47	0.881
7H-6	74-76	63.35	130.14	3.22	1.45	80.57	0.929
8H-1	74-76	65.35	180.92	2.36	1.28	81.03	0.824
8H-2	74-76	66.85	206.99	2.85	1.29	85.49	0.813
8H-3	74-76	68.35	170.15	2.98	1.35	83.43	0.872
8H-4	74-76	69.85	189.88	2.36	1.27	81.76	0.821
8H-5	74-76	71.35	215.87	2.55	1.26	84.62	0.774
8H-6	74-76	72.85	212.27	2.23	1.23	82.58	0.819
9H-1	74-76	74.85	202.18	2.62	1.28	84.08	0.824
9H-2	74-76	76.35	222.59	2.74	1.27	85.91	0.807
9H-3	74-76	77.85	189.74	2.46	1.28	82.31	0.837
9H-4	74-76	79.35	172.68	2.74	1.32	82.45	0.862
9H-5	74-76	80.85	233.64	2.61	1.25	85.94	0.724
9H-6	74-76	82.35	229.68	2.60	1.25	85.68	0.738
10H-1	74-76	84.35	227.41	1.96	1.20	81.81	0.714
10H-2	74-76	85.85	196.17	2.20	1.25	81.19	0.829
10H-3	74-76	87.35	138.74	2.23	1.32	75.47	0.930
10H-4	74-76	88.85	145.41	2.78	1.37	80.04	0.902
10H-5	74-76	90.35	155.31	2.90	1.37	81.73	0.859
10H-6	74-76	91.85	151.04	2.22	1.30	76.94	0.899

the measured values are higher than those determined using the PWL. Figure 41 is a plot of *P*-wave velocity with depth for Hole 678B.

Carbonate Content

Figure 42 is a plot of carbonate content with depth. The values show marked variations over short depth intervals, similar to those evident in the results from Hole 677A.

PWL

Each of the cores recovered from Hole 678B was logged using the PWL. The results were again of high quality. Figure 43 is an example of the data obtained and shows the resolution possible. At the bottom of the logged interval (8.8–9.0 m) a calibration check is visible; this is where a water-filled core liner was placed on the carriage to check the validity of the reading.

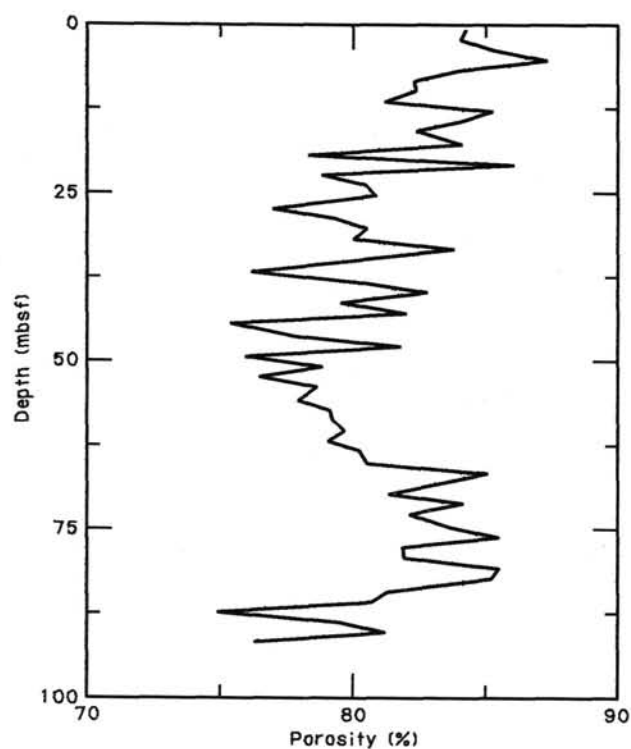


Figure 29. Porosity variation with depth in Hole 677B.

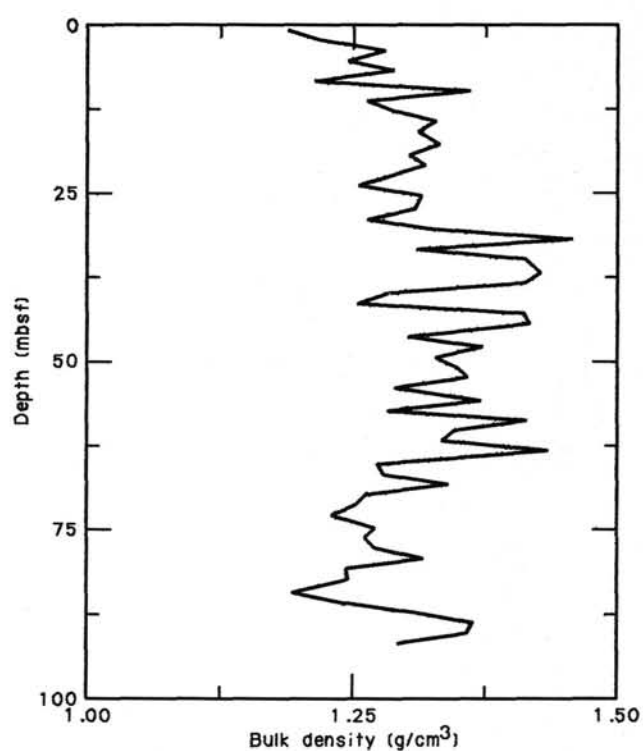


Figure 31. Bulk density variation with depth in Hole 677B.

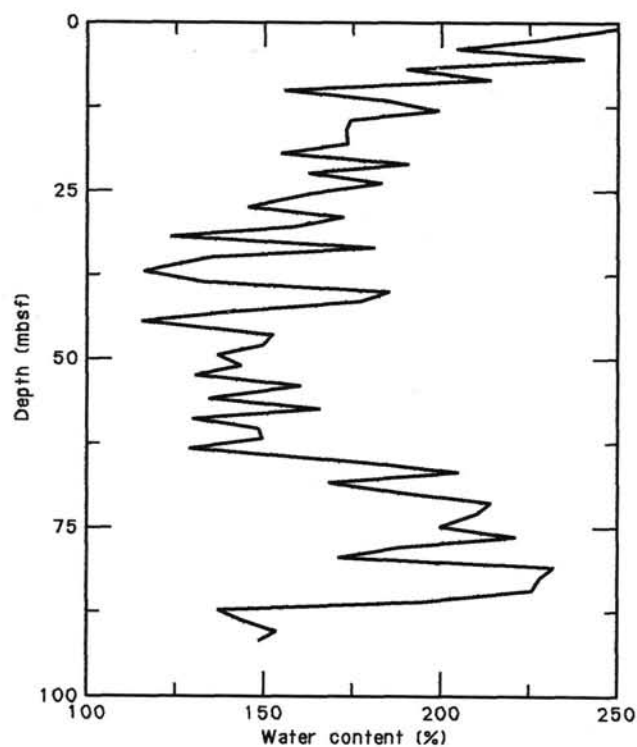


Figure 30. Water content variation with depth in Hole 677B.

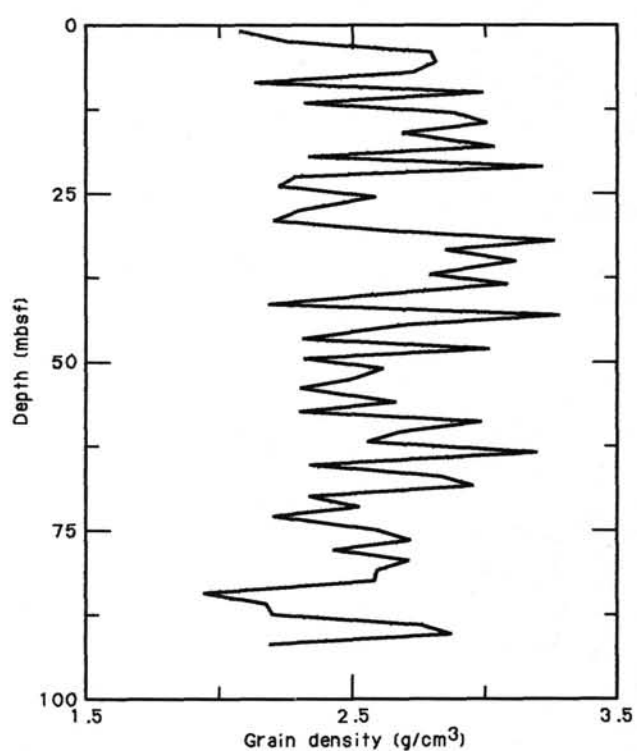


Figure 32. Grain density variation with depth in Hole 677B.

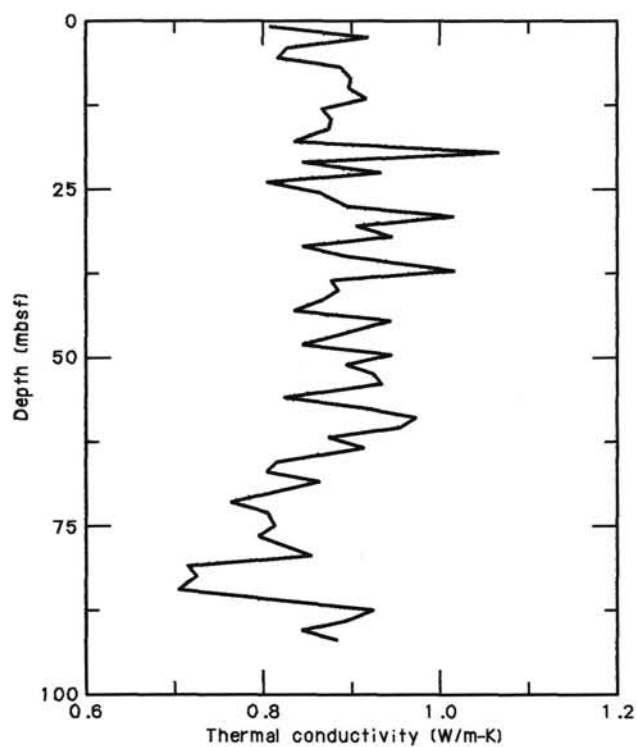


Figure 33. Thermal conductivity variation with depth in Hole 677B.

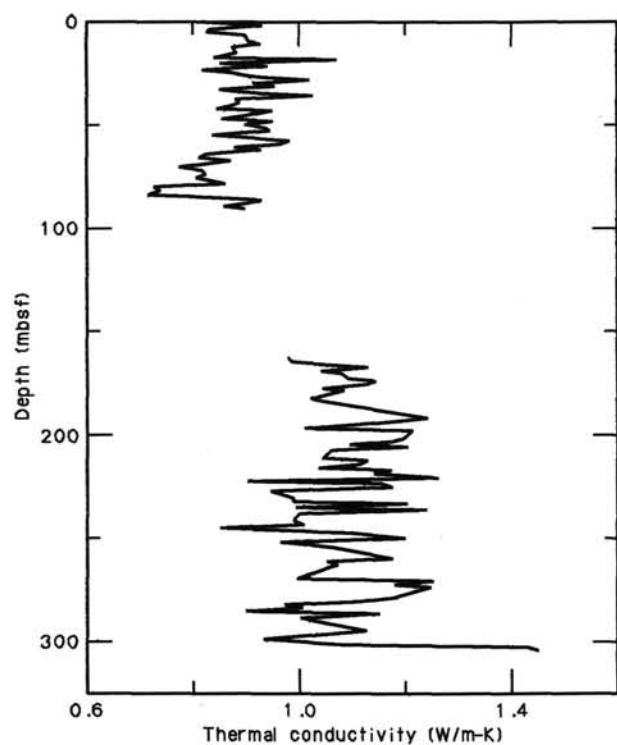


Figure 34. Thermal conductivity variation with depth; composite plot for Holes 677A (lower) and 677B (upper).

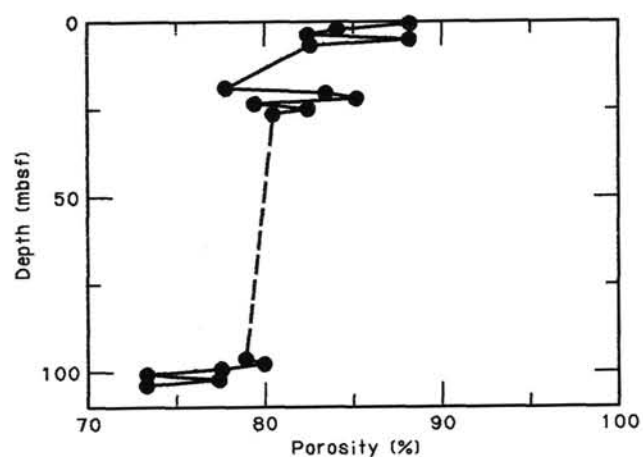


Figure 35. Porosity variation with depth in Hole 678B.

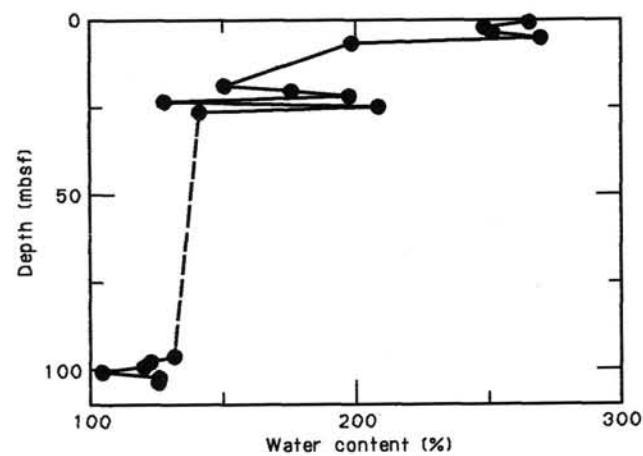


Figure 36. Water content variation with depth in Hole 678B.

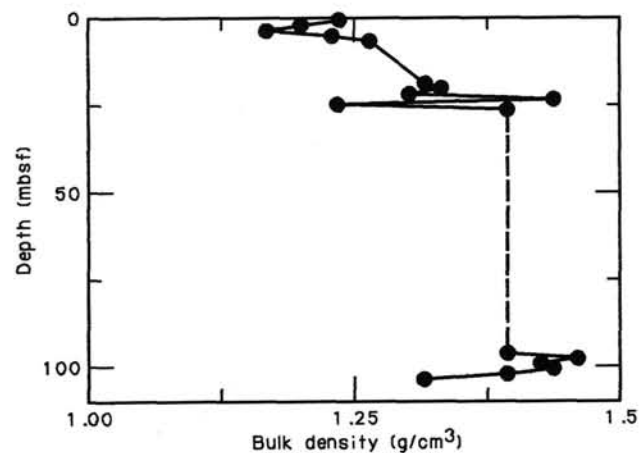


Figure 37. Bulk density variation with depth in Hole 678B.

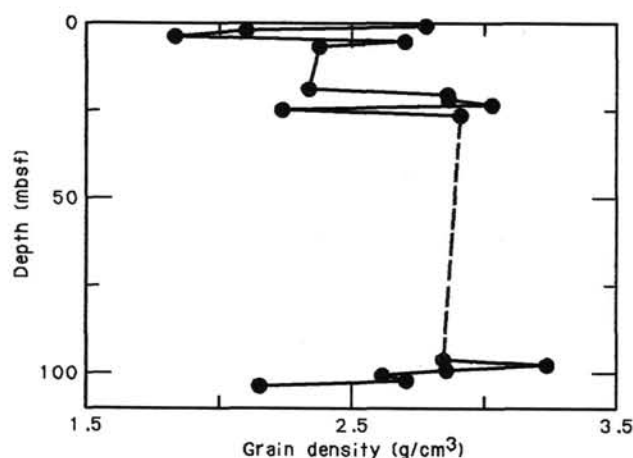


Figure 38. Grain density variation with depth in Hole 678B.

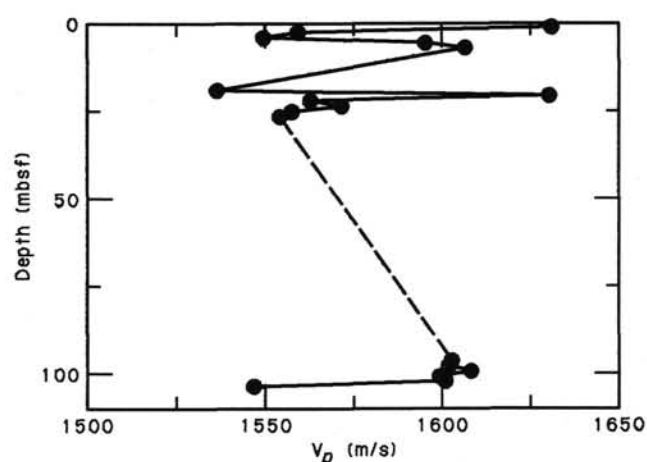
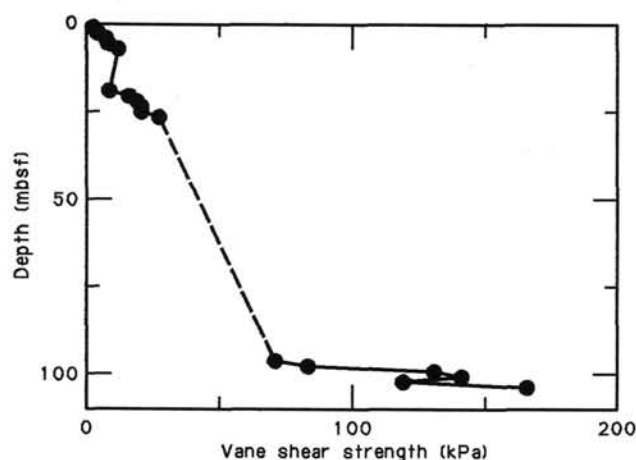
Figure 41. *P*-wave velocity variation with depth in Hole 678B.

Figure 39. Vane shear strength variation with depth in Hole 678B.

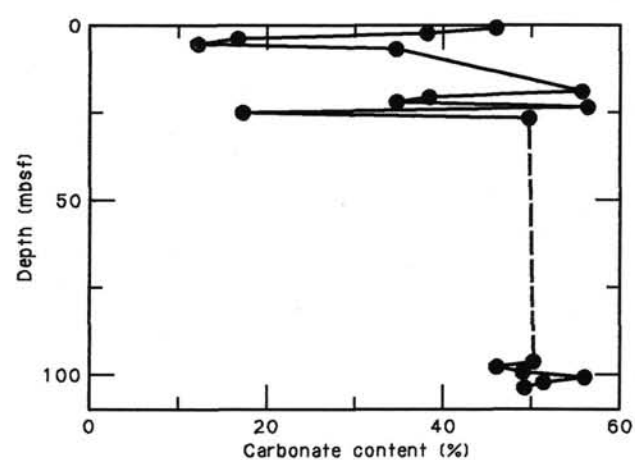


Figure 42. Carbonate content variation with depth in Hole 678B.

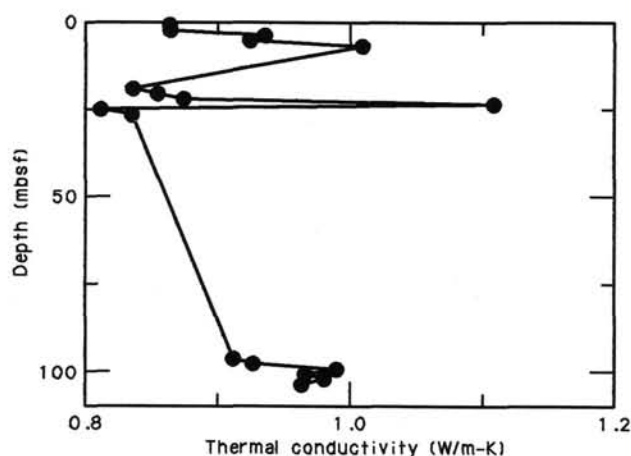


Figure 40. Thermal conductivity variation with depth in Hole 678B.

GRAPE

Simultaneous with the PWL logging, the sections from the same core were run through the GRAPE. Figure 44 shows an example of the data obtained for Hole 678B.

Discussion

Thermal conductivity/porosity relationships: the relationship between thermal conductivity and porosity for marine sediments has been precisely documented over the past 30 yr (Woodside and Messmer, 1961; Sass et al., 1971; Lovell, 1985). Figures 45 and 47 present the results for each of the sediment holes in turn. Figure 46 combines the results for Holes 677A and 677B, while Figure 48 is a composite of the results for both these two and Hole 678B. There is an obvious trend discernible, though in the light of the carbonate content results it may be preferable to consider the results in terms of a dual model involving volumetric components of both quartz and carbonate (e.g., Lovell, 1985).

***P*-wave results:** The velocity of sound in marine sediments is well documented (Clay and Medwin, 1977; Lovell and Ogden, 1985). Generally there is a simple relationship with porosity for saturated sediments (Nafe and Drake, 1957; Taylor-Smith, 1974). Given the porosity measured for Sites 677 and 678, together with the good propagation pulse through the samples which suggests there is little gas present, the values determined using the Hamilton Frame appear to be on the high side. In contrast the results from the *P*-wave logger are more reasonable and, perhaps, if anything, verge on the low side. The errors involved in both measuring systems can be considerable. The *P*-wave logger relies on the maintenance of a good contact between the transducer faces and the core liner, and the complete filling of

Table 10. Summary of physical properties results for Hole 678B.

Core-section	Interval (cm)	Depth (mbsf)	Water content (%)	Grain density (g/cm ³)	Bulk density (g/cm ³)	Porosity (%)	Shear strength (kPa)	Thermal conductivity (W/m-K)	P-wave velocity (m/s)	CaCO ₃ content (%)
1H-1	74-76	0.75	263.17	2.78	1.24	87.99	2.38	0.862	1631.5	46.53
1H-2	74-76	2.25	247.47	2.11	1.20	84.00	4.24	0.862	1560.0	38.71
1H-3	74-76	3.75	250.97	1.83	1.17	82.31	7.07	0.933	1550.7	16.85
1H-4	74-76	5.25	267.79	2.71	1.23	87.91	8.01	0.924	1596.5	12.00
1H-5	74-76	6.75	198.57	2.38	1.26	82.53	11.31	1.007	1607.5	34.98
2H-1	74-76	18.95	150.57	2.34	1.32	77.85	8.39	0.836	1537.3	56.35
2H-2	74-76	20.45	176.37	2.87	1.33	83.46	16.02	0.855	1631.6	38.91
2H-3	74-76	21.95	198.04	2.88	1.30	85.03	19.07	0.874	1564.3	35.12
2H-4	74-76	23.45	128.46	3.04	1.44	79.47	20.59	1.111	1573.3	57.18
2H-5	74-76	24.95	209.22	2.25	1.24	82.48	20.59	0.813	1559.6	17.61
2H-6	74-76	26.45	141.90	2.93	1.40	80.47	27.46	0.836	1556.7	50.52
3H-1	74-76	96.25	133.87	2.88	1.41	79.25	70.94	0.918	1604.9	51.06
3H-2	74-76	97.75	124.82	3.27	1.47	80.15	83.40	0.933	1604.6	46.79
3H-3	74-76	99.25	122.57	2.89	1.44	77.82	131.10	0.996	1610.9	49.60
3H-4	74-76	100.70	106.45	2.65	1.45	73.65	141.80	0.972	1601.1	56.87
3H-5	74-76	102.20	128.06	2.74	1.41	77.67	119.10	0.987	1603.1	52.19
3H-6	74-76	103.70	128.57	2.18	1.33	73.60	166.80	0.970	1549.4	49.86
4W-1	74-76		139.92	2.77	1.38	79.33		0.918		49.91
4W-3	74-76		100.60	2.96	1.52	74.67		1.076		58.03
4W-4	74-76		99.213	2.52	1.45	71.22		1.072		65.04

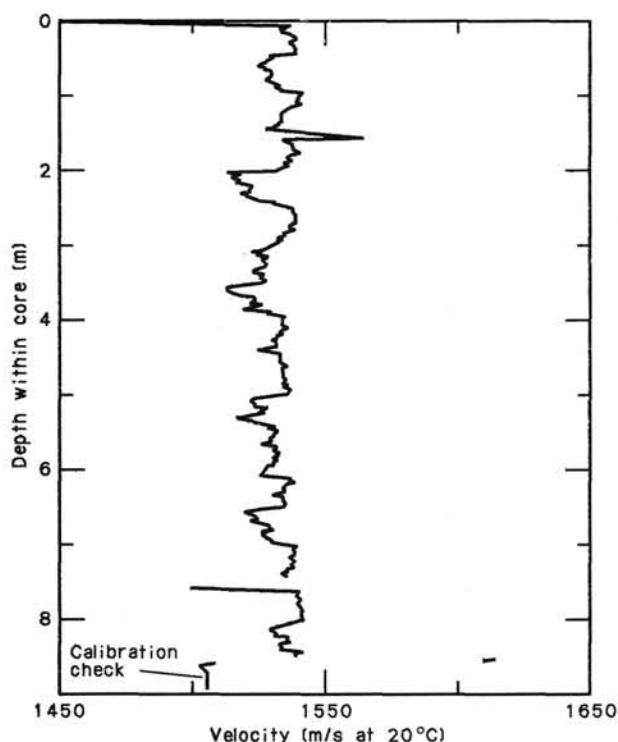


Figure 43. Data record for the P-wave logger; example from Core 111-678B-8H.

the core by the sampled sediment. The presence of gas or air gaps will drastically affect the results, while incompletely filled cores where the remaining space is water filled will yield particularly low velocities. It is possible that some of the core reflects the latter in particular; the XCB cores are especially prone to poor sampling results. Alternately, the Hamilton Frame is not designed for measurements on soft sediments. The propagation of the acoustic pulse again relies on good contact between the transducers and sediment, but in this case necessitates contact and, consequently, pressure between the transducer and split-core sediment surface.

Figures 49 and 50 show plots of Hamilton Frame velocity with porosity for both Sites 677 and 678. Both plots exhibit considerable scatter with no discernible trends evident. In the light of this discussion, velocities determined with the Hamilton Frame should be treated with caution in any detailed analysis.

Vane shear strength patterns: the overall trend discernible in Figure 23 of increasing shear strength with depth for Hole 677A appears at first to be a reasonable supposition. Replotting the data, however, at a larger scale, shows there to be a remarkable cyclicity throughout the hole (Figs. 51 through 53). The visible nature of the oscillations increases with increasing depth. A quick-look analysis, involving no numerical manipulation of the data, produces a figure of around 9 m for the wavelength of the pattern. This suggests that the results may be reflecting the length of the cores and, in turn, be artifacts, at least in part, of the coring procedure. A similar cyclicity is evident in other physical parameters (e.g., porosity as in Fig. 54), but requires further analyses before any firm conclusions can be reached. Initial reaction, however, suggests that the physical properties of sediments sampled by coring should be carefully reviewed to ensure that any effects related to core disturbance are recognized.

TEMPERATURE MEASUREMENTS

A major objective of the 5-day program of sediment coring at Sites 677 and 678 was to obtain detailed profiles of temperature with depth, to assess the modes of heat transfer through the sediments, and to estimate basement temperatures. Sites 677 and 678 were located within 3 km of Site 504, but in different geothermal regimes: Whereas crustal heat flow at Site 504 appears to be conductive, at the value predicted for conductive cooling of 5.9-m.y.-old crust, the surface heat flows at Sites 677 and 678 are respectively lower and higher than the predicted value.

The patterns of surface heat flow (Fig. 1) and chemical gradients in pore waters of piston cores ("Sediment Pore-Water Chemistry" section, this chapter) indicate that convection of pore fluids occurs at slow rates through the 250- to 300-m-thick sediment cover in the region. This is somewhat inconsistent with observations of basically conductive heat transfer and relatively impermeable basement in Hole 504B, except for the upper 100-200 m of basement, which is quite permeable ("High-Temperature Measurements after Return to Thermal Equilibrium" and "Permeability Measurements in the Sheeted Dikes" sections,

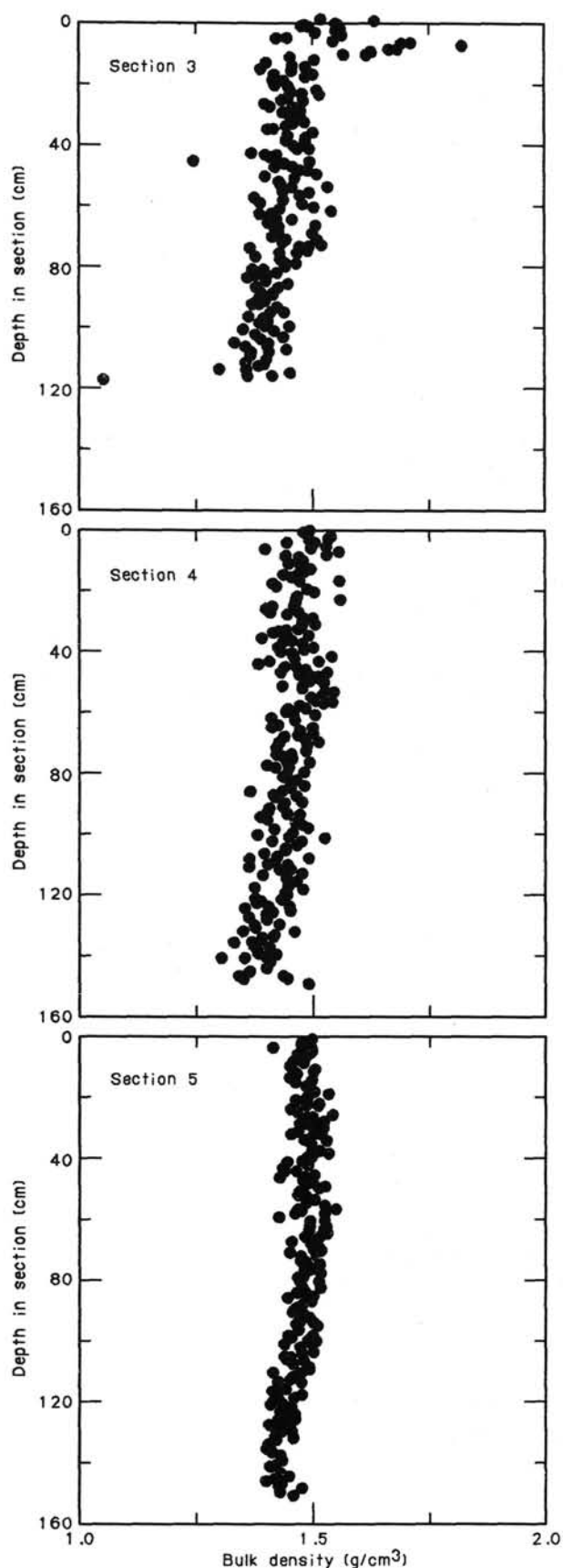


Figure 44. GRAPE data for three sections of Core 111-678B-8H.

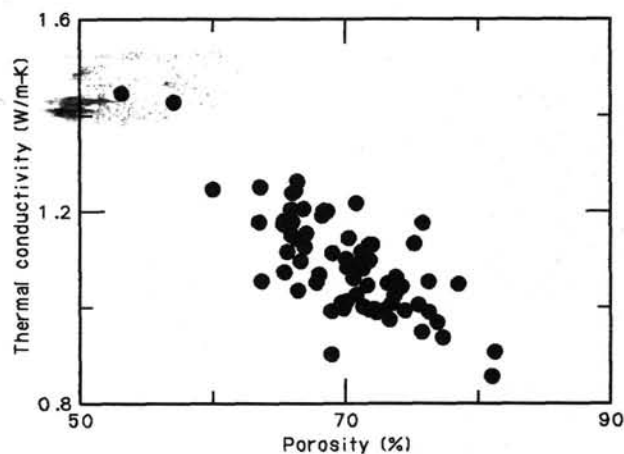


Figure 45. Thermal conductivity variation with porosity for Hole 677A.

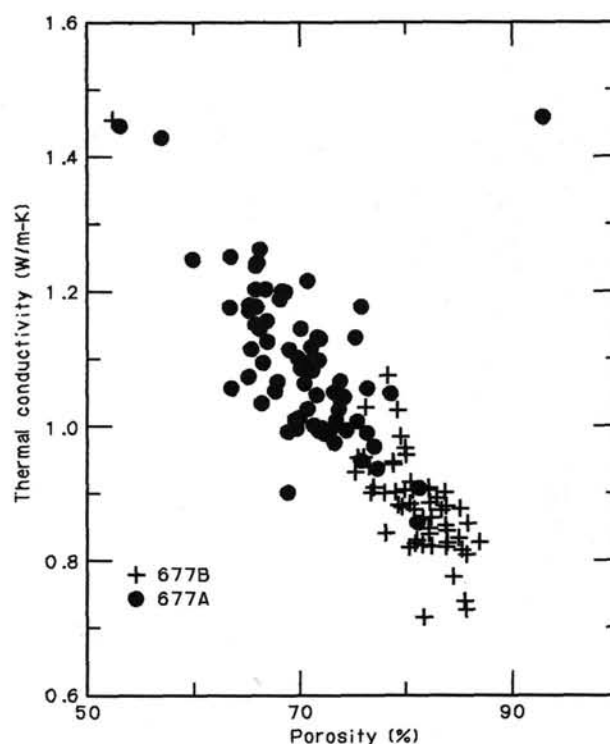


Figure 46. Thermal conductivity variation with porosity for Site 677, Holes 677A and 677B.

Site 504 chapter, this volume). The wavelength of the variation of surface heat flow in the area is on the order of 5 km, which would suggest depths of convection much greater than the 100- to 200-m-thick permeable section of basement (Langseth et al., this volume). It therefore appears that the subdued convection that occurs may be controlled by irregular features in the basement structure—e.g., variations in basement topography or major faults within basement.

Accurate measurements of temperature and thermal conductivity at Sites 677 and 678 were required to provide estimates of velocities of pore-water flow independent of the estimates obtained from chemical gradients in the pore waters ("Sediment Pore-Water Chemistry" section, this chapter). Unfortunately, operational problems and instability of the temperature probes

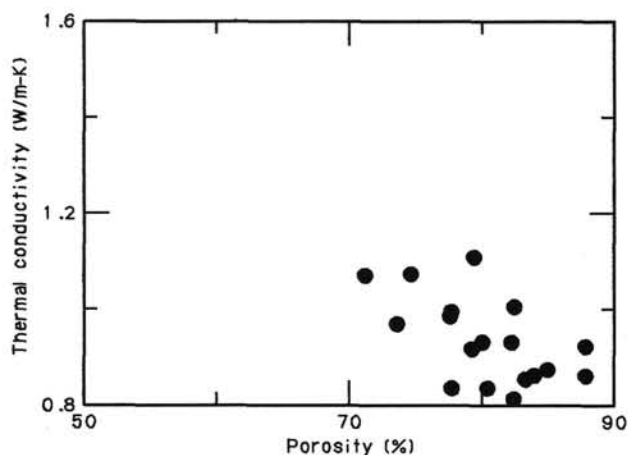


Figure 47. Thermal conductivity variation with porosity for Hole 678B.

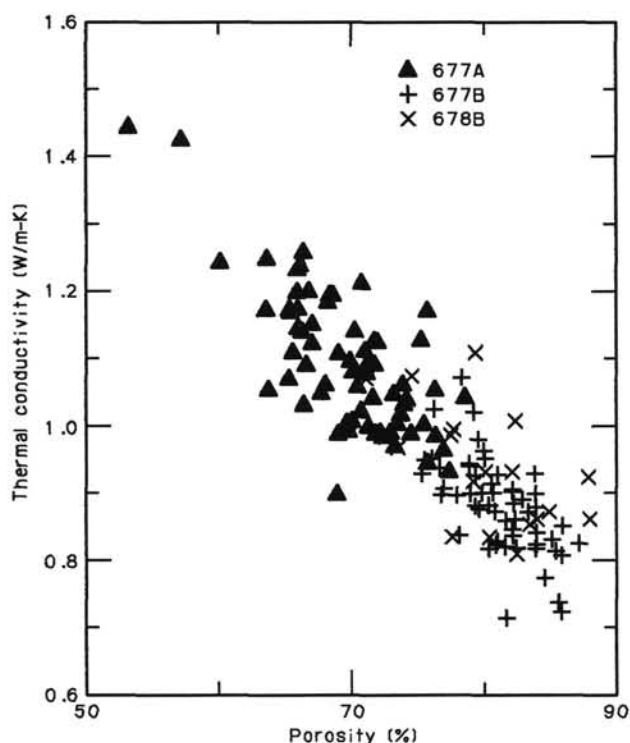


Figure 48. Thermal conductivity variation with porosity for Holes 677A, 677B, and 678B.

in the sediments degraded the temperature data collected at these sites to the extent that we could make no assessment of pore-water movement, and we could make only a preliminary estimate of basement temperature at Site 677.

Methods

We attempted to measure *in-situ* temperatures at five depths in Hole 677A, three depths in Hole 677B, and two depths in Hole 678B. We used the APC temperature recorder (Horai and Von Herzen, 1985) during normal APC cores to depths of about 100 m, where the force required to pull the APC from the sediments reached limits that were unsafe. Deeper in Hole 677A, we used the same tool in tandem with the ODP (Barnes/Current) temperature probe, which samples pore waters and measures

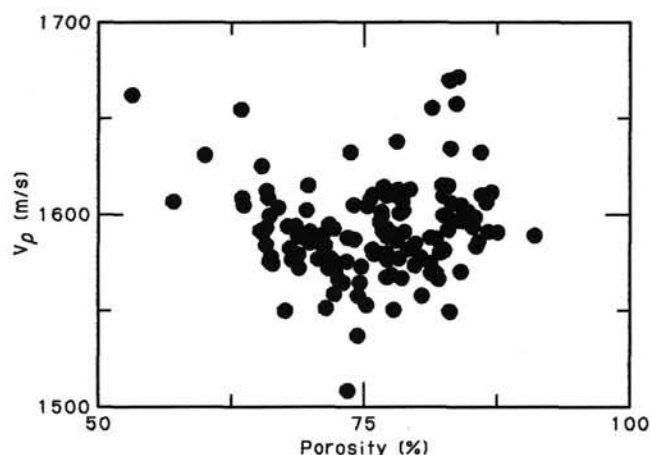


Figure 49. P-wave velocity variation with porosity for Hole 677A.

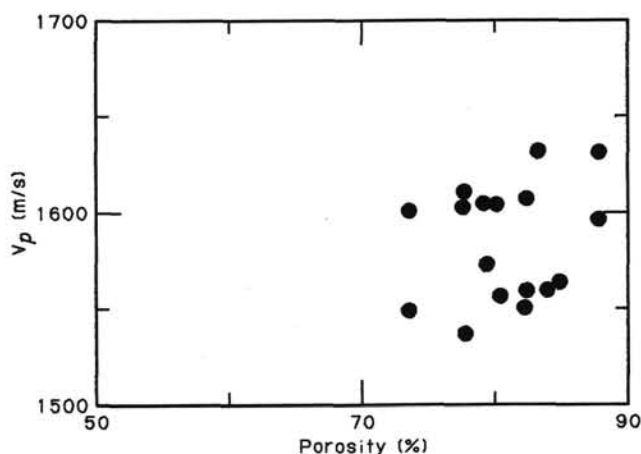


Figure 50. P-wave velocity variation with porosity for Hole 678B.

temperature and pressure (see Mascle, Moore, Taylor, et al., in press).

Unfortunately, of the 10 deployments of the APC tool, 3 collected no data because of battery failures, and the first of the 2 deployments of the ODP temperature probe also failed because of insufficient battery power. The program of temperature measurements at Site 678 was aborted because the last of only three batteries available for the APC tool failed, and because time constraints did not allow extra time to be taken to run the ODP temperature probe tool. The 12 tool deployments at Sites 677 and 678 are summarized in Table 11.

Results

Only 7 of the 12 tool runs collected data, which are shown in Figures 55 through 61. Only one measurement of temperature was made in Hole 678B and it is of questionable quality because the probe and pipe apparently sank slowly through the shallow sediments as the measurement was being made (Fig. 61). Nothing could be concluded from this measurement about thermal processes at Site 678.

Of the six tool runs at Site 677 that actually collected temperature data, three also appeared to have been disturbed by motion of the probe in the sediment (Figs. 56 through 58). Only the measurements at 34.7 mbsf in Hole 677A (Fig. 55) and at 26.6 and 93.1 mbsf in Hole 677B (Figs. 59 and 60) appeared to yield data from which *in-situ* temperatures could be reliably ob-

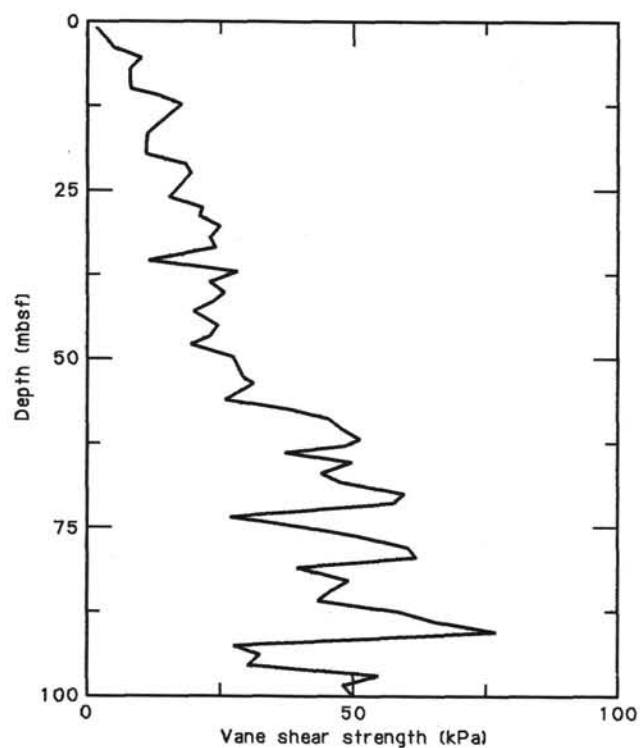


Figure 51. Vane shear strength variation with depth for the upper part of Hole 677A.

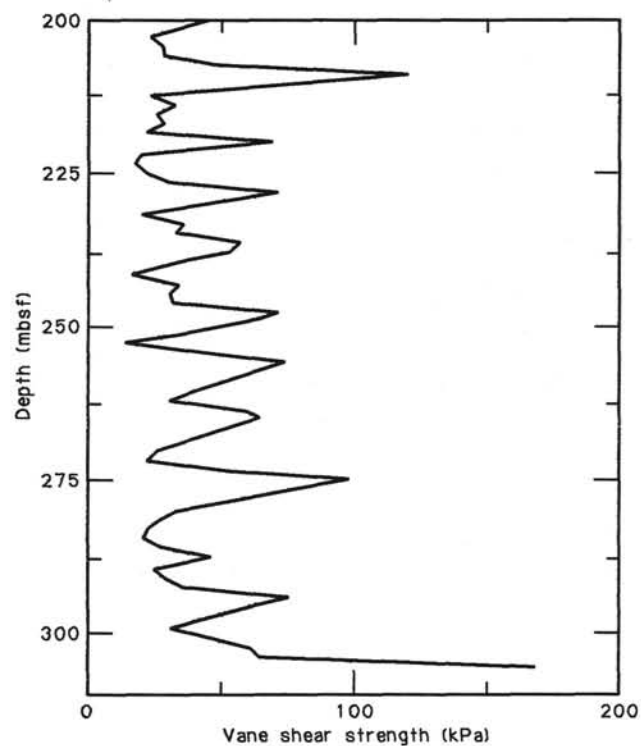


Figure 53. Vane shear strength variation with depth for the lower part of Hole 677A.

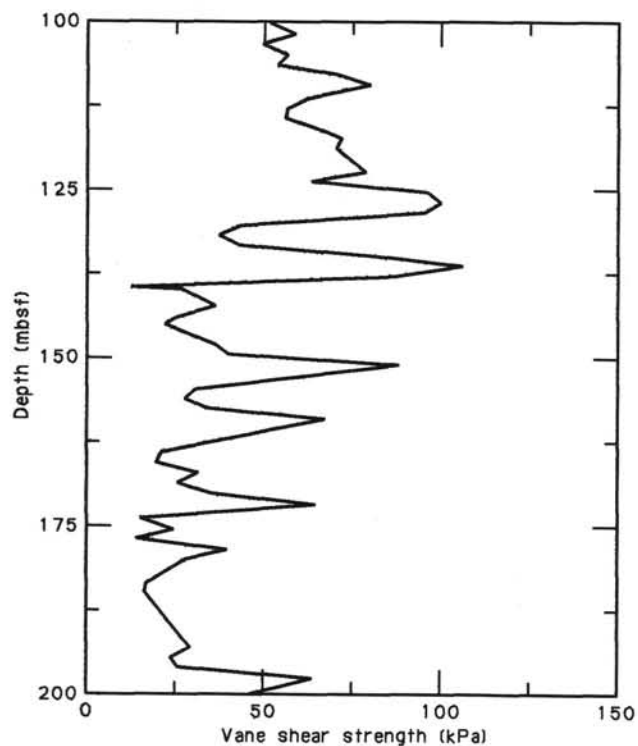


Figure 52. Vane shear strength variation with depth for the middle part of Hole 677A.

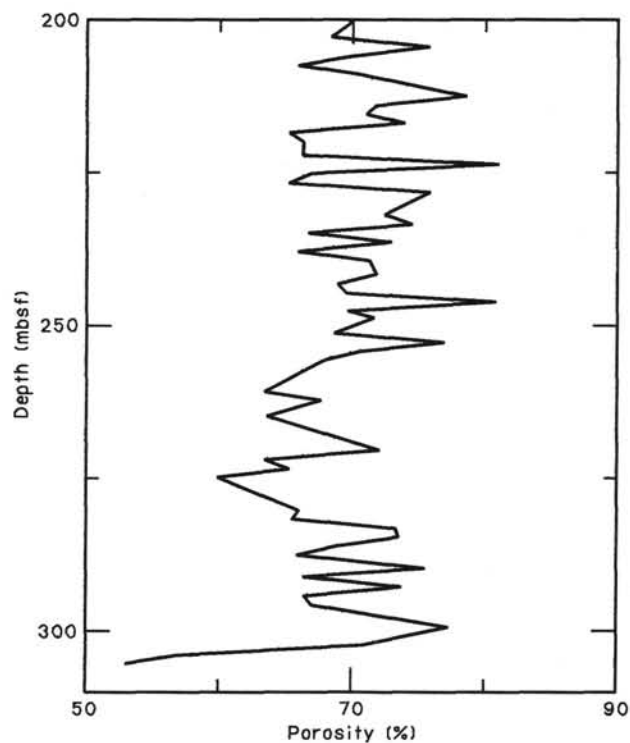


Figure 54. Porosity variation with depth for the lower part of Hole 677A.

Table 11. Summary of attempted temperature measurements, Sites 677 and 678.

Hole	Core	Depth (mbsf)	Data collected?	Data quality
677A	4H	34.7	yes	good
	8H	72.7	no	—
	11H	101.2	yes	fair—probe sinking
	19X	173.2	no - battery failed	—
	19X	173.2	no - battery failed	—
*	23X	212.4	yes	bad—probe motion
	23X	212.4	yes	poor—probe motion
	3H	26.6	yes	good
677B	6H	55.1	no - battery failed	—
	10H	93.1	yes	excellent
	2H	27.7	yes	fair—probe sinking
678B	2H	27.7	yes	fair—probe sinking
	3H	105.0	no - battery failed	—

Note: The APC tool was used, except for the two deployments marked with asterisks which were made with the ODP (Barnes/Current) tool.

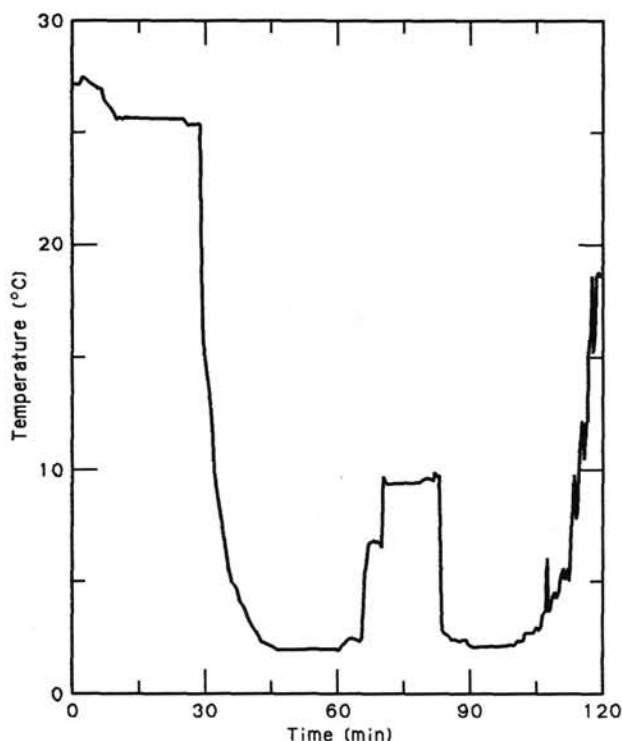


Figure 55. Temperatures measured with the APC temperature tool during Core 111-677A-4H at 34.7 mbsf in Hole 677A.

tained. These data were all obtained with the APC temperature tool, which is frictionally heated on penetration and slowly returns to *in-situ* temperature. The mathematical formulation for the approach to *in-situ* temperature of this tool is very complicated and must be solved numerically (Horai and Von Herzen, 1985); to determine *in-situ* temperature, the measured data must be carefully fit in an iterative program to minimize misfit to the best possible theoretical decay curve. As there were some problems with the shipboard version of the computer program that performs this fitting of data to the best decay curve, the data were not processed during Leg 111.

Nevertheless, Figure 62 shows a first-order attempt to construct a thermal profile at Site 677. The three temperature points plotted were obtained by approximating *in-situ* temperatures directly from the portions of the temperature records that ap-

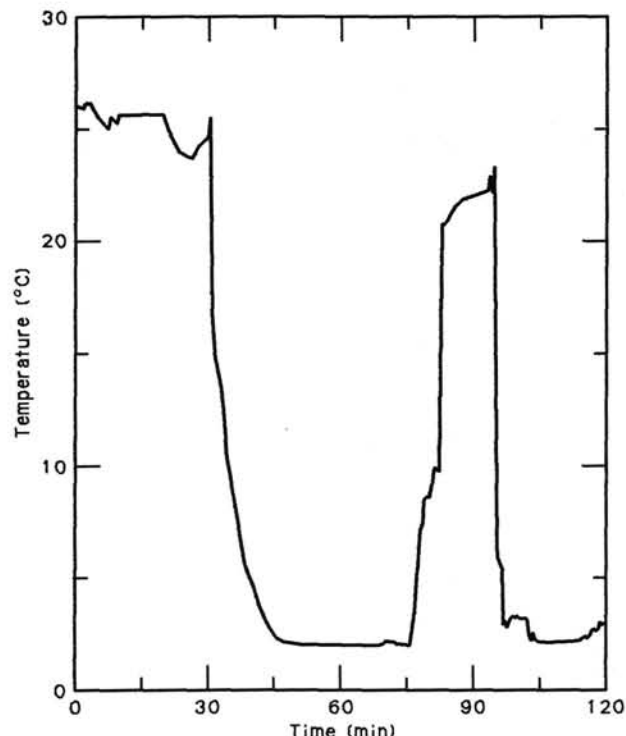


Figure 56. Temperatures measured with the APC temperature tool during Core 111-677A-11H at 101.2 mbsf in Hole 677A.

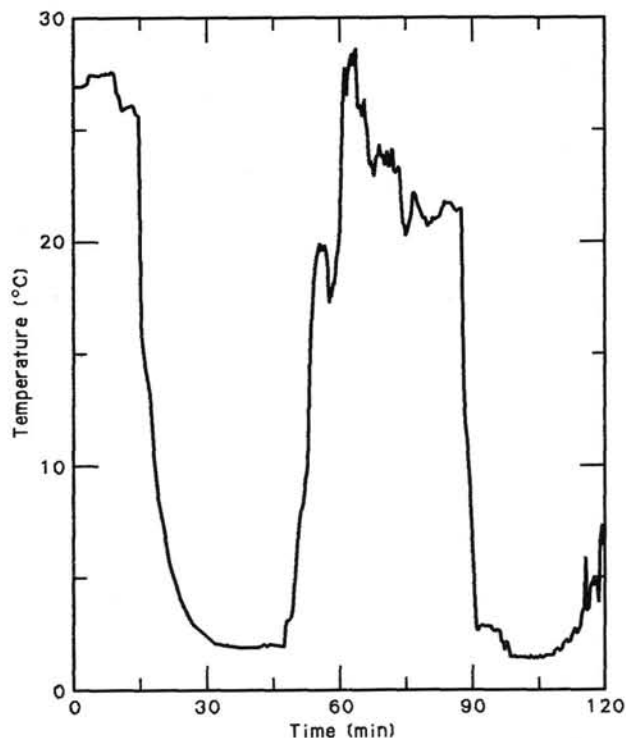


Figure 57. Temperatures measured with the APC temperature tool at 212.4 mbsf in Hole 677A.

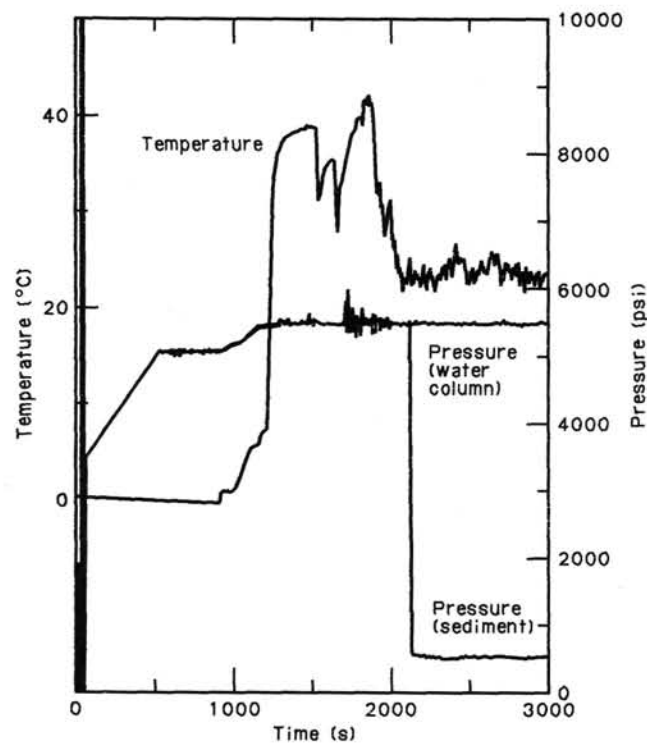


Figure 58. Temperatures and pressures measured with the ODP temperature probe at 212.4 mbsf in Hole 677A.

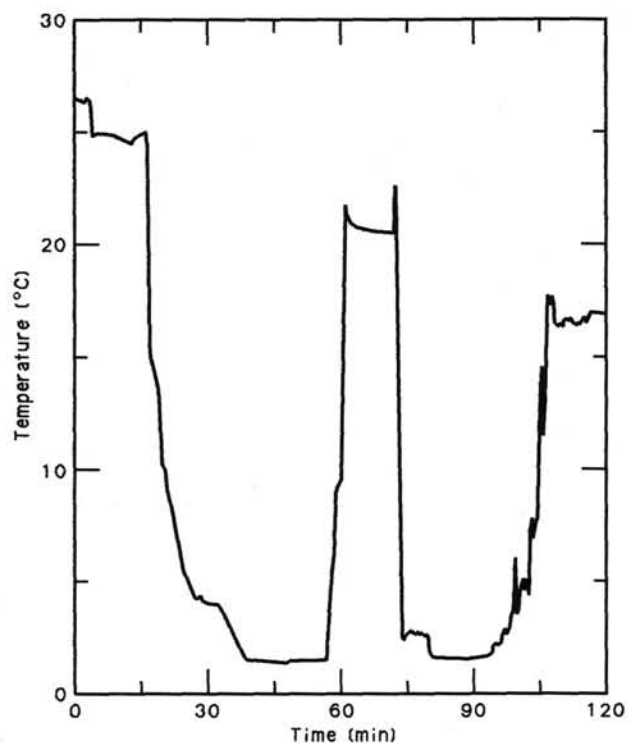


Figure 60. Temperatures measured with the APC temperature tool during Core 111-677B-10H at 93.1 mbsf in Hole 677B.

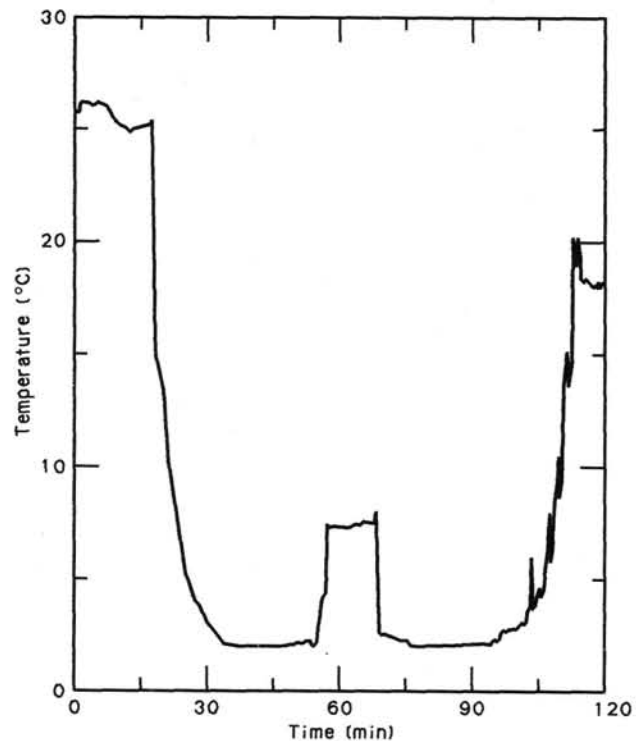


Figure 59. Temperatures measured with the APC temperature tool during Core 111-677B-3H at 26.6 mbsf in Hole 677B.

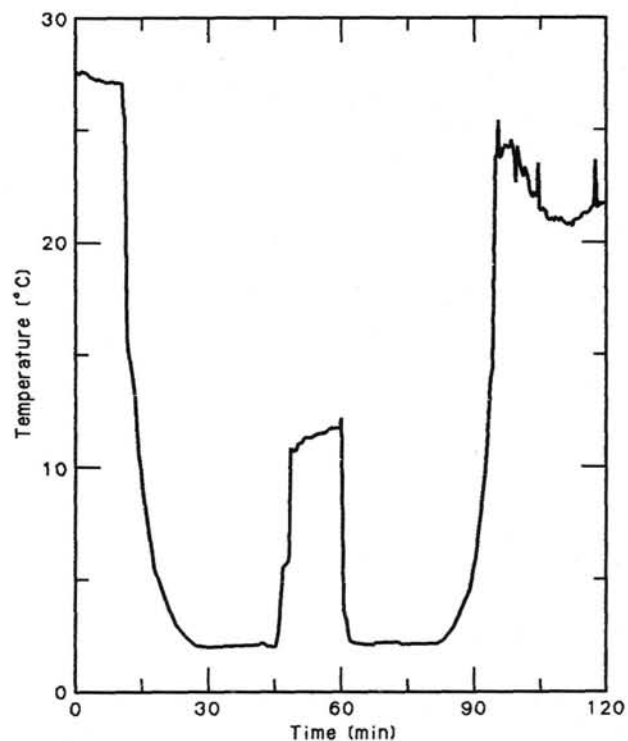


Figure 61. Temperatures measured with the APC temperature tool during Core 111-678B-2H at 27.7 mbsf in Hole 678B.

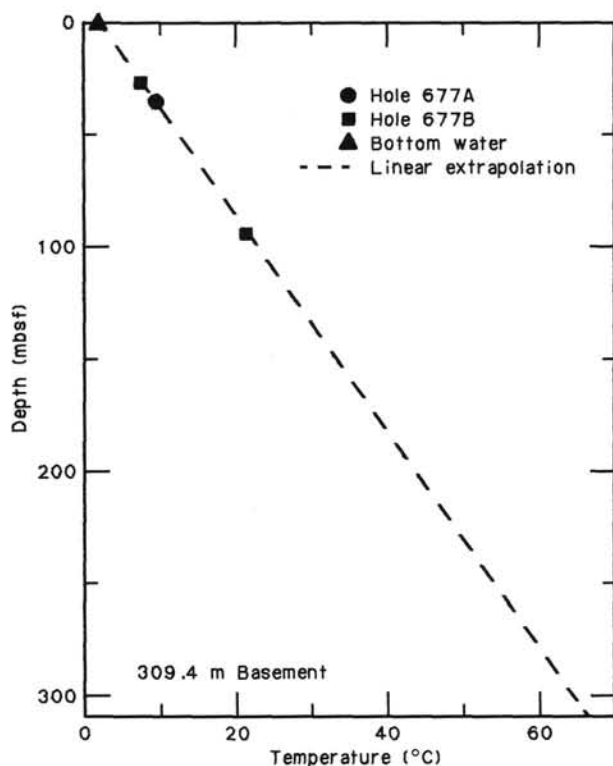


Figure 62. Preliminary profile of temperatures measured in Holes 677A and 677B.

peared to have stabilized after penetration. A constant shift was applied to adjust all temperatures measured in the pipe at mud-line depths to the well-known bottom water temperature value of 2.01°C; this correction was particularly required for the measurement at 93.1 mbsf in Hole 677B, during which the recorded mud-line temperatures were seriously in error—0.6°C too low.

Fig. 62 indicates that temperatures in the upper 100 m of Site 677 are basically linear; this observation is consistent with either purely conductive heat transfer or slow recharge of ocean bottom water through the sediments. The temperature measurements that failed deeper at the site might have allowed us to resolve between these two possibilities. A linear regression of the three data points gives a gradient of 0.208°C/m. Given an average thermal conductivity of 0.9 W/m-K ("Physical Properties" section, this chapter), this yields an estimated surface heat flow of 187 mW/m²—about 10% higher than predicted from site survey data (Fig. 1).

If the gradient in the upper 100 m is extrapolated linearly to the basement depth of 309.4 m, it yields a basement temperature on the order of 60–70 °C. However, this is probably not a valid extrapolation, because it does not account for two probable effects:

1. If mostly conductive heat flow occurs at the site, the increase of thermal conductivity with depth would produce a corresponding decrease in the gradient with depth.
2. If slow recharge of pore fluids or ocean bottom water occurs, as pore fluid chemistry indicates ("Sediment Pore-Water Chemistry" section, this chapter), the gradient would increase close to basement.

It will be possible to produce a more refined estimate of temperature at the sediment-basement contact, once the temperature and thermal conductivity data are fully processed, and given

an estimate of the pore-water recharge rate from gradients in pore-water chemistry.

ORGANIC CARBON

At Sites 677A, 677B, and 678B, sediment residues of the interstitial water squeezing process were analyzed for total carbon content and for carbonate content (Table 12 and Figs. 63 and 64). A 10–30-mg sample sufficed for both analyses. Total organic carbon (TOC) was determined by difference between the total carbon (measured with the CO₂ Coulometer) and the carbonate carbon (measured with the Coulometrics Carbonate Carbon Apparatus, Coulometer). This method is less time consuming than direct measurement of TOC in acidified samples and avoids the loss of organic matter by hydrolysis during treatment with HCl, especially in young, diagenetically immature sediments. Results of the carbonate (inorganic carbon) analyses are discussed in "Sedimentology and Lithostratigraphy" section (this chapter).

Hole 677A

In general, TOC values at Hole 677A range between 0.01 and 2.98 wt%, averaging 0.42 wt%. Lithologic Unit I (0–153.8 mbsf) consists of alternating clayey calcareous siliceous oozes and clayey siliceous calcareous oozes and is characterized by relatively high TOC values, which vary between 0.19 and 2.98 wt% (mean value 0.75 wt%). The maximum value of 2.98 (Sample 111-677A-9H-3, 120–125 cm) occurs in siliceous ooze. In Lithologic Unit II (153.8–303.3 mbsf), which is composed of siliceous nannofossil ooze and siliceous nannofossil chalk, lower TOC values between 0.01 and 0.40 wt% (mean value 0.16 wt%) occur. In Lithologic Unit III (303.3–308.5 mbsf), the organic carbon contents vary between 0.10 and 0.18 wt% (mean value 0.14 wt%). One sample in Lithologic Unit IV (308.5–309.4 mbsf) contains 0.19 wt% TOC.

The sediments between 0 and 100 mbsf are relatively rich in organic carbon. The apparent decrease in TOC content observed as a function of depth may be due to early diagenesis.

Hole 677B

Hole 677B is offset from Hole 677A by 10–30 m. Sediments were recovered from 0 to 93.1 mbsf. All cores consisted of alternating clayey calcareous siliceous ooze and clayey siliceous calcareous ooze, which correlates with Lithologic Unit I in Hole 677A. TOC contents are relatively high, ranging between 0.21 and 10.80 wt%, averaging 2.55 wt%. These values are consistent with those from 0 to about 100 mbsf in Hole 677A despite the much higher mean values. The greatest content of TOC is found around 90 mbsf, just as in Hole 677A.

Hole 678B

In Lithologic Unit I (gray green to olive clayey calcareous radiolarian-diatom ooze), TOC contents range between 0.07 and 5.13 wt%, averaging 1.51 wt%. Near-surface sediments show high contents of TOC, which is consistent with high TOC values in shallow parts of Hole 677A. Lithologic Unit II consists of siliceous nannofossil ooze and siliceous nannofossil chalk. TOC contents range from 0.23 to 0.50 wt%. Lithologic Unit III consists of limestone, which ranges from pink to greenish in color. TOC contents are relatively low, ranging from 0.01 to 1.03 wt%, averaging 0.27 wt%.

High TOC values are found only in sediments within 10 m of the surface. Lower TOC contents which are typical of deeper sediments may be due to early diagenesis.

SUMMARY AND CONCLUSIONS

From 30 September to 5 October, Leg 111 spent slightly more than 5 days in coring the sediments at Sites 677 and 678 near

Table 12. Total organic carbon (TOC) and CaCO₃ in squeezed sediments from Holes 677A, 677B, and 678B.

Core, section (interval in cm)	Depth (mbsf)	CaCO ₃ (wt%)	TOC (wt%)
677A			
1-3, 145-150	4.5	21.19	0.58
2-1, 80-89	7.0	17.37	0.96
3-4, 120-125	21.4	35.34	1.12
4-1, 55-74	25.8	52.29	0.67
5-1, 51-69	35.3	40.42	0.58
6-3, 120-125	48.4	45.43	0.73
9-3, 120-125	76.9	20.10	2.98
12-4, 120-125	106.9	36.58	0.41
13-4, 145-150	116.7	62.97	0.22
14-4, 145-150	126.2	38.92	0.75
15-4, 120-125	135.4	50.41	0.33
16-4, 145-150	145.2	64.81	0.26
17-3, 145-150	148.7	63.16	0.19
18-3, 120-125	158.0	56.06	0.30
19-4, 145-150	169.5	65.70	0.10
20-4, 145-150	179.2	98.10	0.33
22-3, 120-125	196.6	73.59	0.12
23-4, 145-150	208.1	79.06	0.13
24-4, 145-150	217.7	62.03	—
25-4, 120-125	227.1	75.55	0.02
26-4, 145-150	237.1	65.33	0.23
27-4, 145-150	246.8	72.17	0.01
28-3, 120-125	254.6	59.98	0.15
29-3, 145-150	264.5	68.52	0.17
30-3, 145-150	274.2	84.58	0.12
31-4, 120-125	285.0	70.40	0.40
32-4, 145-150	294.9	62.51	0.09
33-2, 145-150	301.6	64.10	0.12
33-4, 145-150	304.6	81.11	0.10
34-CC, 23-31	308.9	56.01	0.19
33-5, 123-140	305.9	77.07	0.18
677B			
1-1, 95-100	1.0	27.68	1.72
1-2, 145-150	3.0	47.78	2.24
2-1, 145-150	9.1	23.41	1.08
2-3, 145-150	12.1	53.88	1.33
3-1, 145-150	18.6	49.47	1.03
3-4, 145-150	23.1	51.12	0.21
4-1, 145-150	28.1	30.86	2.51
4-3, 145-150	31.1	34.98	2.02
5-1, 145-150	37.6	49.32	1.41
5-3, 145-150	40.6	32.21	2.71
6-4, 120-125	51.4	43.45	1.49
7-4, 145-150	61.1	83.05	—
8-2, 145-150	70.6	47.18	1.83
9-1, 145-150	80.1	18.74	5.28
10-4, 145-150	89.6	55.98	10.80
678B			
1-1, 45-50	0.5	12.58	5.13
1-1, 145-150	1.5	11.88	3.88
1-2, 145-150	3.0	40.30	1.19
1-4, 145-150	6.0	40.32	0.69
2-1, 45-50	18.7	52.20	0.49
2-1, 145-150	19.7	41.94	0.07
2-2, 145-150	21.2	41.32	0.81
2-4, 145-150	24.2	34.09	0.75
2-5, 145-150	25.7	52.74	0.61
3-1, 145-150	97.0	60.00	0.23
3-3, 120-125	99.7	40.27	0.50
3-6, 145-150	104.5	58.04	0.38
4-2, 55-67	138.0	65.05	0.08
4-3, 95-107	138.9	60.45	—
4-4, 145-150	139.9	65.14	0.15
4-CC, 3-15	168.9	88.52	—
4-CC, 18-25	169.0	76.75	—
4-CC, 30-42	169.2	53.63	—
4-CC, 50-60	169.4	5.20	0.08
5-CC, 36-47	169.7	37.97	1.03
4-CC, 3-15	168.9	81.72	0.01

Note: Carbonate contents were measured by carbonate bomb technique.

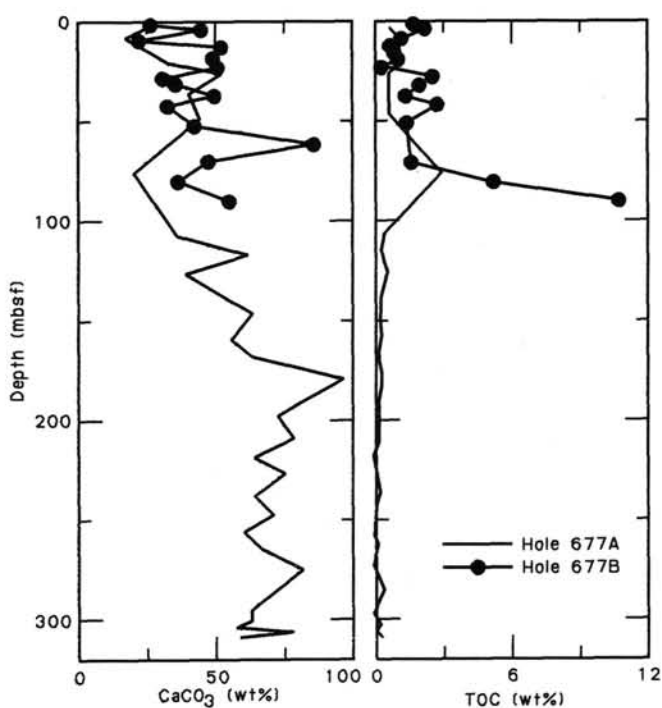


Figure 63. Total organic carbon (TOC) and carbonate carbon contents as a function of depth below seafloor in Site 677.

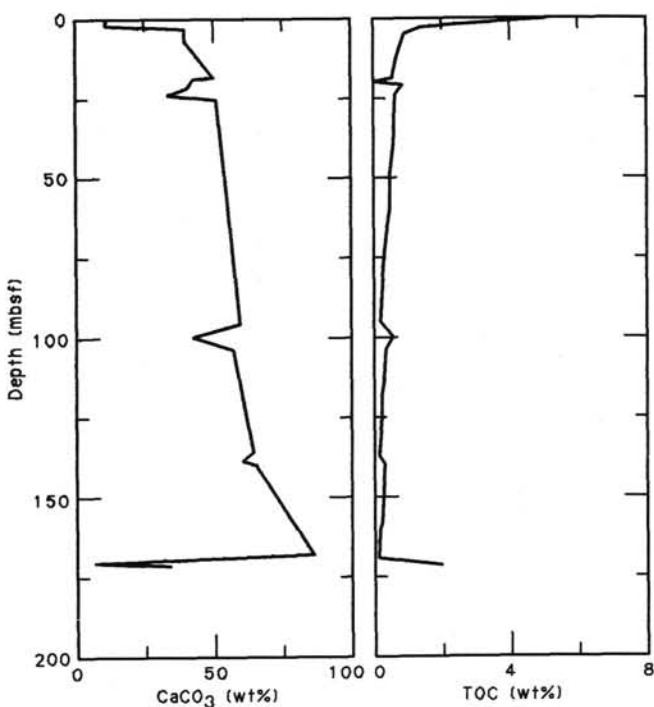


Figure 64. Total organic carbon (TOC) and carbonate carbon contents as a function of depth below seafloor in Site 678.

Site 504. Site 677 was located on a local minimum of heat flow, 3 km south of Hole 504B, in a water depth of 3461 m; Site 678 was located in a sharp maximum of heat flow about 1.5 km northeast of Site 677, in a water depth of 3425 m. Major objectives of the sediment coring at these sites were: (1) to recover a complete Pliocene-Pleistocene sedimentary record, especially at

the low-heat-flow site, for biostratigraphic and paleoceanographic studies, (2) to obtain sediment pore waters for chemical study of advective vs. diffusive exchange between the ocean bottom water and the basement underlying the sediment section, and (3) to compare diagenetic alteration in sediments between high- and low-heat-flow sites.

Two holes were drilled at Site 677, Hole 677A to basal sediments and altered basalt at 309.4 mbsf and Hole 677B, offset 10–30 m from Hole 677A, to 93.1 mbsf. The original drilling program at Site 677 had been to core two holes with the APC to refusal, then continue one of the holes to basement with the XCB. However, because time was short, the second hole, 677B, was terminated when Pliocene sediment was first recovered, thus assuring a complete Pleistocene sedimentary section.

The time problem was more severe at Site 678, where Hole 678B was cored only at specific stratigraphic intervals at 0–7.5, 18.2–27.7, 95.5–105.0, and 169.5–171.8 mbsf, with intervening intervals being washed down. The last core recovered fragments of basal basalt. Hole 678A was abandoned after two successive failures to obtain a good mud-line core.

Three major sedimentary units and a basal basalt unit are recognized at Site 677: Unit I consists of alternating clayey biogenic calcareous siliceous oozes and clayey biogenic siliceous calcareous oozes of early Pliocene to late Pleistocene ages, Unit II is composed of siliceous nannofossil oozes and chalk of late Miocene to early Pliocene ages, Unit III consists of cherty limestone and nannofossil chalk of late Miocene age, and Unit IV consists of iron oxide- and smectite-rich sediments intermixed with glassy basement basalts of late Miocene age. The sedimentary section of Site 678 may be divided into four similar units, although spot coring at this site makes precise comparison with Site 677 difficult.

The biochronological boundary between Pliocene and Pleistocene lies within Cores 111-677A-9H (72.7–82.2 mbsf) and 111-677B-9H (74.1–83.6 mbsf). The early/late Pliocene boundary is within Core 111-677A-17A. The Miocene/Pliocene boundary is placed in the middle of Core 111-677A-23X. The oldest sediment recovered in Hole 677A has an age of 5.6–5.9 m.y. The rate of sedimentation is surprisingly constant with a mean value of 42 m/m.y. over the last 5.6 m.y., although the first 0.3 m.y. of deposition had a much higher rate.

Unit IV in both Holes 677A and 678B consists of dark green and gray muds, intercalated with basalt pebbles and conglomerates, and calcite veins and aggregates. A 2 x 3 cm concretion of pyrite and marcasite was noted within these poorly indurated conglomerates of Hole 677A. Alteration of the basalts represents early diagenesis with very shallow burial, and possibly low-pressure/low-temperature hydrothermal processes. It is of special interest for interpretation of the pore-water chemistry (see below).

Pore waters were squeezed from the sediments including the smectite- and iron oxide-rich alteration products from the upper basement sections, at an interval of approximately 10 m in Holes 677A and 677B and at an interval of approximately 3 m in the spot cores of Hole 678B. The pore waters were analysed on board *JOIDES Resolution* for major (Ca, Mg, SO₄, Cl) and minor (Si, NH₄, NO₂ + NO₃, PO₄, H₂S) components. Except for the basal alteration products, sufficient amounts of pore-water samples could be squeezed from sediments to split aliquots for shore-based analyses of stable isotopes of water, trace heavy metals, amino acids, and sugars.

In pore waters squeezed from sediments from Holes 677A and 677B, Ca and Mg maintain almost the same concentrations to about 110 mbsf as those in overlying ocean bottom water. Below that, to just above the smectite-rich alteration products, Ca slowly increases, while Mg decreases, respectively reaching concentrations approximately 2 and 0.7 times those in the ocean

bottom water. However, Ca and Mg show drastic changes in concentration in the underlying basal alteration products of 14 m thickness; Ca increases to 7 times and Mg decreases to 0.2 times the concentration in the ocean bottom water.

In the pore waters from the sediments of Hole 678B, Ca and Mg exhibit depth profiles that contrast sharply with those at the low-heat-flow site; Ca quickly rises to a concentration close to 5 times that in seawater in the topmost 40 m of sediment, maintains the same concentration thereafter to the basement, where it again sharply increases to the same concentration as that encountered in Hole 677A. Mg shows a correspondingly rapid decrease to nearly 15% of the ocean bottom seawater value within the topmost 40 m of the Hole 678B sediments and, in the basal altered basalt, almost the same concentration as in Hole 677A was found.

Profiles for NH₄, Si, and PO₄ are dominated by reactions in the sediments. All of these species except PO₄ show large gradients near basement at Site 677 and near the seafloor at Site 678, again contrasting to each other. Alkalinity also is convex upward at Site 678.

These observations clearly indicate that ocean bottom seawater flows down through the 300-m-thick sediment into basement at the low heat flow Site 677, whereas significantly altered seawater formed in basement wells up through the 180-m-thick sediment into overlying seawater at the high-heat-flow Site 678. The rate of these flows estimated from the depth-composition profiles is approximately a few millimeters/year at both sites. The similarity in composition of pore water from the basal alteration products at both sites, however, suggests that the advective flow rates in sediment are negligible compared to those in basement.

In order to verify advective flow rates of pore water obtained from the chemical gradients, accurate measurements of temperature-depth profiles at both sites were attempted using the Von Herzen temperature probe and the Barnes/Current tool. However, battery failures resulted in only three acceptable temperature measurements in the upper 100 m at Site 677, from which the temperature at the sediment-basement contact is estimated to be roughly 60°C–70°C. The temperature profile measurement at Site 678 could not be determined.

In spite of the limitations in time and problems with equipment, the coring and subsequent shipboard studies at Sites 677 and 678 unambiguously demonstrated that the ocean bottom water and sediment-covered basement still exchange materials and heat, though slowly, through localized advection-recharge systems in the area of Sites 677/678, even though conductive heat loss predominates on a regional scale in this area. Further, a more comprehensive coring program including temperature measurements will help clarify the relative importance of advective vs. diffusive transport in sediments, in terms of thickness and nature of sediment, basement age, etc. The present results clearly indicated the usefulness of pore-water chemistry in such studies.

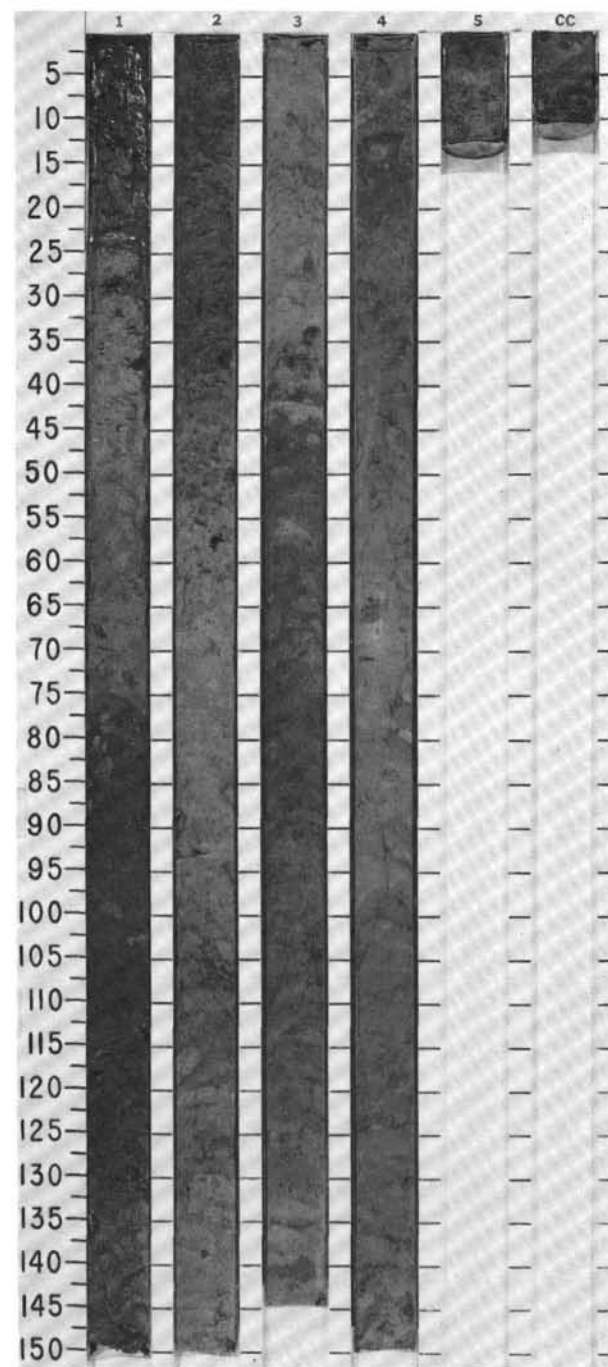
REFERENCES

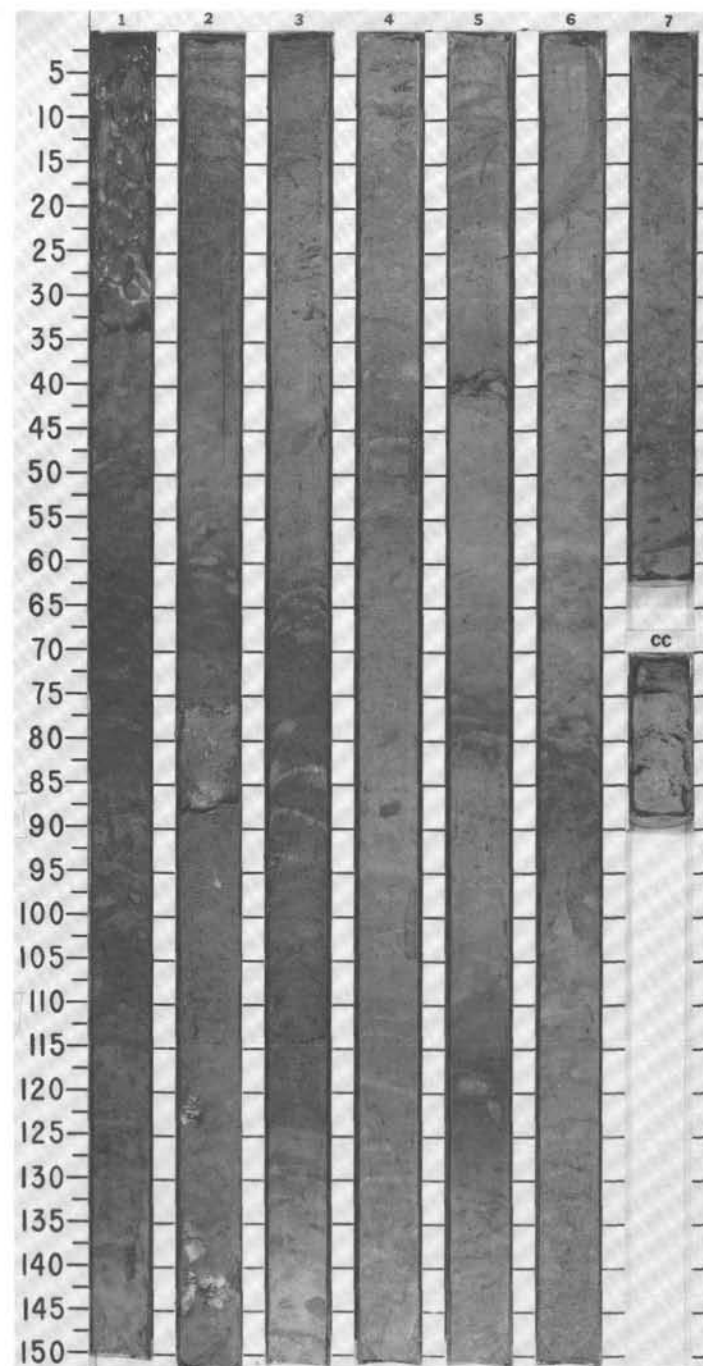
- Anderson, R. N., and Hobart, M. A., 1976. The relation between heat flow, sediment thickness, and age in the eastern Pacific. *J. Geophys. Res.*, 81:2968–2989.
- Backman, J., and Shackleton, N. J., 1983. Quantitative biochronology of Pliocene and early Pleistocene calcareous nannofossils from the Atlantic, Indian and Pacific Oceans. *Mar. Micropaleontol.*, 8:141–170.
- Boyce, R. E., 1973. Appendix I. Physical properties—methods. In Edgar, N. T., Saunders, J. B., et al., *Init. Repts. DSDP*, 15: Washington (U.S. Govt. Printing Office), 1115–1127.
- Bukry, D., 1980. Coccolith stratigraphy, tropical eastern Pacific Ocean, DSDP, Leg 54. In Hekinian, R., and Rosendahl, B. R., et al., *Init.*

- Repts. DSDP, 15: Washington (U.S. Govt. Printing Office), 535-545.
- Cann, J. R., Langseth, M. G., Honnorez, J., Von Herzen, R. P., White, S. M., et al., 1983. *Init. Repts. DSDP*, 69: Washington (U.S. Govt. Printing Office).
- Clay, C. S., and Medwin, H., 1977. *Acoustical Oceanography*: New York (John Wiley).
- Gartner, S., Jr., 1977. Calcareous nannofossil biostratigraphy and revised zonation of the Pliocene, *Mar. Micropaleontol.*, 2:1-25.
- Gieskes, J. L., and Peretsman, G., 1986. Water chemistry procedures aboard JOIDES Resolution—some comments. *ODP Tech. Note* 5.
- Goll, R. M., 1980. Pliocene-Pleistocene radiolarians from the East Pacific Rise and the Galapagos spreading center, DSDP Leg 54. In Rasendahl, B. R., Hakenian, R., et al., *Init. Repts. DSDP*, 54: Washington (U.S. Govt. Printing Office), 425-453.
- Hays, J. D., and Shackleton, N. J., 1976. Globally synchronous extinction of the radiolarian *Stylatractus universus*. *Geology*, 4:649-652.
- Horai, K., and Von Herzen, R. P., 1985. Measurement of heat flow on Leg 86 of the Deep Sea Drilling Project. In Heath, G. R., Burckle, L. H., et al., *Init. Repts. DSDP*, 86: Washington (U.S. Govt. Printing Office), 759-777.
- Jenkins, D. G., and Orr, W. N., 1972. Planktonic foraminifera biostratigraphy of the eastern equatorial Pacific, Leg 9. In Hays, J. D., et al., *Init. Repts. DSDP*, 9: Washington (U.S. Govt. Printing Office), 1059-1205.
- Johnson, D. A., and Nigrini, C. A., 1985. Synchronous and time-transgressive Neogene radiolarian datum levels in the equatorial Indian and Pacific oceans. *Mar. Micropaleontol.*, 9:489-523.
- Keigwin, L. D., Jr., 1982. Neogene planktonic foraminifera from Deep Sea Drilling Project Sites 502 and 503. In Prell, W. L., Gardner, J. V., et al., *Init. Repts. DSDP*, 68: Washington (U.S. Govt. Printing Office), 269-288.
- Kent, D. V., and Spariosu, D. J., 1983. Magnetostratigraphy of equatorial Pacific Site 503 hydraulic piston cores. In Prell, W. L., Gardner, J. V., et al., *Init. Repts. DSDP*, 68: Washington (U.S. Govt. Printing Office), 435-440.
- Langseth, M. G., Cann, J. R., Natland, J. H., and Hobart, M., 1983. Geothermal phenomena at the Costa Rica Rift: background and objectives for drilling at Deep Sea Drilling Project Sites 501, 504, and 505. In Cann, J. R., Langseth, M. G., Honnorez, J., Von Herzen, R. P., White, S. M., et al., *Init. Repts. DSDP*, 69: Washington (U.S. Govt. Printing Office), 461-473.
- Langseth, M. G., and Mottl, M., 1982. Geochemical and geothermal mapping of crustal circulation patterns near DSDP sites 501/504. *Trans. Am. Geophys. Union*, 63:1116. (Abstract).
- Lovell, M. A., 1985. Thermal conductivity and permeability assessment by electrical resistivity measurements in marine sediments. *Mar. Geotechnol.*, 6(2):205-240.
- Lovell, M. A., and Ogden, P., 1985. Remote assessment of permeability/thermal diffusivity of consolidated clay sediments. *Report to the European Atomic Energy Community*, EUR 9206EN, Luxembourg.
- Martini, E., 1971. Standard Tertiary and Quaternary calcareous nannoplankton zonation. *Proc. Internat. Conf. Plank. Organisms* (1st), 2: 739.
- Masle, A., Moore, J. C., Taylor, E., et al., in press. *Proc., Init. Rept., ODP*, 110.
- Mottl, M. J., Lawrence, J. R., and Keigwin, L. D., 1983. Elemental and stable-isotope composition of pore waters and carbonate sediments from Deep Sea Drilling Project Sites 501/504 and 505. In Cann, J. R., Langseth, M. G., Honnorez, J., Von Herzen, R. P., White, S. M., et al., *Init. Repts. DSDP*, 69: Washington (U.S. Govt. Printing Office), 461-473.
- Nafe, J. E., and Drake, C. L., 1957. Variation with depth in shallow and deep water marine sediments of porosity, density and the velocities of compressional and shear waves. *Geophysics*, 22:523-552.
- Prell, W. L., Gardner, J. V., et al., 1982. *Init. Repts. DSDP*, 68: Washington (U.S. Govt. Printing Office).
- Riech, V., and von Rad, U., 1979. Silica diagenesis in the Atlantic Ocean: diagenetic potential and transformations. In Talwani, M., Hay, W., and Ryan, W.B.F. (Eds.), *Deep Drilling Results in the Atlantic Ocean: Passive Margins and Paleoenvironment* (Maurice Ewing Series 2): Washington (Am. Geophys. Union), 315-341.
- Riedel, W. R., and Sanfilippo, A., 1978. Stratigraphy and evolution of tropical Cenozoic radiolarians. *Micropaleontology*, 24:61-96.
- Saito, T., Burkle, L. H., and Hays, J. D., 1975. Late Miocene to Pleistocene biostratigraphy of equatorial Pacific sediments. In Late Neogene Epoch Boundaries: *Micropaleontol. Spec. Publ.* 1: New York (Micropaleontology Press), 226-244.
- Sancetta, C. A., 1983. Biostratigraphic and paleoceanographic events in the eastern Equatorial Pacific: Results of Deep Sea Drilling Project Leg 69. In Cann, J. R., Langseth, M. G., Honnorez, J., Von Herzen, R. P., White, S. M., et al., *Init. Repts. DSDP*, 69: Washington (U.S. Govt. Printing Office), 311-320.
- Sass, J. H., Lachenbruch, A. H., and Munroe, R. J., 1971. Thermal conductivity of rocks from measurements on fragments and its application to heat-flow determinations. *J. Geophys. Res.*, 76:3391-3401.
- Shackleton, N. J., and Hall, M. A., 1983. Stable isotopic record of Hole 504B sediments: High resolution record of the Pleistocene. In Cann, J. R., Langseth, M. G., Honnorez, J., Von Herzen, R. P., White, S. M., et al., *Init. Repts. DSDP*, 69: Washington (U.S. Govt. Printing Office), 431-441.
- Taylor-Smith, D., 1974. Acoustic and mechanical loading of marine sediments. In Hampton, L. (Ed.), *Physics of Sound in Marine Sediments*: New York (Plenum Press), 122-139.
- Woodside, W., and Messmer, J. H., 1961. Thermal conductivity of porous media. I. Unconsolidated sands. *J. Appl. Phys.*, 32:1688-1699.

SITE 677 HOLE A										CORE 1H		CORED INTERVAL		0 -6.2 mbsf	
TIME-ROCK UNIT	BIOSTRAT. ZONE/ FOSSIL CHARACTER				PALEOMAGNETICS	PHYS. PROPERTIES	CHEMISTRY	SECTION	METERS	GRAPHIC LITHOLOGY	DRILLING DISTURB.	SED. STRUCTURES	SAMPLES	LITHOLOGIC DESCRIPTION	
	FORAMINIFERS	NANNOFOSSILS	RADIOLARIANS	DIATOMS											
LATE PLEISTOCENE	<i>P. obliquiloculata</i> Zone				▲	■	●	1	0.5				*	CLAYEY DIATOM-RADIOLARIAN-NANNOFOSSIL-FORAMINIFER OOZE AND CALCAREOUS RADIOLARIAN-DIATOM OOZE (SOMETIMES CLAY-BEARING)	
	NN21 <i>E. huxleyi</i> Zone								1.0						
	<i>L. haysi</i> Zone														
	F/M														
					●	■	●	2					*	The core consists predominantly of olive gray (10Y 4/2) ooze mottled with darker gray green (5Y 3/2 to 10Y 4/1) material. Bioturbation intense with numerous fat <i>Zoophycos</i> burrows (5Y 4/3), and open burrows in Section 1.	
					●	■	●	3					*	CHEMISTRY wt % CO ₃ /wt % total C:	
									1.70 2.75 3.76 4.76						
									51.35/7.99 42.79/6.11 16.62/3.61 29.12/4.49						
					●	■	●	4					*	PHYSICAL PROPERTIES:	
									1.70 2.75 3.76 4.76						
									WC (%) 240.26 219.41 264.14 239.31						
									ρ _g (g/cm ³) 4.27 2.77 2.25 2.81						
									ρ _b (g/cm ³) 1.31 1.27 1.20 1.26						
					●	■	●	5					*	SMEAR SLIDE SUMMARY (%):	
									1.6 1.49 1.113 2.70 3.51 4.70 4.81						
									M D D D D M D						
					●	■	●	6					*	TEXTURE:	
									Sand 8 10 7 10 3 1 3						
									Silt 22 20 20 20 10 10 7						
									Clay 70 70 73 70 87 89 90						
					●	■	●	7					*	COMPOSITION:	
									Quartz Tr — — Tr Tr — —						
									Feldspar Tr Tr Tr Tr — 5 1						
									Clay 14 15 15 15 10 25 10						
									Calcite/dolomite 40 20 8 10 5 7 5						
					●	■	●	8					*	Accessory minerals — Tr — — — 3 3	
									Pyrite — — 2 1 1 — 1						
									Foraminifers 13 20 20 25 10 5 5						
									Nannofossils 5 10 25 15 10 5 5						
									Diatoms 7 15 20 20 40 40 45						
					●	■	●	9					*	Radiolarians 20 20 10 13 15 10 15	
									Sponge spicules — — — 2 9 — 10						
									Silicoflagellates Tr — — Tr Tr — Tr						
									Fish remains Tr — — — — — —						
									Pellets 1 — — — — — —						

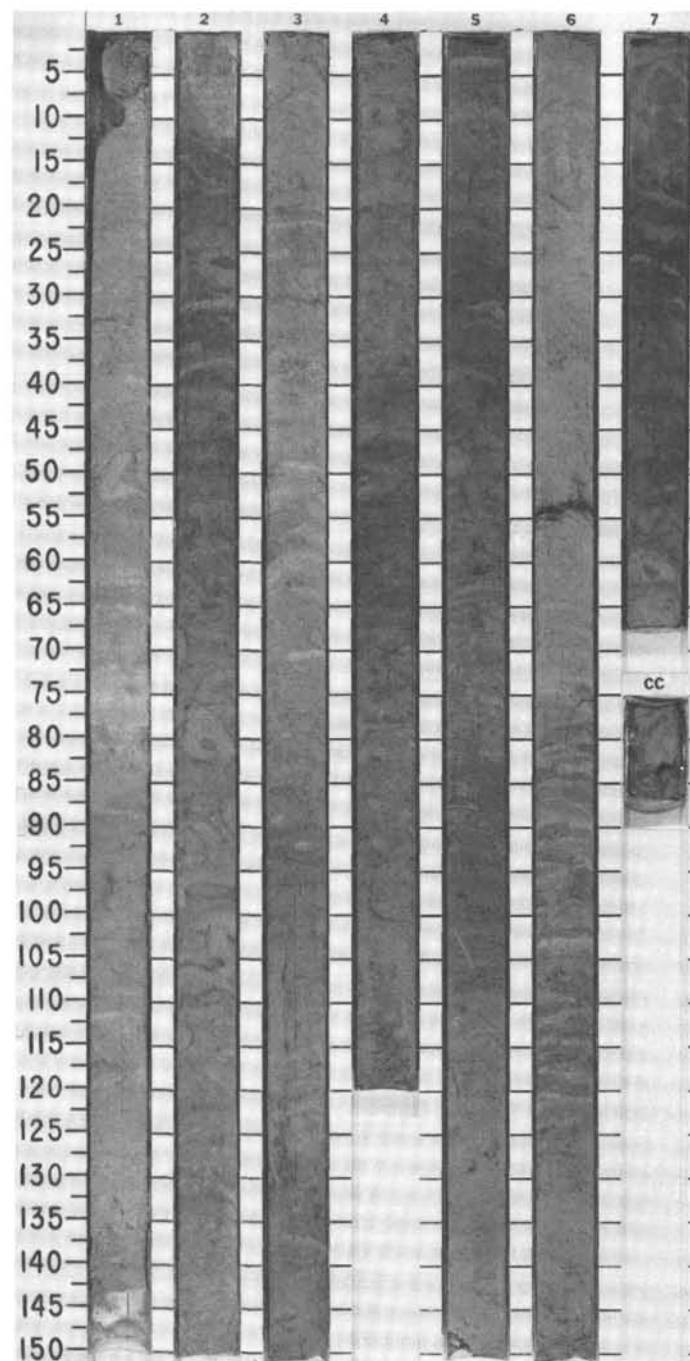
Information on Core Description Forms, for ALL sites, represents field notes taken aboard ship. Some of this information has been refined in accord with post-cruise findings, but production schedules prohibit definitive correlation of these forms with subsequent findings. Thus the reader should be alerted to the occasional ambiguity or discrepancy.

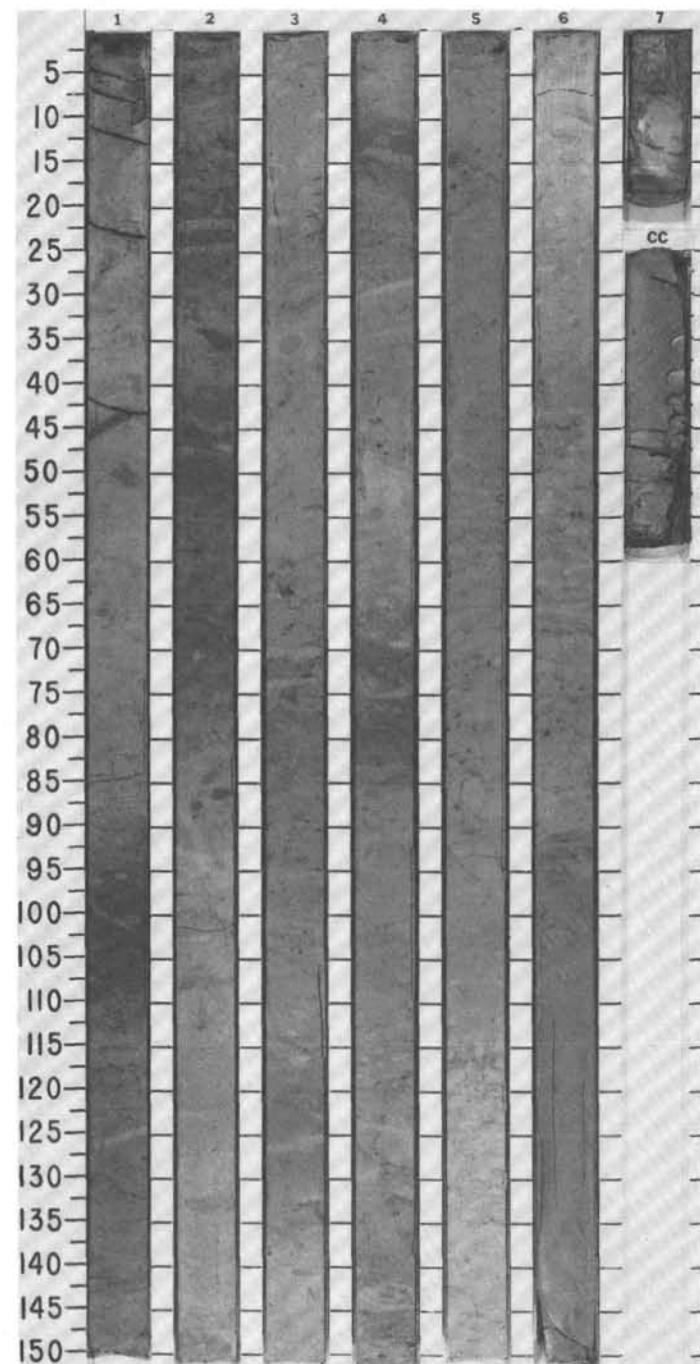




SITE 677 HOLE A CORE 3H CORED INTERVAL 15.7-25.2 mbsf

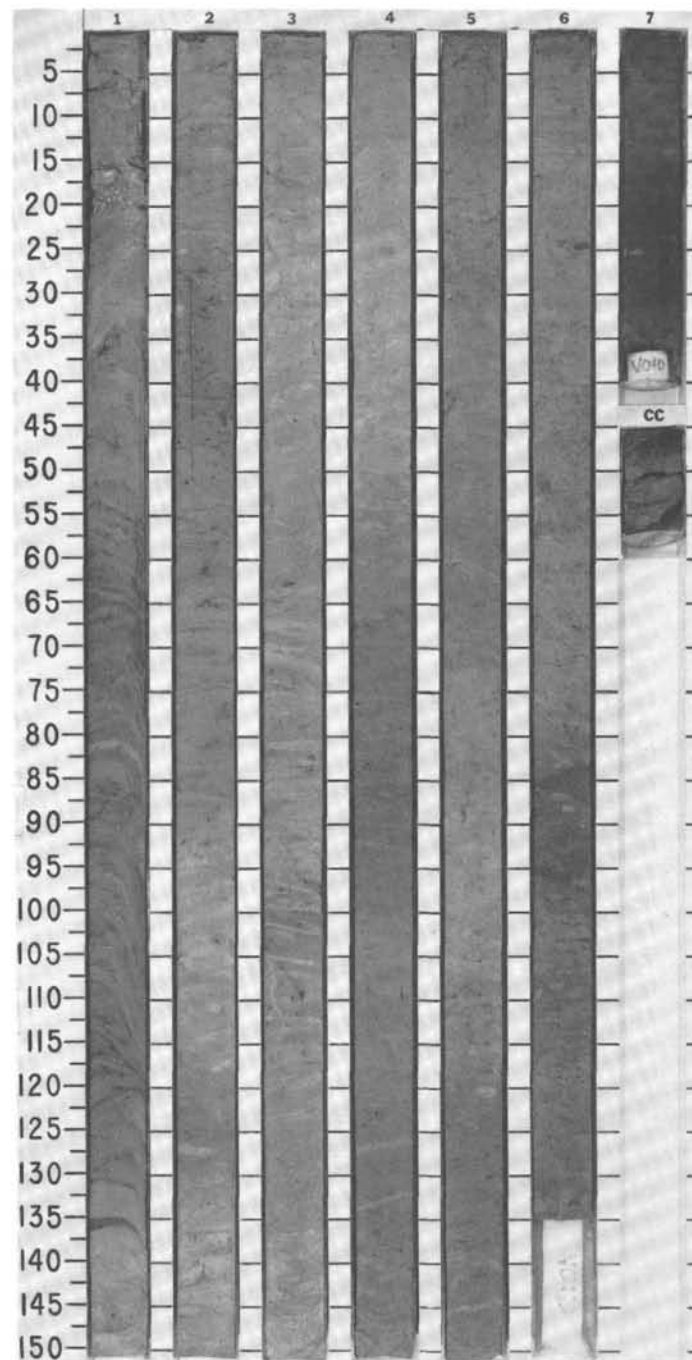
TIME-ROCK UNIT	BIOSTRAT. ZONE/ FOSSIL CHARACTER			PALEOMAGNETICS	PHYS. PROPERTIES	CHEMISTRY	SECTION	METERS	GRAPHIC LITHOLOGY	DRILLING DISTURB.	SED. STRUCTURES	SAMPLES	LITHOLOGIC DESCRIPTION
	FORAMINIFERS	NANNOFOSSILS	RADIOLARIANS										
LATE PLEISTOCENE	NN20			▲	●	■	1	0.5				*	SILICEOUS NANNOFOSSIL OOZE, SOMETIMES CLAY-BEARING, SOMETIMES PYRITE-BEARING Light gray green (10Y 6/2) ooze alternating with dusky yellow green (5GY 5/2) ooze, moderately bioturbated. Simple Zoophycos burrows (10Y 7/2), pyrite streaking and and burrow haloing are common. Sulfur-rich layers (10GY 2.5/1) in Section 6 (804 cm).
								1.0					
	NN19	<i>Pseudoemiliania lacunosa</i> Zone		▲	●	■	2					*	CHEMISTRY wt % CO ₂ /wt % total C: 1, 70 2, 70 3, 70 4, 70 5, 70 6, 70 59.75/7.52 41.20/5.72 52.14/6.27 32.63/5.11 40.22/5.26 52.00/6.98 PHYSICAL PROPERTIES: 1, 70 2, 70 3, 70 4, 70 5, 70 6, 70 WC (%) 133.50 165.47 159.30 187.40 178.97 142.89 P _g (g/cm ³) 2.48 2.99 2.97 2.84 2.06 2.47 P _b (g/cm ³) 1.36 1.36 1.37 1.31 1.24 1.34 φ (%) 76.69 83.11 82.46 84.13 78.64 77.79 σ (kPa) 11.78 11.78 10.84 18.85 19.80 17.91 V _p (m/s) 1602.0 1598.0 1615.8 1571.0 — 1590.8
	L. haysi Zone			▲	●	■	3					*	SMEAR SLIDE SUMMARY (%): 1, 75 2, 75 3, 46 4, 66 5, 91 6, 54 7, 38 D D D D D M D TEXTURE: Sand 7 15 15 10 15 50 25 Silt 20 10 25 25 25 30 20 Clay 63 75 60 65 60 20 55 COMPOSITION: Quartz — — — Tr — 10 — Feldspar 1 3 — Tr 1 — 1 Mica — — — — Tr — — Clay 7 7 15 7 12 5 10 Calcite/dolomite 5 10 4 8 5 5 10 Accessory minerals 2 — 1 3 1 5 5 Pyrite 2 5 5 3 5 30 2 Foraminifers 10 15 7 10 15 5 15 Nannofossils 50 30 40 35 40 30 20 Diatoms 15 10 15 20 10 4 14 Radiolarians 5 10 5 5 5 3 15 Sponge spicules 3 10 7 7 6 3 7 Silicoflagellates — Tr 1 1 Tr — 1 Fish remains — — — — — — Tr
	F/M			▲	●	■	4					*	
				▲	●	■	5					*	
				▲	●	■	6					*	
				▲	●	■	7					*	



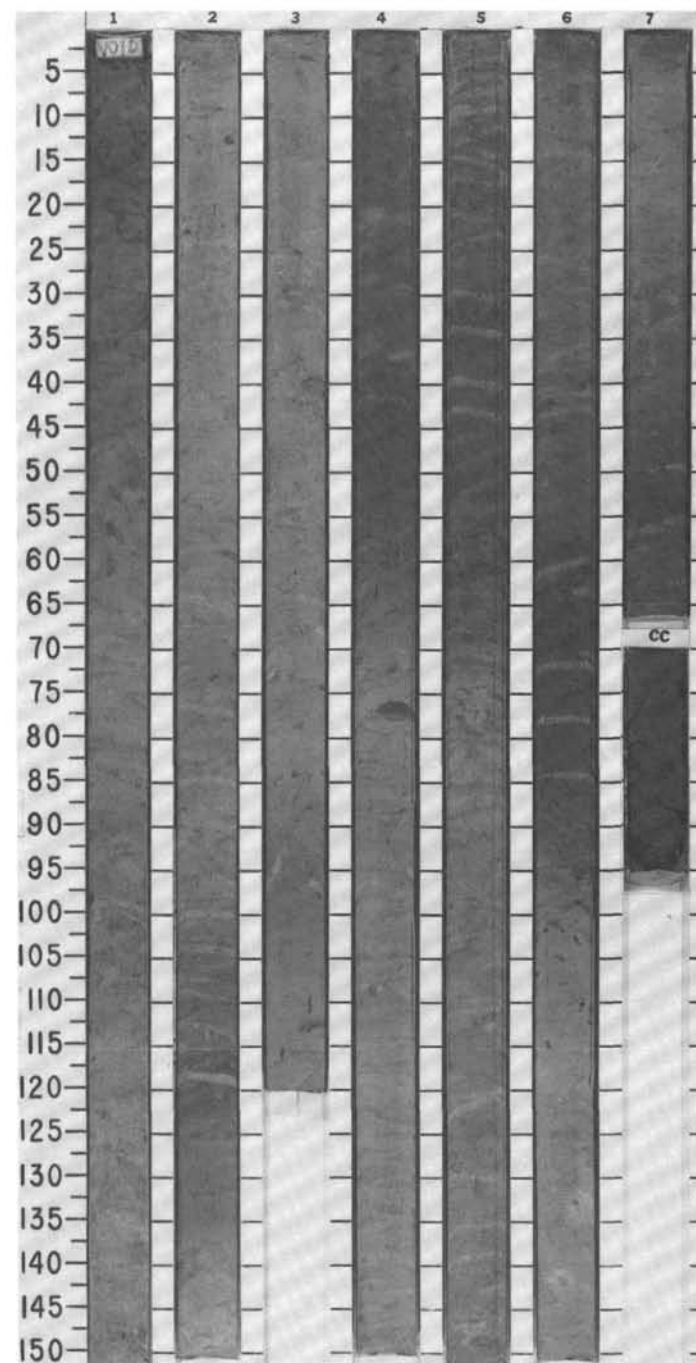


SITE 677 HOLE A CORE 5 H CORED INTERVAL 34.7-44.2 mbsf

TIME-ROCK UNIT	BIOSTRAT. ZONE/ FOSSIL CHARACTER				PALEOMAGNETICS	PHYS. PROPERTIES	CHEMISTRY	SECTION	METERS	GRAPHIC LITHOLOGY	DRILLING DISTURB.	SED. STRUCTURES	SAMPLES	LITHOLOGIC DESCRIPTION
	FORAMINIFERS	NANNOFOSSILS	RADIOLARIANS	DIATOMS										
MIDDLE PLEISTOCENE	<i>P. obliquiloculata</i> Zone	NN19 <i>P. lacunosa</i> Zone	<i>L. haysi</i> Zone		▲	● ■		1	0.5					
					▲	● ■		2	1.0					
					▲	● ■		3						
					▲	● ■		4						
					▲	● ■		5						
					▲	● ■		6						
					▲	● ■		7						
	</													



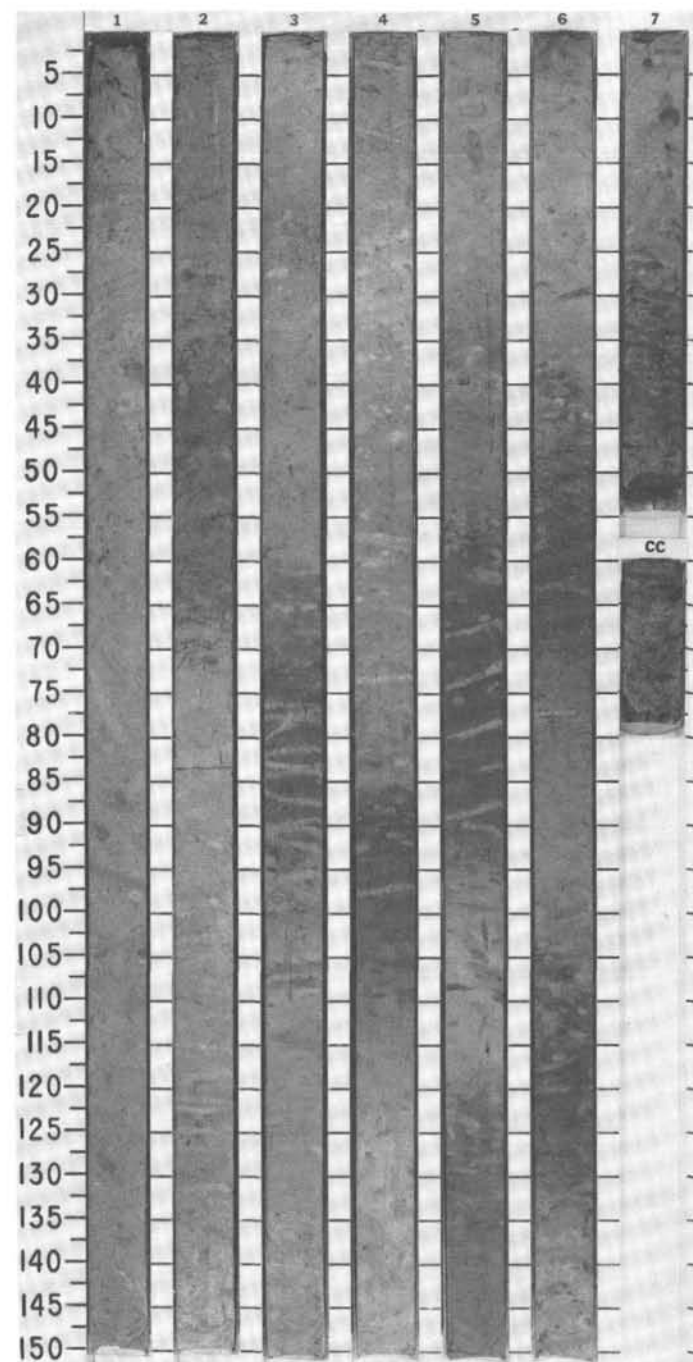
TIME-ROCK UNIT	BIOSTRAT. ZONE / FOSSIL CHARACTER				PALEOMAGNETICS	PHYS. PROPERTIES	CHEMISTRY	SECTION	METERS	GRAPHIC LITHOLOGY	DRILLING DISTURB.	SED. STRUCTURES	SAMPLES	LITHOLOGIC DESCRIPTION
	FORAMINIFERS	NANNOFOSSILS	RADIOLARIANS	DIATOMS										
MIDDLE PLEISTOCENE	<i>P. obliquiloculata</i> Zone NN19	<i>P. lacunosa</i> Zone			▲	●	■	1	0.5	VOID			*	RADIOLARIAN-FORAMINIFER-NANNOFOSSIL OOZE, SOMETIMES CLAY-BEARING Predominantly olive gray ooze (10Y 6/2 to 5Y 4/3). Intensely bioturbated at top of core, less so at bottom. Solid <i>Cylindrichnus</i> in Sections 1 and 3. Simple <i>Zoophycos</i> burrows common.
									1.0					
									2					
	<i>P. prismatium</i> Zone	<i>L. haysi</i> Zone			▲	●	■	3					*	CHEMISTRY wt % CO ₂ /wt % total C: 1, 74 2, 75 3, 54 4, 73 5, 76 6, 69 7, 31 48.93/6.69 35.75/6.17 55.42/7.22 39.27/5.31 45.18/5.88 25.36/— 40.78/2.47
									4					
					▲	●	■	5						PHYSICAL PROPERTIES: 1, 74 2, 75 3, 54 4, 73 5, 76 6, 69 7, 31 WC (%) 121.13 159.37 121.11 144.04 149.16 197.15 1 61.07 p _g (g/cm ³) 2.74 3.13 3.96 2.38 3.10 1.71 2.32 p _b (g/cm ³) 1.42 1.38 1.54 1.33 1.40 1.18 1.30 φ (%) 76.71 83.19 82.59 77.31 82.12 77.25 78.82 σ (kPa) 25.45 24.04 20.27 28.28 29.70 30.17 32.05 V _p (m/s) 1600.0 1550.1 1581.9 1576.7 1566.5 1588.8 1602.0
									6					
				▲	●	■	7					*	SMEAR SLIDE SUMMARY (%): 1, 63 3, 110 6, 50 D D D TEXTURE: Sand 25 30 25 Silt 40 30 20 Clay 35 40 55 COMPOSITION: Quartz — — 1 Feldspar — — Tr Clay 15 9 20 Calcite/dolomite 5 10 8 Accessory minerals 1 1 — Pyrite 2 7 3 Foraminifers 15 15 10 Nannofossils 30 30 25 Diatoms 8 8 10 Radiolarians 20 15 15 Sponge spicules 1 2 5 Silicoflagellates 3 3 3 Fish remains — — Tr	
				▲	●	■								



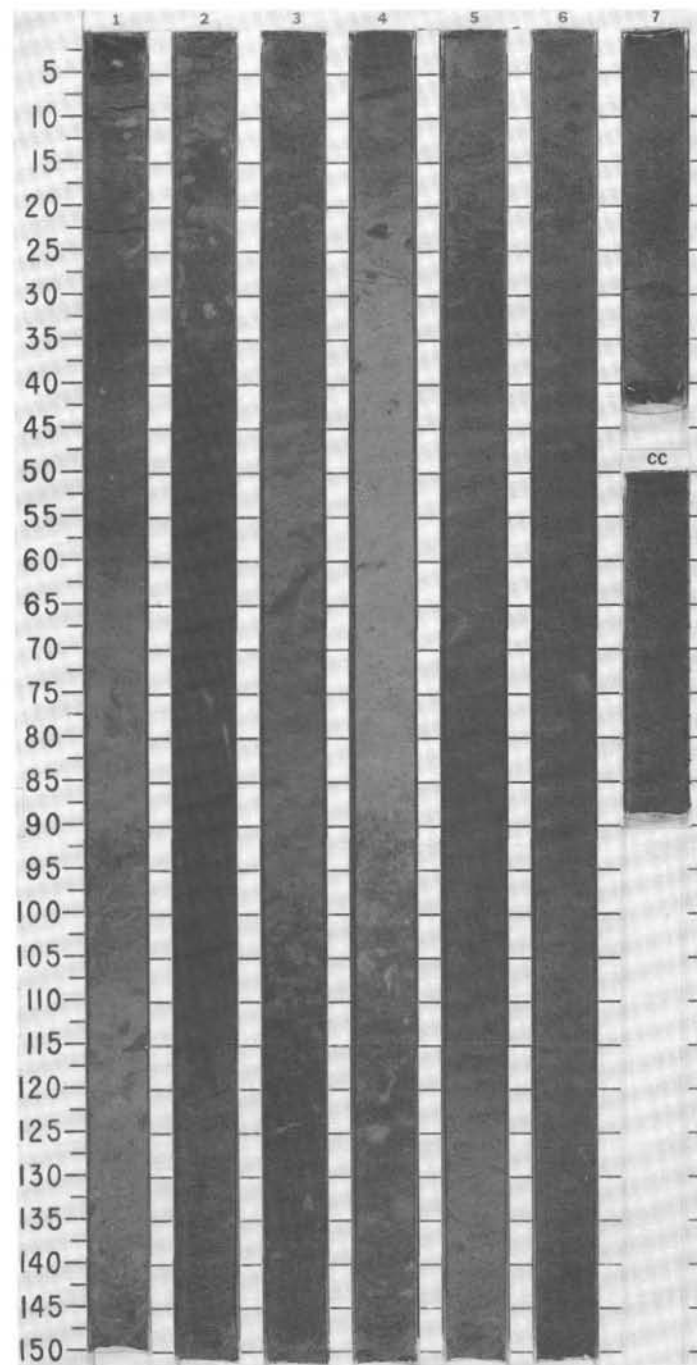
SITES 677 AND 678

SITE 677 HOLE A CORE 7H CORED INTERVAL 53.7-63.2 mbsf

TIME-ROCK UNIT	BIOSTRAT. ZONE/ FOSSIL CHARACTER				PALEOMAGNETICS	PHYS. PROPERTIES	CHEMISTRY	SECTION	METERS	GRAPHIC LITHOLOGY	DRILLING DISTURB.	SED. STRUCTURES	SAMPLES	LITHOLOGIC DESCRIPTION
	FORAMINIFERS	NANNOFOSSILS	RADIOLARIANS	DIATOMS										
EARLY PLEISTOCENE <i>P. obliquiloculata</i> Zone NN19 <i>P. lacunosa</i> Zone <i>P. prismatium</i> Zone F/M					▲	●	■		0.5					CLAYEY RADIOLARIAN-FORAMINIFER-NANNOFOSSIL OOZE Olive green (10Y 5/2 to 10Y 4/2) ooze with gray green layers (5Y 5/2 to 5Y 6/2) and occasional black streaks and mottles (pyrite). Intensely bioturbated. Abundant <i>Zoophycos</i> burrows. CHEMISTRY wt % CO ₃ /wt % total C: 1, 76 2, 76 3, 72 4, 77 5, 75 6, 75 57.04/7.41 49.44/6.38 24.95/6.20 42.07/5.88 15.67/3.48 32.88/5.40 PHYSICAL PROPERTIES: 1, 76 2, 76 3, 72 4, 77 5, 75 6, 75 7, WC (%) 145.82 149.82 171.17 152.26 199.31 176.71 174.70 ρ _g (g/cm ³) 2.46 2.43 2.58 2.36 2.19 3.65 2.61 ρ _b (g/cm ³) 1.34 1.33 1.31 1.32 1.24 1.38 1.32 φ (%) 78.10 78.36 81.45 78.13 81.37 86.50 82.33 σ (kPa) 29.75 26.70 39.66 46.53 48.82 52.63 49.58 V _p (m/s) 1610.4 1613.3 1601.7 1637.8 1576.0 1607.3 1580.9 SMEAR SLIDE SUMMARY (%): 2, 90 4, 70 6, 84 D D D TEXTURE: Sand 30 20 20 Silt 10 7 15 Clay 60 73 65 COMPOSITION: Feldspar 1 2 1 Mica — — Tr Clay 15 25 20 Calcite/dolomite 10 10 7 Accessory minerals Tr Tr — Pyrite 5 3 1 Foraminifers 15 15 10 Nannofossils 25 25 25 Diatoms 10 7 12 Radiolarians 15 10 10 Sponge spicules 3 2 3 Silicoflagellates 1 1 1
					▲	●	■		1.0					
					▲	●	■		2					
					▲	●	■		3					
					▲	●	■		4					
					▲	●	■		5					
					▲	●	■		6					
									7					

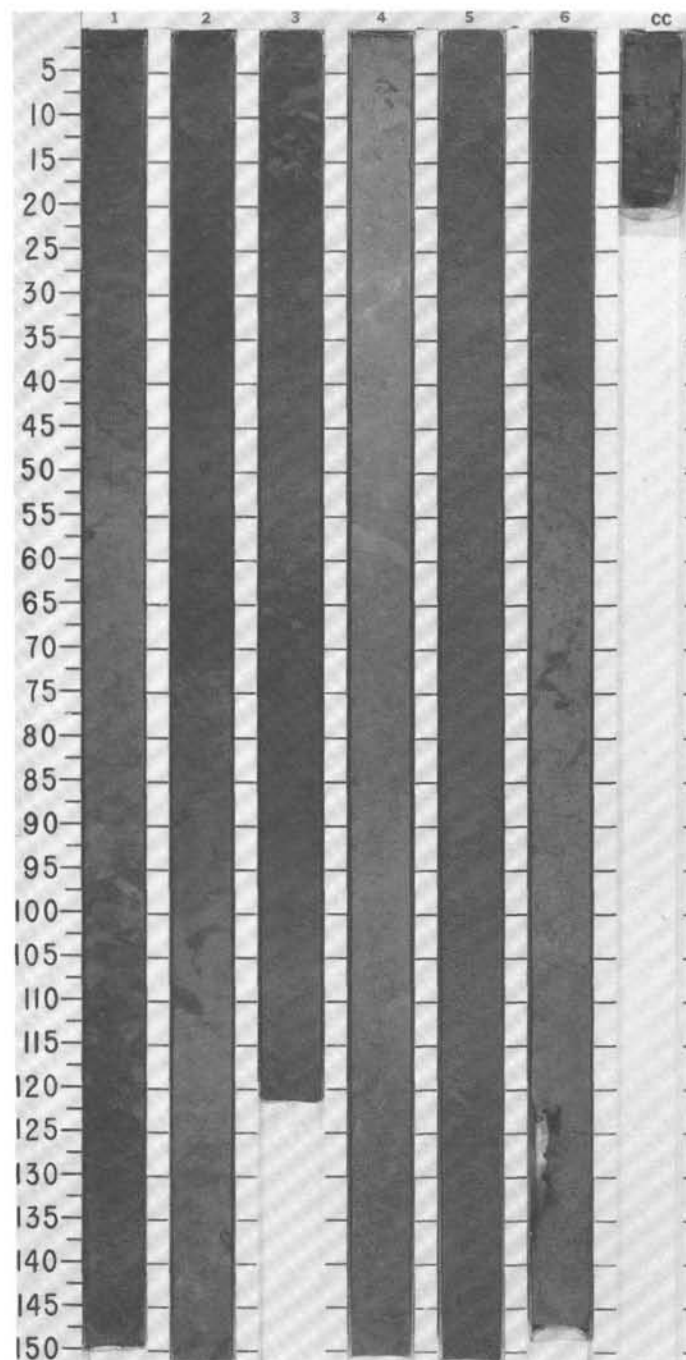


TIME- ROCK UNIT	BIOSTRAT. ZONE/ FOSSIL CHARACTER				PALEOMAGNETICS	PHYS. PROPERTIES	CHEMISTRY	SECTION	METERS	GRAPHIC LITHOLOGY	DRILLING DISTURB.	SED. STRUCTURES	SAMPLES	LITHOLOGIC DESCRIPTION
	FORAMINIFERS	NANNOFOSSILS	RADIOLARIANS	DIATOMS										
EARLY PLEISTOCENE	F/M	<i>P. obliquiloculata</i> Zone	NN 19 <i>P. lacunosa</i> Zone	<i>P. prismatium</i> Zone	▲	●	■		1					CLAYEY NANNOFOSSIL-RADIOLARIAN-DIATOM OOZE Olive green (10Y 5/2 to 10Y 4/2) ooze interlayered with gray green (5Y 2.5/2 to 5Y 4/3) ooze. Moderate to intense bioturbation. There are several burrows filled with pyrite, and pyrite streaking is common. Foraminifers have become less abundant. CHEMISTRY wt % CO ₂ /wt % total C: 1, 76 2, 69 3, 77 4, 76 5, 77 6, 77 34.32/6.46 10.06/6.15 17.17/4.12 35.48/5.67 13.91/4.67 14.47/3.9 6 PHYSICAL PROPERTIES: 1, 76 2, 69 3, 77 4, 76 5, 77 6, 77 WC (%) 166.75 243.94 216.42 181.48 188.46 195.63 p _g (g/cm ³) 3.11 2.41 2.25 2.63 2.90 2.47 p _b (g/cm ³) 1.36 1.22 1.23 1.30 1.32 1.27 φ (%) 83.75 85.50 83.00 82.61 84.47 82.86 σ (kPa) 38.14 51.11 45.00 48.82 61.02 59.50 V _p (m/s) 1658.2 1599.2 1615.6 1610.7 1602.5 1592.2 SMEAR SLIDE SUMMARY (%): 4, 50 D TEXTURE: Sand 20 Silt 25 Clay 55 COMPOSITION: Feldspar 3 Clay 20 Calcite/dolomite 15 Accessory minerals 1 Pyrite 1 Foraminifers 5 Nannofossils 15 Diatoms 20 Radiolarians 17 Sponge spicules 7 Silicoflagellates Tr Fish remains Tr



SITE 677 HOLE A CORE 9H CORED INTERVAL 72.7-82.2 mbsf

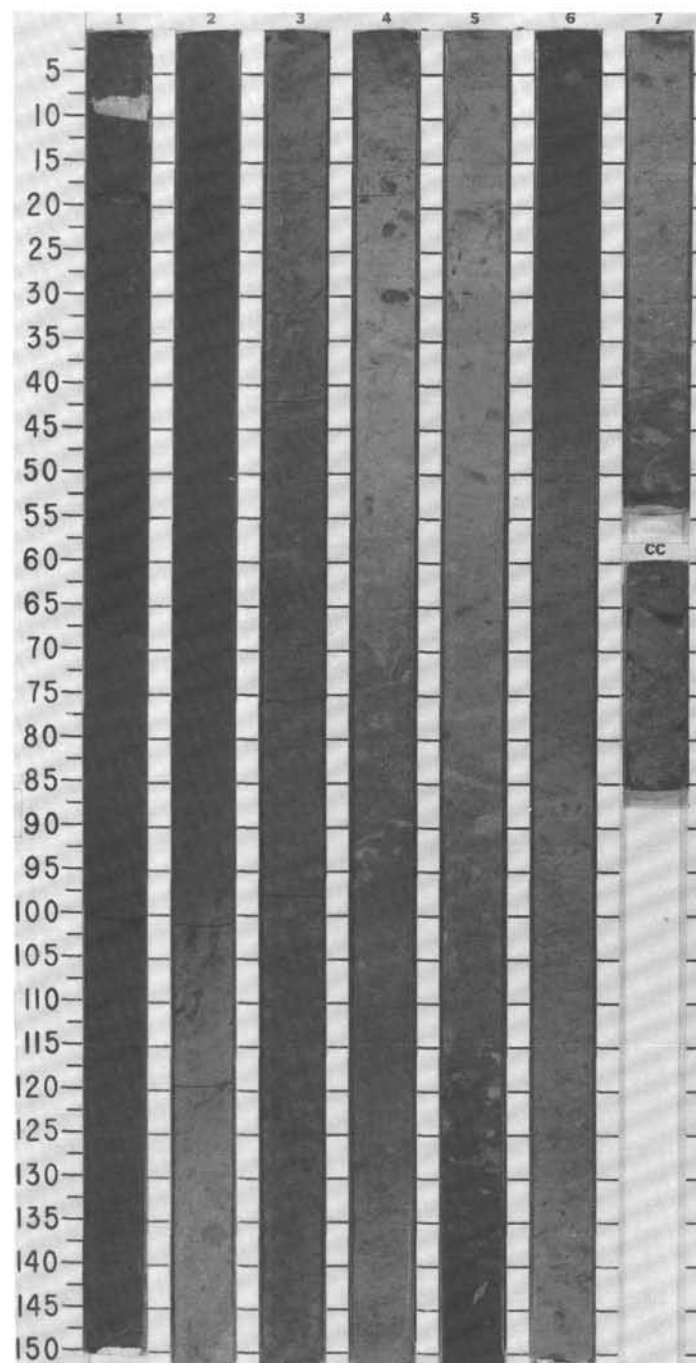
TIME-ROCK UNIT	BIOSTRAT. ZONE/ FOSSIL CHARACTER				PALEOMAGNETICS		PHYS. PROPERTIES	CHEMISTRY	SECTION	METERS	GRAPHIC LITHOLOGY	DRILLING DISTURB.	SED. STRUCTURES	SAMPLES	LITHOLOGIC DESCRIPTION	
	FORAMINIFERS	NANNOFOSSILS	RADIOLARIANS	DIATOMS												
E. PLEISTOCENE	F/M	G. fistulosus Zone NN 19 P. lacunosa Zone P. prismatium Zone			▲	●	■			0.5 1.0					CLAYEY NANNOFOSSIL-RADIOLARIAN-DIATOM OOZE	
															Olive green (10Y 6/2 to 10Y 4/3) and gray green (5Y 3/2 to 5Y 4/2) ooze predominate with occasional gray (10Y 4/1) pyritic streaks. Bioturbation moderate at top to slight at bottom of core.	
															CHEMISTRY wt % CO ₂ /wt % total C:	
															1, 76 2, 76 3, 75 4, 76 5, 77 6, 77	
															25.40/5.10 17.67/5.19 16.70/5.97 33.36/5.84 27.19/5.52 32.97/5.7 4	
															PHYSICAL PROPERTIES:	
LATE PLOECENE					▲	●	■			2				* IW OG	1, 76 2, 76 3, 75 4, 76 5, 77 6, 77	
															WC (%) 211.18 206.22 243.19 172.21 235.07 192.05	
															ρ _w (g/cm ³) 2.95 2.38 2.14 2.41 2.63 2.60	
															ρ _s (g/cm ³) 1.29 1.25 1.20 1.30 1.25 1.29	
															φ (%) 86.13 83.09 83.94 80.57 86.09 83.27	
															σ (kPa) 27.40 41.70 52.42 61.96 63.15 40.51	
					▲	●	■			3					V _p (m/s) 1610.7 1669.7 1672.0 1606.8 1632.7 1634.8	
															SMEAR SLIDE SUMMARY (%):	
															2, 80	
															D	
															TEXTURE:	
															Sand 20 Silt 30 Clay 50	
					▲	●	■			4					COMPOSITION:	
															Feldspar 2	
															Clay 15	
															Calcite/dolomite 7	
															Accessory minerals 1	
															Pyrite 3	
					▲	●	■			5					Foraminifers 3	
															Nannofossils 25	
															Diatoms 25	
															Radiolarians 15	
															Sponge spicules 3	
															Silicoflagellates 1	
					▲	●	■			6					CC	

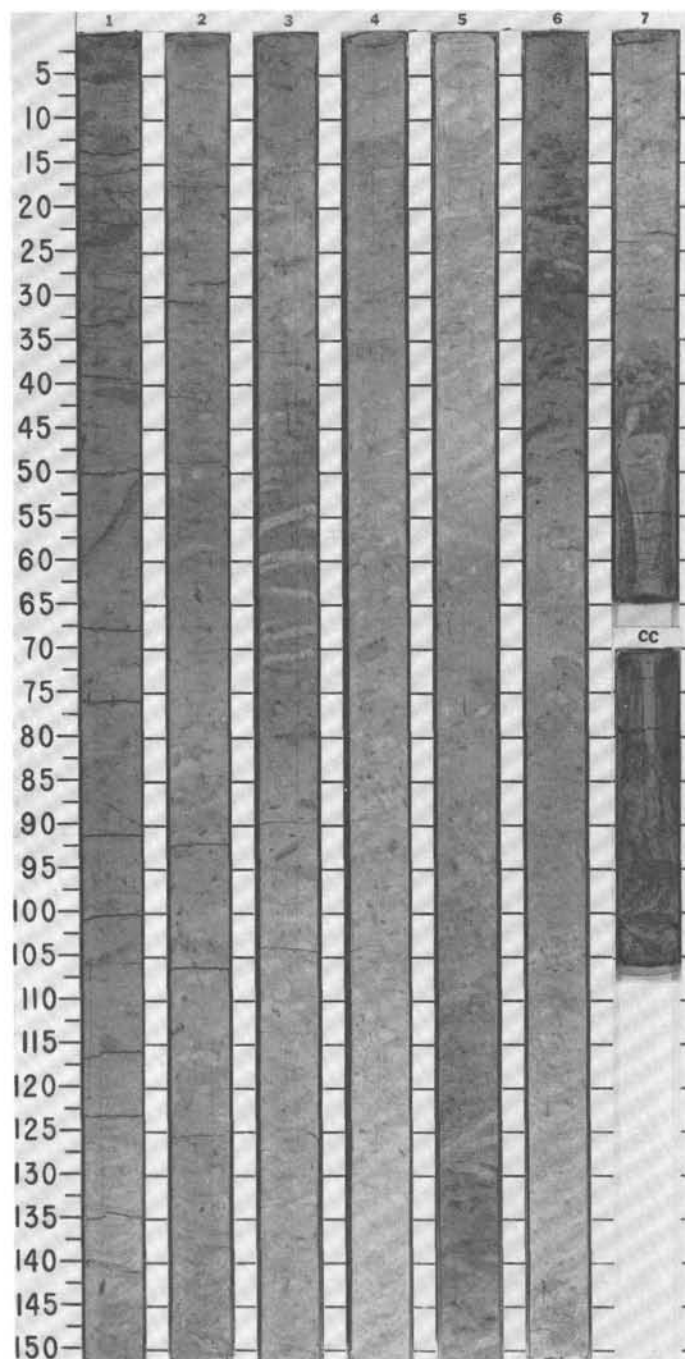


SITES 677 AND 678

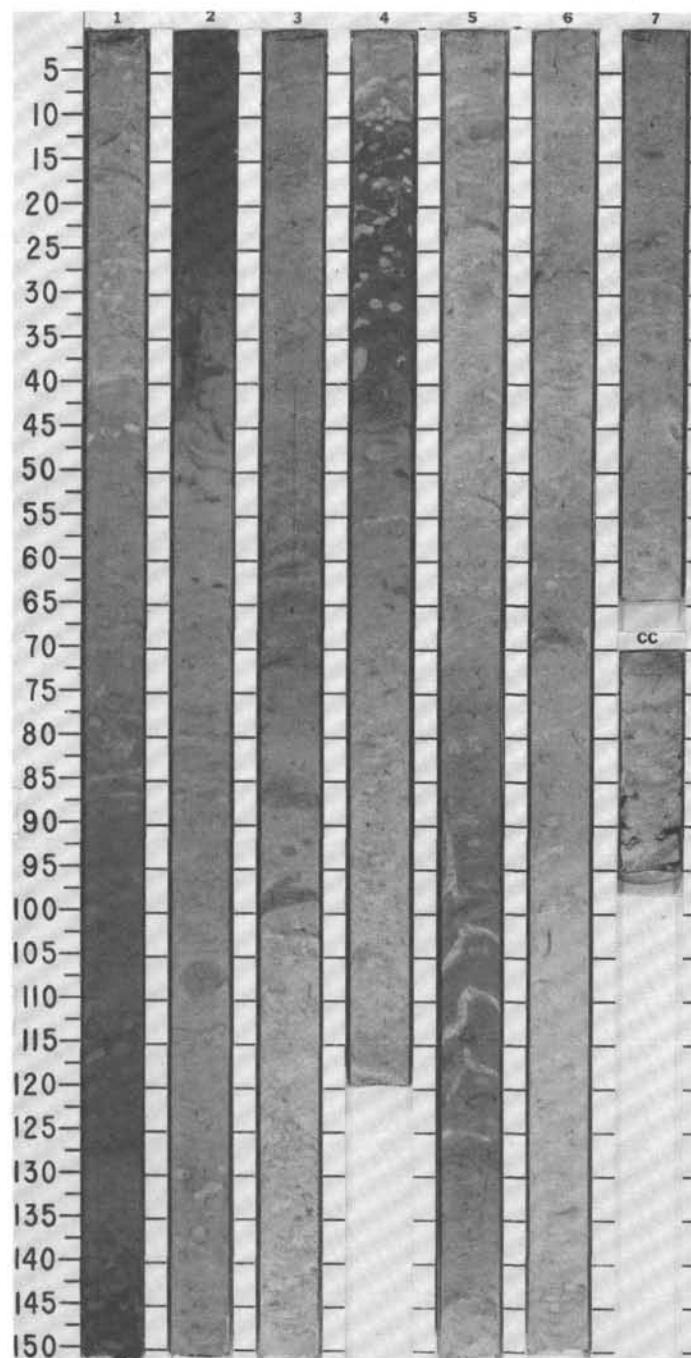
SITE 677 HOLE A CORE 10H CORED INTERVAL 82.2 - 91.7 mbsf

TIME-ROCK UNIT	BIOSTRAT. ZONE/ FOSSIL CHARACTER				PALEOMAGNETICS	PHYS. PROPERTIES	CHEMISTRY	SECTION	METERS	GRAPHIC LITHOLOGY	DRILLING DISTURB.	SED. STRUCTURES	SAMPLES	LITHOLOGIC DESCRIPTION
	FORAMINIFERS	NANNOFOSSILS	RADIOLARIANS	DIATOMS										
LATE PLIOCENE	NN19 <i>P. lacunosa</i> Zone				▲	●	■		0.5			*	CLAYEY NANNOFOSSIL-RADIOLARIAN-DIATOM OOZE Predominantly gray green (5Y 3/2 to 5Y 5/3) ooze with layers of olive green (10Y 4/2 to 10Y 5/2) and yellow green (5GY 5/2) ooze. Bioturbation ranges from slight at top of core to intense in Sections 3, 4 and 5. Black and gray (5GY 4/1) streaks and mottles common. Between 7 and 10 cm there is an inclusion of clayey siliceous nannofossil ooze which probably is a coring artifact derived from higher in the hole. CHEMISTRY wt % CO ₂ /wt % total C: 1, 78 2, 77 3, 76 4, 76 5, 78 6, 78 30.86/8.87 9.31/6.13 14.30/2.82 49.71/9.91 41.80/6.39 34.17/5.26 PHYSICAL PROPERTIES: 1, 78 2, 77 3, 76 4, 76 5, 78 6, 78 WC (%) 215.05 247.87 224.37 208.82 151.49 166.41 p _g (g/cm ³) 2.04 1.80 2.37 2.28 2.30 2.71 p _b (g/cm ³) 1.21 1.17 1.24 1.24 1.31 1.33 φ (%) 81.47 81.90 84.21 82.63 77.65 81.78 σ (kPa) 50.04 46.47 44.08 60.76 66.72 78.64 V _p (m/s) 1570.1 1588.3 1605.5 1599.9 — 1605.7 SMEAR SLIDE SUMMARY (%): 1, 9 3, 61 M D TEXTURE: Sand 25 20 Silt 15 40 Clay 60 40 COMPOSITION: Feldspar 1 2 Clay 15 19 Calcite/dolomite 10 10 Accessory minerals — 1 Pyrite 1 2 Foraminifers 10 Tr Nannofossils 40 15 Diatoms 10 25 Radiolarians 10 20 Sponge spicules 3 5 Silicoflagellates Tr 1 Fish remains — Tr	
					▲	●	■		1.0					
					▲	●	■		2					
					▲	●	■		3					
					▲	●	■		4					
					▲	●	■		5					
					▲	●	■		6					
F/M	NN18 <i>D. brouweri</i>								7					
	<i>P. prismatium</i> Zone													



[illegible]

SITES 677 AND 678

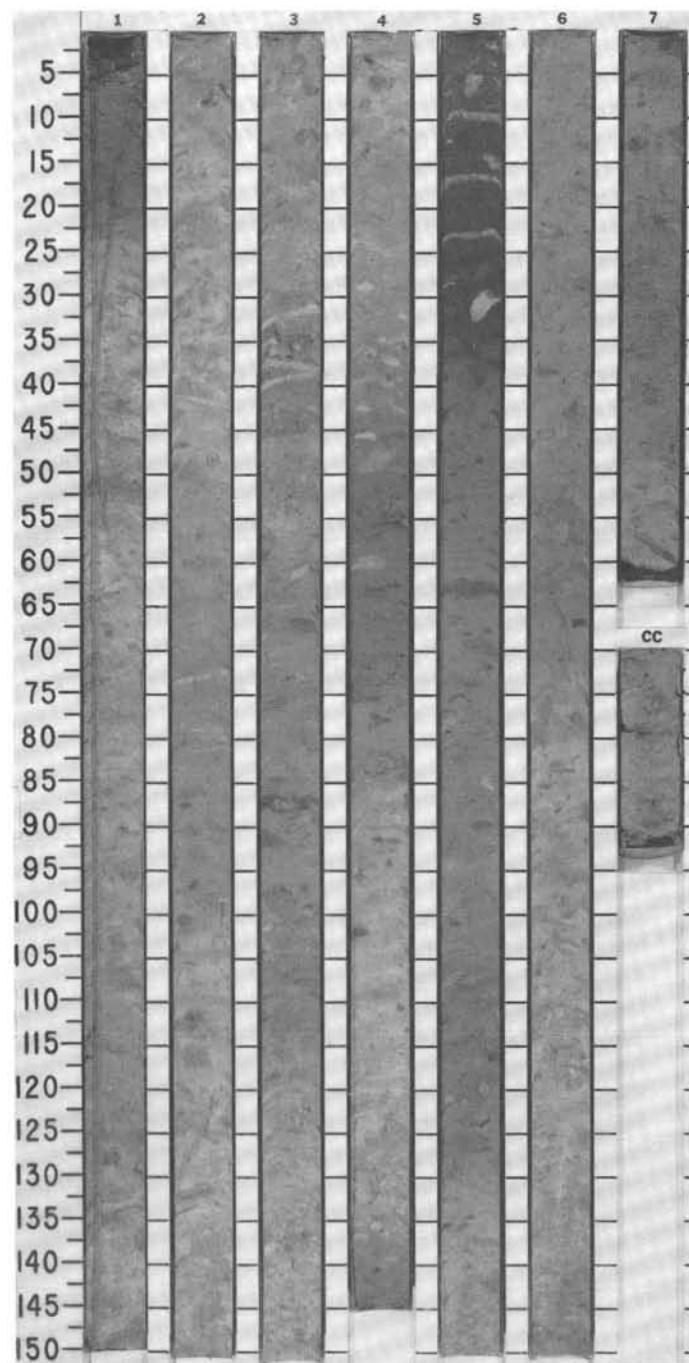


SITE 677 HOLE A CORE 13H CORED INTERVAL 110.7-120.2 mbsf

TIME-ROCK UNIT	BIOSTRAT. ZONE/ FOSSIL CHARACTER				PALEOMAGNETICS	PHYS. PROPERTIES	CHEMISTRY	SECTION	METERS	GRAPHIC LITHOLOGY	DRILLING DISTURB.	SED. STRUCTURES	SAMPLES	LITHOLOGIC DESCRIPTION	
	FORAMINIFERS	NANNOFOSSILS	RADIOLARIANS	DIATOMS											
LATE PLIOCENE	<i>G. fistulosus</i> Zone NN17 <i>D. pentaradiatus</i> Zone <i>S. pentas</i> Zone														
C/M					▲	●	■	1	0.5						CLAYEY DIATOM-NANNOFOSSIL OOZE Predominantly gray green (10Y 5/2 to 10Y 7/2) ooze, with a grayish yellow green (5GY 7/1) layer in Section 5. Mottled with burrows and disseminated pyrite throughout. Moderately to intensely bioturbated. CHEMISTRY wt % CO ₂ /wt % total C: 1, 70 2, 70 3, 70 4, 70 5, 70 6, 70 40.86/5.90 52.15/6.59 21.86/6.17 38.10/5.55 58.68/7.28 52.94/6.72 PHYSICAL PROPERTIES: 1, 70 2, 70 3, 70 4, 70 5, 70 6, 70 WC (%) 158.04 143.45 143.70 136.74 118.68 117.77 ρ _g (g/cm ³) 2.73 2.74 2.53 2.25 2.59 2.70 ρ _b (g/cm ³) 1.35 1.37 1.35 1.33 1.41 1.43 φ (%) 81.11 79.62 78.31 75.38 75.33 75.93 σ (kPa) 63.15 57.19 57.10 65.53 72.68 71.49 V _p (m/s) 1602.8 1598.8 1578.2 1605.6 — 1610.9 SMEAR SLIDE SUMMARY (%): 2, 70 D TEXTURE: Sand 10 Silt 30 Clay 60 COMPOSITION: Quartz T Feldspar Y Clay 15 Calcite/dolomite 5 Accessory minerals 1 Pyrite 3 Foraminifers 5 Nannofossils 40 Diatoms 18 Radiolarians 10 Sponge spicules 2 Silicoflagellates 1 Fish remains Tr
					▲	●	■	2	1.0						
					▲	●	■	3							
					▲	●	■	4							
					▲	●	■	5							
					▲	●	■	6							
								7							
								CC							

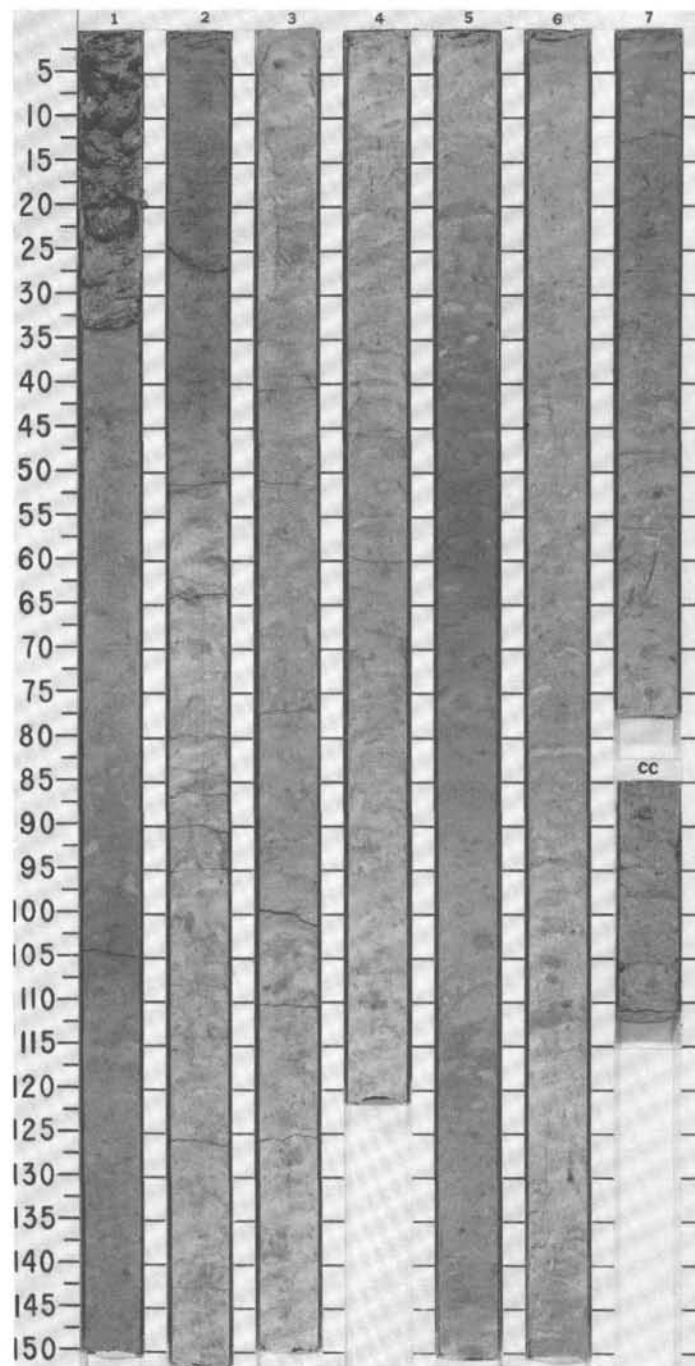
120.2-123.7 MUSE

TIME-ROCK UNIT	BIOSTRAT. ZONE/ FOSSIL CHARACTER				PALEOMAGNETICS	PHYS. PROPERTIES	CHEMISTRY	SECTION	METERS	GRAPHIC LITHOLOGY	DRILLING DISTURB.	SED. STRUCTURES	SAMPLES	LITHOLOGIC DESCRIPTION										
	FORAMINIFERS	NANNOFOSSILS	RADIOLARIANS	DIATOMS																				
LATE PLIOCENE	NN17 <i>D. pentaradiatus</i> Zone					● ■			0.5 1.0					CLAYEY NANNOFOSSIL-RADIOLARIAN-DIATOM OOZE Light (5Y 7/2) to dark (10Y 6/2 to 10Y 7/2) gray oozes alternate in Sections 1 through 4. Olive (10Y 5/4) and yellow green (2.5GY 5/2 to 5GY 5/2) oozes dominate Section 5 and the upper part of 6. Gray oozes return in lower part of core. Abundant Zoophycos burrows, solid <i>Cylindrichnus</i> , <i>planolites</i> . Diffuse pyrite bands and disseminations throughout. CHEMISTRY wt % CO ₃ /wt % total C: 1, 70 2, 70 3, 70 4, 70 5, 70 6, 70 43.11/5.84 37.05/5.42 38.42/5.26 29.23/4.32 35.87/4.96 3.98/4.52 PHYSICAL PROPERTIES: 1, 70 2, 70 3, 70 4, 70 5, 70 6, 70 WC (%) 143.57 156.65 144.94 161.05 161.87 163.95 p _g (g/cm ³) 3.05 2.70 2.59 2.31 2.22 2.76 p _b (g/cm ³) 1.40 1.35 1.36 1.30 1.29 1.34 φ (%) 81.30 80.77 78.86 78.79 78.18 81.85 σ (kPa) 76.25 79.83 64.34 97.70 101.30 96.51 V _p (m/s) 1589.2 1595.7 1591.7 1607.1 1586.9 1570.0 SMEAR SLIDE SUMMARY (%): 6, 66 D TEXTURE: Sand 15 Silt 30 Clay 55 COMPOSITION: Clay 20 Calcite/dolomite 10 Accessory minerals 1 Pyrite 2 Foraminifers 3 Nannofossils 25 Diatoms 20 Radiolarians 15 Sponge spicules 3 Silicoflagellates 1 Fish remains Tr										
						● ■			2															
					▲	● ■			3															
						● ■			4															
					▲	● ■			5															
					▲	● ■			6															
						● ■			7															

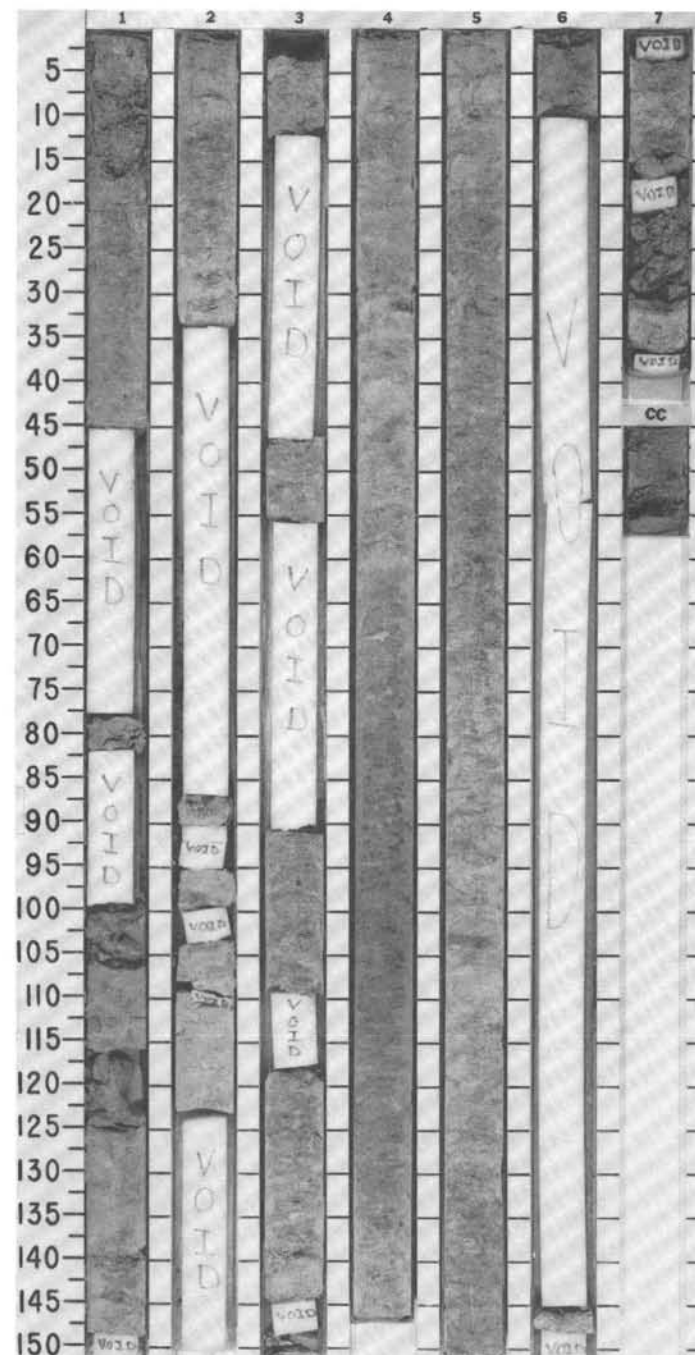


SITE 677 HOLE A CORE 15H CORED INTERVAL 129.7-139.2 mbsf

TIME-ROCK UNIT	BIOSTRAT. ZONE/ FOSSIL CHARACTER				PALEOMAGNETICS	PHYS. PROPERTIES	CHEMISTRY	SECTION	METERS	GRAPHIC LITHOLOGY	DRILLING DISTURB.	SED. STRUCTURES	SAMPLES	LITHOLOGIC DESCRIPTION
	FORAMINIFERS	NANNOFOSSILS	RADIOLARIANS	DIATOMS										
LATE PLIOGENE	<i>S. dehiscentis</i> Zone	NN16	<i>D. surculus</i> Zone	<i>S. pentas</i> Zone	▲	●	■	1	0.5					CLAYEY DIATOM-NANNOFOSSIL OOZE Dark gray green (10Y 5/2 to 10Y 6/2) and lighter olive green (5Y 5/2 to 5Y 5/3) oozes alternate throughout most of core, with occasional gray (5Y 7/1) and dark green (10Y 5/4) layers. Intensely bioturbated with abundant fat <i>Zoophycos</i> burrows. Diffuse pyrite bands and disseminations throughout. CHEMISTRY wt % CO ₂ /wt % total C: 1, 70 3, 70 4, 70 5, 70 6, 70 47.75/6.05 47.96/5.44 42.07/5.43 42.08/6.03 40.40/5.44 PHYSICAL PROPERTIES: 1, 70 2, 70 3, 70 4, 70 5, 70 6, 70 WC (%) 134.71 136.81 152.73 144.79 139.49 132.31 ρ _g (g/cm ³) 3.04 2.81 2.42 2.41 3.10 2.57 ρ _b (g/cm ³) 1.42 1.40 1.32 1.34 1.41 1.38 φ (%) 80.22 79.21 78.64 77.66 81.12 77.19 σ (kPa) 44.08 38.13 44.08 82.21 107.20 88.17 V _p (m/s) — 1583.0 1567.8 1590.2 1600.3 1610.6 SMEAR SLIDE SUMMARY (%): 6, 60 7, 62 D D TEXTURE: Sand 30 35 Silt 10 5 Clay 60 60 COMPOSITION: Quartz — Tr Clay 10 15 Calcite/dolomite 10 10 Accessory minerals Pyrite 1 Tr Foraminifers fragments 5 5 Nannofossils 45 40 Diatoms 15 13 Radiolarians 4 5 Sponge spicules 6 9 Silicoflagellates 4 3 Fish remains — Tr
									1.0					
									2					
									3					
									4					
									5					
									6					
									7					
									CC					

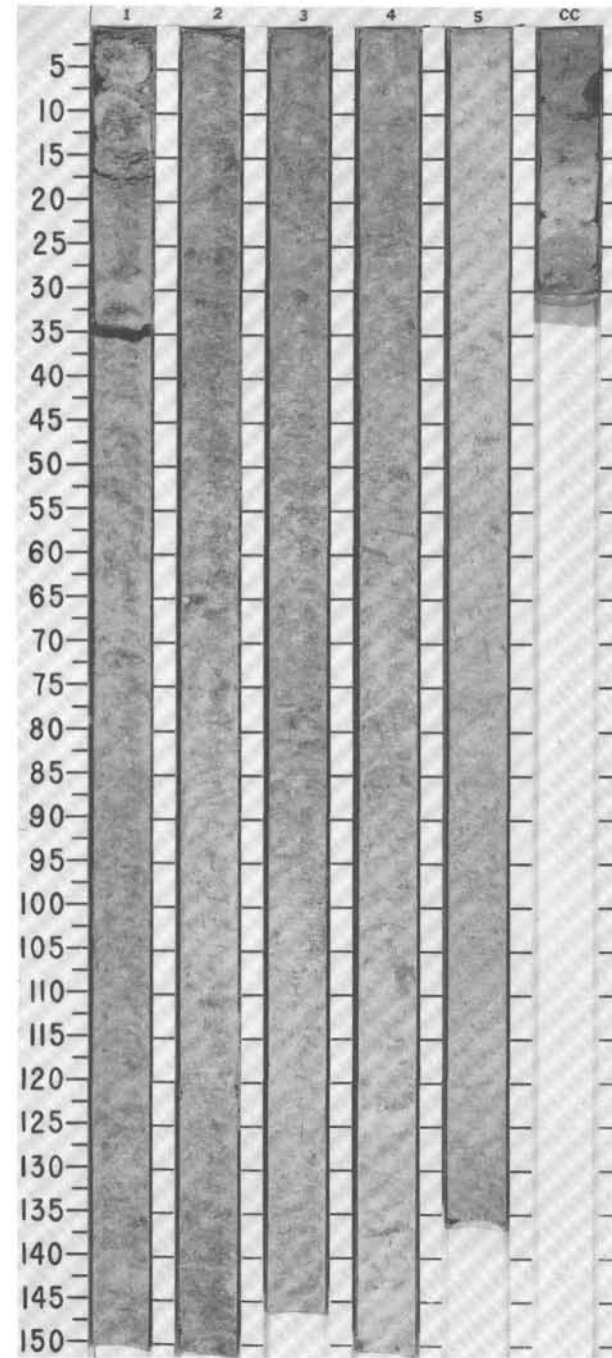


TIME-ROCK UNIT	BIOSTRAT. ZONE/FOSSIL CHARACTER				PALEOMAGNETICS	PHYS. PROPERTIES	CHEMISTRY	SECTION	METERS	GRAPHIC LITHOLOGY	DRILLING DISTURB.	SED. STRUCTURES	SAMPLES	LITHOLOGIC DESCRIPTION
	FORAMINIFERS	NANNOFOSSILS	RADIOLARIANS	DIATOMS										
LATE PLEISTOCENE	C/M	S. dehiscentes Zone NN16 D. surculus Zone S. pentas Zone							0.5 1.0	VOID				CLAYEY DIATOM-NANNOFOSSIL OOZE Light gray (5Y 6/1 to 5Y 7/2) to darker gray green (10Y 5/2 to 10Y 7/2) oozes alternate, with abundant black and olive (5Y 5/3) patches. This core had high recovery, which explains the voids, most of which formed during splitting (5 meters spread out in 9.5-meter core barrel). Probable moderate bioturbation, but splitting damage makes interpretation difficult. CHEMISTRY wt % CO ₂ /wt % total C: 1, 41 2, 11 3, 46 4, 78 5, 77 39.88/5.08 54.56/6.82 62.91/7.63 46.40/5.77 59.50/7.23 PHYSICAL PROPERTIES: 1, 41 2, 11 4, 78 5, 77 WC (%) 131.44 152.58 141.88 120.77 p _g (g/cm ³) 2.59 3.01 2.25 2.43 p _b (g/cm ³) 1.38 1.38 1.32 1.38 φ (%) 77.19 82.00 76.04 74.49 σ (kPa) 13.11 27.40 36.94 26.21 V _p (m/s) 1580.5 — 1580.2 1558.5 SMEAR SLIDE SUMMARY (%): 5, 100 D TEXTURE: Sand 25 Silt 10 Clay 65 COMPOSITION: Clay 17 Calcite/dolomite 7 Accessory minerals Pyrite Tr Foraminifers 3 Nannofossils 50 Diatoms 14 Radiolarians 2 Sponge spicules 4 Silicoflagellates 3

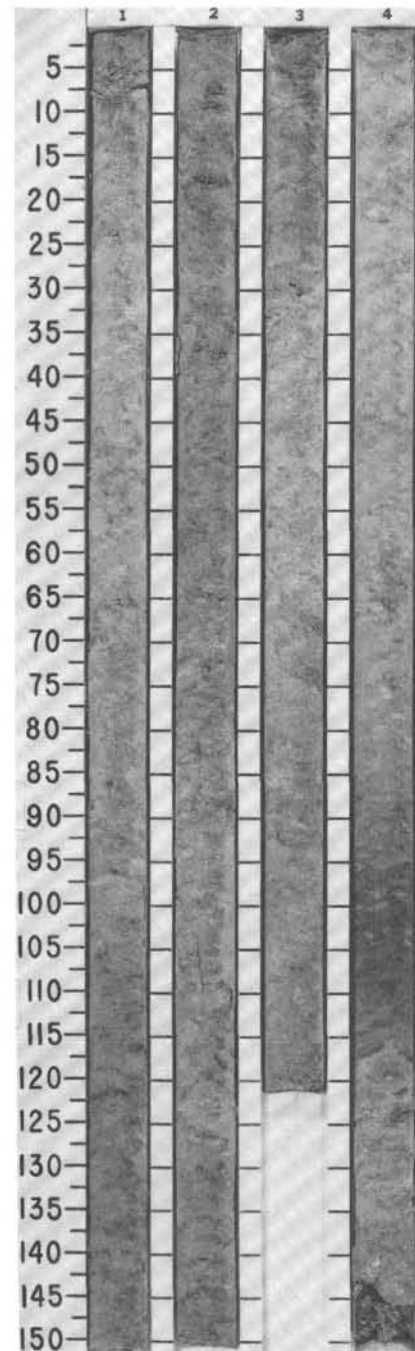


SITE 677 HOLE A CORE 17X CORED INTERVAL 144.2-153.8 mbsf

TIME-ROCK UNIT	BIOSTRAT. ZONE/ FOSSIL CHARACTER				PALEOMAGNETICS	PHYS. PROPERTIES	CHEMISTRY	SECTION	METERS	GRAPHIC LITHOLOGY	DRILLING DISTURB.	SED. STRUCTURES	SAMPLES	LITHOLOGIC DESCRIPTION
	FORAMINIFERS	NANNOFOSSILS	RADIOLARIANS	DIATOMS										
EARLY PLIOCENE	C/M	NN14-NN15												CLAYEY SILICEOUS NANNOFOSSIL OOZE Uniformly light olive gray (5Y 6/2) ooze forms Sections 1 through 4, with occasional black layers and olive (5Y 5/3) patches. Bioturbation moderate. Section 5 consists of pale olive (5Y 6/3) and gray green (10Y 7/1 to 10Y 6/2) material with only slight bioturbation. CHEMISTRY wt % CO ₃ /wt % total C: 1, 78 3, 78 4, 78 5, 75 58.99/7.14 54.65/6.84 64.00/7.80 63.11/7.69 PHYSICAL PROPERTIES: 1, 78 3, 78 4, 78 5, 75 WC (%) 110.63 92.35 110.40 88.00 P _g (g/cm ³) 2.37 2.52 2.39 2.69 P _b (g/cm ³) 1.40 1.48 1.40 1.52 φ (%) 72.25 69.78 72.36 70.10 σ (kPa) 22.64 36.94 40.51 89.36 V _p (m/s) 1559.5 1616.1 1571.1 — SMEAR SLIDE SUMMARY (%):

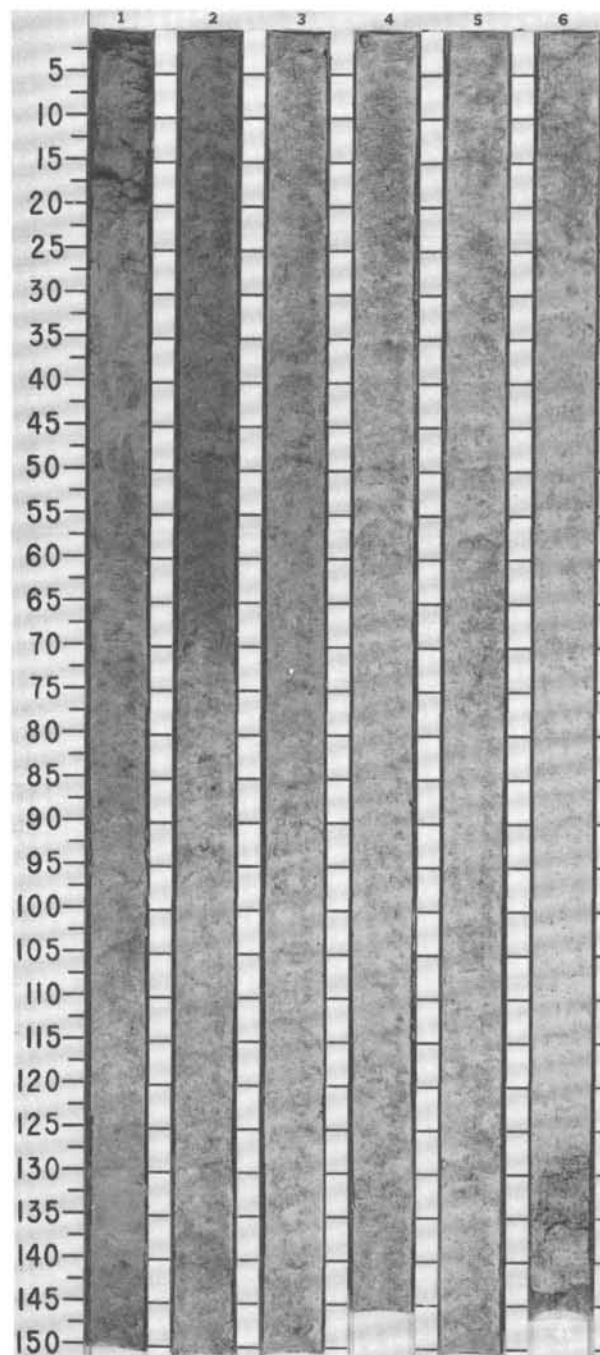


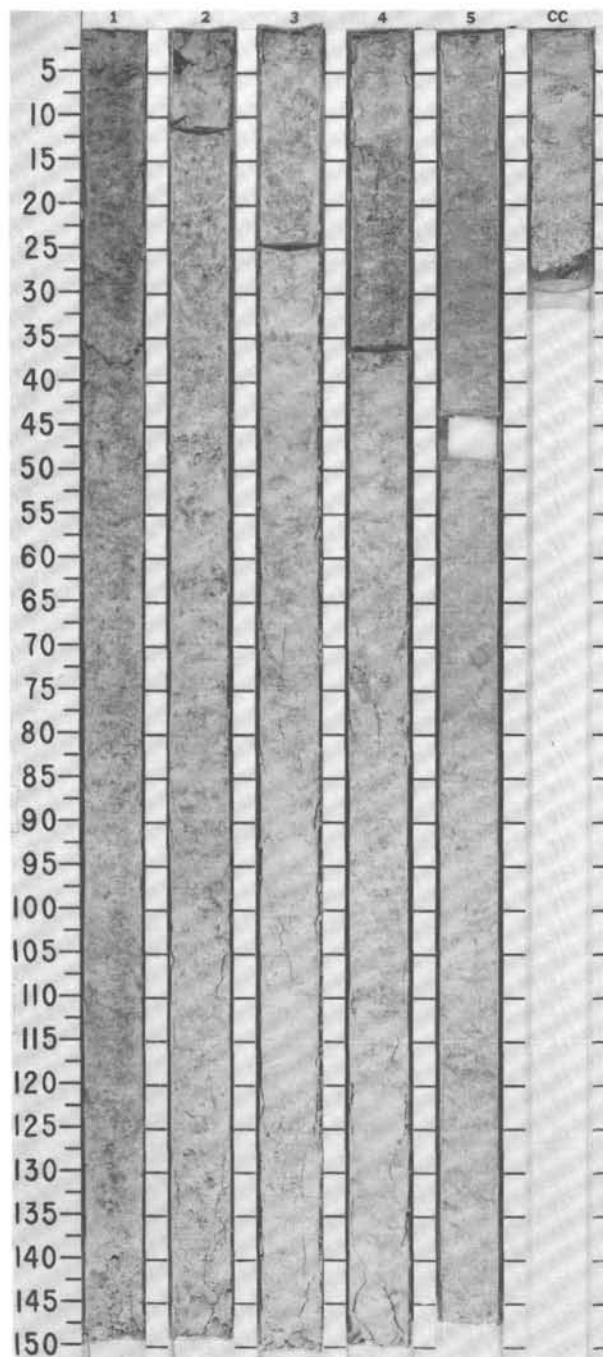
TIME-ROCK UNIT	BIOSTRAT. ZONE/ FOSSIL CHARACTER				PALEOMAGNETICS	PHYS. PROPERTIES	CHEMISTRY	SECTION	METERS	GRAPHIC LITHOLOGY	DRILLING DISTURB.	SED. STRUCTURES	SAMPLES	LITHOLOGIC DESCRIPTION
	FORAMINIFERS	NANNOFOSSILS	RADIOLARIANS	DIATOMS										
EARLY PLIOCENE	C/M	NN14 -NN15 Zones	S. pentas Zone											
					● ■			1	0.5 1.0					SILICEOUS NANNOFOSSIL OOZE AND CHALK
					● ■			2						Light gray (5Y 7/1) to gray green (5GY 7/1) ooze and chalk, ranging from predominantly ooze with indurated chalk in patches and layers in Sections 1 and 2, with transition to chalk complete in Section 3. Transition from predominantly ooze to predominantly chalk occurred over 3 to 5 m. Yellowish (10Y 8/2) and gray (2.5Y 3/0) mottles common. Moderately bioturbated.
					● ■			3						CHEMISTRY wt % CO ₂ /wt % total C:
					● ■									1, 78 2, 78 3, 78 4, 78
					● ■									67.28/8.24 58.94/7.18 52.96/7.09 64.12/7.90
					● ■									PHYSICAL PROPERTIES:
					● ■									1, 78 2, 78 3, 78 4, 78
					● ■									WC (%) 98.84 112.11 127.84 99.18
					● ■									p _g (g/cm ³) 2.33 2.40 3.29 3.03
					● ■									p _b (g/cm ³) 1.42 1.40 1.46 1.53
					● ■									φ (%) 69.55 72.75 80.65 74.81
					● ■									σ (kPa) 30.98 28.59 34.55 67.91
					● ■									V _p (m/s) 1588.7 1566.7 1557.8 1573.3
					● ■									SMEAR SLIDE SUMMARY (%):
					● ■									3, 58
					● ■									D
					● ■									TEXTURE:
					● ■									Sand 10
					● ■									Silt 20
					● ■									Clay 70
					● ■									COMPOSITION:
					● ■									Clay 5
					● ■									Calcite/dolomite 15
					● ■									Accessory minerals
					● ■									Pyrite Tr
					● ■									Foraminifers
					● ■								 fragments 10
					● ■									Nannofossils 50
					● ■									Diatoms 6
					● ■									Radiolarians 5
					● ■									Sponge spicules 5
					● ■									Silicoflagellates 4



SITE 677 HOLE A CORE 19X CORED INTERVAL 163.5 - 173.2 mbsf

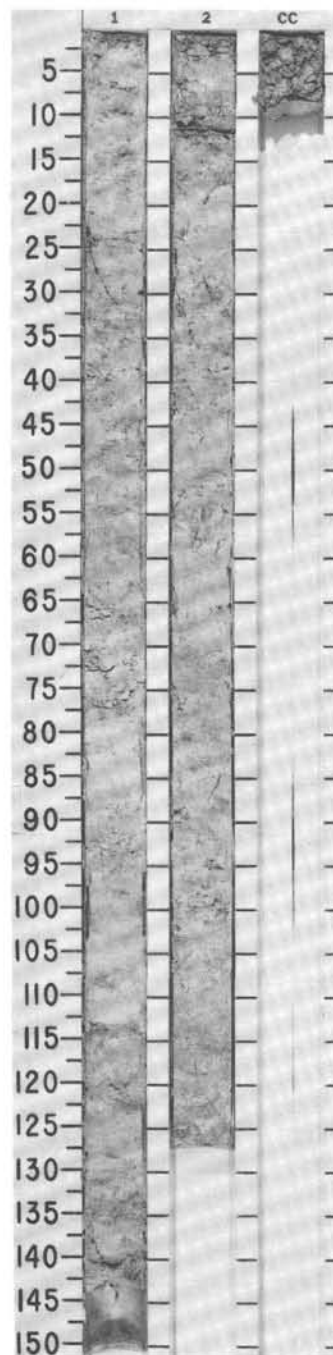
TIME-ROCK UNIT	BIOSTRAT. ZONE/ FOSSIL CHARACTER				PALEOMAGNETICS	PHYS. PROPERTIES	CHEMISTRY	SECTION	METERS	GRAPHIC LITHOLOGY	DRILLING DISTURB.	SED. STRUCTURES	SAMPLES	LITHOLOGIC DESCRIPTION
EARLY PLIOCENE	FORAMINIFERS	NANNOFOSSILS	RADIOLARIANS	DIATOMS										
	<i>G. tumida</i> Zone													
	C/M NN14 - NN15													
	<i>S. pentas</i> Zone													

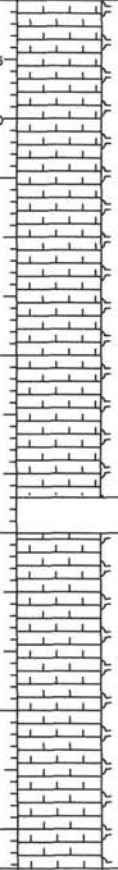



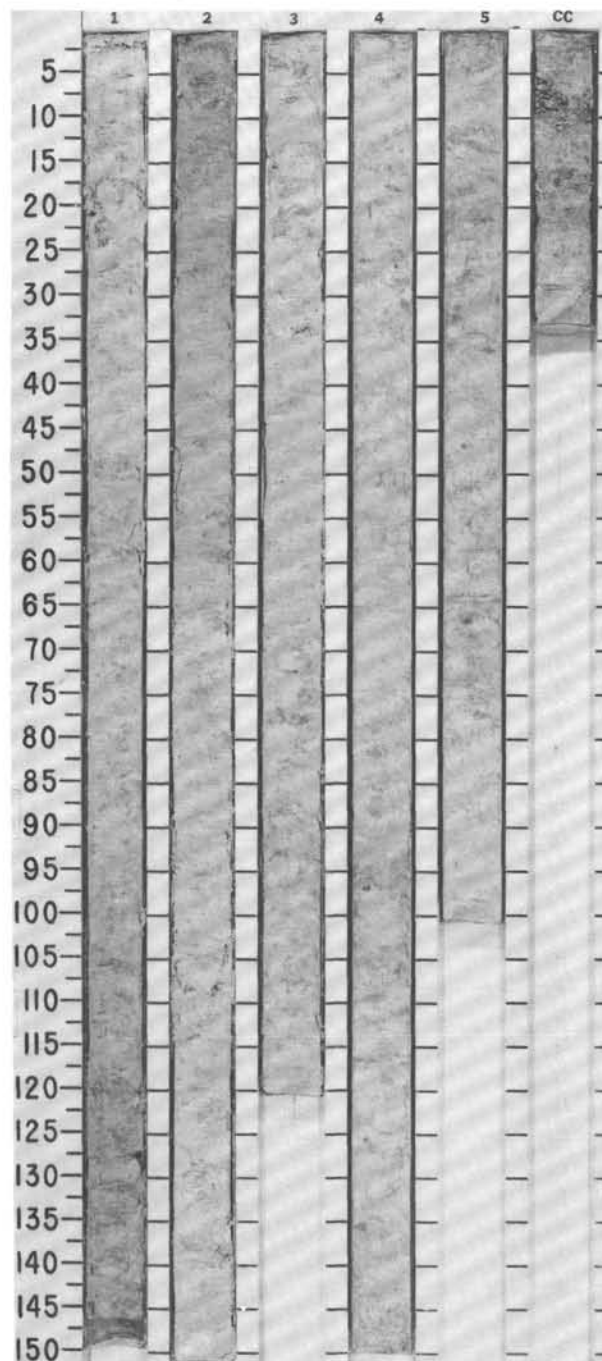
[illegible]

SITE 677 HOLE A CORE 21 X CORED INTERVAL 182.8-192.4 mbsf

TIME-ROCK UNIT	BIOSTRAT. ZONE/ FOSSIL CHARACTER				PALEOMAGNETICS	PHYS. PROPERTIES	CHEMISTRY	SECTION	METERS	GRAPHIC LITHOLOGY	DRILLING DISTURB.	SED. STRUCTURES	SAMPLES	LITHOLOGIC DESCRIPTION	
	FORAMINIFERS	NANNOFOSSILS	RADIOLARIANS	DIATOMS											
EARLY PLIOCENE															
	<i>G. tumida</i> Zone														
	C/M NN13	<i>Ceratulithus rugosus</i>	NN14 -NN15												
	<i>S. pentas</i> Zone														

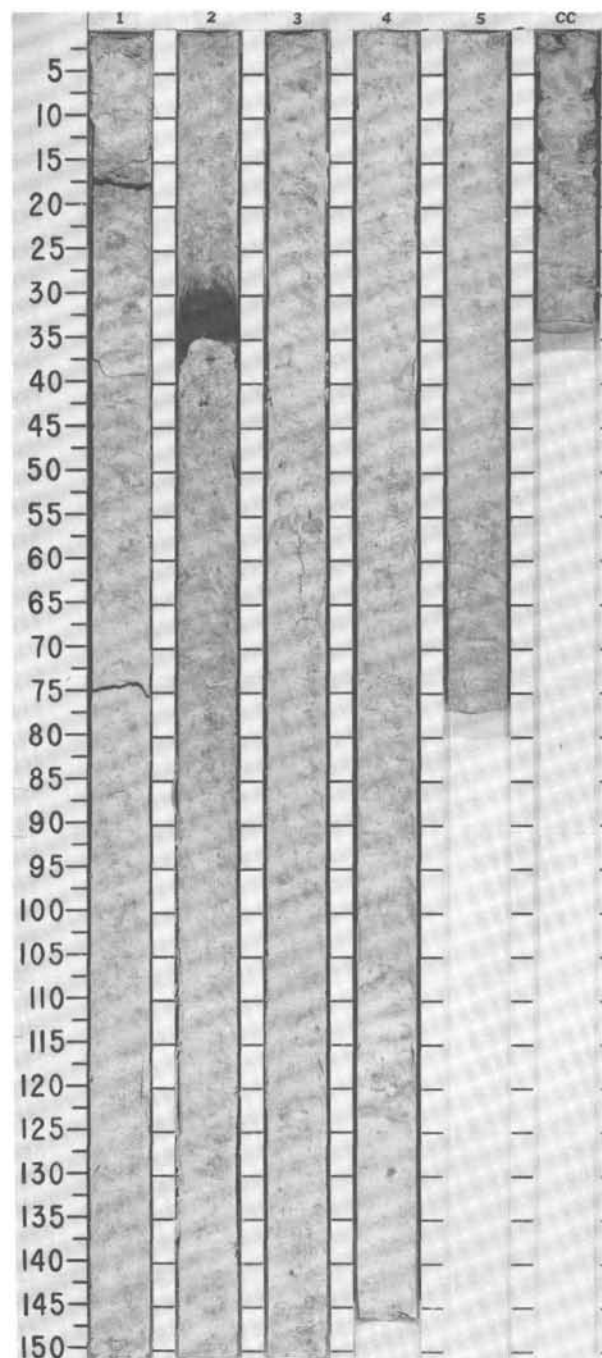


TIME-ROCK UNIT	BIOSTRAT. ZONE/ FOSSIL CHARACTER				PALEOMAGNETICS	PHYS. PROPERTIES	CHEMISTRY	SECTION	METERS	GRAPHIC LITHOLOGY	DRILLING DISTURB.	SED. STRUCTURES	SAMPLES	LITHOLOGIC DESCRIPTION						
	FORAMINIFERS	NANNOFOSSILS	RADIOLARIANS	DIATOMS																
EARLY PLIOCENE	NN13 <i>C. rugosus</i> Zone								0.5					SILICEOUS NANNOFOSSIL CHALK Grayish yellow green (5GY 7/1) and gray green (10Y 7/1 to 10Y 7/2) chalk. Relatively few burrows observed. Top of Section 5 is dark gray (10Y 4/1), and includes a pyrite haloed burrow at 664 cm. Mottled with gray (2.5Y 3/0, 5Y 8/1) and gray green (5G 7/1, 5Y 7/3). CHEMISTRY wt % CO ₂ /wt % total C: 1, 70 2, 70 3, 70 4, 70 5, 70 86.03/10.26 79.23/9.67 79.51/9.71 74.83/9.04 73.82/8.95 PHYSICAL PROPERTIES: 1, 70 2, 70 3, 70 4, 70 5, 70 WC (%) 66.08 76.19 74.94 83.49 83.90 P _g (g/cm ³) 3.00 2.86 3.02 2.84 2.94 P _b (g/cm ³) 1.69 1.61 1.64 1.57 1.58 φ (%) 66.16 68.29 69.12 70.10 70.92 σ (kPa) 29.79 23.83 26.21 64.34 53.62 K (W/mk) 1.243 1.191 1.113 1.012 1.217 V _p (m/s) 1609.9 1583.5 1573.0 1592.0 — SMEAR SLIDE SUMMARY (%): 2, 22 D TEXTURE: Sand 10 Silt 15 Clay 75 COMPOSITION: Quartz Tr Feldspar Tr Clay 7 Calcite/dolomite 3 Accessory minerals Tr Pyrite 1 Foraminifers 3 Nannofossils 72 Diatoms 10 Radiolarians 3 Sponge spicules 1 Silicoflagellates Tr						
									1.0											
	G. tumida Zone																			
	C/M <i>Ceratolithus tricorniculatus</i> Zone NN12																			
	S. pentas Zone																			



SITE 677 HOLE A CORE 23X CORED INTERVAL 202.1-211.7 mbsf

TIME-ROCK UNIT	BIOSTRAT. ZONE/ FOSSIL CHARACTER			PALEOMAGNETICS	PHYS. PROPERTIES	CHEMISTRY	SECTION	METERS	GRAPHIC LITHOLOGY	DRILLING DISTURB.	SED. STRUCTURES	SAMPLES	LITHOLOGIC DESCRIPTION
	FORAMINIFERS	NANNOFOSSILS	RADIOLARIANS										
EARLY PLIOCENE	<i>G. tumida</i> Zone							0.5					SILICEOUS NANNOFOSSIL CHALK Uniform light gray green (10Y 7/1 and 10Y 7/2) chalk. Moderately bioturbated, mottled with burrows and wisps of pyrite. Dark brown (10Y 3/1) volcanic ash layer (6 cm) in Section 2 contains biotite flakes. CHEMISTRY wt % CO ₂ /wt % total C: 1, 70 2, 70 3, 70 4, 70 5, 70 79.66/9.60 65.03/8.04 71.22/8.80 70.92/8.75 59.66/7.60 PHYSICAL PROPERTIES: 1, 70 2, 70 3, 70 4, 70 5, 70 WC (%) 74.85 96.47 93.71 90.25 101.75 p _g (g/cm ³) 2.93 3.32 2.52 2.17 2.38 p _b (g/cm ³) 1.63 1.57 1.47 2.17 2.38 φ (%) 68.44 75.98 70.06 65.97 70.62 σ (kPa) 23.83 28.59 28.59 47.66 120.30 K (W/mk) 1.201 1.176 1.101 1.204 1.062 V _p (m/s) 1577.4 1581.9 1586.3 1585.2 — SMEAR SLIDE SUMMARY (%): 2, 33 4, 80 M D TEXTURE: Sand 50 5 Silt 45 15 Clay 5 80 COMPOSITION: Quartz 2 — Feldspar 10 Tr Clay — 5 Volcanic glass 70 — Calcite/dolomite Tr 3 Accessory minerals — Tr Pyrite 15 1 Amphibole Tr — Phillipsite Tr — Foraminifers — 2 Nannofossils 3 75 Diatoms — 10 Radiolarians — 3 Sponge spicules — 1
	<i>C. tricorniculatus</i> Zone							1.0					
	<i>S. pentas</i> Zone												
LATE MIOCENE													



TIME-ROCK UNIT	BIOSTRAT. ZONE/ FOSSIL CHARACTER				PALEOMAGNETICS	PHYS. PROPERTIES	CHEMISTRY	SECTION	METERS	GRAPHIC LITHOLOGY	DRILLING DISTURB.	SED. STRUCTURES	SAMPLES	LITHOLOGIC DESCRIPTION								
	FORAMINIFERS	NANNOFOSSILS	RADIOLARIANS	DIATOMS																		
LATE MIOCENE	G. tumida Zone C. tricorniculatus Zone S. pentas Zone	C/M												SILICEOUS NANNOFOSSIL CHALK								
															Gray green (10Y 7/2, 10Y 6/1) bioturbated chalks. Burrows are filled with light gray sediment (5Y 7/2). Occasional layers of pale yellow green (5GY 7/1). Diffuse bands of pyrite occur in lower part of core.							
																CHEMISTRY wt % CO ₂ /wt % total C:						
																	1, 70 2, 70 3, 70 4, 70 5, 70 6, 70					
																		59.76/7.30 71.80/8.77 75.44/9.30 69.0/8.40 77.80/9.34 75.98/9.09				
																			PHYSICAL PROPERTIES:			
																				* 1, 70 2, 70 3, 70 4, 70 5, 70 6, 70		
																					WC (%) 118.26 84.36 83.37 104.00 75.09 80.84	
																						p _g (g/cm ³) 3.17 3.07 3.00 2.78 2.54 2.46
φ (%) 78.77 71.92 71.23 74.12 65.35 66.35																						
	σ (kPa) 23.83 33.36 26.21 28.59 22.64 69.10																					
		K (W/mk) 1.046 1.131 1.117 1.038 1.174 1.145																				
			V _p (m/s) — — 1590.2 1587.7 1592.6 1600.5																			
				SMEAR SLIDE SUMMARY (%):																		
					2, 10 D																	
						TEXTURE:																
							Sand 10 Silt 10 Clay 80															
								COMPOSITION:														
									Feldspar Tr Clay 5 Calcite/dolomite 1 Accessory minerals Pyrite Tr Foraminifers 3 Nannofossils 75 Diatoms 10 Radiolarians 5 Silicoflagellates Tr													

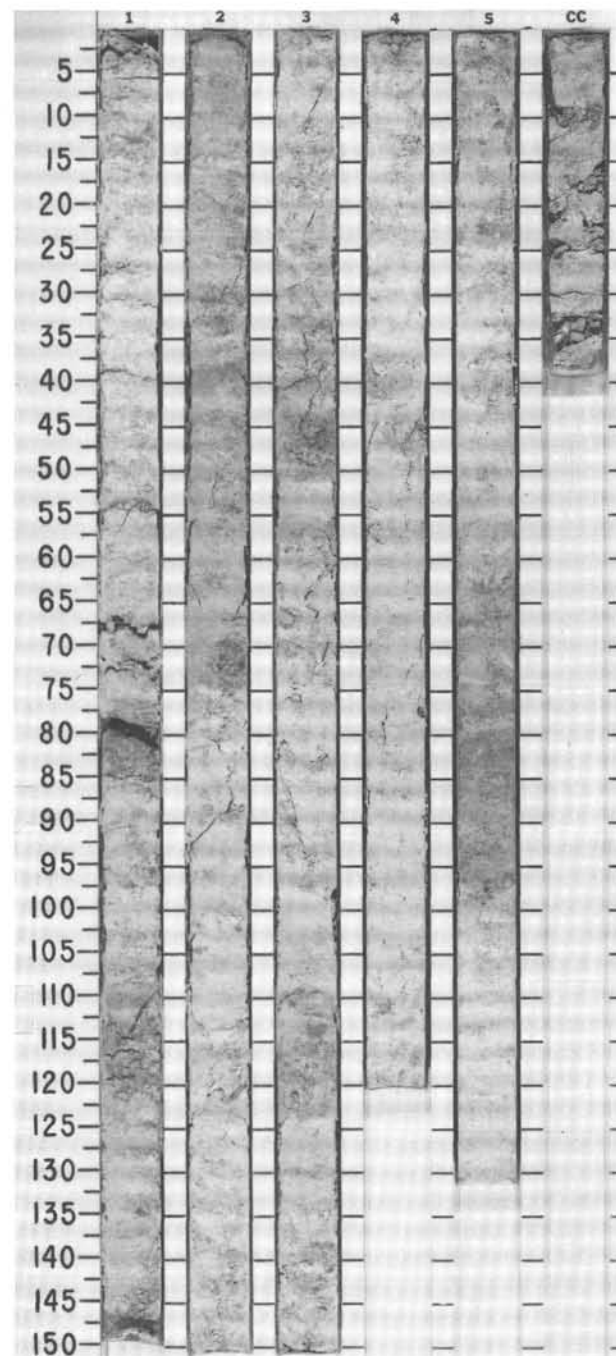
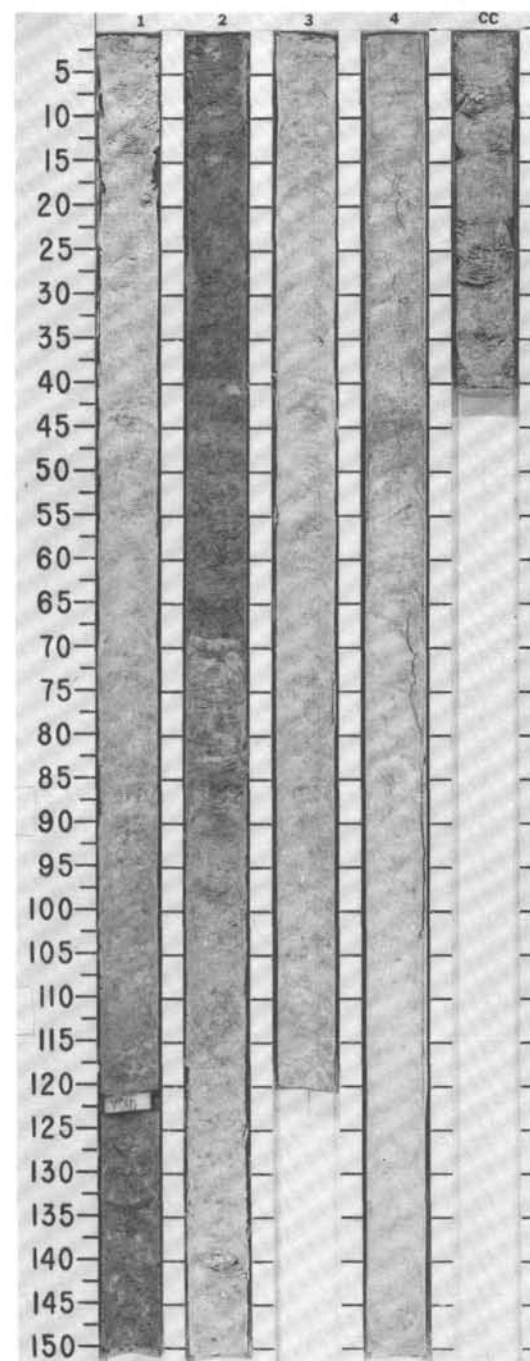
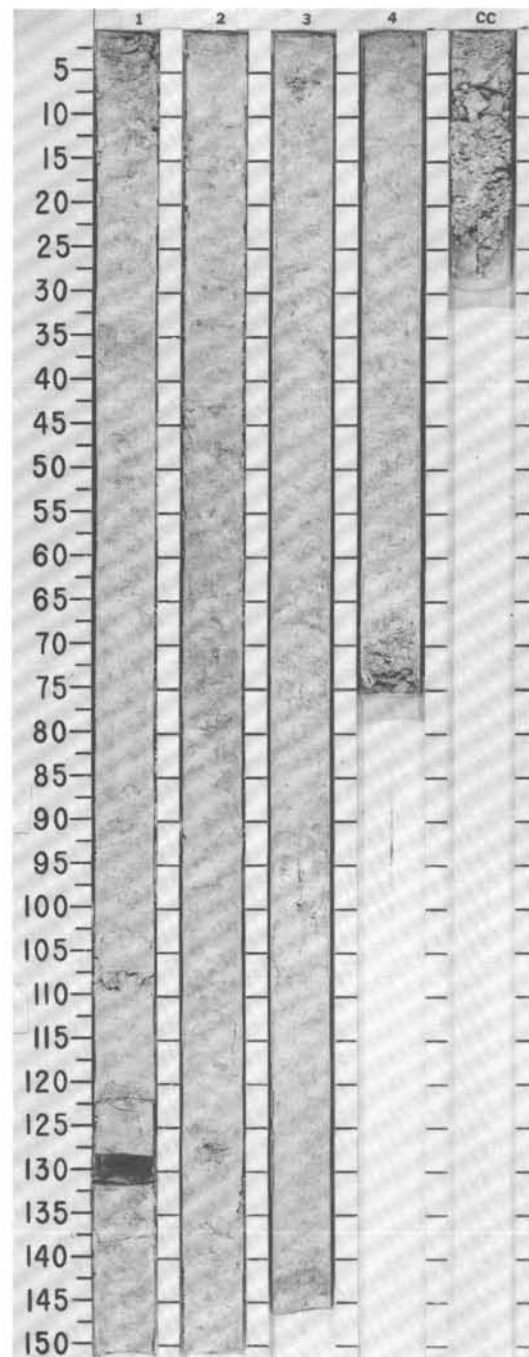
[illegible]

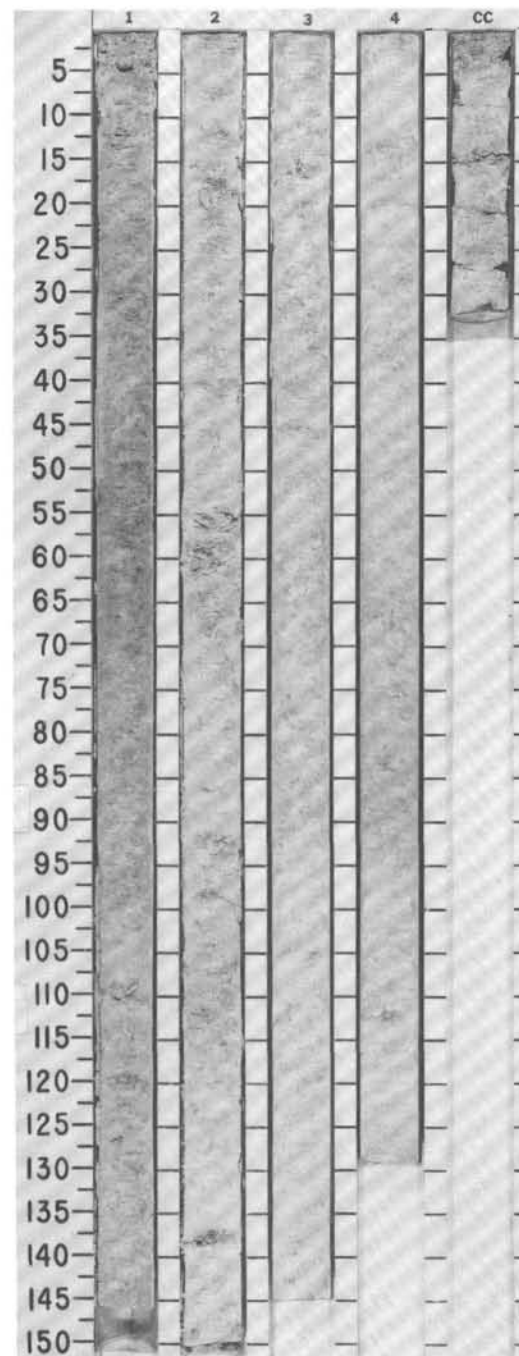
Figure 1 shows a vertical scale from 5 to 150 cm. Six vertical bars, labeled 1 through 6, and a control bar labeled 'CC', are shown. The bars represent different concentrations of the substance being tested. The bars are arranged vertically, with the scale on the left. The bars show varying degrees of darkening and texture, indicating the effect of the substance at different concentrations.



SITE 677		HOLE A		CORE 29X		CORED INTERVAL		260.0 - 269.7 mbsf						
TIME-ROCK UNIT	BIOSTRAT. ZONE/ FOSSIL CHARACTER				PALEOMAGNETICS	PHYS. PROPERTIES	CHEMISTRY	SECTION	METERS	GRAPHIC LITHOLOGY	DRILLING DISTURB.	SED. STRUCTURES	SAMPLES	LITHOLOGIC DESCRIPTION
	FORAMINIFERS	NANNOFOSSILS	RADIOLARIANS	DIATOMS										
LATE MIOCENE	<i>G. plesiotumida</i> Zone	NN11	<i>D. quinqueringus</i> Zone	<i>S. peregrina</i> Zone		● ■		1	0.5					SILICEOUS NANNOFOSSIL CHALK Uniformly gray (10Y 7/1) mottled with light gray (5Y 7/1 to 5Y 7/2) chalk in Sections 1 through 3, changing to light gray (5Y 7/2) in the lower part of Section 3 and Section 4. Moderately bioturbated. The chalk is becoming more indurated, and begins to show cracking, fragmentation, and an undulating split surface (due to variations in degree of induration). CHEMISTRY wt % CO ₂ /wt % total C: 1, 76 2, 76 3, 75 4, 36 81.29/9.67 70.34/8.57 77.72/9.32 72.81/8.74 PHYSICAL PROPERTIES: 1, 76 2, 76 3, 75 4, 36 WC (%) 65.52 80.60 66.29 73.20 p _g (g/cm ³) 2.70 2.63 2.88 2.43 p _b (g/cm ³) 1.63 1.54 1.67 1.53 φ (%) 63.57 67.75 65.34 63.76 σ (kPa) 39.32 30.98 59.57 64.34 K (W/mk) 1.178 1.052 1.074 1.057 V _p (m/s) 1655.2 1550.6 — 1605.9 SMEAR SLIDE SUMMARY (%): 2, 70 D TEXTURE: Sand 7 Silt 15 Clay 78 COMPOSITION: Feldspar Tr Clay 5 Calcite/dolomite 5 Accessory minerals Tr Pyrite Tr Foraminifers 2 Nannofossils 75 Diatoms 10 Radiolarians 2 Sponge spicules 1 Silicoflagellates Tr Fish remains Tr
									1.0					
	2													
	3													
4														
CC														



TIME-ROCK UNIT	BIOSTRAT. ZONE/ FOSSIL CHARACTER				PALEOMAGNETICS	PHYS. PROPERTIES	CHEMISTRY	SECTION	METERS	GRAPHIC LITHOLOGY	DRILLING DISTURB.	SED. STRUCTURES	SAMPLES	LITHOLOGIC DESCRIPTION
	FORAMINIFERS	NANNOFOSSILS	RADIOLARIANS	DIAATOMS										
LATE MIOCENE														SILICEOUS NANNOFOSSIL CHALK
	G. plesiotumida Zone								0.5					Predominantly light gray (5Y 7/1 to 5Y 7/2) chalk with minor olive gray (5Y 6/2) component in Section 1. Generally homogeneous and competent with some broken fragments (from coring) of more indurated chalk. Diffuse patches and layers of pyrite. Moderate to slight bioturbation.
	D. quinqueramus Zone								1.0					CHEMISTRY wt % CO ₃ /wt % total C:
														1. 74 2. 76 3. 75 4. 65
	S. peregrina Zone													59.39/7.20 77.11/9.25 80.73/9.59 79.99/9.64
														PHYSICAL PROPERTIES:
														1. 74 2. 76 3. 75 4. 65
														WC (%) 100.59 72.01 59.36 58.82
														p _a (g/cm ³) 2.62 2.46 3.23 2.59
														p _b (g/cm ³) 1.47 1.54 1.79 1.65
														φ (%) 72.30 63.62 65.43 60.04
														σ (kPa) 26.21 22.64 52.42 97.70
														K (W/mk) 0.996 1.252 1.181 1.248
														V _p (m/s) 1593.8 1610.4 1625.9 1632.1
														SMEAR SLIDE SUMMARY (%):
														4. 80
														D
														TEXTURE:
														Sand 5
														Silt 20
														Clay 75
														COMPOSITION:
														Feldspar Tr
														Clay 7
														Calcite/dolomite 7
														Accessory minerals
														Pyrite Tr
														Foraminifers Tr
														Nannofossils 70
														Diatoms 10
														Radiolarians 3
														Sponge spicules 3
														Silicoflagellates Tr



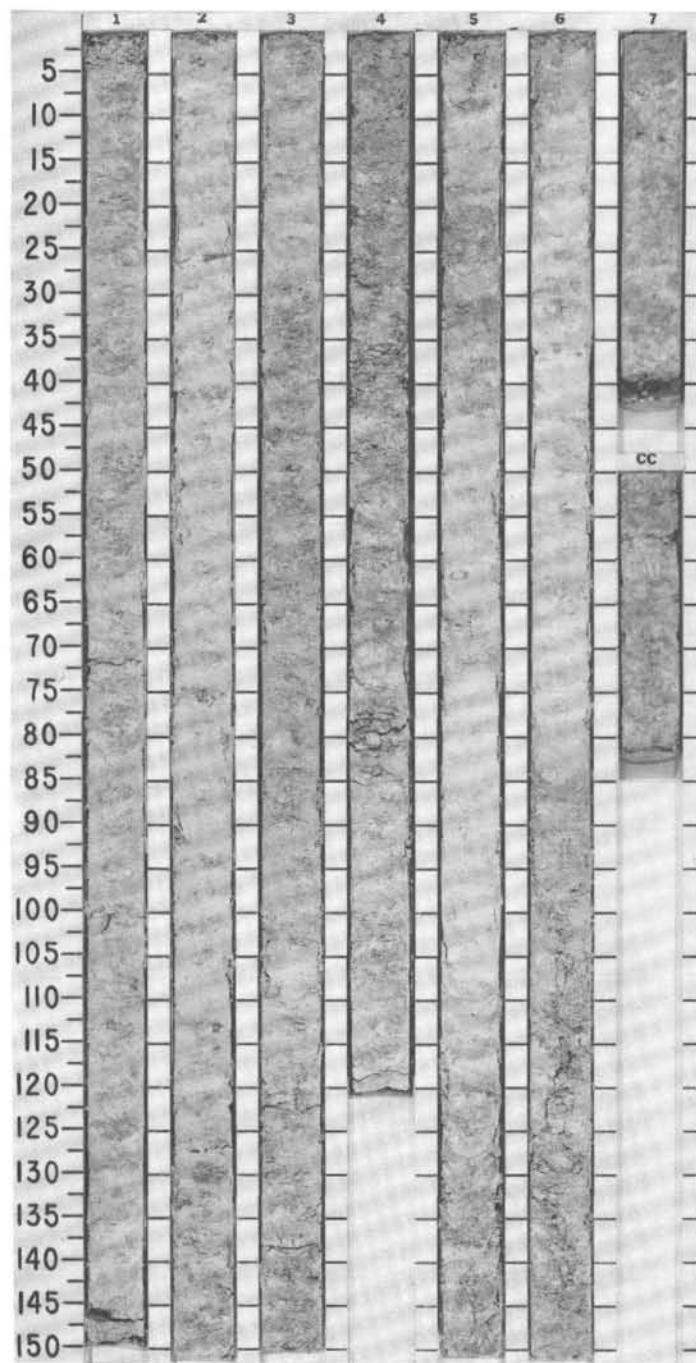
SITE 677 HOLE A

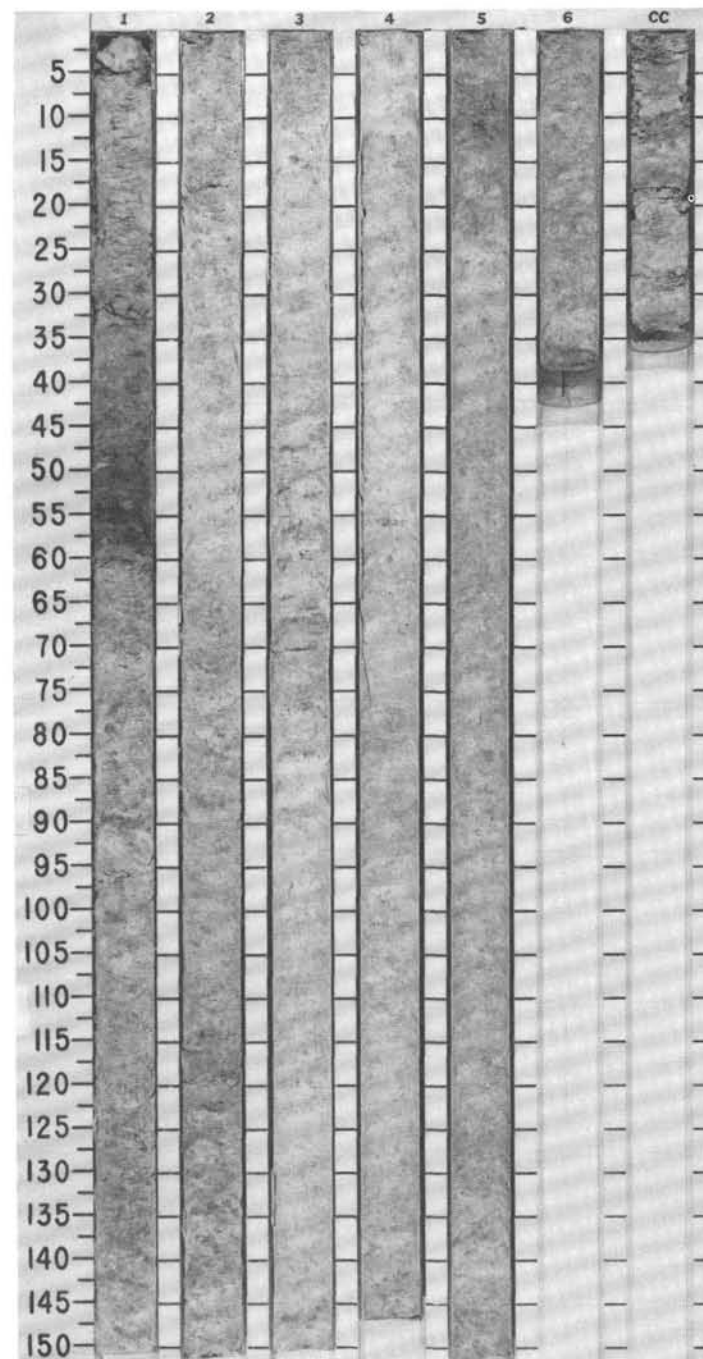
CORE 31X

CORED INTERVAL

279.3 - 288.9 mbsf

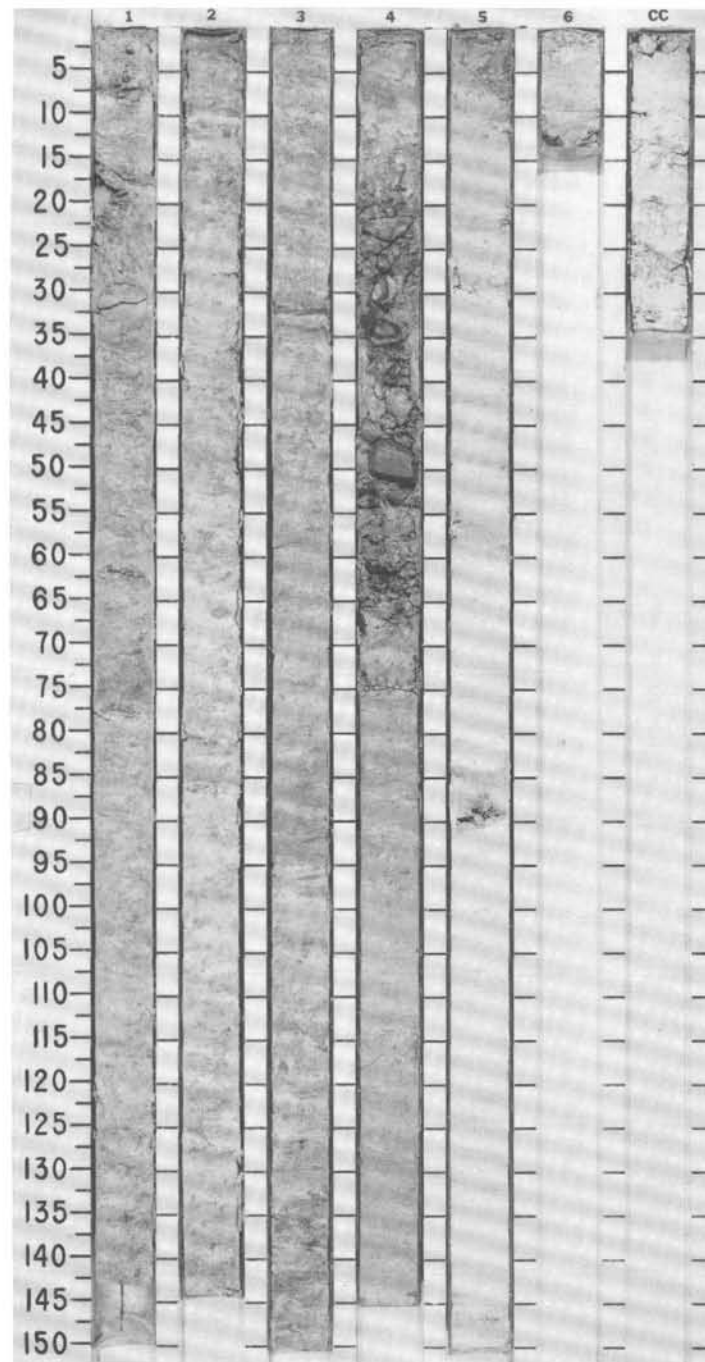
TIME-ROCK UNIT	BIOSTRAT. ZONE/ FOSSIL CHARACTER				PALEOMAGNETICS	PHYS. PROPERTIES	CHEMISTRY	SECTION	METERS	GRAPHIC LITHOLOGY	DRILLING DISTURB.	SED. STRUCTURES	SAMPLES	LITHOLOGIC DESCRIPTION
	FORAMINIFERS	NANNOFOSSILS	RADIOLARIANS	DIATOMS										
LATE MIOCENE	<i>G. plesiotumida</i> Zone	NN11	<i>D. quinqueramus</i> Zone	<i>S. peregrina</i> Zone	● ■	■ ■	● ■	1	0.5				NANNOFOSSIL CHALK	
									1.0					Sections 1 and 2 consist of homogeneous grayish yellow green (5GY 7/1) chalk with alternating competent and less competent layers, mottled with 2.5Y 4/0, 5Y 6/3, 5G 7/2, and 5Y 7/1. The lower part of Section 2 and all of Sections 3 and 4 consist of light gray (5Y 7/1 and 10Y 7/1) chalk mottled with 2.5Y 4/0, 2.5Y 7/3 and 5G 7/1. Sections 5 and 6 consist of light gray (5Y 7/1) chalk intercalated with pale yellowish green (5GY 7/1) chalk. Thin layer of pyrite in Section 5 at 145 cm. Bioturbation moderate throughout.
	C/M					● ■	■ ■	● ■	2				CHEMISTRY wt % CO ₃ /wt % total C: 2.78 3.76 4.78 5.85 6.74 70.17/8.32 56.61/6.86 58.67/7.13 70.41/8.32 87.21/8.74	
						● ■	■ ■	● ■	3				PHYSICAL PROPERTIES: 1, 2.78 3.76 4.78 5.85 6.74 WC (%) 80.18 80.95 105.62 92.10 81.55 81.05 p _g (g/cm ³) 2.45 2.38 2.64 3.07 2.76 2.42 p _b (g/cm ³) 1.51 1.49 1.45 1.56 1.56 1.50 φ (%) 66.04 65.61 73.46 73.67 69.00 65.98 σ (kPa) 33.36 27.40 22.64 21.45 27.40 46.47 K (W/mk) 1.179 1.115 0.973 1.007 0.901 1.151 V _p (m/s) — 1591.8 1588.7 1508.8 1580.1 1594.2	
						● ■	■ ■	● ■	4				SMEAR SLIDE SUMMARY (%): 2.53 D	
					● ■	■ ■	● ■	5				TEXTURE: Sand 5 Silt 10 Clay 85		
					● ■	■ ■	● ■	6				COMPOSITION: Clay 7 Calcite/dolomite 3 Accessory minerals Tr Pyrite 1 Foraminifers Tr Nannofossils 80 Diatoms 7 Radiolarians 1 Sponge spicules 1		
					● ■	■ ■	● ■	7						
					● ■	■ ■	● ■	CC						



[illegible]

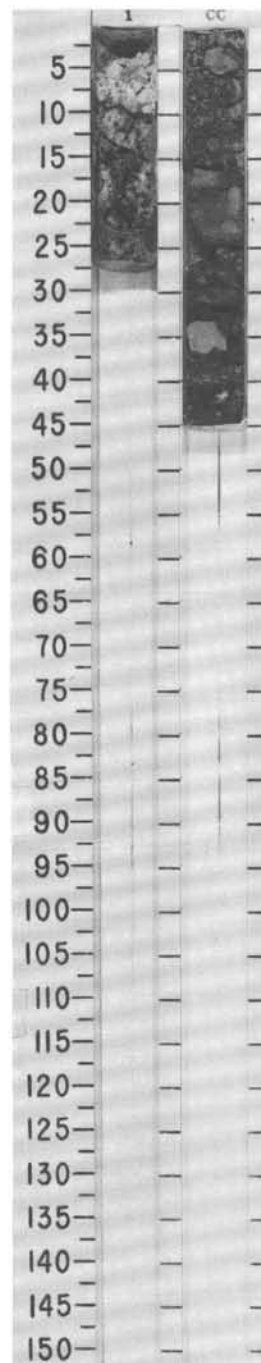
SITE 677 HOLE A CORE 33X CORED INTERVAL 298.6-308.4 mbsf

TIME-ROCK UNIT	BIOSTRAT. ZONE/ FOSSIL CHARACTER				PALEOMAGNETICS	PHYS. PROPERTIES	CHEMISTRY	SECTION	METERS	GRAPHIC LITHOLOGY	DRILLING DISTURB.	SED. STRUCTURES	SAMPLES	LITHOLOGIC DESCRIPTION
	FORAMINIFERS	NANNOFOSSILS	RADIOLARIANS	DIATOMS										
LATE MIOCENE	NN11 <i>D. quinqueramus</i> Zone	C/P							0.5					DIATOM-NANNOFOSSIL CHALK, CHERTY LIMESTONE, AND NANNOFOSSIL CHALK
									1.0				Predominantly light gray (5Y 7/1, 5Y 7/2, 10Y 7/1) chalk mottled with 2.5Y 7/2, 2.5Y 4/0, and 10G 6/2. Four large (3-6 cm diameter) pieces of cherty limestone were found in Section 4 (467-516 cm). They are brownish (5Y) in color and are thinly laminated with silicified areas cutting across primary bioturbation features. Many small pieces of this cherty limestone are found within the 467-516 cm interval. Lower part of Section 5 and Section 6 are filled with pale green (5G 8/1 and 5GY 7/1) chalk. Moderately bioturbated, competent, little visible structure.	
														2
													CHEMISTRY wt % CO ₂ /wt % total C:	
														3
														1, 68 2, 68 3, 79 4, 85 5, 77
														52.63/6.19 67.74/8.15 60.45/7.59 75.68/9.46 81.67/9.36
													* PHYSICAL PROPERTIES:	
														6
													1, 68 3, 79 4, 85 5, 77	
														CC
													WC (%) 117.99 98.60 48.37 41.75 ρ_g (g/cm ³) 2.95 2.52 2.78 2.75 ρ_b (g/cm ³) 1.46 1.46 1.78 1.84 ϕ (%) 77.54 71.08 57.05 53.13 σ (kPa) 30.98 60.76 64.34 168.00 K (W/mk) 0.935 1.084 1.429 1.447 V_p (m/s) 1568.8 — 1608.1 1662.7	
													SMEAR SLIDE SUMMARY (%):	
													2, 84 4, 110 D D	
													TEXTURE:	
													Sand 5 1 Silt 25 5 Clay 70 94	
													COMPOSITION:	
													Feldspar Tr 1 Clay 3 5 Calcite/dolomite 2 — Accessory minerals Tr Tr Pyrite — 2 Foraminifers Tr 2 Nannofossils 69 90 Diatoms 25 Tr Radiolarians 1 — Silicoflagellates Tr —	



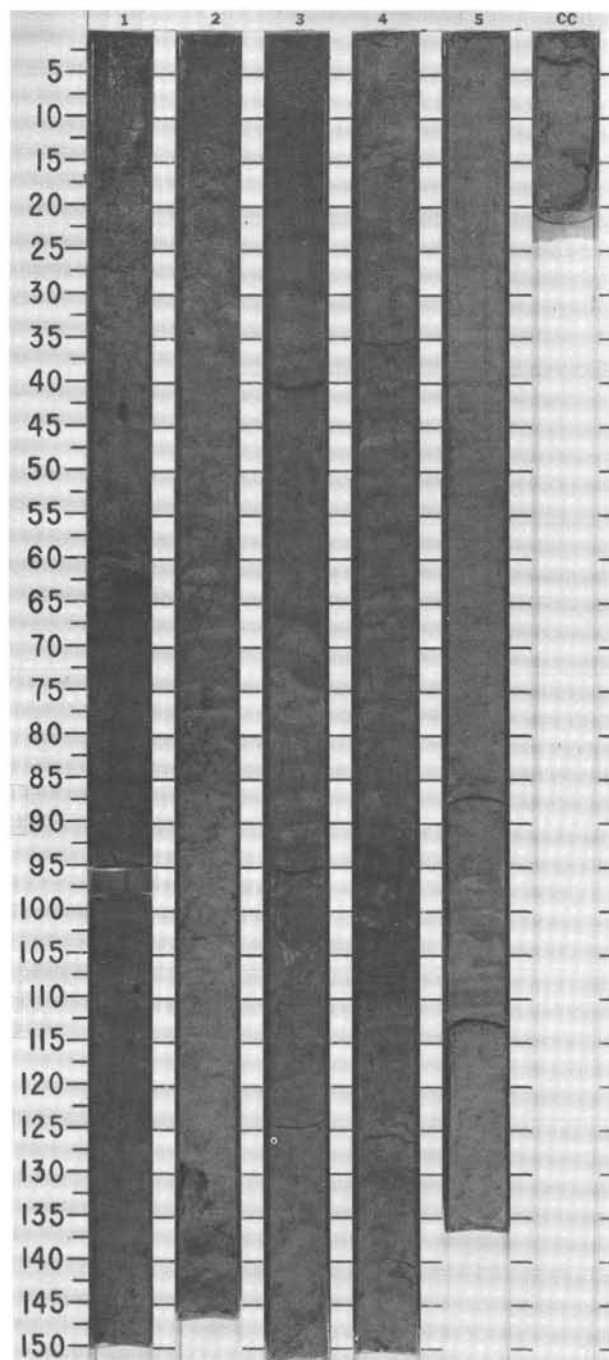
SITES 677 AND 678

TIME-ROCK UNIT	BIOSTRAT. ZONE/ FOSSIL CHARACTER				SECTION	METERS	GRAPHIC LITHOLOGY	DRILLING DISTURB.	SED. STRUCTURES	SAMPLES	LITHOLOGIC DESCRIPTION
	FORAMINIFERS	NANNOFOSSILS	RADIOLARIANS	DIAZONES							
LATE MIOCENE	C/P NN11 D. <i>quinqueramus</i>										SILICEOUS NANNOFOSSIL CHALK, METALLIFEROUS CLAYS, WEATHERED BASALT, AND BASALT Section 1 consists of pale green (10GY 8/1) chalk in upper 9 cm, followed by a mixture of soft pale green (10GY 8/1) and dark green (7.5 G 4/2) ooze mixed with black glassy basalt fragments. CC is filled with brecciated mixture of weathered and fresh basalt and sediments. SMEAR SLIDE SUMMARY (%): 1, 5

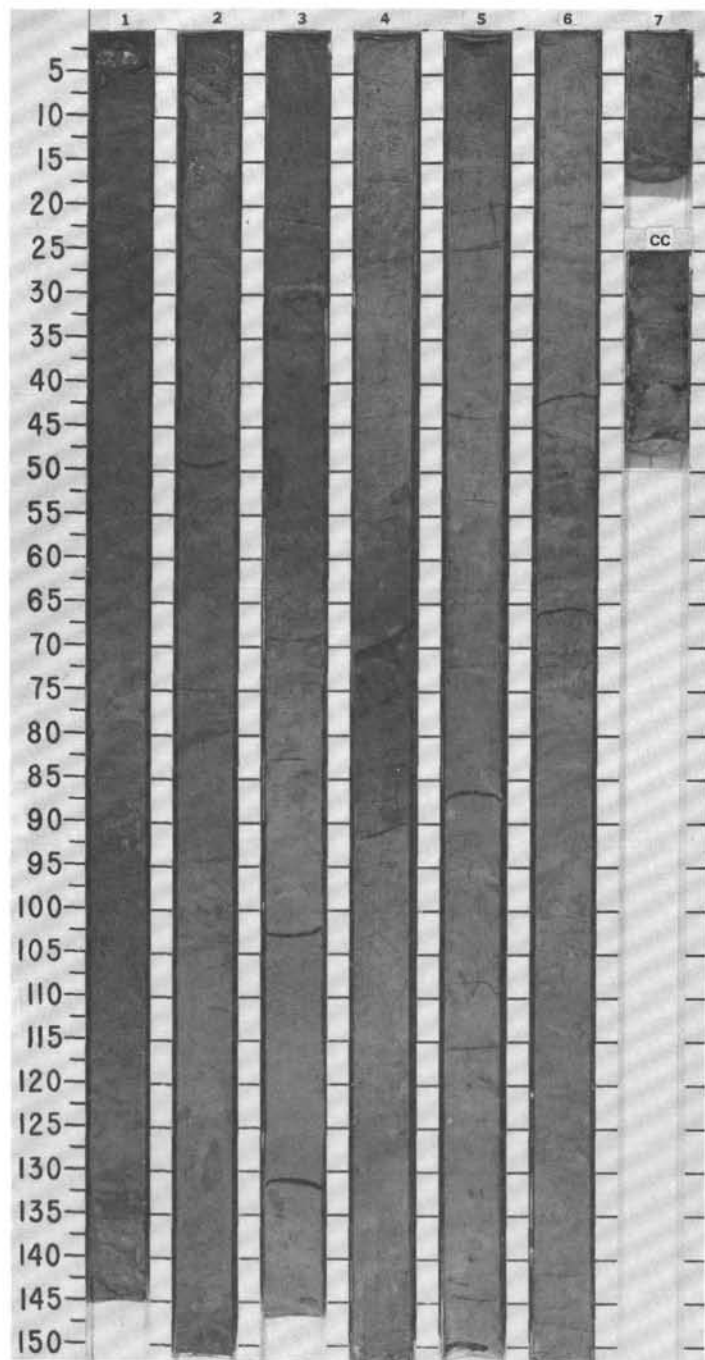


SITE 677 HOLE B CORE 1H CORED INTERVAL 0-7.6 mbsf

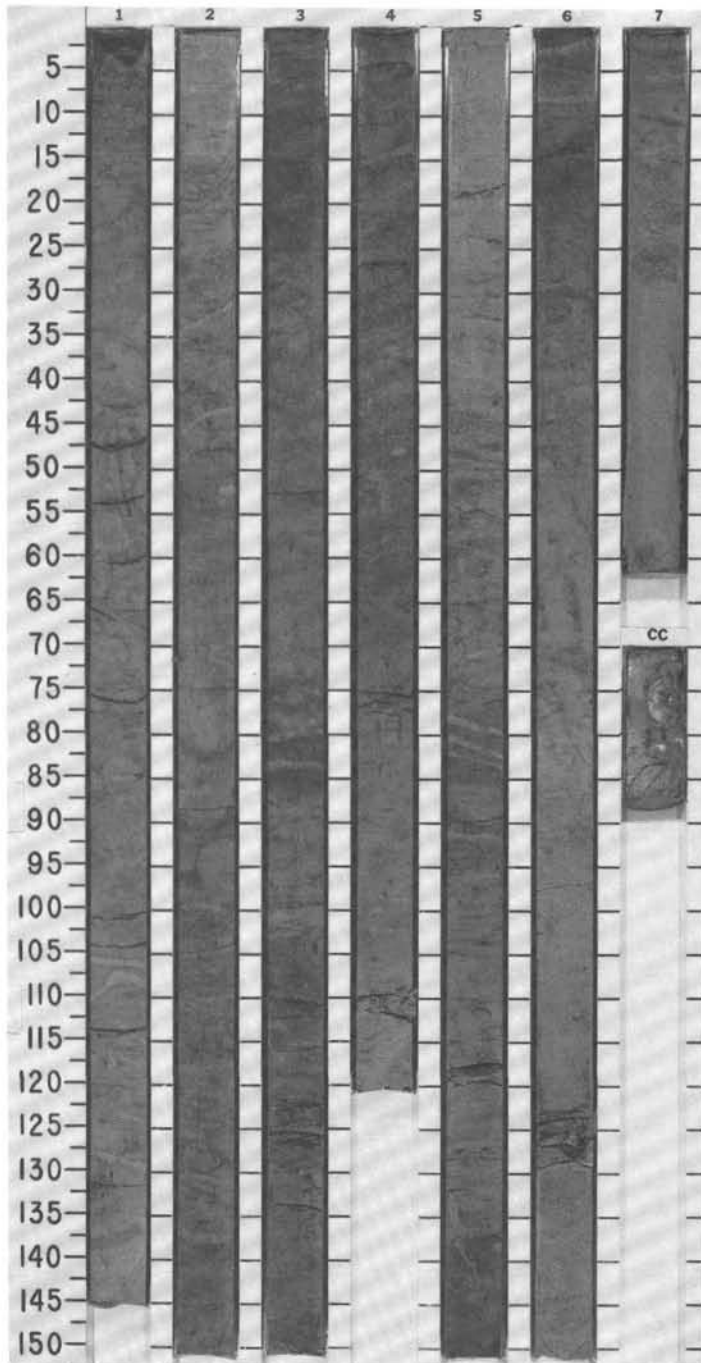
TIME-ROCK UNIT	BIOSTRAT. ZONE/ FOSSIL CHARACTER				PALEOMAGNETICS	PHYS. PROPERTIES	CHEMISTRY	SECTION	METERS	GRAPHIC LITHOLOGY	DRILLING DISTURB.	SED. STRUCTURES	SAMPLES	LITHOLOGIC DESCRIPTION
	FORAMINIFERS	NANNOFOSSILS	RADIOLARIANS	DIATOMS										
LATE PLEISTOCENE	<i>P. obliquiloculata</i> Zone <i>NN21 E. huxleyi</i> Zone F/M													



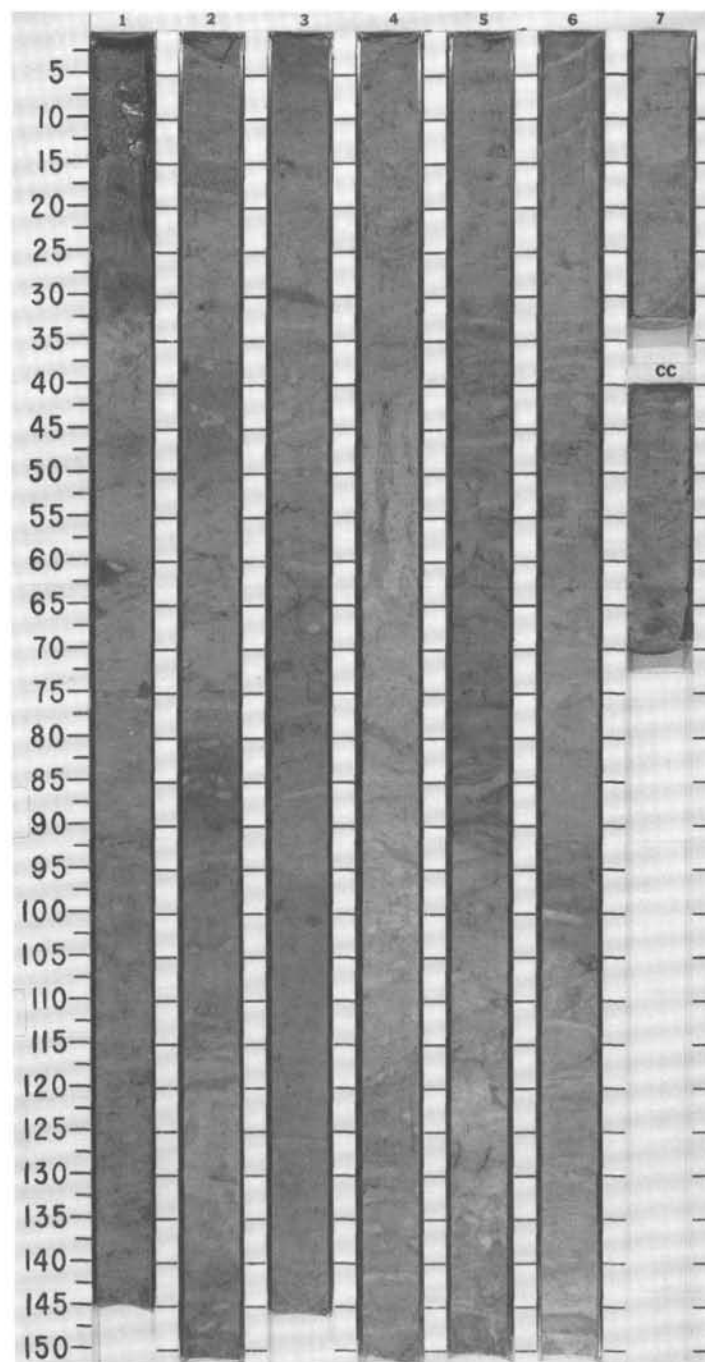
TIME-ROCK UNIT	BIOSTRAT. ZONE/ FOSSIL CHARACTER				PALEOMAGNETICS	PHYS. PROPERTIES	CHEMISTRY	SECTION	METERS	GRAPHIC LITHOLOGY	DRILLING DISTURB.	SED. STRUCTURES	SAMPLES	LITHOLOGIC DESCRIPTION																																																																																													
	FORAMINIFERS	NANNOFOSSILS	RADIOLARIANS	DIATOMS																																																																																																							
LATE PLEISTOCENE	NN21 <i>E. huxleyi</i> Zone				•			1	0.5 1.0					RADIOLARIAN-DIATOM-NANNOFOSSIL OOZE AND VOLCANIC ASH Dusky yellow green (5GY 5/2) ooze intercalated with olive green (10Y 4/2, 10Y 4/3, 10Y 5/2, 10Y 5/3, 10Y 6/2) ooze. Common simple <i>Zoophycos</i> burrows. Volcanic ash layer (Gley N6) and patches occur in Sections 2 and 6. Moderate to slight bioturbation throughout. PHYSICAL PROPERTIES: <table><tr><td></td><td>1,</td><td>2,</td><td>3,</td><td>4,</td><td>5,</td><td>6,</td></tr><tr><td>WC (%)</td><td>215.35</td><td>155.90</td><td>184.88</td><td>200.24</td><td>174.81</td><td>173.97</td></tr><tr><td>ρ_g (g/cm³)</td><td>2.15</td><td>3.00</td><td>2.34</td><td>2.90</td><td>3.02</td><td>2.70</td></tr><tr><td>ρ_b (g/cm³)</td><td>1.22</td><td>1.38</td><td>1.27</td><td>1.30</td><td>1.34</td><td>1.32</td></tr><tr><td>ϕ (%)</td><td>82.27</td><td>82.30</td><td>81.20</td><td>85.26</td><td>84.00</td><td>82.41</td></tr><tr><td>K (W/mk)</td><td>0.903</td><td>0.906</td><td>0.928</td><td>0.875</td><td>0.880</td><td>0.884</td></tr></table> SMEAR SLIDE SUMMARY (%): <table><tr><td></td><td>2, 7</td><td>4, 96</td></tr><tr><td></td><td>M</td><td>D</td></tr></table> TEXTURE: <table><tr><td>Sand</td><td>35</td><td>20</td></tr><tr><td>Silt</td><td>60</td><td>30</td></tr><tr><td>Clay</td><td>5</td><td>50</td></tr></table> COMPOSITION: <table><tr><td>Feldspar</td><td>10</td><td>1</td></tr><tr><td>Clay</td><td>—</td><td>10</td></tr><tr><td>Volcanic glass</td><td>80</td><td>—</td></tr><tr><td>Calcite/dolomite</td><td>—</td><td>10</td></tr><tr><td>Accessory minerals</td><td>10</td><td>2</td></tr><tr><td>Pyrite</td><td>—</td><td>Tr</td></tr><tr><td>Foraminifers</td><td>—</td><td>7</td></tr><tr><td>Nannofossils</td><td>Tr</td><td>30</td></tr><tr><td>Diatoms</td><td>—</td><td>20</td></tr><tr><td>Radiolarians</td><td>—</td><td>15</td></tr><tr><td>Sponge spicules</td><td>—</td><td>5</td></tr><tr><td>Silicoflagellates</td><td>—</td><td>Tr</td></tr></table>		1,	2,	3,	4,	5,	6,	WC (%)	215.35	155.90	184.88	200.24	174.81	173.97	ρ_g (g/cm ³)	2.15	3.00	2.34	2.90	3.02	2.70	ρ_b (g/cm ³)	1.22	1.38	1.27	1.30	1.34	1.32	ϕ (%)	82.27	82.30	81.20	85.26	84.00	82.41	K (W/mk)	0.903	0.906	0.928	0.875	0.880	0.884		2, 7	4, 96		M	D	Sand	35	20	Silt	60	30	Clay	5	50	Feldspar	10	1	Clay	—	10	Volcanic glass	80	—	Calcite/dolomite	—	10	Accessory minerals	10	2	Pyrite	—	Tr	Foraminifers	—	7	Nannofossils	Tr	30	Diatoms	—	20	Radiolarians	—	15	Sponge spicules	—	5	Silicoflagellates	—	Tr
		1,	2,	3,	4,	5,	6,																																																																																																				
	WC (%)	215.35	155.90	184.88	200.24	174.81	173.97																																																																																																				
	ρ_g (g/cm ³)	2.15	3.00	2.34	2.90	3.02	2.70																																																																																																				
	ρ_b (g/cm ³)	1.22	1.38	1.27	1.30	1.34	1.32																																																																																																				
	ϕ (%)	82.27	82.30	81.20	85.26	84.00	82.41																																																																																																				
	K (W/mk)	0.903	0.906	0.928	0.875	0.880	0.884																																																																																																				
	2, 7	4, 96																																																																																																									
	M	D																																																																																																									
Sand	35	20																																																																																																									
Silt	60	30																																																																																																									
Clay	5	50																																																																																																									
Feldspar	10	1																																																																																																									
Clay	—	10																																																																																																									
Volcanic glass	80	—																																																																																																									
Calcite/dolomite	—	10																																																																																																									
Accessory minerals	10	2																																																																																																									
Pyrite	—	Tr																																																																																																									
Foraminifers	—	7																																																																																																									
Nannofossils	Tr	30																																																																																																									
Diatoms	—	20																																																																																																									
Radiolarians	—	15																																																																																																									
Sponge spicules	—	5																																																																																																									
Silicoflagellates	—	Tr																																																																																																									
	NN20 <i>G. oceanica</i> Zone				•			2																																																																																																			
	<i>P. obliquiloculata</i> Zone				•			3																																																																																																			
	C/M				•			4																																																																																																			
					•			5																																																																																																			
					•			6																																																																																																			
								7																																																																																																			
								CC																																																																																																			



SITES 677 AND 678

[illegible]

TIME-ROCK UNIT	BIOSTRAT. ZONE/ FOSSIL CHARACTER				PHYS. PROPERTIES	CHEMISTRY	SECTION	METERS	GRAPHIC LITHOLOGY	DRILLING DISTURB.	SED. STRUCTURES	SAMPLES	LITHOLOGIC DESCRIPTION
	FORAMINIFERS	NANNOFOSSILS	RADIOLARIANS	DIATOMS									
MIDDLE PLEISTOCENE	<i>P. obliquiloculata</i> Zone NN19 <i>P. lacunosa</i> Zone C/G						1	0.5					DIATOM-NANNOFOSSIL OOZE Yellow green (5GY 5/2 to 5GY 6/2) interlayered with olive green (10Y 4/2 to 10Y 5/3) and gray green (10Y 6/2) ooze. Vertical and subhorizontal pyrite tracks, patches and banding common. Moderately bioturbated throughout.
								1.0					
							2						PHYSICAL PROPERTIES: 1. 2. 3. 4. 5. 6. WC (%) 146.06 173.26 158.92 124.50 182.51 135.77 ρ_g (g/cm ³) 2.32 2.23 2.64 3.27 2.87 3.14 ρ_b (g/cm ³) 1.32 1.27 1.34 1.47 1.32 1.43 ϕ (%) 77.14 79.41 80.67 80.15 83.90 80.85 K (W/mk) 0.907 1.021 0.914 0.954 0.851 0.901
							3						SMEAR SLIDE SUMMARY (%): 2, 69 6, 80 D D TEXTURE: Sand 20 15 Silt 40 25 Clay 40 60 COMPOSITION: Feldspar 1 Tr Clay 7 7 Calcite/dolomite 10 10 Accessory minerals 1 1 Pyrite 1 2 Foraminifers 5 5 Nannofossils 30 40 Diatoms 25 20 Radiolarians 10 7 Sponge spicules 10 7 Silicoflagellates 1 1
							4						
							5						
							6						
							7						
							CC						



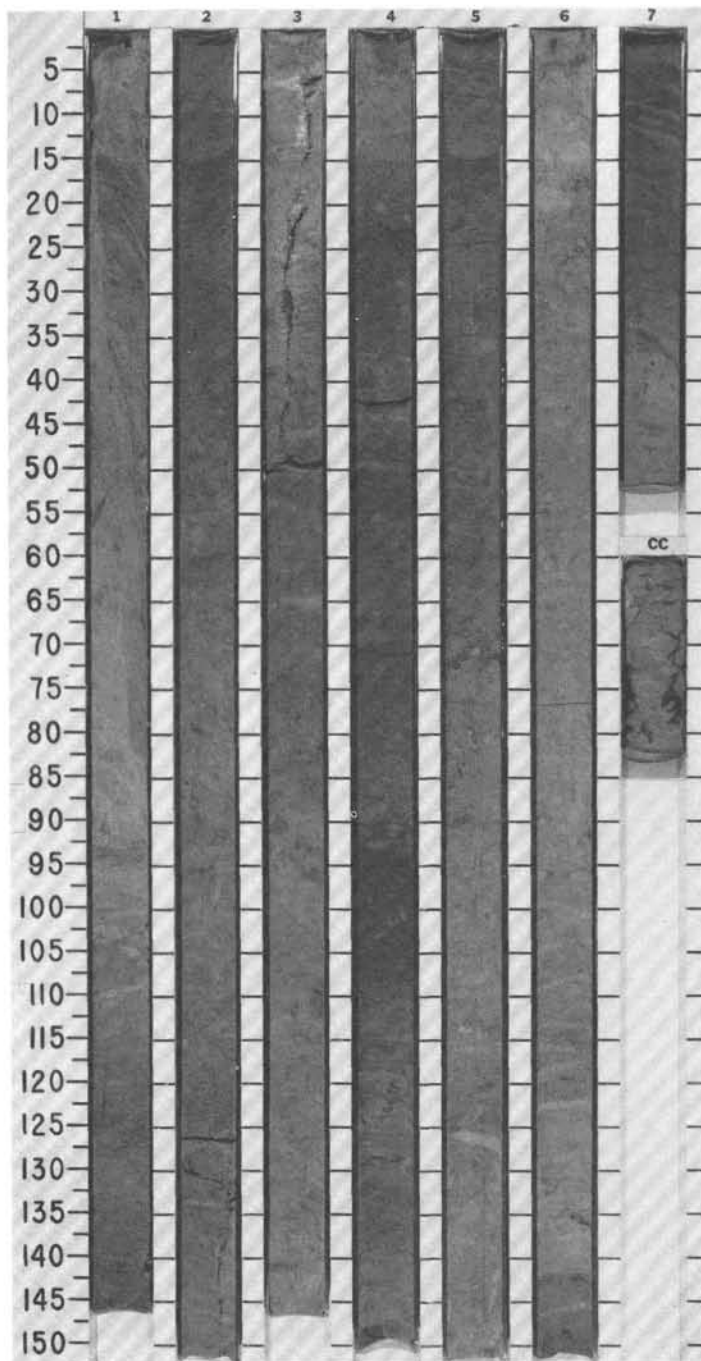
SITE 677 HOLE B CORE 5H CORED INTERVAL 36.1-45.6 mbsf

TIME-ROCK UNIT	BIOSTRAT. ZONE/ FOSSIL CHARACTER				PALEOMAGNETICS	PHYS. PROPERTIES	CHEMISTRY	SECTION	METERS	GRAPHIC LITHOLOGY	DRILLING DISTURB.	SED. STRUCTURES	SAMPLES	LITHOLOGIC DESCRIPTION
	FORAMINIFERS	NANNOFOSSILS	RADIOLARIANS	DIATOMS										
MIDDLE PLEISTOCENE														
<i>P. obliquiloculata</i> Zone														
NN19 <i>P. lacunosa</i> Zone														
F/G														

MIDDLE PLEISTOCENE

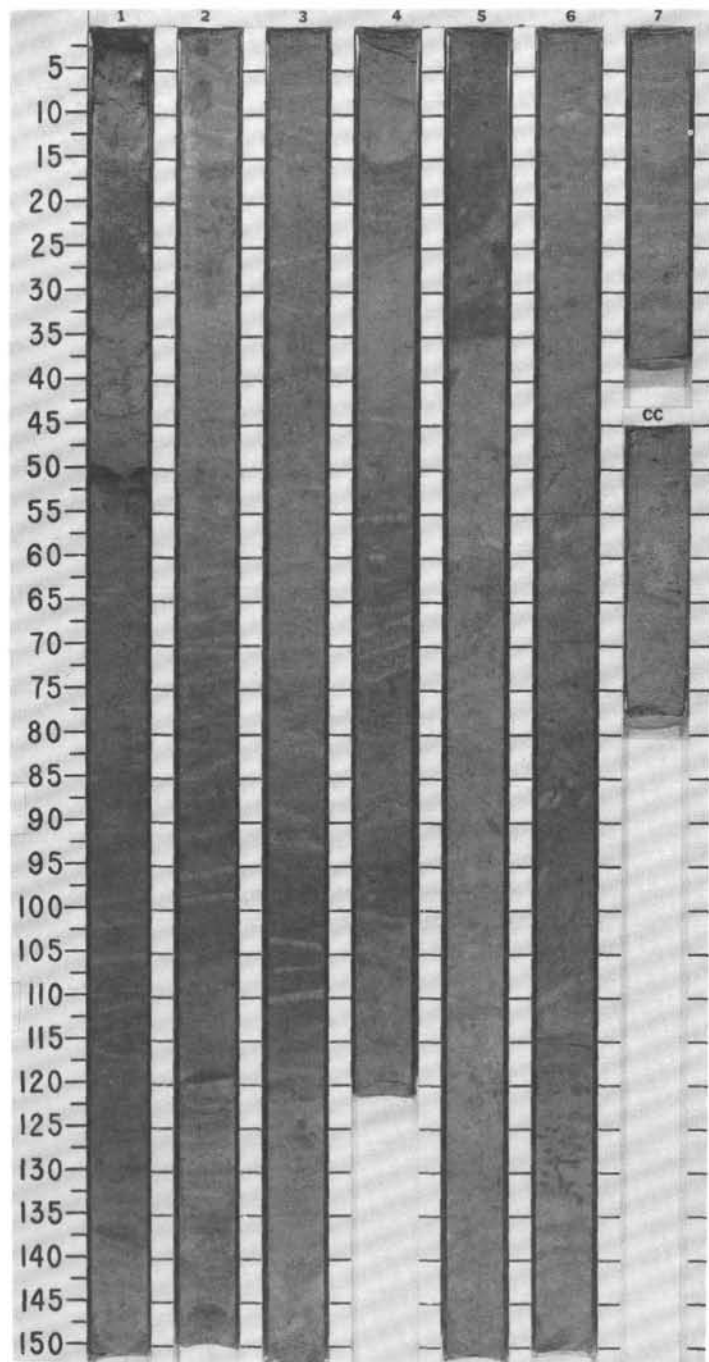
P. obliquiloculata ZoneNN19 *P. lacunosa* Zone

F/G



SITE 677 HOLE B CORE 6H CORED INTERVAL 45.6-55.1 mbsf

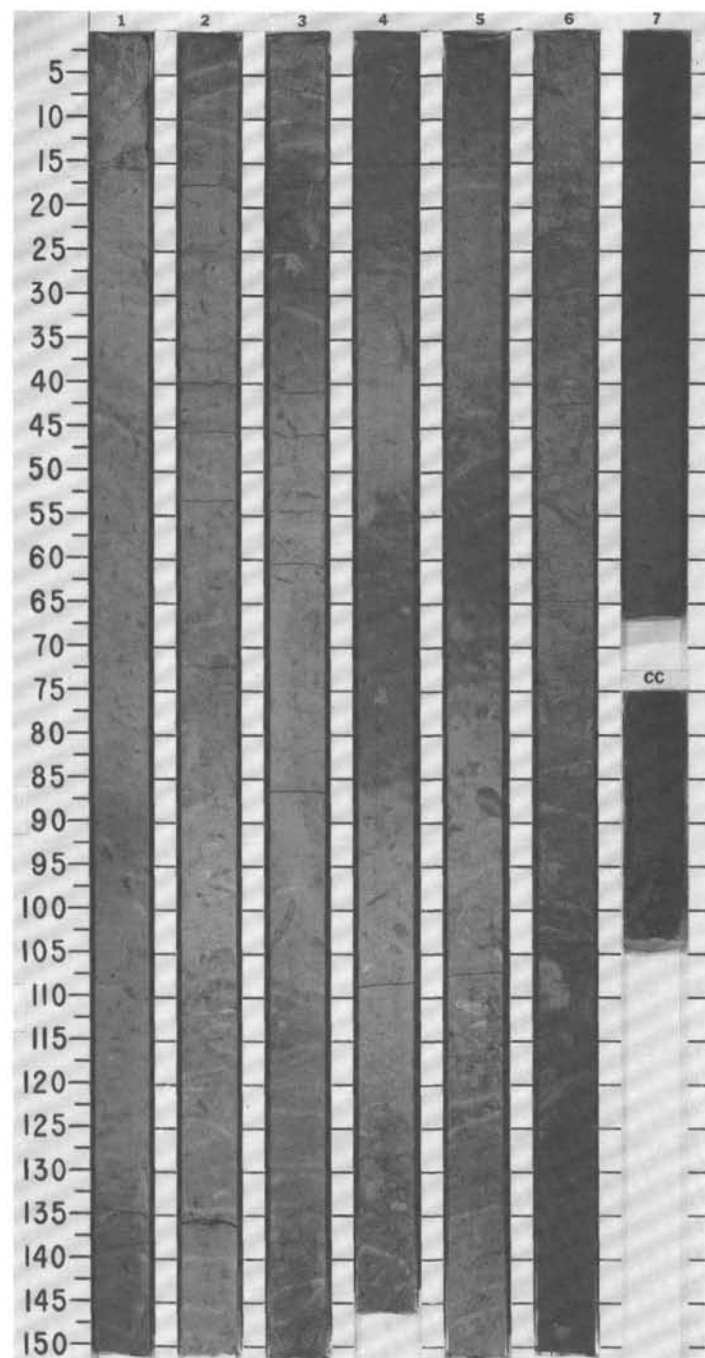
TIME-ROCK UNIT	BIOSTRAT. ZONE/ FOSSIL CHARACTER				PALEOMAGNETICS	PHYS. PROPERTIES	CHEMISTRY	SECTION	METERS	GRAPHIC LITHOLOGY	DRILLING DISTURB.	BED. STRUCTURES	SAMPLES	LITHOLOGIC DESCRIPTION
	FORAMINIFERS	NANNOFOSSILS	RADIOLARIANS	DIATOMS										
MIDDLE PLEISTOCENE	<i>P. obliquiloculata</i> Zone													
	NN19 <i>P. lacunosa</i>													

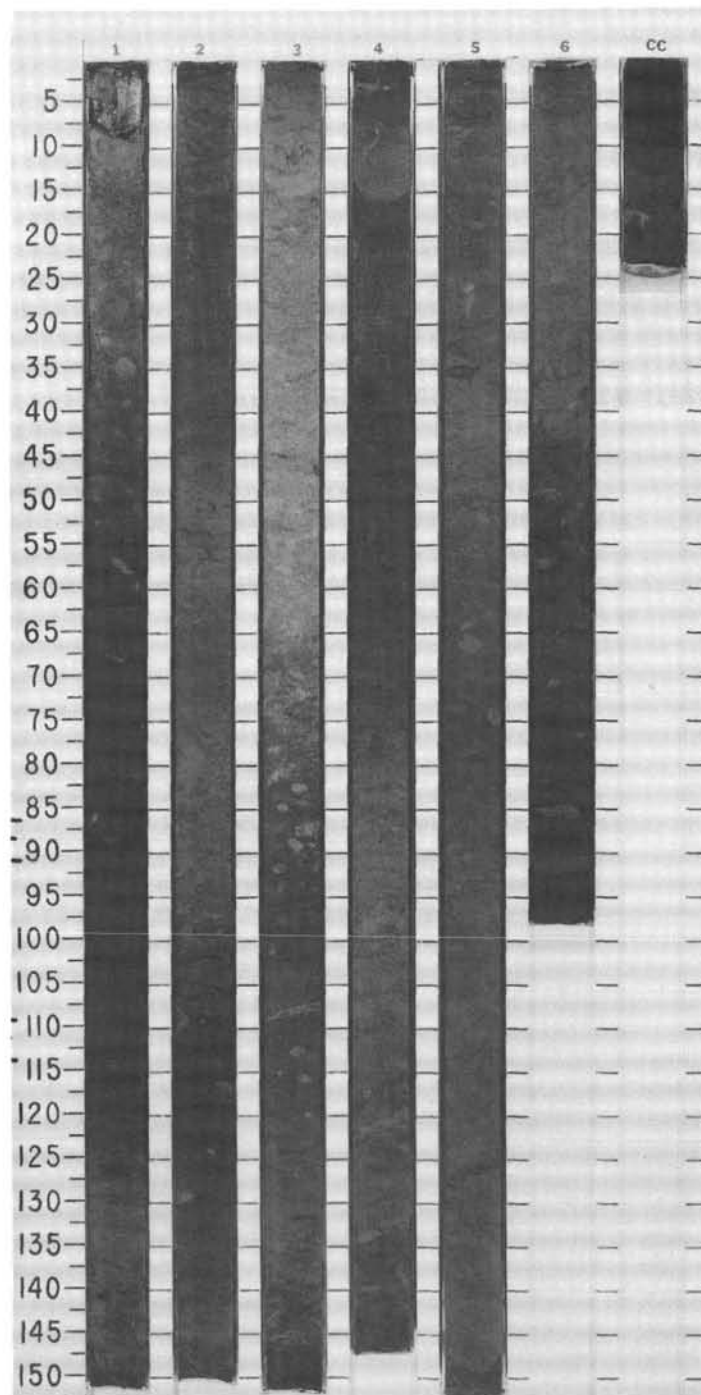


SITES 677 AND 678

SITE 677 HOLE B CORE 7H CORED INTERVAL 55.1-64.6 mbsf

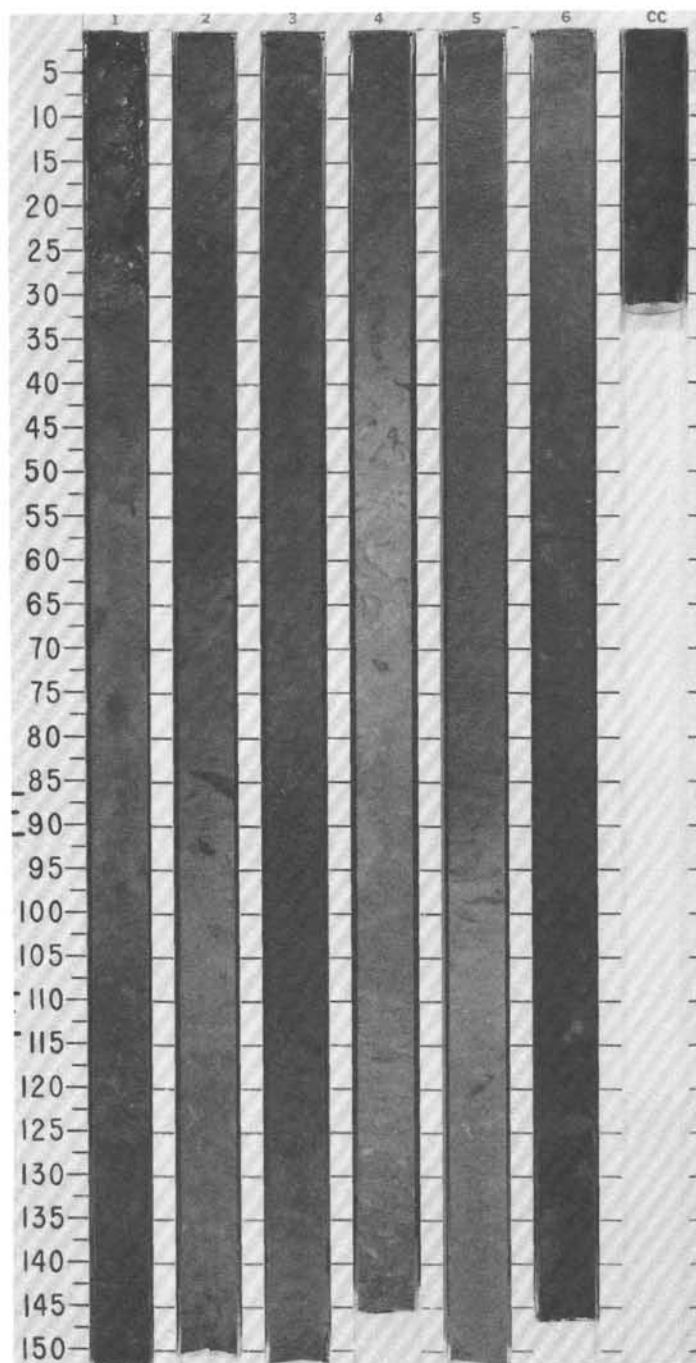
TIME-ROCK UNIT	BIOSTRAT. ZONE/ FOSSIL CHARACTER				PALEOMAGNETICS	PHYS. PROPERTIES	CHEMISTRY	SECTION	METERS	GRAPHIC LITHOLOGY	DRILLING DISTURB.	SED. STRUCTURES	SAMPLES	LITHOLOGIC DESCRIPTION
	FORAMINIFERS	NANNOFOSSILS	RADIOLARIANS	DIATOMS										
EARLY PLEISTOCENE														





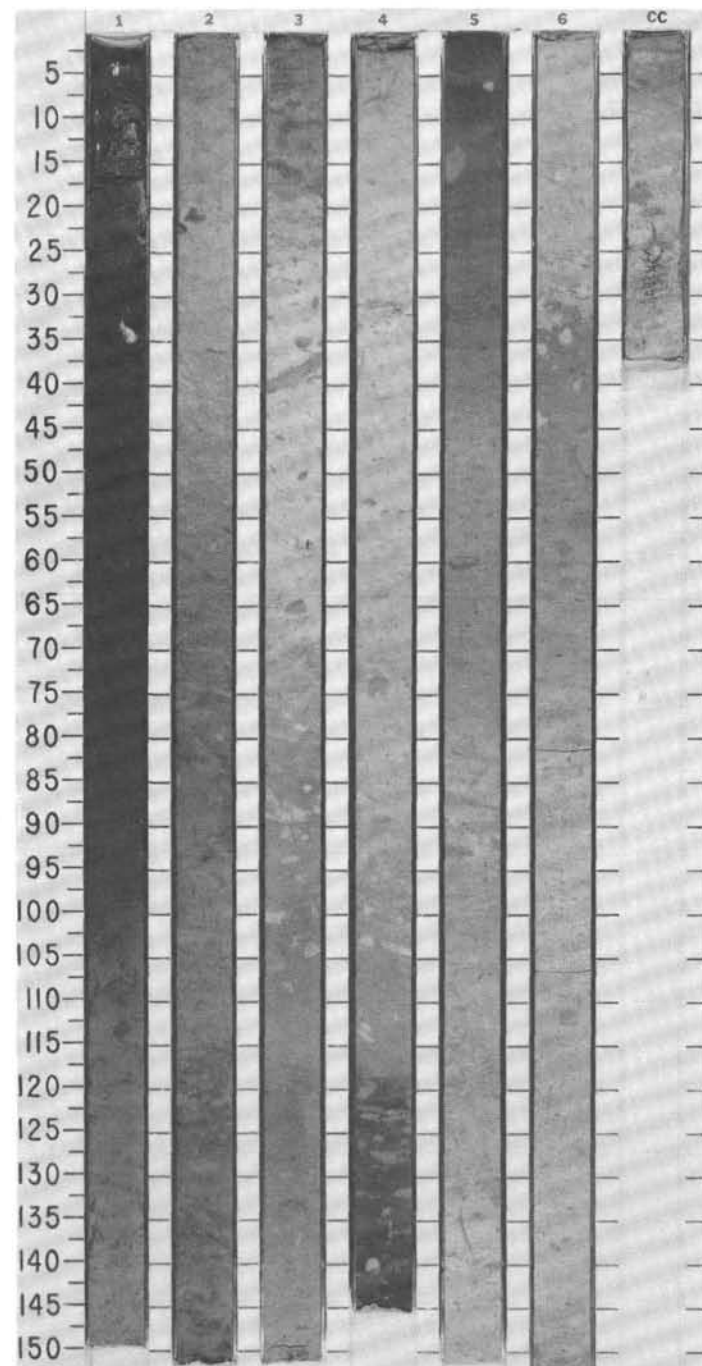
SITE 677 HOLE B CORE 9H CORED INTERVAL 74.1-83.6 mbsf

TIME-ROCK UNIT	BIOSTRAT. ZONE/ FOSSIL CHARACTER				PALEOMAGNETICS	PHYS. PROPERTIES	CHEMISTRY	SECTION	METERS	GRAPHIC LITHOLOGY	DRILLING DISTURB.	SED. STRUCTURES	SAMPLES	LITHOLOGIC DESCRIPTION																																																																								
	FORAMINIFERS	NANNOFOSSILS	RADIOLARIANS	DIATOMS																																																																																		
EARLY PLEISTOCENE	<i>P. obliquiloculata</i> Zone NN19 <i>P. lacunosa</i> Zone					•		1	0.5 1.0					CLAYEY CALCAREOUS DIATOM OOZE Homogeneous, nearly structureless, intercalated dark olive green (10Y 4/2, 10Y 5/2) and dark olive gray (5Y 3/2 and 5Y 4/2) ooze. 2 1/4-cm long shark tooth at 26-29 cm Section 1. Minor bioturbation and mottling. PHYSICAL PROPERTIES: <table><tr><td></td><td>1,</td><td>2,</td><td>3,</td><td>4,</td><td>5,</td><td>6,</td></tr><tr><td>WC (%)</td><td>202.18</td><td>222.59</td><td>189.74</td><td>172.68</td><td>233.64</td><td>229.68</td></tr><tr><td>ρ_g (g/cm³)</td><td>2.62</td><td>2.74</td><td>2.46</td><td>2.74</td><td>2.61</td><td>2.60</td></tr><tr><td>ρ_b (g/cm³)</td><td>1.28</td><td>1.27</td><td>1.28</td><td>1.32</td><td>1.25</td><td>1.25</td></tr><tr><td>ϕ (%)</td><td>84.08</td><td>85.91</td><td>82.31</td><td>82.45</td><td>85.94</td><td>85.68</td></tr><tr><td>K (W/mk)</td><td>0.824</td><td>0.807</td><td>0.837</td><td>0.862</td><td>0.724</td><td>0.738</td></tr></table> SMEAR SLIDE SUMMARY (%): <table><tr><td></td><td>6, 80</td></tr><tr><td>D</td><td></td></tr></table> TEXTURE: <table><tr><td>Sand</td><td>20</td></tr><tr><td>Silt</td><td>50</td></tr><tr><td>Clay</td><td>30</td></tr></table> COMPOSITION: <table><tr><td>Clay</td><td>25</td></tr><tr><td>Calcite/dolomite</td><td>15</td></tr><tr><td>Accessory minerals</td><td></td></tr><tr><td>Pyrite</td><td>5</td></tr><tr><td>Foraminifers</td><td>1</td></tr><tr><td>Nannofossils</td><td>7</td></tr><tr><td>Diatoms</td><td>35</td></tr><tr><td>Radiolarians</td><td>7</td></tr><tr><td>Sponge spicules</td><td>3</td></tr><tr><td>Silicoflagellates</td><td>2</td></tr></table>		1,	2,	3,	4,	5,	6,	WC (%)	202.18	222.59	189.74	172.68	233.64	229.68	ρ_g (g/cm ³)	2.62	2.74	2.46	2.74	2.61	2.60	ρ_b (g/cm ³)	1.28	1.27	1.28	1.32	1.25	1.25	ϕ (%)	84.08	85.91	82.31	82.45	85.94	85.68	K (W/mk)	0.824	0.807	0.837	0.862	0.724	0.738		6, 80	D		Sand	20	Silt	50	Clay	30	Clay	25	Calcite/dolomite	15	Accessory minerals		Pyrite	5	Foraminifers	1	Nannofossils	7	Diatoms	35	Radiolarians	7	Sponge spicules	3	Silicoflagellates	2
	1,	2,	3,	4,	5,	6,																																																																																
WC (%)	202.18	222.59	189.74	172.68	233.64	229.68																																																																																
ρ_g (g/cm ³)	2.62	2.74	2.46	2.74	2.61	2.60																																																																																
ρ_b (g/cm ³)	1.28	1.27	1.28	1.32	1.25	1.25																																																																																
ϕ (%)	84.08	85.91	82.31	82.45	85.94	85.68																																																																																
K (W/mk)	0.824	0.807	0.837	0.862	0.724	0.738																																																																																
	6, 80																																																																																					
D																																																																																						
Sand	20																																																																																					
Silt	50																																																																																					
Clay	30																																																																																					
Clay	25																																																																																					
Calcite/dolomite	15																																																																																					
Accessory minerals																																																																																						
Pyrite	5																																																																																					
Foraminifers	1																																																																																					
Nannofossils	7																																																																																					
Diatoms	35																																																																																					
Radiolarians	7																																																																																					
Sponge spicules	3																																																																																					
Silicoflagellates	2																																																																																					
LATE PLIOCENE	F/M					•		2						* CC																																																																								
						•		3																																																																														
						•		4																																																																														
						•		5																																																																														
						•		6																																																																														



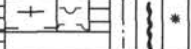

SITE 677 HOLE B CORE 10H CORED INTERVAL 83.6-93.1 mbsf

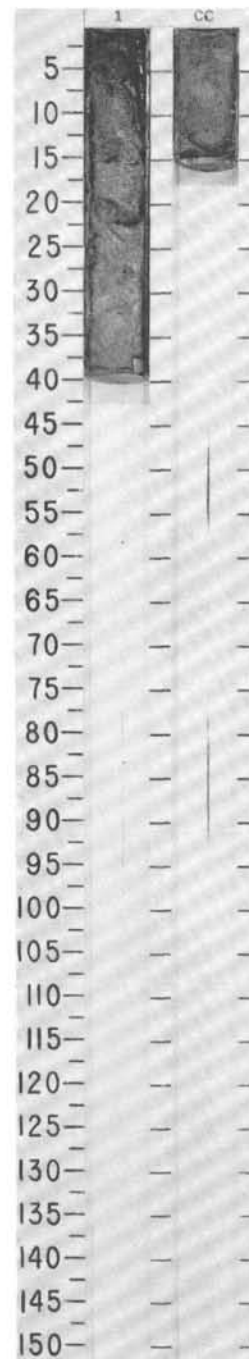
TIME-ROCK UNIT	BIOSTRAT. ZONE/ FOSSIL CHARACTER				PALEOMAGNETICS	PHYS. PROPERTIES	CHEMISTRY	SECTION	METERS	GRAPHIC LITHOLOGY	DRILLING DISTURB.	SED. STRUCTURES	SAMPLES	LITHOLOGIC DESCRIPTION
	FORAMINIFERS	NANNOFOSSILS	RADIOLARIANS	DIATOMS										
LATE PLIOCENE														
	G. fistulosus Zone													
	NN19 P. lacunosa Zone													



SITES 677 AND 678

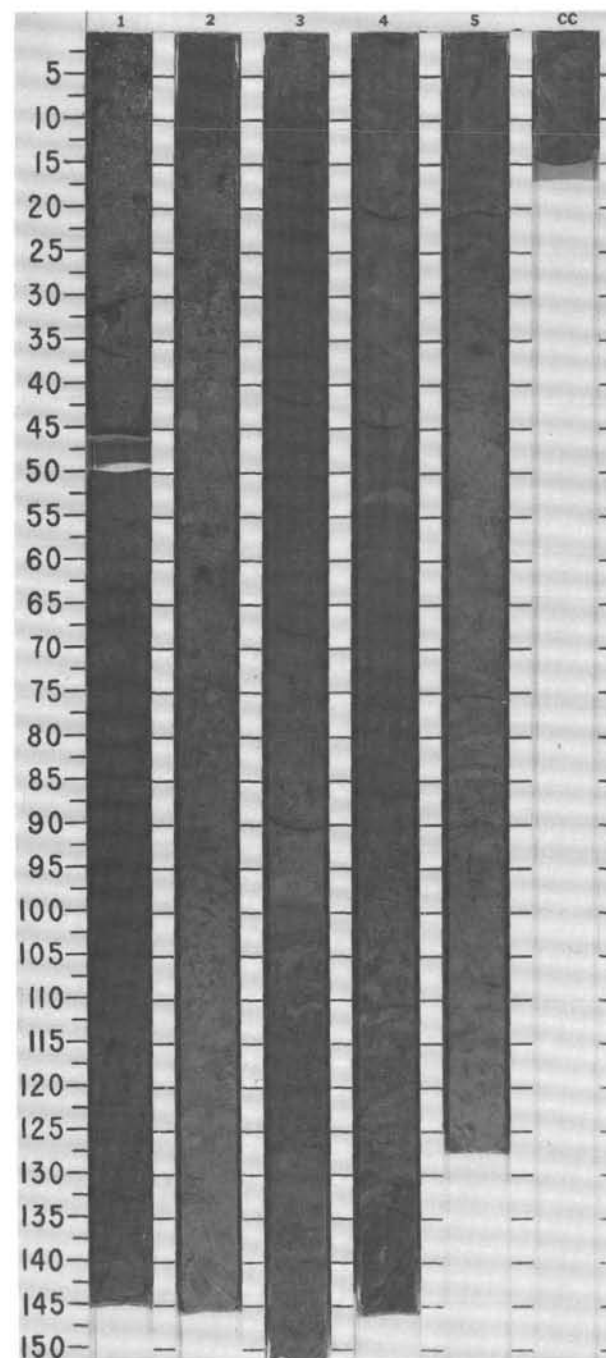
SITE 678 HOLE A CORE 1H CORED INTERVAL 0-0.6 mbsf

TIME-ROCK UNIT	BIOSTRAT. ZONE/ FOSSIL CHARACTER				SECTION	METERS	GRAPHIC LITHOLOGY	DRILLING DISTURB. SED. STRUCTURES	SAMPLES	LITHOLOGIC DESCRIPTION
	FORAMINIFERS	NANNOFOSSILS	RADIOLARIANS	DIATOMS						
LATE PLEISTOCENE										
F/M	NN21 E. <i>huxleyi</i> Zone				1	0.5			*	<p>CLAYEY RADIOLARIAN-NANNOFOSSIL-FORAMINIFER OOZE</p> <p>Olive gray (5Y 4/2, 5Y 5/2) ooze with gray (2.5Y 2/0) streaky mottling in Section 1. CC contains dark olive (10Y 4/2) ooze mottled with 10Y 6/2, 2.5Y 3/0, and 5Y 4/3. Moderately bioturbated.</p> <p>SMEAR SLIDE SUMMARY (%):</p> <p>1, 32 D</p> <p>TEXTURE:</p> <p>Sand 30 Silt 25 Clay 45</p> <p>COMPOSITION:</p> <p>Feldspar 2 Clay 20 Calcite/dolomite 5 Accessory minerals Pyrite 1 Foraminifers 25 Nannofossils 15 Diatoms 10 Radiolarians 20 Sponge spicules 2</p>



SITE 678 HOLE B CORE 1H CORED INTERVAL 0-7.5 mbsf

TIME-ROCK UNIT	BIOSTRAT. ZONE/ FOSSIL CHARACTER				PALEOMAGNETICS	PHYS. PROPERTIES	CHEMISTRY	SECTION	METERS	GRAPHIC LITHOLOGY	DRILLING DISTURB.	BED. STRUCTURES	SAMPLES	LITHOLOGIC DESCRIPTION
	FORAMINIFERS	NANNOFOSSILS	RADIOLARIANS	DIATOMS										
LATE PLEISTOCENE	NN21 <i>E. huxleyi</i> Zone													
F/P														



SITES 677 AND 678

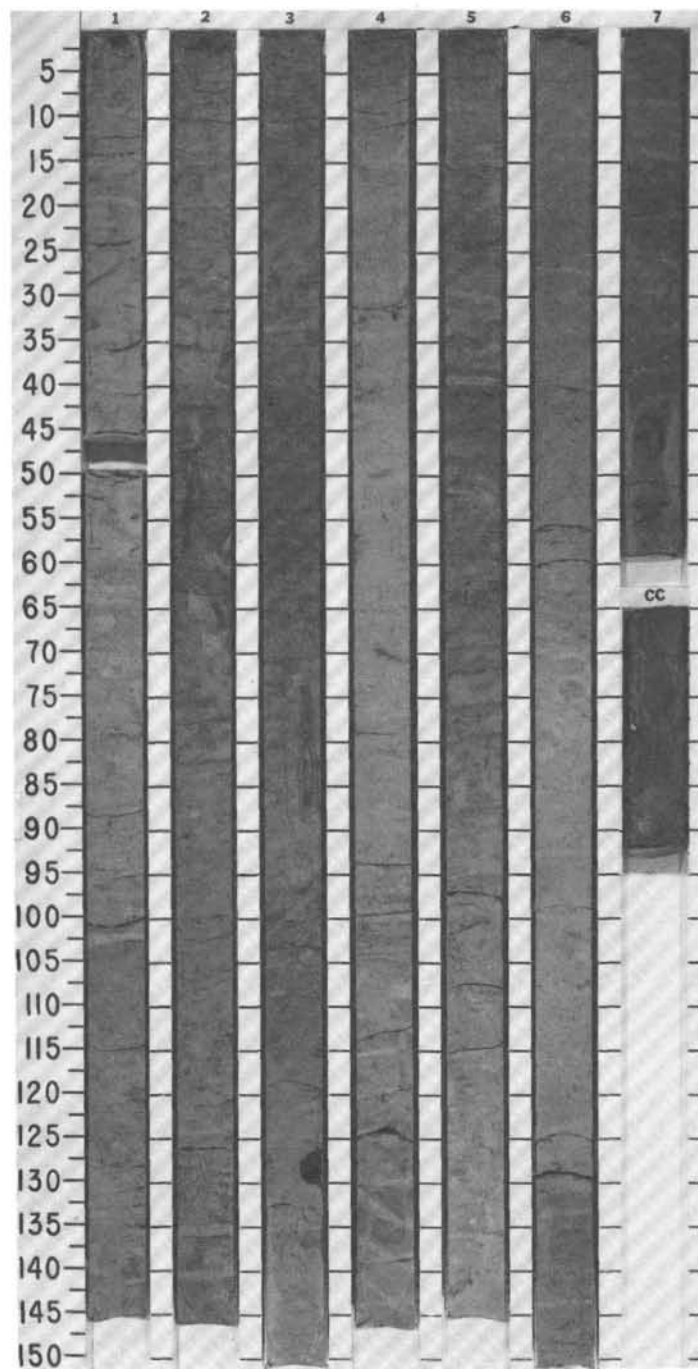
SITE 678HOLE B

CORE 2H

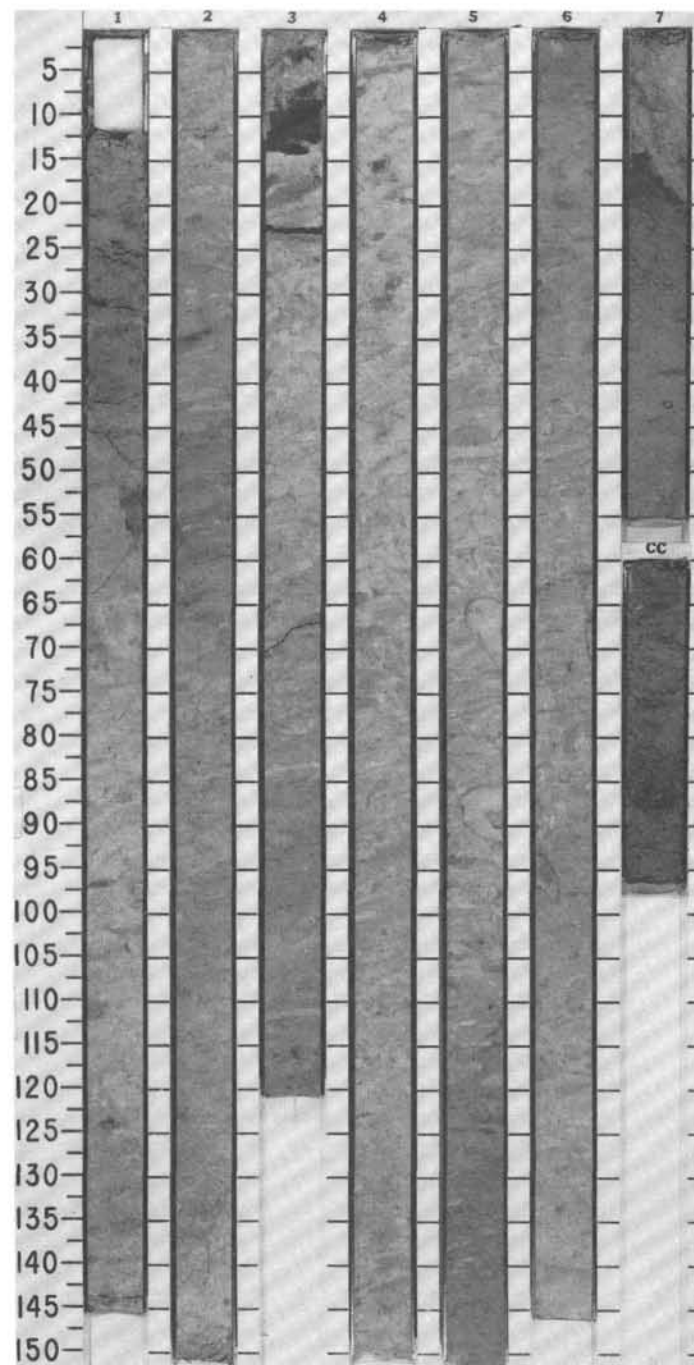
CORED INTERVAL

18.2-27.7 mbsf

TIME-ROCK UNIT	BIOSTRAT. ZONE/ FOSSIL CHARACTER				PALEOMAGNETICS	PHYS. PROPERTIES	CHEMISTRY	SECTION	METERS	GRAPHIC LITHOLOGY	DRILLING DISTURB.	SED. STRUCTURES	SAMPLES	LITHOLOGIC DESCRIPTION																																																																																																																										
	FORAMINIFERS	NANNOFOSSILS	RADIOLARIANS	DIATOMS																																																																																																																																				
LATE PLEISTOCENE	NN19 <i>P. lacunosa</i> Zone	F/M							1				IWV	<p>NANNOFOSSIL RADIOLARIAN-DIATOM OOZE</p> <p>Uniformly olive gray green (10Y 5/2, 10Y 6/2) ooze, moderately to intensely bioturbated. One 70-cm thick layer of yellow green (5GY 5/2) ooze at top of Section 6. Simple <i>Zoophycos</i> burrows common. Pyrite staining ubiquitous. Drilling disturbance flow-in structure at 940 cm which continues in the CC.</p> <p>CHEMISTRY wt % CO₂/wt % total C:</p> <table><tr><td>1.75</td><td>2.75</td><td>3.75</td><td>4.75</td><td>5.75</td><td>6.75</td></tr><tr><td>56.35/7.10</td><td>38.91/5.34</td><td>35.12/4.75</td><td>57.18/7.3</td><td>17.61/2.8</td><td>50.52/6.84</td></tr></table> <p>PHYSICAL PROPERTIES:</p> <table><tr><td></td><td>1.75</td><td>2.75</td><td>3.75</td><td>4.75</td><td>5.75</td><td>6.75</td></tr><tr><td>WC (%)</td><td>150.57</td><td>176.37</td><td>198.04</td><td>128.46</td><td>209.22</td><td>141.90</td></tr><tr><td>ρ_g (g/cm³)</td><td>2.34</td><td>2.87</td><td>2.88</td><td>3.04</td><td>2.25</td><td>2.93</td></tr><tr><td>ρ_b (g/cm³)</td><td>1.32</td><td>1.33</td><td>1.30</td><td>1.44</td><td>1.24</td><td>1.40</td></tr><tr><td>ϕ (%)</td><td>77.85</td><td>83.46</td><td>85.03</td><td>79.47</td><td>82.48</td><td>80.47</td></tr><tr><td>σ (kPa)</td><td>8.39</td><td>16.02</td><td>19.07</td><td>20.59</td><td>20.59</td><td>27.46</td></tr><tr><td>K (W/mk)</td><td>0.836</td><td>0.855</td><td>0.874</td><td>1.111</td><td>0.813</td><td>0.836</td></tr><tr><td>V_p (m/s)</td><td>1537.3</td><td>1631.6</td><td>1564.3</td><td>1573.3</td><td>1559.6</td><td>1556.7</td></tr></table> <p>SMEAR SLIDE SUMMARY (%):</p> <table><tr><td></td><td>3, 128</td><td>5, 50</td></tr><tr><td></td><td>M</td><td>D</td></tr></table> <p>TEXTURE:</p> <table><tr><td>Sand</td><td>—</td><td>15</td></tr><tr><td>Silt</td><td>15</td><td>40</td></tr><tr><td>Clay</td><td>85</td><td>45</td></tr></table> <p>COMPOSITION:</p> <table><tr><td>Quartz</td><td>—</td><td>Tr</td></tr><tr><td>Feldspar</td><td>—</td><td>1</td></tr><tr><td>Rock fragments</td><td>3</td><td>—</td></tr><tr><td>Clay</td><td>45</td><td>10</td></tr><tr><td>Calcite/dolomite</td><td>—</td><td>10</td></tr><tr><td>Accessory minerals</td><td>2</td><td>—</td></tr><tr><td>Pyrite</td><td>60</td><td>1</td></tr><tr><td>Foraminifers</td><td>Tr</td><td>3</td></tr><tr><td>Nannofossils</td><td>Tr</td><td>15</td></tr><tr><td>Diatoms</td><td>—</td><td>40</td></tr><tr><td>Radiolarians</td><td>Tr</td><td>15</td></tr><tr><td>Sponge spicules</td><td>—</td><td>4</td></tr><tr><td>Silicoflagellates</td><td>—</td><td>1</td></tr></table>	1.75	2.75	3.75	4.75	5.75	6.75	56.35/7.10	38.91/5.34	35.12/4.75	57.18/7.3	17.61/2.8	50.52/6.84		1.75	2.75	3.75	4.75	5.75	6.75	WC (%)	150.57	176.37	198.04	128.46	209.22	141.90	ρ_g (g/cm ³)	2.34	2.87	2.88	3.04	2.25	2.93	ρ_b (g/cm ³)	1.32	1.33	1.30	1.44	1.24	1.40	ϕ (%)	77.85	83.46	85.03	79.47	82.48	80.47	σ (kPa)	8.39	16.02	19.07	20.59	20.59	27.46	K (W/mk)	0.836	0.855	0.874	1.111	0.813	0.836	V _p (m/s)	1537.3	1631.6	1564.3	1573.3	1559.6	1556.7		3, 128	5, 50		M	D	Sand	—	15	Silt	15	40	Clay	85	45	Quartz	—	Tr	Feldspar	—	1	Rock fragments	3	—	Clay	45	10	Calcite/dolomite	—	10	Accessory minerals	2	—	Pyrite	60	1	Foraminifers	Tr	3	Nannofossils	Tr	15	Diatoms	—	40	Radiolarians	Tr	15	Sponge spicules	—	4	Silicoflagellates	—	1
1.75	2.75	3.75	4.75	5.75	6.75																																																																																																																																			
56.35/7.10	38.91/5.34	35.12/4.75	57.18/7.3	17.61/2.8	50.52/6.84																																																																																																																																			
	1.75	2.75	3.75	4.75	5.75	6.75																																																																																																																																		
WC (%)	150.57	176.37	198.04	128.46	209.22	141.90																																																																																																																																		
ρ_g (g/cm ³)	2.34	2.87	2.88	3.04	2.25	2.93																																																																																																																																		
ρ_b (g/cm ³)	1.32	1.33	1.30	1.44	1.24	1.40																																																																																																																																		
ϕ (%)	77.85	83.46	85.03	79.47	82.48	80.47																																																																																																																																		
σ (kPa)	8.39	16.02	19.07	20.59	20.59	27.46																																																																																																																																		
K (W/mk)	0.836	0.855	0.874	1.111	0.813	0.836																																																																																																																																		
V _p (m/s)	1537.3	1631.6	1564.3	1573.3	1559.6	1556.7																																																																																																																																		
	3, 128	5, 50																																																																																																																																						
	M	D																																																																																																																																						
Sand	—	15																																																																																																																																						
Silt	15	40																																																																																																																																						
Clay	85	45																																																																																																																																						
Quartz	—	Tr																																																																																																																																						
Feldspar	—	1																																																																																																																																						
Rock fragments	3	—																																																																																																																																						
Clay	45	10																																																																																																																																						
Calcite/dolomite	—	10																																																																																																																																						
Accessory minerals	2	—																																																																																																																																						
Pyrite	60	1																																																																																																																																						
Foraminifers	Tr	3																																																																																																																																						
Nannofossils	Tr	15																																																																																																																																						
Diatoms	—	40																																																																																																																																						
Radiolarians	Tr	15																																																																																																																																						
Sponge spicules	—	4																																																																																																																																						
Silicoflagellates	—	1																																																																																																																																						
2				IWV																																																																																																																																				
3				IWV	*																																																																																																																																			
4				IWV	*																																																																																																																																			
5				IWV	*																																																																																																																																			
6				IWV	*																																																																																																																																			
7																																																																																																																																								
CC																																																																																																																																								

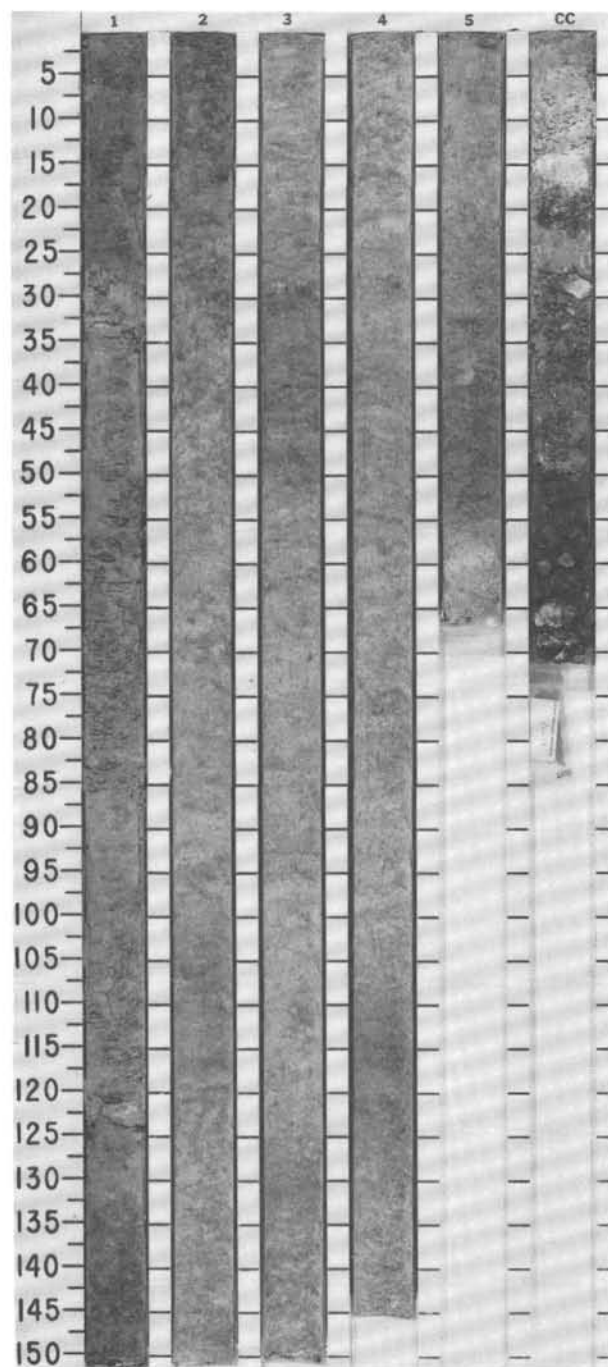


SITES 677 AND 678



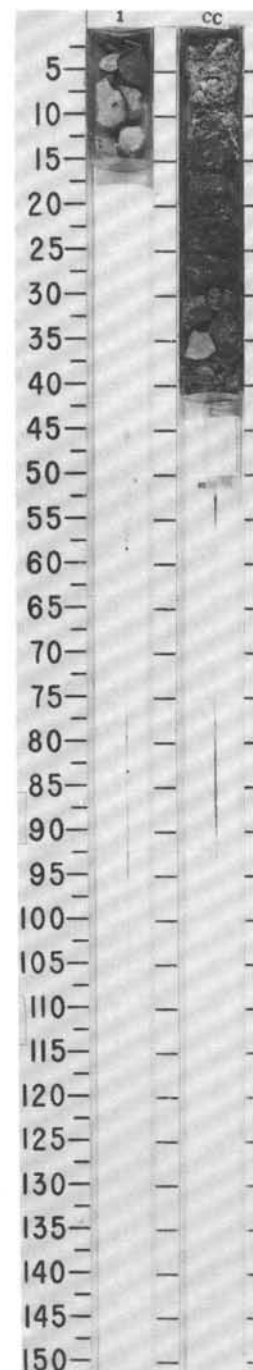
SITE 678 HOLE B CORE 4W CORED INTERVAL 105.0-169.5 mbsf

TIME-ROCK UNIT	BIOSTRAT. ZONE/ FOSSIL CHARACTER	PALEOMAGNETICS	PHYS. PROPERTIES	CHEMISTRY	SECTION	METERS	GRAPHIC LITHOLOGY	DRILLING DISTURB.	SED. STRUCTURES	SAMPLES	LITHOLOGIC DESCRIPTION
LATE MIOCENE	NN11 D. <i>quinqueramus</i> Zone										CLAYEY SILICEOUS NANNOFOSSIL CHALK, LIMESTONE, AND BASALT CONGLOMERATE
					1	0.5 1.0					Yellow-gray olive green (5GY 5/2, 10Y 4/2, 10Y 6/2, 5Y 7/1) chalk fills Sections 1 through 4. Moderate to intense bioturbation. CC grades from massive yellow green (5GY 6/1) ooze through firm pinkish gray (5YR 6/2) limestone fragments mixed with yellow green (5GY 6/1) ooze to a basalt conglomerate in which dark gray (10G 6/1) basalt fragments are angular to subrounded, ranging up to 3 cm in size, many with reddish-brown stained surfaces. These fragments are cemented with fine-grained, firm gray mud containing common white zeolite(?).
					2						Bottom of CC is filled with hard pinkish gray (5YR 7/2) mud containing greenish patches and white zeolite(?) within fractures, and a 3-cm long concretion of marcasite with cubic pyrite on the surface at 60 cm in the CC.
					3						CHEMISTRY wt % CO ₂ /wt % total C: 1, 75 3, 75 4, 75 49.91/6.28 58.03/6.99 65.04/7.82
					4						PHYSICAL PROPERTIES: 1, 75 3, 75 4, 75 WC (%) 139.92 100.60 99.213 p _g (g/cm ³) 2.77 2.96 2.52 p _b (g/cm ³) 1.38 1.52 1.45 φ (%) 79.33 74.67 71.22 K (W/mk) 0.918 1.076 1.072
					5						SMEAR SLIDE SUMMARY (%): 3, 80 CC, 15 D D
					CC						TEXTURE: Sand 7 3 Silt 20 10 Clay 73 87
											COMPOSITION: Feldspar 1 Tr Clay 20 7 Calcite/dolomite 10 4 Accessory minerals Tr 1 Pyrite 3 Tr Foraminifers 1 3 Nannofossils 45 85 Diatoms 15 — Radiolarians 5 — Sponge spicules Tr —



SITE 678 HOLE B CORE 5X CORED INTERVAL 169.5-171.8 mbsf

TIME-ROCK UNIT	BIOSTRAT. ZONE/ FOSSIL CHARACTER				PALEOMAGNETICS	PHYS. PROPERTIES	CHEMISTRY	SECTION	METERS	GRAPHIC LITHOLOGY	DRILLING DISTURB.	SED. STRUCTURES	SAMPLES	LITHOLOGIC DESCRIPTION
	FORAMINIFERS	NANNOFOSSILS	RADIOLARIANS	DIATOMS										
R/P	?							1	0.5		X	X	*	<p>LIMESTONE AND BRECCIATED BASALT</p> <p>Section 1 consists primarily of pale red (10R 6/2) lithified limestone pebbles, 2-6 cm in size. A single basalt pebble, rounded, black 4 cm diameter, fine-grained, glassy at one end; pillow fragment? CC contents range from 0-11 cm very firm yellow-green (5GY 6/1) mud forming a conglomerate with abundant pebbles of pinkish gray (5YR 6/2) limestone (up to 2.5 cm in diameter), plus rounded pieces of yellow green (5GY 6/1) limestone (up to 5 mm in diameter), and a white (zeolite?) cement, disseminated and in fractures. From 11-29 cm dense dark brown-gray (5YR 3/1) to dark green (7.5G 3/2) mud containing rounded mm-sized reddish (2.5YR 5/4) granules and several rounded basalt pebbles (up to 1.5 cm diameter); common white (zeolite?) material occurs in mm-sized spots and along fractures. The final (29-41 cm) consists of a conglomerate of dark gray (10G 4/1) rounded pebbles of basalt (up to 3 cm diameter), cemented by very firm gray mud. White (zeolite?) material is common in mm-sized spots within mud.</p>



THIN SECTION DESCRIPTION

111-678B-4W-CC (Piece 55, 51-53 cm)

ROCK NAME: Plagioclase porphyritic basalt

WHERE SAMPLED: Pillow margin(?)

TEXTURE: Quenched, fluidal

GRAIN SIZE: Fine

OBSERVER: Malpas

PRIMARY MINERALOGY	PERCENT PRESENT	PERCENT ORIGINAL	SIZE RANGE (mm)	APPROX. COMPOSITION	MORPHOLOGY	COMMENTS
PHENOCRYSTS						
Plagioclase	5	5	< 1	An 70	Euhedral	Tabular crystals in glomerocrysts (10-12 crystals). Some solitary phenocrysts.
Spinel	< 1	< 1	< 0.02	Chromite	Subhedral-anhedral	Rare crystals associated with glomerocrysts of plag and with cpx clusters.
GROUNDMASS						
Plagioclase	50	50	< 1		Skeletal	Acicular. Fluidised texture.
Pyroxene	10	20	< 0.6		Plumose	Occurs in patches. Palagonitised.
Glass	—	12				Devitrified.
Oxides	2	2			Some euhedral, dusty	Patchy. Form around glomerocrysts plus px-rich patches.
SECONDARY MINERALOGY	PERCENT	REPLACING/ FILLING				COMMENTS
Clays	22					Palagonite from glass. Replacing some cpx.
Oxides	8					Associated with glass devitrification.
Celadonite(?)	2					Associated with cpx alteration.
VESICLES / CAVITIES	PERCENT	LOCATION	SIZE RANGE (mm)	FILLING	SHAPE	COMMENTS
Vesicles	<< 1	Dispersed	0.2	None	Round	Rare empty vesicles.

COMMENTS: Quenched texture. Typical features of groundmass glass devitrification.

THIN SECTION DESCRIPTION

111-678B-5X-1 (5-8 cm)

ROCK NAME: Plagioclase porphyritic basalt

WHERE SAMPLED: Pillow margin(?)

TEXTURE: Hyalopilitic

GRAIN SIZE: Fine

OBSERVER: Malpas

PRIMARY MINERALOGY	PERCENT PRESENT	PERCENT ORIGINAL	SIZE RANGE (mm)	APPROX. COMPOSITION	MORPHOLOGY	COMMENTS
PHENOCRYSTS						
Olivine	—	(?)				
Plagioclase	5	5	< 1.5	An 70	Euhedral	Possibly altered olivine crystal ≈ 0.1 mm, now chlorite. Glomerocrysts. Show additional skeletal growth at margins. Some show subtle zoning. Generally cluster of 10-12 crystals.
GROUNDMASS						
Plagioclase	30	30	0.5		Acicular	Microlites with some alignment.
Clinopyroxene	—	15	< 0.1		Plumose	Patches of plumose cpx. Altered to oxides plus clay.
Glass	—	50				Altered to oxides and crystallites. Palagonitised.
Chromite	< 1	< 1	< 0.05		Euhedral	Rare grains close to glomerocrysts of plag.
SECONDARY MINERALOGY	PERCENT	REPLACING/ FILLING				
Clays	55	Glass, cpx				Celadonite, sepiolite.
Oxides	10	Glass				
VESICLES / CAVITIES	PERCENT	LOCATION	SIZE RANGE (mm)	FILLING	SHAPE	COMMENTS
Vesicles		Dispersed	0.1	None	Elliptical	Open vesicles.

COMMENTS: Rock shows typical quench texture with minor flow alignment of some microlites. Pyroxene is developed in patches in groundmass especially close to glomerocrysts of plag. Phenocrysts show skeletal growth on margins.